DEVELOPMENT OF BIOPOLYMER HYDROGELS AS COMPLEX TISSUE ENGINEERING SCAFFOLDS

SAMUEL ROBERT MOXON

A thesis submitted to the University of Huddersfield in partial fulfilment of the requirements for the degree of Doctor of Philosophy

The University of Huddersfield

Submission date – December 2016

Copyright statement

Abstract

As global life expectancy increases, so does the demand for new technologies to address healthcare issues associated with disease and degradation of biological tissues and organs. Implantation is still a heavily relied upon method but patient demand is far greater than donor availability. Tissue engineering continues to show promise as a potential alternative to the reliance on donors and is fundamentally based on the concept of using a patient's own cells to create new, healthy tissue. Strategies often include incorporation of cells into 3D culture scaffolds as a means of replicating *in vivo* culture environments *in vitro*, thus stimulating expression of more native cellular phenotypes. Biopolymer hydrogels are popular tools for this approach due to lack of cytotoxicity, high porosity and a capacity to both introduce chemical cues and tune mechanical properties. Research, however, often focuses on culturing a single cell type and scaffolds often only exhibit a single mechanical property. Additionally, there is difficulty in delivering different chemical cues to a single encapsulated population due to limitations in controlling diffusion of small molecules through hydrogel matrices. This places limitations on the capacity to fabricate scaffolds for repair of complex layered structures comprised of multiple matrix components and cell types. The work presented in this thesis focuses on development of biopolymer hydrogel culture systems for providing cells with multiple chemical and mechanical cues. This could provide a platform for creating scaffolds for regeneration of more complex, layered structures such as articular cartilage and osteochondral tissue.

Chapter 4 presents a study into using pulsed sonication to tune mechanical properties of hydrogel scaffolds of gellan gum (gellan). By applying different amplitudes of sonication, molecular weight was successfully tuned as evidenced by changes in intrinsic viscosity. This resulted in changes in both the dynamic viscosity of gellan solutions and the matrix stiffness and elasticity of gellan hydrogels. The impact on tuning mechanical properties of gellan hydrogels on cell behaviour was

investigated using MC3T3 mouse pre-osteoblasts. A reduction in matrix stiffness via sonication coincided with a drop in expression of a key osteogenic marker, namely alkaline phosphatase. This demonstrated how tuning mechanical properties of gellan scaffolds with sonication could potentially be used to influence phenotype expression of many cell types with a possibility to influence cell differentiation.

Chapters 5 and 6 build on this concept of manipulating mechanical properties to influence cell behaviour *in vitro*. Fluid gels are presented as a material for supporting deposition of biopolymer solutions for additive layer manufacturing of tissue culture scaffolds. The aim was to use this system to fabricate scaffolds exhibiting multiple mechanical properties and multiple cell types. Chapter 5 presents development of the method with investigation into how fluid gel mechanical properties impacted on self-healing properties and a capacity to suspend gellan solutions. Furthermore, the effect of multiple deposition parameters (gellan viscosity, needle aperture and deposition speed) on the resolution of suspended structures was evaluated. Complex structures were fabricated including a mineralised gellan helix and layered, biphasic osteochondral-like scaffolds which were further investigated in Chapter 6. Cell-loaded, autologous osteochondral scaffolds were formed, implanted into human osteochondral tissue and cultured for 30 days. Analysis of mRNA expression revealed evidence of expression of chondrogenic and osteogenic phenotypes in the cartilage and bone regions of the scaffold. Moreover, there was evidence of an interface between both cell types and materials providing support to the conclusion that a 3D osteochondral culture model had been successfully generated.

Chapter 7 presents an alternative approach to creating gradient structures such as an osteochondral tissue culture scaffold. A fluidic hydrogel system is presented for controlled delivery of multiple chemical cues to a single rBMSC population. Delivery of osteogenic and chondrogenic differentiation cues was controlled by restricting diffusion of small molecules through the porous hydrogel network. After 6 weeks of culture, rBMSC’s displayed evidence of controlled differentiation down both

osteogenic and chondrogenic lineages. Analysis of alkaline phosphatase activity paired with type I and II collagen mRNA synthesis revealed evidence of segregated populations of osteoblasts and chondrocytes. Additionally, there was evidence of an interface between the two, thus presenting another possible osteochondral culture model.

Acknowledgements

I would like to start by thanking my supervisors Dr. Alan Smith and Prof. Barbara Conway for their guidance throughout my PhD. I believe they have taught me how to function as a researcher and have helped inspire my passion for research. Additionally I would like to thank the technicians, particularly Hayley Markham, for all their assistance in the lab. Without them our labs simply would not function.

I would also like to acknowledge researchers at the University of Birmingham for all they have contributed to my studies both in an advisory and collaboratory role. In particular I want to thank Prof. Liam Grover, Dr. Richard Williams, Dr. Sophie Cox, Erik Hughes and Megan Cooke for the integral roles they have played in this research.

Thirdly, I would like to thank my best friend James for halving my rent over the course of my PhD. They say living with your best mate is a bad thing but we managed to not kill each other! Thanks for always supporting me.

I would like to acknowledge Louise and Oscar for keeping me sane throughout the business end of my PhD. Especially when I struggled to switch off and relax!

I also want to thank many members of my family for their on-going support throughout my career. Thanks to my parents, Robert and Jayne, my grandparents, Desmond and Margaret and my Great Auntie Helen for their support and for funding my education, ensuring I have the best possible chances to succeed. Additionally thanks to my grandparents, Olga and Geoff and my Uncle Ian for always encouraging me. Finally thanks to my big sister Lauren for always being there to help!

This thesis is dedicated to the memory of my Great Uncle, the late Prof. Sidney Pollard. Born in Vienna in 1925, Sidney was forced to leave his homeland to flee the grasp of Nazi Germany. He arrived on British soil via the Kindertransport with no possessions and would never see his parents again. He began life in England on a farm where he would often clean out the pig sty. In doing so he developed a great fondness for pigs that he kept throughout his life. However, as the war went on Sidney felt the need to contribute to the British effort. As a German speaker, Sidney worked as an interpreter for the British Army in occupied Germany knowing full well that, were he to be captured, he would not be sent to a POW camp. Instead, he would be sent to one of the many concentration camps established by Nazi Germany. After the war ended, he returned to London to study Economics. He quickly became a world renowned academic in the field of Economic History as highlighted by his award of Professorship at the age of 36. Sidney became a giant of his field delivering guest lectures worldwide and he is held in high regard by all who knew him, in particular the University of Sheffield where he spent a lot of his career. While I was only young when he died, retellings of his lifetime achievements despite an incredibly difficult start have always inspired me to strive for excellence.

Contents

Abstract I

Acknowledgements IV

Chapter 1 – General Introduction 19

1.1 Introduction to Tissue Engineering 19

1.2 Native Tissue 20

1.3 Bone Tissue 20

1.3.1 Osteoblasts 21

1.3.2 Osteocytes 22

1.3.3 Osteoclasts 22

1.3.4 Bone lining cells 23

1.4 Articular cartilage tissue 23

1.4.1 Superficial layer 24

1.4.2 Transitional zone 25

1.4.3 Radial zone 25

1.4.4 Calcified cartilage 25

1.5 Tissue Engineering Scaffolds 26

1.5.1 Mechanical properties 26

1.5.2 Scaffold architecture 27

1.6 Current Developments in Bone and Cartilage Tissue Engineering 27

1.6.1 Bone ECM-mimetic scaffolds 28

1.6.2 Progress in cartilage tissue engineering 30

1.7 Current Limitations in Engineering of Complex Tissues 32
1.8 Hypothesis, Aims and Objectives 33
1.9 Thesis Outline 34
1.10 Publications and Conference Presentations 35
1.10.1 - Publications 35
1.101.2 - Conferences Presentations 36
Chapter 2 – Biopolymer Hydrogel Scaffolds 38
2.1 Introduction to Medical Biopolymers 38
2.1.1 Biopolymer hydrogel scaffolds 39
2.1.2 Porosity 41
2.1.3 Structural and mechanical properties 42
2.1.4 Tunability 42
2.2 Polysaccharide Hydrogels 44
2.2.1 Gellan gum 44
2.2.2 Agarose 46
2.2.3 Alginate 47
2.3 Protein Hydrogels 49
2.3.1 Collagen 49
2.3.2 Gelatin 50
2.4 – Recent Innovations in Tissue Engineering Applications of Biopolymers 51
Chapter 3 – Rheological Characterisation of Biopolymer Materials 59
3.1 Introduction to Rheology 59

3.2 Stress and Strain 60
3.2.1 Young's modulus 60
3.2.2 Shear modulus 61
3.2.3 Bulk relaxation modulus 61
3.3 Rheological Analysis of Biopolymers 62
3.3.1 Viscosity 63
3.3.2 Newtonian vs. Non-Newtonian systems 63
3.3.3 Characterising flow behaviour 65
3.3.4 Intrinsic Viscosity 66
3.3.5 Viscoelasticity 69
3.3.6 The linear viscoelastic region 74
3.3.7 LVR determination 75
3.3.8 Frequency Sweeps 76
3.3.9 Temperature sweeps 77
Chapter 4 – Tuning the Rheology of Gellan Gum Hydrogels for Cell Culture Applications 79
4.1 Introduction 79
4.2 Materials and Methods 82
4.2.1 Materials 82
4.2.2 Preparation of gellan gum solutions 82
4.2.3 Sonication of gellan solutions 82
4.2.4 Rheology 83
4.2.5 Stress sweeps 84

4.2.6 Dynamic measurements of modulus during cooling....84
4.2.7 Frequency sweeps....85
4.2.8 Viscosity measurements....85
4.2.9 Intrinsic viscosity and molecular weight....85
4.2.10 Rheology in cell culture conditions....87
4.2.11 Effect of sonication on gelation time of gellan in cell culture conditions....87
4.2.12 Frequency sweeps in cell culture conditions....88
4.2.13 Cell culture....88
4.2.14 Cell culture – aseptic technique....88
4.2.15 – Seeding and expansion of MC3T3 cultures....88
4.2.16 Passaging of confluent cultures....89
4.2.17 Encapsulation of MC3T3 preosteoblasts in sonicated and un-sonicated gellan....89
4.2.18 Live/dead staining....90
4.2.19 Cell viability....90
4.2.20 Alkaline phosphatase activity....91
4.2.21 Statistical analysis....91
4.3 Results....91
4.3.1 Stress Sweeps of sonicated and un-sonicated gellan hydrogels....91
4.3.2 Temperature sweeps of gellan before and after sonication....94
4.3.3 Frequency sweeps....96
4.3.4 Shear sweeps of gellan gum....97
4.3.5 Determination of intrinsic viscosity and molecular weight....98

4.3.6 Gelation in cell culture conditions 99
4.3.7 Frequency sweeps of hydrogels formed in cell culture conditions 100
4.3.8 Cell-loaded hydrogels 101
4.3.9 Live/dead staining 102
4.3.10 Cell viability 103
4.3.11 Effect of gellan sonication on ALP activity in encapsulated MC3T3 cells 104
4.4 Discussion 106
4.5 Conclusions 110
Chapter 5 – Development of an Additive Layer Manufacturing Technique for 3D Rapid Prototyping of Hydrogel Substrates 111
5.1 Introduction 111
5.2 Materials and Methods 117
5.2.1 Materials 117
5.2.2 Fluid gel formation 118
5.2.3 Fluid gel concentration tests 118
5.2.4 Rheology 119
5.2.5 Frequency Sweeps 119
5.2.6 Shear Ramps 120
5.2.7 Particle size analysis 120
5.2.8 Tuning construct resolution 120
5.2.9 Creating complex hydrogel structures using suspended manufacture 121
5.2.10 Fabricating layered structures of specific dimensions 121

5.2.11 Fabrication of mineralised polymer helical structures 123
5.2.12 Initial evaluation of cell culture applications 124
5.3 Results 124
5.3.1 Fluid gel concentration tests 124
5.3.2 Rheology of gellan fluid gels 125
5.3.3 Rheology of agarose fluid gels 127
5.3.4 Particle size analysis 130
5.3.5 Tuning construct resolution 133
5.3.6 Formation of multi-layered structures 136
5.3.7 Fabrication of mineralised gellan helices 137
5.3.8 Cell culture proof-of-concept 138
5.4 Discussion 139
5.5 Conclusions 144
Chapter 6 – Fabrication of a Layered Tissue Culture Scaffold for Repair of Human Osteochondral Defects 145
6.1 Introduction 145
6.2 Materials and Methods 150
6.2.1 Materials 150
6.2.2 Extraction and culture of primary human cells 151
6.2.3 Defect creation and reconstruction 151
6.2.4 Stress sweeps of osteochondral implants 152
6.2.5 Culture of osteochondral implants 152

6.2.6 Reverse transcription PCR (RT-PCR) – RNA Isolation 152
6.2.7 RT-PCR 153
6.3 Results 153
6.3.1 Fabrication of cell-loaded osteochondral implant scaffolds 153
6.3.2 Stress sweeps of osteochondral scaffolds 154
6.3.3 RT-PCR 155
6.4 Discussion 158
6.5 Conclusions 160
Chapter 7 – Controlled Multi-Lineage Differentiation of Rat Bone Marrow Stromal Cells within a Single Hydrogel Structure 162
7.1 Introduction 162
7.2.1 Materials 166
7.2.2 Preparation of agarose hydrogels 166
7.2.3 Gelation properties 167
7.2.4 Diffusion studies 167
7.2.5 Channelled hydrogel cell culture proof of concept 167
7.2.6 Live/dead assay 168
7.2.7 Culture and encapsulation of rBMSC's 168
7.2.8 Histological Staining of encapsulated rBMSC's 169
7.2.9 Histology of stained cultures 170
7.2.10 Alkaline Phosphatase Assay 170
7.2.11 Reverse transcription PCR (RT-PCR) – RNA Isolation 171

7.2.12 Real-time quantitative PCR 171

7.3 Results 172

7.3.1 Rheology 172

7.3.2 Diffusion studies 173

7.3.3 Culture of 3t3 fibroblasts in a channelled structure 174

7.3.4 Live/dead assay of encapsulated rBMSC's 175

7.3.5 Histological analysis of encapsulated cultures 176

7.3.6 ALP Assay 177

7.3.7 RT-PCR 178

7.4. Discussion 181

7.5 Conclusions 185

Chapter 8 – Summary, Conclusions and Future Recommendations 186

8.1 Tuning the Rheology of Gellan Gum Hydrogels for Cell Culture Applications 186

8.2 Fluid Gel as a Supporting Media for ALM of Biological Structures 187

8.3 Controlled Multi-Lineage Differentiation of MSCs within a Single Hydrogel Structure 189

References 191

List of Figures

Figure 1.1- A cartoon representation showing the organisation of structural components in bone ECM (Gaharwar et al., 2016) 21

Figure 1.2 - A schematic demonstrating the organisation of chondrocytes and collagen in four layers of articular cartilage tissue 24

Figure 1.3 – Repair of bone defects in adult rats after 8 weeks treatment with acellular and MSC-loaded porous hydroxyapatite scaffolds (adapted from Yoshikawa and Myoui, 2005 with permissions from Springer) 29

Figure 1.4 – Tissue engineered 'ear-like' structures after 6 weeks subcutaneous incubation in mice (adapted from Xue et al., 2013 with permissions from Elsevier) 32

Figure 2.1– A freeze-dried, porous gellan gum hydrogel network observed with scanning electron microscopy/SEM 41

Figure 2.2 - The chemical structure of the tetrasaccharide repeat of low acyl and high acyl gellan (reproduced from Stevens et al. 2016 with permissions from Elsevier) 44

Figure 2.3 - A cartoon representation of phase transitions of gellan molecules from random coils to an ordered, cross-linked network during hydrogel formation 45

Figure 2.4 - Chemical structure of the repeat unit of agarose shows the 1,3 linked β-D-galactose residue and the 1,4 linked 3,6-anhydro-α-L-galactose residue (reproduced from Thermo Fisher Scientific) 46

Figure 2.5 - Chemical structures of G and M block confirmations in alginate (reproduced from Park et al., 2009 with permissions from Elsevier) 47

Figure 2.6 - A simplified representation of a left-handed collagen triple helix 49

Figure 2.7 - A simplified representation of conformational differences between collagen and gelatin helices 51

Figure 2.8 - CAD and subsequent manufacture of a cell-seeded collagen hydrogel supported by a porous PCL network and implantation into an *in vivo* culture model (reproduced from Zopf et al. 2015 with permissions from SAGE Publishing).....53
Figure 2.9 – High viability (indicated by green fluorescence) of human hepatocytes encapsulated in a 3D printed, porous gelatin scaffold. A) shows bright field microscopy images of the ordered 'waffle-like' scaffold architecture while B) shows live human hepatocytes attached to the scaffold network (reproduced from Billiet et al. with permissions from Elsevier – scale bar represents 500 µm).....54
Figure 2.10 – Repair of rabbit cartilage defects using cell-loaded gellan gum hydrogels (reproduced from Oliveira et al. 2012 with permissions from John Wiley & Sons) 55
Figure 2.11 – Induction of native phenotype expression in neuronal cells (A-C) and endothelial cells (D-F) when seeded on modified cell-adhesive agarose matrices of varying matrix stiffness (adapted from Yamada et al. 2012 with permissions from Elsevier – scale bar = 100 µm).....56
Figure 2.12 – Organisation of cardiomyocytes and myofibrils in A) RGD-alginate, B) native alginate and C) native tissue (reproduced from Shachar et al. 2011 with permissions from Elsevier – arrows in A and B represent non-myocytes (red), green represents cardiomyocytes in myofibril network.....57
Figure 2.13 – A layered gellan/gellan-hydroxyapatite scaffold for osteochondral tissue engineering (reproduced from Perreira et al. 2014 with permissions from Trans Tech Publications Ltd.) 58
Figure 3.1 – A schematic demonstrating differences between types of force applied in longitudinal, lateral and isotopic stress testing of solid materials (Mahdi, 2016).....62
Figure 3.2 – Flow curves outlining differences between flow behaviour of Newtonian and Non-Newtonian systems (Adapted from Miri 2011) 64
Figure 3.3 – Typical changes in dynamic viscosity of shear thinning and shear thickening materials in response to increasing shear rate.....66
Figure 3.4 – Cartoon representation of and Otswald Viscometer immersed in a water bath 67

Figure 3.5 - An example of a Huggins/Kraemer plot used for determination of intrinsic viscosity (Reproduced from Harding, 1997 with permissions from Elsevier).....69
Figure 3.6 – Differences in phase lag between stress and strain when transmitted in purely elastic, purely viscous and viscoelastic materials 71
Figure 3.7 – Differences in mechanical spectra exhibited by dilute polymer solutions, concentrated polymer solutions, ordered polymer solutions and true gels 74
Figure 3.8 – Commonly observed relationships between stress in strain both within and outside the linear viscoelastic region of viscoelastic materials.....75
Figure 3.9 – Trends in elastic and viscous moduli associated with a linear to non-linear transition in response to increasing shear stress.....76
Figure 3.10 – A diagrammatical representation of changes in elastic and viscous moduli during a characteristic, temperature-dependant biopolymer sol-gel transition.....77
Figure 4.1 – Schematic demonstrating cell attachment to ECM via integrin-fibronectin binding complexes and application of tension to the matrix by actin filaments.....80
Figure 4.2– Controlled ion delivery system mounted on a Bohlin Gemini rheometer used to study gelation time of gellan hydrogels (adapted from Mahdi et al. 2016 with permissions from Elsevier) 87
Figure 4.3 - Elastic and viscous modulus of un-sonicated (A) and 100% sonicated (B) 0.5% w/w gellan hydrogels in response to increasing shear stress 93
Figure 4.4 – Oscillatory cooling scans displaying both the elastic modulus (G′) and viscous modulus (G″) of 0.5% low acyl gellan hydrogels gelled using DMEM after no sonication (A), 30% amplitude sonication (B), 70% amplitude sonication (C) and 90% amplitude sonication (D).....95
Figure 4.5 – A comparison of the G′ of 0.5% low acyl gellan gum hydrogels at 10 °C and 37 °C with no sonication, sonication at 30% amplitude, sonication at 70% amplitude and sonication at 90% amplitude 96

Figure 4.6 – Frequency sweeps of 0.5% low acyl gellan gum mixed with DMEM at 60 °C and gelled at room temperature after no sonication, sonication at 50% amplitude and sonication at 100% amplitude.....97
Figure 4.7 – The effect of increasing amplitude (%) of sonication on viscosity of 0.5% low acyl gellan gum in response to increasing shear rate.....98
Figure 4.8 – The effect of increasing the amplitude (%) of sonication on the intrinsic viscosity of low acyl gellan gum (error bars represent +/- 1 standard deviation, n = 3).....99
Figure 4.9 – Elastic and viscous moduli (G′ and G″) vs. time for sonicated and un-sonicated gellan when gelation is triggered by ions present in DMEM 100
Figure 4.10 – Effect of sonication at (A) 0% amplitude, (B) 50% amplitude and (C) 100% amplitude on G′ and G″ of 0.5% gellan gum cell culture scaffolds in response to increasing oscillatory frequency.....101
Figure 4.11 – Cell-loaded hydrogels created with A) un-sonicated gellan, B) gellan sonicated at 50% amplitude and C) gellan sonicated at 100% amplitude 102
Figure 4.12 – Live/dead staining results for MC3T3's encapsulated in A) un-sonicated gellan, B) gellan sonicated at 50% amplitude and C) gellan sonicated at 100% amplitude – (colour corrected using Microsoft PowerPoint - green spots indicate presence of a live cell) 103
Figure 4.13 – Number of viable cells 7 days post encapsulation determined via MTT assay in un-sonicated gellan, gellan sonicated at 50% amplitude and gellan sonicated at 100% amplitude (error bars represent +/- 1 standard deviation, n = 12).....104
Figure 4.14 – The effect of increasing the amplitude (%) of sonication on the concentration of p-nitrophenol produced per 1000 encapsulated cells provided with p-nitrophenyl phosphate (error bars represent +/- 1 standard deviation, n = 12) 105
Figure 5.1 - Transition of a fluid gel from a self-supporting paste-like material to a pourable viscoelastic liquid after application of a small shear force 114

Figure 5.2 – Schematic diagram showing differences between polymer gels subjected to quiescent and sheared gelation (Mahdi, 2016).....115
Figure 5.3 - Schematic showing a proposed fluid gel ALM technique. A) Cell loaded biopolymer injected into fluid gel. The polymer remains in liquid form but does not flow due to support from self -healing fluid gel. B) Multiple layers added containing different cell types or molecules such as growth factors (all biopolymers still in liquid form). C) Cross-linker added to completed structure to trigger gelation and immobilise the cells. D) Solidified gel structure/implant can be recovered from the fluid gel when required 116
Figure 5.4 - Suspended deposition, gelation and recovery of 1% gellan in fluid gels with a varying gellan concentration and a constant NaCl concentration of 100 mM.....125
Figure 5.5 - Elastic modulus (G') in response to an increasing frequency of fluid gels made with 1% gellan (clear squares), 0.75% gellan (black circles), 0.5% gellan (black triangles), 0.25% gellan (black squares) and 0.1% gellan (black diamonds and a constant concentration of NaCl of 100 mM 126
Figure 5.6 - Dynamic viscosity in response to an increasing shear rate of fluid gels made with 1% gellan (clear squares), 0.75% gellan (black circles), 0.5% gellan (black triangles), 0.25% gellan (black squares) and 0.1% gellan (black diamonds and a constant concentration of NaCl of 100 mM 127
Figure 5.7 - Elastic modulus (G') in response to an increasing frequency of fluid gels made with 1% agarose (black squares), 0.75% agarose (black diamonds), 0.5% agarose (black triangles) and 0.25% agarose (black circles) 128
Figure 5.8 - Elastic modulus (G') in response to an increasing frequency of fluid gels made with 1% agarose (black squares), 0.75% agarose (black diamonds), 0.5% agarose (black triangles) and 0.25% agarose (black circles) 129
Figure 5.9 – Microscope images of 0.1% gellan, 1% gellan and 0.5% agarose fluid gel particles .130

Figure 5.10 – Particle size distribution of 0.1% gellan fluid gels represented by average number of particles in a specific size range and % of particles under a specific size (error bars represent +/- 1 standard deviation, n = 8).....131
Figure 5.11 – Particle size distribution of 1% gellan fluid gels represented by average number of particles in a specific size range and % of particles under a specific size (error bars represent +/- 1 standard deviation, n = 8).....132
Figure 5.12 – Particle size distribution of 0.5% agarose fluid gels represented by average number of particles in a specific size range and % of particles under a specific size (error bars represent +/- 1 standard deviation, n = 8).....133
Figure 5.13 – The effect of solution viscosity at 1 s^{-1} on width and height of resulting extruded constructs deposited at a rate of 125 µl/s (error bars represent +/- 1 standard deviation, n = 6).....134
Figure 5.14 – The effect needle inner diameter on width and height of resulting extruded constructs deposited at a rate of 125 µl/s (error bars represent +/- 1 standard deviation, n = 6).....135
Figure 5.15 – The effect of lateral deposition speed on width and height of resulting extruded constructs deposited at a rate of 125 µl/s (error bars represent +/- 1 standard deviation, n = 6).....136
Figure 5.16 – Fabrication and extraction of structures containing a layer of 1.5% gellan and a second layer of A) 0.5% type I collagen, (construct appears pink due to being dyed with culture media for easier deposition) B) 3% alginate with 5% nano HA, C) 30% gelatin with 5% nano HA and D) 1.5% gellan with nano HA (scale bars represent 5 mm).....137
Figure 5.17 – Fabrication of a mineralised gellan helix (A), micro CT image demonstrating complexity of suspended helical structure (B) and extraction of mineralised gellan helix (C) (scale bars represent 5 mm).....138
Figure 5.18 - Recovery and live/dead staining of 3T3 fibroblast-loaded gellan hydrogels suspended in A) linear 3D structures B) the shape of the Greek symbol ‘Sigma’/Σ and C) the shape of a spiral 139

Figure 6.1 – A schematic demonstrating transition from a superficial layer of articular cartilage through an osteochondral interface and into porous, cancellous bone (Adapted from Li et al. 2015 with permissions from Oxford University Press) 147
Figure 6.2 – Simulation of a human osteochondral defect and subsequent reconstruction and fabrication of a cell-loaded scaffold for osteochondral repair 150
Figure 6.3 – Layered, multicellular scaffolds comprised of chondrocyte-loaded gellan and osteoblast-loaded gellan/HA (scale bar represents 5 mm) 154
Figure 6.4 – A comparison of storage moduli in 4 regions of osteochondral scaffolds with nanoindentation moduli osteochondral tissue (Nanoindentation moduli extrapolated from Campbell et al. 2012 where Region A represents hyaline cartilage, Region B represents calcified cartilage and regions C and D represent subchondral bone (error bars represent +/- 1 standard deviation, n = 3) 155
Figure 6.5 – Expression of COL1A1 and COL2A1 30 days post implantation in three regions of a fabricated osteochondral scaffold seeded with human primary osteoblasts and chondrocytes (error bars represent +/- 1 standard deviation, n = 3, PCR data annotated to show ratios of COL1A1 to COL2A1 gene expression) 157
Figure 7.1 – Concept image of how channels could be used to deliver different media types to regions of a cell-loaded hydrogel 164
Figure 7.2 – A schematic demonstrating how cell-loaded gels were sliced and arranged. Gel A was stained with alizarin red and gel B was stained with alcian blue 169
Figure 7.3 – Elastic modulus (G′) and viscous modulus (G″) of 0.5% agarose (w/w) during cooling 173
Figure 7.4 – Diffusion of methylene blue through a 0.5% agarose hydrogel over 48 hours after injection into channels 174
Figure 7.5 – Calcein AM/propidium iodide staining from various regions of a 0.5% agarose hydrogel containing 3t3 fibroblasts cultured for 7 days using a single media channel 175

Figure 7.6 – Calcein AM/propidium iodide staining results from osteogenic (A) and chondrogenic (B) regions of a 0.5% agarose hydrogel containing rBMSC's after 7 days of culture 176
Figure 7.7 – Histology of osteogenic and chondrogenic regions of rBMSC-loaded gel when stained with alizarin red and alcian blue after 6 weeks culture.....177
Figure 7.8 – A photographic image demonstrating (A) how cell-loaded gels were sliced for bioassays and PCR combined with (B) results indicating alkaline phosphatase activity as a function of [p-nitrophenol] produced by hydrolysis of p-nitrophenyl phosphate (error bars represent +/- 1 standard deviation, n = 8).....178
Figure 7.9 – RT-PCR results showing Col1 and Col2 expression relative to GAPDH in three regions of a cell loaded hydrogel (error bars represent +/- 1 standard deviation, n = 6).....180

List of Tables

Table 4.1 – Ionic composition of Dulbecco's Modified Eagle's Medium.....84

Table 4.2 - The effect of sonication amplitude on the modulus of 0.5% gellan gels in response to increasing stress 94

Table 4.3 – The effect of sonication amplitude on the modulus and gelation temperatures of 0.5% gellan gum gels 95

Table 4.4 - Intrinsic viscosity and resulting calculated molecular weights of gellan subjected to varying amplitudes of sonication 99

Table 4.5 – A summary of results obtained from statistical analysis of ALP assay data 105

Table 5.1 – Fluid gel samples prepared for rheological analysis.....119

Table 5.2 – Materials used for creation of osteochondral mimetic constructs 122

Table 6.1 - Primers used for real-time PCR.....153

Table 7.1 - Primers used for real-time PCR.....171

List of Abbreviations

ALM – Additive Layer Manufacturing
ALP – Alkaline Phosphatase
$CaCl_2$ – Calcium Chloride
CAD – Computer Aided Design
Col1 – Type I Collagen
Col2 – Type II Collagen
COL1A1 – Type I Collagen Gene
COL2A1 – Type II Collagen Gene
DMEM – Dulbecco's Modified Eagle's Medium
ECM – Extracellular Matrix
GAG - Glycosaminoglycan
G′ - Elastic Modulus
G″ - Viscous Modulus
HA – Hydroxyapatite
LVR – Linear Viscoelastic Region
MSC – Mesenchymal Stem Cell
NaCl – Sodium Chloride
nano-HA – Nanocrystalline Hydroxyapatite
PCL - Polycaprolactone
RGD – Lysine, Arginine, Aspartic Acid
RNA – Ribonucleic Acid
RT PCR – Reverse Transcription Polymerase Chain Reaction
TGF-β – Transforming Growth Factor Beta

Chapter 1 – General Introduction

1.1 Introduction to Tissue Engineering

The average life span of the global population has increased in recent years as a result of medical advancements and improvements in technologies to prolong life (Wang et al., 2012). While this has resulted in an overall increase in quality of life, particularly in the developed world, there has also been a rise in occurrence of tissue disease and degradation (often associated with aging). Tissue/organ donation and transplantation is a method that is heavily relied upon to address such issues, but therapy is often hindered by issues such as donor availability, immune rejection or morbidity at the donor site (Vats et al., 2003).

Tissue engineering has emerged as a promising field for addressing issues with transplantation. The main focus is on regeneration rather than replacement with an aim to restore and, in some cases, improve tissue function (Ma, 2008). Research within the field has grown rapidly over recent years with a wide variety of techniques explored but the underlying theory is often the same and involves attempting to replicate *in vivo* tissue development environments *in vitro*. An ideal therapeutic model for tissue engineering would involve isolation, extraction and expansion of cells from the patient requiring treatment, subsequent culture in fabricated structures and re-introduction to the target site leading to tissue repair.

Due to their multipotency, mesenchymal stem cells (MSC's) are often utilised in tissue engineering applications. MSC's can be isolated from the bone marrow of patients and expanded *in vitro* while retaining multipotency. A population of MSC's can then be manipulated by mechanical or biochemical cues to trigger differentiation into specific cell types (osteoblasts, chondrocytes, myoblasts and adipocytes), providing a platform for repair of a wide variety of tissues (Eberli and Atala, 2006). Cell numbers rapidly decline with age however, and extraction from bone marrow causes a great deal of patient discomfort (Caplan, 2007). As a result, there is also a large amount of

research in the regeneration of tissue from native cell types which can be more easily isolated and cultured e.g. chondrocytes for cartilage tissue engineering or myoblasts for muscle (Wang et al., 2006, Conconi et al., 2005). While a range of cell types have been explored, the common aim is to design a cell culture environment that mimics extracellular matrix (ECM) properties so that tissue can be cultured using *in vivo* conditions *in vitro*. This work focuses on development of new approaches to regeneration of bone and articular cartilage tissue, two structurally different connective tissues. Therefore, composition and structure of both tissue types should be considered when designing potential new mechanisms for regeneration.

1.2 Native Tissue

Human tissue can be categorised as either connective, muscle, epithelial or nervous tissue. Each tissue type has a specific function and thus structural and mechanical properties vary amongst and within tissue categories (Voskerician, 2012). Bone and cartilage are connective tissues with specific cellular and material compositions. They often function in synergy with bone providing primary structural support and cartilage providing a gliding surface in joints and preventing damage to subchondral bone by acting as a shock absorber. However, both the cellular and ECM composition of bone and cartilage vary greatly in order to facilitate their differences in function.

1.3 Bone Tissue

A primary component of bone tissue is the extracellular matrix. Bone ECM is comprised of two main components, namely the inorganic and organic. The organic component of bone ECM is primarily formed by collagenous proteins, most of which is type I collagen. However, non-collagenous proteins (e.g. osteocalcin, osteonectin and osteopontin), growth factors, bone morphogenic proteins and proteoglycans such as decorin and biglycan are also present (Florencio-Silva et al., 2015). The resulting scaffold is mineralised by an inorganic component with a calcium based compound called hydroxyapatite (HA) deposited on the collagenous network (Fig. 1.1).

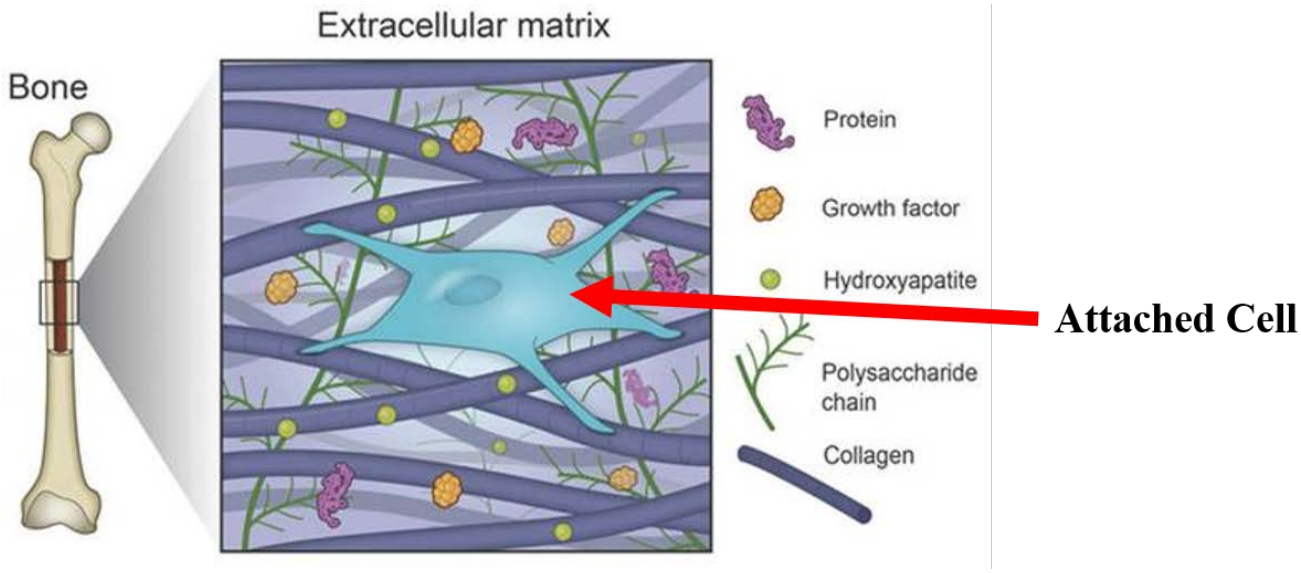

Figure 1.1- A cartoon representation showing the organisation of structural components in bone ECM (Gaharwar et al., 2016)

Both components combine to create a matrix that is stiff, tough and has a high tensile strength. Deposited throughout bone ECM are four different cell types that interact with the matrix and play their own role in formation, maintenance and repair of bone tissue.

1.3.1 Osteoblasts

Osteoblasts account for approximately 4-6% of cells present in bone tissue and are heavily associated with early bone formation. The main role of an osteoblast is the synthesis and subsequent mineralisation of collagenous bone ECM (Capulli et al., 2014). In the early stages of bone formation osteoblasts synthesise and deposit collagenous proteins, primarily type I collagen, non-collagenous proteins such as osteopontin and osteonectin and proteoglycans including decorin and biglycan. An increase in activity of alkaline phosphatase (ALP), an extracellular enzyme, by osteoblasts promotes mineralization of the collagenous matrix. ALP both hydrolyses extracellular pyrophosphate and increases concentrations of intracellular phosphate (Bellows et al., 1991b). At this stage, osteoblasts are classified as being primary osteoblasts and are differentiated from mesenchymal stem cells located in bone marrow. Primary osteoblasts undergo maturation during osteogenesis which can be

characterised by changes in activity of multiple key markers for bone repair. Transition into mature osteoblasts is marked by a change in morphology and an increase in expression of other matrix proteins such as osteocalcin and osteopontin at the expense of ALP expression (Weinreb et al., 1990a). Mature osteoblasts continue to deposit bone matrix components until they are fully encased in ECM. At this point, mature osteoblasts halt proliferation and become osteocytes.

1.3.2 Osteocytes

Osteocytes are the most abundant cells in bone tissue accounting for 90-95% of all cells. They are embedded within bone ECM and can have a lifespan of up to 25 years. For many years osteocytes had been incorrectly assumed to have a passive role in regulation of bone tissue but more recent discoveries have highlighted osteocytes as regulators of bone formation and resorption. Osteocytes function as dendrites in bone tissue and can respond to mechanical strain and bone deformation by sending signals to trigger bone resorption and repair by osteoclasts and osteoblasts (Bonewald and Johnson, 2008). It is also thought that osteocytes can deliver signals to cells in bone marrow resulting in both the recruitment of osteoclast precursors and the differentiation of MSC's (Heino et al., 2004).

1.3.3 Osteoclasts

Osteoclasts play a key role in resorption and remodelling in bone repair and are thought to function in synergy with osteoblasts. In the early stages of bone repair osteoclasts polarise along bone ECM to create a border known as a resorption domain. Proteinases are secreted into the domain by osteoclasts resulting in breakdown of proteins in the organic matrix. Acidification inside the domain also leads to demineralisation of the matrix and components are subsequently removed in vesicles and absorbed by osteoclasts which either undergo apoptosis or revert to a non-resorbant phenotype (Schindeler et al., 2008). Osteoclasts then secrete mediators which promote migration of MSC's to the site and differentiation into osteoblasts. Cytokines are also secreted by osteoclasts which trigger recruitment of primary osteoblasts to the healing site (Gamblin et al., 2014).

1.3.4 Bone lining cells

Bone lining cells are relatively inactive osteoblasts with a flattened phenotype present at the bone surface. They are not directly involved in bone repair or resorption and are thought to play a more protective role in maintenance of bone tissue. They prevent interaction between osteoclasts and ECM when healing is not required to ensure healthy bone is not resorbed and release calcium into bone tissue when supply from the blood is insufficient (Florencio-Silva et al., 2015).

1.4 Articular cartilage tissue

Articular cartilage serves as a shock absorbing tissue to prevent stress and damage in subchondral bone. Its primary components are water (up to 80% of weight), collagen (mostly type II with some type X – up to 20% of wet weight) and proteoglycans (up to 20% of wet weight). Water facilitates deformation of cartilage in a load-bearing manner and the amount present is critical. When cartilage contains too much water load-bearing capabilities are impaired leading to osteoarthritis (Liess et al., 2002). Tensile strength of cartilage tissue is provided by collagenous proteins as in bone, while proteoglycans provide strength under compression. Matrix components are synthesised, deposited and maintained by chondrocytes creating a matrix that is comprised of 4 layers (Fig. 1.2).

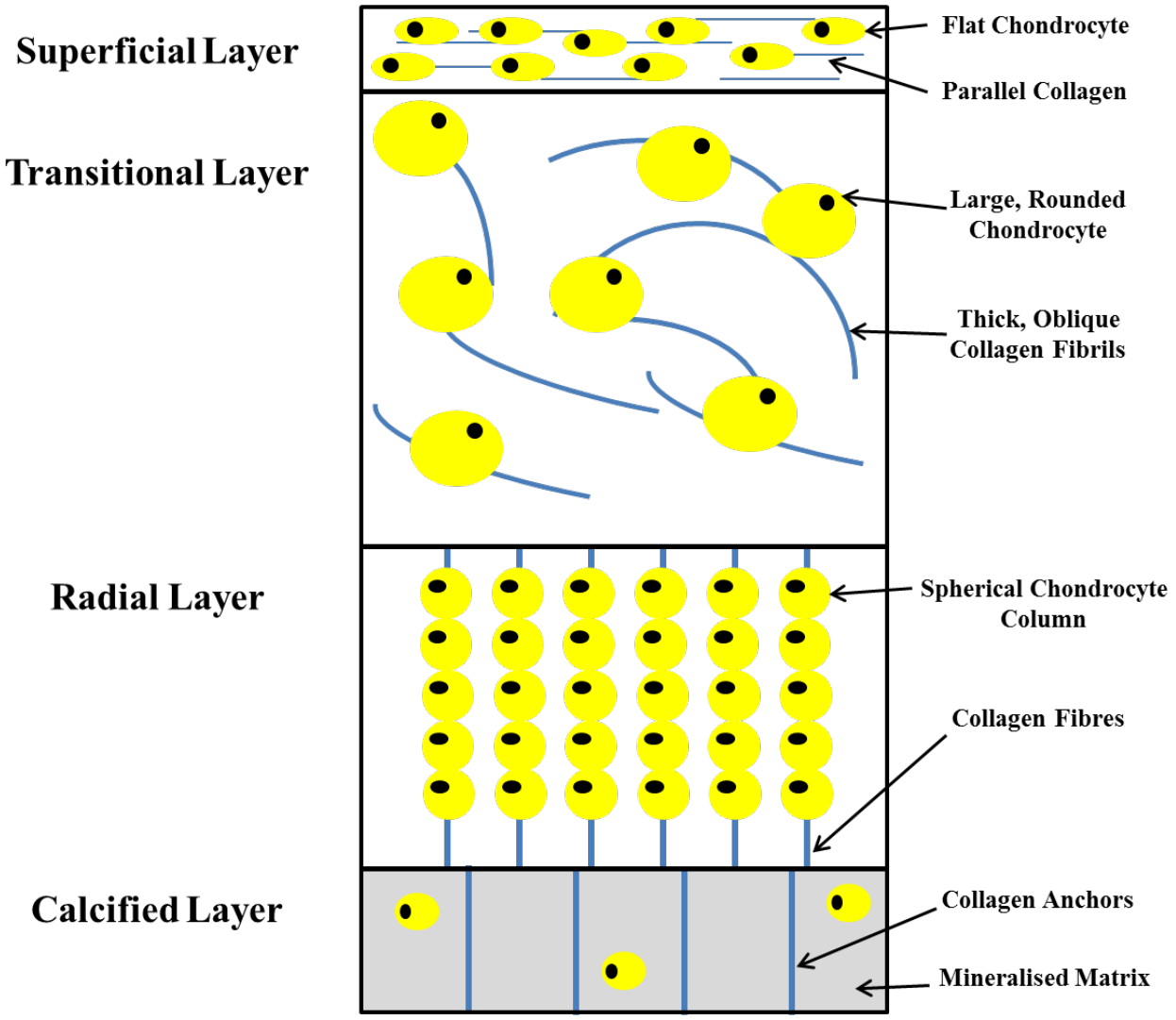

Figure 1.2 - A schematic demonstrating the organisation of chondrocytes and collagen in four layers of articular cartilage tissue

1.4.1 Superficial layer

The superficial layer is the thinnest layer of articular cartilage and has the highest water content. It is covered by synovial fluid which acts as a lubricant providing a gliding surface (Buckwalter and Mankin, 1998). Additionally, surface topography of the superficial layer further facilitates lubrication. On a micro scale, the surface of superficial cartilage contains grooves that trap and maximise the volume of synovial fluid at a joint, thus increasing lubrication (Shekhawat et al., 2009).

Damage to the superficial zone leads to a change in mechanical properties and ultimately results in osteoarthritis. Chondrocytes in the superficial zone are flat and synthesise a much greater amount of collagen than proteoglycans. Collagen fibres are ordered and arranged in parallel to superficial

chondrocytes giving the matrix a high tensile strength. The layer also provides a barrier protecting articular cartilage from the immune system (Bhosale and Richardson, 2008b).

1.4.2 Transitional zone

This zone acts as a functional connection between the superficial and radial zones and accounts for 40-60% of the cartilage volume. Transitional chondrocytes display a large, rounded appearance and are present at a low density. They synthesise and organise collagen into thick fibrils arranged in random, oblique structures and deposit proteoglycans to form the ECM. The transitional zone's main function is to protect cartilage tissue against compressive forces (Fox et al., 2009).

1.4.3 Radial zone

The radial zone is approximately 30% of cartilage volume and provides the greatest resistance against any compressive force placed on the tissue. Chondrocytes in this zone are spherical and arranged in columns parallel to thick collagen fibres. The radial zone contains both the highest concentration of proteoglycans and the lowest water content, thus giving it high tensile strength (Fox et al., 2009).

1.4.4 Calcified cartilage

Calcified cartilage acts as a bridge between articular cartilage and bone. Within this region, collagen fibres present in the radial zone are anchored into subchondral bone (Bhosale and Richardson, 2008a). As such, the calcified layer contains an overlap between hyaline cartilage and subchondral bone and is often considered to be the focal point of an osteochondral interface. The osteochondral interface is key to the function of joints and serves to transfer forces into subchondral bone. It contains both bone and cartilage ECM components with sufficient interplay to prevent separation of the two tissue types in the presence of high shear stresses. Chondrocytes synthesise type X collagen providing subchondral bone with a capacity to absorb shock while subchondral osteoblasts calcify the matrix via increased ALP activity. Degeneration of osteochondral tissue often leads to osteoarthritis and, thus, research into osteochondral tissue engineering therapies is as widespread as individual bone and cartilage studies. Engineering of such tissues is complex and involves design of specific materials to

facilitate native cellular function. A tissue is a three dimensional structure because it develops in a 3D environment *in vivo*. In order to engineer more native tissues *in vitro* it is therefore, necessary to replicate this using a 3D cell culture platform as opposed to conventional 2D flask culture. Intelligently designed tissue engineering scaffolds have therefore emerged as promising tools for replicating *in vivo* tissue culture environments *in vitro* (Carletti et al., 2011).

1.5 Tissue Engineering Scaffolds

Any scaffold for tissue engineering applications must exhibit a number of key properties in order to facilitate engineering of tissues with a native architecture. Generally, scaffolds must not inhibit normal cell behaviour such as, proliferation, differentiation, ECM production and they should act as a substitute for missing ECM by providing structural support to developing tissues. Requirements for a tissue engineering scaffold can, therefore, be divided into two categories, namely mechanical properties and microarchitecture.

1.5.1 Mechanical properties

Mechanical properties of a scaffold are key to success of tissue culture. Orientations of cells in a tissue and interactions with the surrounding matrix, both have an integral effect on their phenotype/behaviour. As a result it is desirable for cell culture scaffolds to exhibit mechanical properties similar to that in native tissue development environments. For example, a scaffold for bone regeneration should present a strong, stiff matrix with a high tensile strength. The influence of the mechanical properties of scaffolds have even been shown to directly influence stem cell lineage specification (Engler et al., 2006).

Tissue culture scaffolds also need to have sufficient strength to withstand stresses placed by cells without undergoing significant deformation and maintaining shape during tissue development. Ideally, they should also have sufficient degradation properties to facilitate replacement by newly synthesised tissue or ECM (Hutmacher, 2000).

1.5.2 Scaffold architecture

Equally key to the success of tissue culture is scaffold architecture. Tissue culture substrates should display a microarchitecture that is reflective of native ECM. Porosity is integral to scaffold design with a necessity to facilitate introduction of nutrients, growth factors and other chemical cues and the removal of waste products. In some cases scaffolds also require sufficient porosity to allow cell migration through the network and vascularisation of developing tissues. Additionally, it may be necessary to consider the nanoarchitecture of a scaffold in the context of surface topography and chemistry as this can also have a profound impact on cell behaviour (Roach et al., 2007).

Specific requirements vary depending upon the target tissue and scaffolds should be designed with native tissue architecture in mind. For example, it has been shown that a scaffold for bone engineering requires larger pores than that for endothelial cell culture (Karageorgiou and Kaplan, 2005, Salem et al., 2002). Such diversity in required properties has led to a wide variety of materials being researched for use as tissue engineering scaffolds. One such class of materials are biopolymer hydrogels, which have shown great promise as tissue engineering scaffolds and are the primary focus of this thesis.

1.6 Current Developments in Bone and Cartilage Tissue Engineering

The concept of using scaffold structures for repairing bone tissue has been recognised for over 40 years with a wide variety of materials investigated. One of the most notable materials for bone tissue engineering is bioactive glass/bioglass first proposed by the late Prof. Larry Hench in 1971 (Hench et al., 1971). Since its inception, bioglass has been extensively researched and utilised as a material for implantation into the human body for bone repair. Bioglass is a non-crystalline ceramic comprised of a primary layer rich in silicon covered by a second layer that is rich in calcium phosphate (Schepers et al., 1991). Bioactive glass is described as being osteoconductive meaning it can serve as a scaffold around which new bone tissue can develop from existing bone. Bioglass can be seeded with multiple cell types and has been reported to degrade into products that show anti-bacterial and angiogenic activity (Baino et al., 2016). It is FDA approved and is used routinely to treat critical sized bone

defects. However, limitations have been observed due to mechanical weakness and insufficient load-bearing strength. This has led to investigation into using materials more analogous of native bone tissue and ECM for induction of bone repair.

1.6.1 Bone ECM-mimetic scaffolds

While bioglass has shown a great deal of promise for bone regeneration, there is no single solution for the treatment of critical sized bone defects. As a result other materials have also been explored with a lot of focus on using materials present in bone ECM to design osteoconductive culture scaffolds with varying levels of complexity.

On a simpler scale, research groups have designed osteogenic scaffolds formulated from one of the two principal components of bone ECM, namely type I collagen and hydroxyapatite. Seeding of stem cells into porous collagen scaffolds has been shown to induce osteogenesis. For example, Kakudo et al., (2008) demonstrated seeding 'honeycomb' collagen scaffolds with adult stem cells resulted in a mineralised collagen network *in vitro*. When stem cell-laden collagen scaffolds were implanted into mice, evidence of osteocalcin expression and activity was observed after 8 weeks (Kakudo et al., 2008). This alludes to a presence of mature osteoblasts and relates to latter stages of bone formation. A second study revealed applying a mechanical load to pre-osteoblasts seeded on a collagen scaffold enhanced osteogenesis with an up regulation in several osteogenic markers such as osteocalcin, alkaline phosphatase and type I collagen (Ignatius et al., 2005).

More recent studies have built on such results by designing substrates that further mimic the organic component of bone ECM. Non-collagenous bone ECM proteins such as fibronectin, osteocalcin and proteoglycans have been incorporated into collagen scaffolds with encapsulated cells showing even greater enhanced osteogenic activity (Kim et al., 2015, Murphy et al., 2010).

A lot of research has also been conducted investigating the potential of designing osteogenic scaffolds comprised of inorganic bone ECM. Scaffolds of hydroxyapatite have been widely investigated both

with and without the incorporation cells. One notable study by Nishikawa et al., (2005) compared bone healing properties of porous hydroxyapatite scaffolds seeded with mesenchymal stem cells against acellular scaffolds (Yoshikawa and Myoui, 2005). At a time point of 8-weeks post implantation, rats treated with cell-laden HA showed a much greater degree of regeneration than those treated with HA alone. Bone unions were observed at the defect site paired with an increase in mineral density (Fig. 1.3). This was attributed to MSC's in the cell-laden scaffolds undergoing differentiation into osteoblasts and subsequent synthesis of new bone ECM; something not possible in the absence of stem cells with the acellular scaffold.

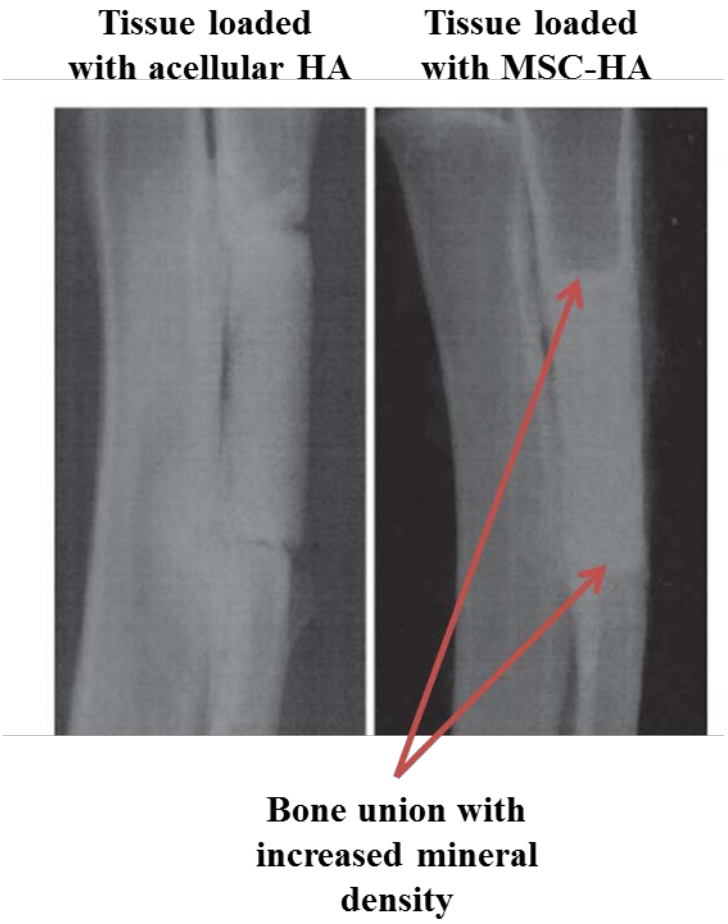

Figure 1.3 – Repair of bone defects in adult rats after 8 weeks treatment with acellular and MSC-loaded porous hydroxyapatite scaffolds (adapted from Yoshikawa and Myoui, 2005 with permissions from Springer)

Combination of both major bone ECM components is perhaps the most successful method for replicating *in vivo* regeneration environments *in vitro*. Recent studies have demonstrated the potential

of combining both type I collagen and hydroxyapatite for greatly enhanced osteogenesis. Many groups have presented research demonstrating the native mechanical and biochemical properties of collagen/HA scaffolds and subsequent effects on promoting bone formation and maintenance. A notable example is successful regeneration of new, healthy periodontal bone with periodontal fibres and cementum, a highly complex structure (Liu et al., 2016). This was achieved via incorporation of MSC's into collagen/HA scaffolds and implantation into beagle dogs. After 3 months, a 70% increase in periodontal bone regeneration was observed when compared with control samples of un-treated dogs.

1.6.2 Progress in cartilage tissue engineering

One notable example of progress in cartilage tissue engineering is the development of a clinically approved product named ChondroCelect®. ChondroCelect® has been used since 2011 in the treatment of adult knee defects. The treatment involves removal of chondrocytes from the patient via biopsy. The cells are then expanded *in vitro* and placed back into the patient defect which is sealed with a membrane, comprised of collagen. Despite successful clinical implementation, however, ChondroCelect® has been recently scheduled for removal from the market due to poor sales. This places further emphasis on the requirement of novel tissue engineering techniques for cartilage regeneration.

While progress with both soft materials and hard ceramics has been made in the field of bone tissue engineering, a majority of research in cartilage regeneration involves the use of soft biopolymer hydrogel scaffolds (see Chapter 2 for further details). Focus tends to be on fabricating scaffolds that are reflective of the high glycosaminoglycan/GAG content of cartilage ECM, although some research has also been conducted on collagen scaffolds for cartilage regeneration.

An example of research into collagen for cartilage tissue engineering involved the use of collagen scaffolds derived from jellyfish (Hoyer et al., 2014). Scaffolds were seeded with MSC's and chondrogenic responses were analysed. Encapsulated cells deposited matrix components associated

with early chondrogenesis such as type II collagen and hyaluronic acid. Paired with an up regulation of genes coding for synthesis of mRNA for aggrecan and type II collagen, it was concluded that MSC-laden collagen scaffolds could enhance chondrogenesis via chondrogenic differentiation and deposition of new cartilage ECM. However, the release kinetics of important growth factors for chondrogenesis in collagen have been shown inferior to those seen in other cartilage ECM materials (Haleem and Chu, 2010).

One such material is hyaluronic acid and a number of research groups have investigated its potential for chondrogenesis. A study published by Jin et al., (2010) demonstrated the potential of using hyaluronic acid based substrates to enhance chondrogenesis (Jin et al., 2010). Bovine chondrocytes were encapsulated in hydrogels based on hyaluronic acid and polyethylene glycol and cultured for 21 days. When compared with control samples, chondrocytes encapsulated in scaffolds showed enhanced levels of type II collagen and GAG expression with evidence of deposition throughout the matrix. While this shows promise, however, hyaluronic acid scaffolds implanted for *in vivo* chondrogenesis have been shown to degrade into by-products that can induce lysis and subsequent necrosis of chondrocytes (Haleem and Chu, 2010).

Another class of materials explored for chondrogenesis is biopolymers as they are often chemically similar to GAG's. GAG's are polysaccharides formed of long, un-branched repeating chains often containing carboxylated and sulphated functional groups. Two such examples of chemically similar tissue engineering biopolymers are gellan gum and alginate, both of which contain carboxylate groups.

Arguably one of the most notable applications of biopolymers in cartilage tissue engineering was a study published by Xue et al., (2013). Electrospun membranes were fabricated with gelatin and polycaprolactone (PCL) into the shape of a human ear and seeded with chondrocytes. Structures were then cultured *in vivo* using a mouse model before removal after 6-weeks cultivation. Removed tissue

retained an ear-like morphology (Fig. 1.4) with a similarity of over 91% to a titanium mould (Xue et al., 2013).

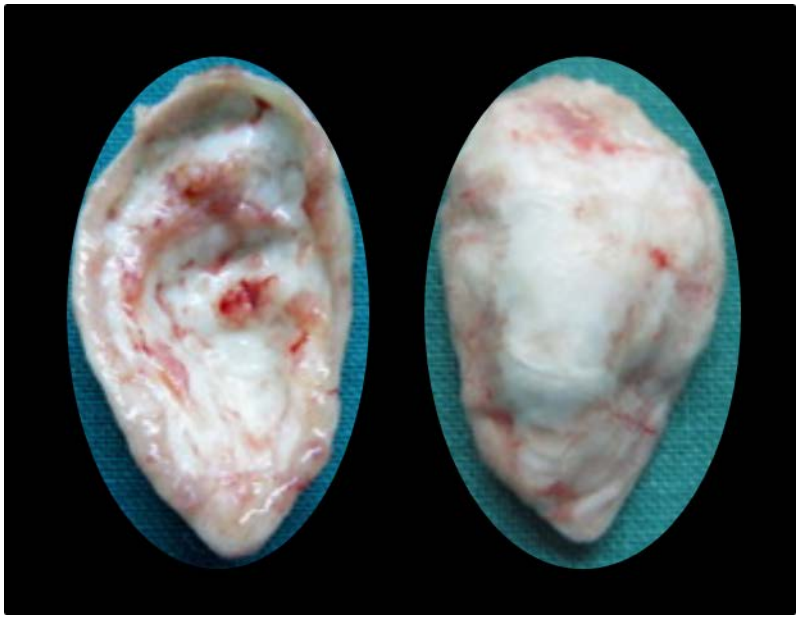

Figure 1.4 – Tissue engineered 'ear-like' structures after 6 weeks subcutaneous incubation in mice (adapted from Xue et al., 2013 with permissions from Elsevier)

1.7 Current Limitations in Engineering of Complex Tissues

While such studies represent a great deal of progress in the field of tissue engineering, research tends to focus on regeneration of a single tissue. While this has led to advancements in areas such as repair of simple bone and cartilage defects, applications in regeneration of more complex structures are limited. A perfect example is the 4-tier structure of cartilage outlined in Fig. 1.2 where each layer contains a different cellular and structural composition. While regeneration of cartilage with single, homogenous scaffolds has shown promise, newly formed tissue often does not reflect native cartilage both structurally and mechanically (Moutos and Guilak, 2008). A similar issue falls in replication of the osteochondral interface (the critical interface between cartilage and bone) outlined in 1.4.4. A scaffold for osteochondral engineering would require multiple properties to facilitate simultaneous bone and cartilage ECM synthesis, with most current techniques falling short of such requirements. The work presented in this thesis has focused on the development of biopolymer hydrogel scaffolds

for regeneration of complex tissues with an aim to address current issues in *in vitro* replication of the heterogeneous *in vivo* environment for tissue development.

1.8 Hypothesis, Aims and Objectives

The overall aim of this work was to develop novel tissue culture methods using natural biopolymers to address current issues with regeneration of complex tissues. Consequently, this tested the hypothesis that naturally sourced biopolymers can be used to replicate complex *in vivo* environments thus facilitating fabrication of scaffolds that stimulate expression of native, tissue-specific cellular phenotypes. The main objective in testing this hypothesis was to study the effect of manipulating multiple scaffold properties in order to fabricate structures that further mimic *in vivo* environments in terms of material, cellular and chemical content. This was explored in the context of tissues such as bone, cartilage and the osteochondral interface.

Initially, sonication was investigated as a method for tuning mechanical properties of gellan gum scaffolds. The effect of modifying matrix stiffness on cell behaviour in an osteogenic culture model was evaluated. Consequently, a model for modification of mechanical properties for specific tissue culture applications was outlined.

Building on this, scaffolds composed of multiple materials and containing multiple cell types were fabricated using a novel rapid prototyping method. A system was developed using fluid gels as supporting media for ALM of biopolymer materials, with a study conducted on applications in human osteochondral tissue repair.

Finally, an alternative approach to modelling the osteochondral environment was evaluated. Instead of fabricating scaffolds of multiple materials and cell types, a single, channelled scaffold containing a population of MSC's was developed. Osteogenic and chondrogenic differentiation media were injected into separate channels with a view to trigger controlled simultaneous differentiation of osteoblasts and chondrocytes from a single MSC population within a single structure.

1.9 Thesis Outline

This thesis consists of 2 further introductory chapters followed by 4 results chapters and a final, concluding chapter.

Chapter 2 introduces biopolymer hydrogel scaffolds and their significance to the field of tissue engineering. Advantages of using hydrogels as tissue engineering substrates are outlined with a focus on a capacity to encapsulate cells in a micro-porous network that mimics ECM properties. Five separate biopolymers are discussed, namely gellan gum, agarose, alginate, collagen and gelatin, all of which are explored in later chapters. Chemical structures, physical properties and current biomedical applications of each biopolymer are detailed.

Each results chapter contains data showing multiple rheological properties of biopolymer solutions and hydrogels. In Chapter 3, fundamental principles behind methods for the rheological characterisation of biomedical biopolymers are outlined. Details of the relationship between stress and strain in determining moduli in soft solid materials are presented along with flow models for pourable fluids. The principle of viscoelasticity and its relevance to hydrogel properties is described with a final section detailing intrinsic viscosity and how it can be determined and used to inform about molecular weight and rheological behaviour of biopolymers.

The first results chapter is comprised of a study that is published in the International Journal of Biological Macromolecules (Moxon and Smith, 2016). Sonication was used to tune rheological properties of gellan gum hydrogels with a focus on the effects on tissue culture applications. Data are presented outlining changes in intrinsic viscosity, fundamental rheology and mechanical properties in a cell culture environment. Results conclude with a final study showing the effect of tuning gellan hydrogel properties on behaviour of encapsulated MC3T3 pre-osteoblasts.

Chapters 5 and 6 builds on the principle of tuning mechanical properties to influence behaviour of encapsulated cells. An innovative ALM method for fabricating a single hydrogel structure containing

multiple materials and, thus, exhibiting varied mechanical properties is proposed. Chapter 5 focuses on method development and determination of mechanical boundaries for the system with Chapter 6 presenting results from a study implementing this technique into an osteochondral tissue engineering model. Results highlight the potential benefits of using this technique to manufacture constructs for repair of complex, layered tissues.

The final results chapter offers an alternative approach to engineering of complex, layered tissues. Channelled hydrogel structures are proposed for stimulating multi-lineage differentiation of stem cells within a single structure. The chapter details the development and initial evaluation of channelled hydrogels. A final study detailing results of inducing controlled, simultaneous chondrogenic and osteogenic differentiation from a single MSC population in a single structure is also outlined.

Chapter 8 provides a final conclusion and details potential future work to build on each concept outlined in Chapters 4-7.

1.10 Publications and Conference Presentations

1.10.1 - Publications

Moxon, S.R. & Smith, A.M. (2016), Controlling the rheology of gellan gum hydrogels in cell culture conditions. International Journal of Biological Macromolecules, 84, 79-86

Smith, A.M. **Moxon, S.R.** Morris, G.A. (2016). Biopolymers as wound healing materials. In: Agren, M.S. Wound Healing Biomaterials. Duxford, UK: Woodhead Publishing. 261-287.

Moxon, S.R. Cooke, M. Jones S.W. Snow, M. Jeys, L. Cox, S.C. Smith, A.M. Grover, L.M. Suspended Manufacture of Biological Structures – Submitted for review in Advanced Materials

Moxon, S.R. Cooke, M. Smith, A.M. Grover, L.M. Controlled Multi-Lineage Differentiation of MSCs within a Single Structure – In preparation for submission to Biomaterials

1.10.2 - Conferences Presentations

17th - 22nd May 2016 – 10th World Biomaterials Congress, Montreal (Canada)

Poster Presentation - Channelled Polysaccharide Hydrogel Structures for Tissue Engineering Applications (S.R Moxon & A.M Smith)

Poster Presentation - Bioprinting Multilayered Hydrogels Using 3D Suspended Manufacturing

(S.R Moxon, M.E. Cooke, S.C. Cox, L.M. Grover, A.M Smith)

25th – 29th October 2015 – AAPS Annual Meeting, Orlando (USA)

Channelled Polysaccharide Hydrogel Structures for Tissue Engineering Applications (S.R Moxon & A.M Smith)

10th September 2015 – 2nd UK Hydrocolloids Symposium, Birmingham (UK)

Oral Presentation - Tuning the Rheology of Gellan Gum Hydrogels for Cell Culture Applications (S.R Moxon & A.M Smith)

25th- 26th June 2015 – UKSB Annual Conference, Belfast (UK)

Oral Presentation - Channelled Polysaccharide Hydrogels as Tissue Engineering Substrates (S.R Moxon & A.M Smith)

31st August – September 3rd - 6th European Conference on Biomaterials, Liverpool (UK)

Poster with Oral Presentation - Controlling the Modulus of Gellan Gum Hydrogels for Cell Culture Substrates (S.R Moxon & A.M Smith)

5th – 9th May 2014 – 12th International Hydrocolloids Conference, Taipei (Taiwan)

Oral Presentation – An Initial Evaluation of Channelled Hydrogel Structures to Engineer Complex Tissues (S.R Moxon, L.M Grover & A.M Smith)

Poster Presentation - Controlling the Modulus of Gellan Gum Hydrogels by Sonication (S.R Moxon & A.M Smith)

Chapter 2 – Biopolymer Hydrogel Scaffolds

2.1 Introduction to Medical Biopolymers

Biopolymers are polymers derived from a natural source. They are produced either by extraction of a fully synthesised polymer from a living organism or by chemical synthesis from a starting material of biological origin. They have many therapeutic applications ranging from drug delivery, wound healing, gene therapy and tissue regeneration (Reddy et al., 2015). The natural source of biopolymers means end products harbour little cytotoxicity and degrade into benign products (Zopf et al., 2015), which has obvious advantages for use as a biomaterial biopolymers have a wide variety of applications in the field of tissue engineering and a number of biopolymer systems have been developed. The most notable forms are electrospun fibres, sponges and hydrogels, each with unique bulk properties and applications. Electrospun fibres, for example, are formed by ejecting biopolymer solutions through a needle with an applied electrical charge. Application of an electrical force triggers evaporation of solvent during ejection resulting in the formation of fibres (Zhu et al., 2015). This allows for fabrication of a scaffold that has the potential to mimic the fibrous structure of native ECM. However, there are issues associated with tissue culture applications of electrospun fibres. One noteworthy disadvantage is a difficulty in incorporation of cells into electrospun fibrous networks (Lipson and Kurman, 2013). Without post-processing, electrospun fibrous scaffolds often lack sufficient porosity to facilitate infiltration and migration of cells making fabrication of cell-loaded structures challenging.

Conversely, biopolymer sponges are highly porous and allow for cell seeding and migration without the requirement for post-processing (Reddy et al., 2015). Pore size is sufficient to allow for cell migration and delivery of nutrients, growth factors and chemical cues. Similarly, waste products can diffuse out of sponges. However, biopolymer sponges have been reported to exhibit insufficient

mechanical properties and a lack of structural stability for a number of tissue culture applications. Additionally, cells encapsulated in sponges have been shown to exhibit non-uniform phenotypes with one example demonstrating that chondrocytes seeded in sponges exhibit heterogeneity in terms of morphology (Yamada et al., 2012).

This work focuses on hydrogels because they have the capacity to address a number of the issues associated with sponges and electrospun fibrous networks. Hydrogels can exhibit sufficient porosity to facilitate cell migration and diffusion of small molecules without post-processing modifications (Shachar et al., 2011). Additionally, hydrogels have the capacity to exhibit sufficient mechanical properties to support a wide variety of tissue culture applications (Oliveira et al., 2010, Sakai et al., 2007, Annabi et al., 2013). Also, cells encapsulated in hydrogels have been shown to exhibit uniform morphology with the previously mentioned Zhang et al. 2013 study demonstrating expression of a more native phenotype of chondrocytes in hydrogels versus sponges.

2.1.1 Biopolymer hydrogel scaffolds

A hydrogel is an organised, gelled polymer network with high (often >90%) water content (Coviello et al., 2007). Polymer chains in hydrogel networks are characterised as being swollen and hydrophilic and show varied levels of hydrophobicity dependent upon the polymer used. Generally, hydrogels are formed either by passage through a sol-gel transition or via phase separation (Ahmed, 2015). However, the biopolymers explored in this thesis form a hydrogel via sol-gel transitions. When a hydrogel is formed in this way, polymer molecules undergo conformational changes triggering a shift from a disordered solution to an ordered network of cross-linked polymer molecules. Consequently, passage through the sol-gel transition is characterised by a pronounced change in mechanical properties (Tsao et al., 2015, Ruel-Gariépy and Leroux, 2004). Cross-linking of polymer molecules can be triggered in a number of ways.

Physical cross-linking of polymer molecules is often utilised in biomedical applications as it is a relatively gentle mechanism of forming hydrogels from natural polymers (Pereira et al., 2014).

Natural polymers disperse in water to form a disordered solution often initiated by heating or cooling, sometimes additionally mediated by ionic interaction. Upon changes in temperature, certain biopolymers can undergo a rapid phase transition from a disordered to an ordered conformation. The temperature at which this occurs is defined as the critical solution temperature. For some biopolymers, ionic interaction is required for cross-linking to occur. This can be triggered either with the addition of ions such as sodium and calcium or alternatively by incorporating a second polymer of opposite charge, resulting in complex coacervation. For example, alginate can be cross-linked with the addition of Ca^{2+} ions but it can also be cross-linked with a positively charged biopolymer such as chitosan (Çelik et al., 2016, Ghorbal et al., 2013).

Natural biopolymers can also be modified to contain chemical groups (often methacrylates) that facilitate photo-crosslinking by exposure to UV light. When these modified biopolymers are exposed to UV light, free radicals are generated by energy transfer, initiating polymer network formation. However, free radicals can also react with proteins, DNA and cell membranes causing cell damage. Careful control must therefore be placed on the level and type of radiation used to initiate photo-crosslinking of biopolymer networks (Fedorovich et al., 2009).

Finally, polymers can also be chemically cross-linked into ordered networks. Similar to physical cross-linking, this involves the addition of cross-linkers to trigger gelation. However, chemical cross-linking is mediated by direct interaction between cross-linkers and functional groups on a polymer side chain (Hezaveh and Muhamad, 2013). Natural or synthetic cross-linkers can be used to form covalent bonds between polymer functional groups. However, chemical cross-linking is rarely used in biomedical applications. This is due to chemical cross-linkers often harbouring cytotoxic effects, thus compromising viability of encapsulated cells.

Biopolymers explored throughout this thesis are all examples of polymers that can be physically cross-linked. The ability to transition a biopolymer solution into an ordered, hydrogel network is something that is often exploited for tissue engineering applications. Cells can be seeded into

biopolymers in a sol state to create a cell-laden suspension. Gelation can then be triggered, thus fabricating a cell-loaded hydrogel scaffold. Such structures are promising tools for tissue engineering applications due to a number of advantageous properties.

2.1.2 Porosity

Porosity is important in a tissue engineering scaffold (see Chapter 1 Section 1.5.2) and hydrogel networks are often highly porous due to a large water content. This facilitates diffusion of nutrients, key growth factors and biochemical cues to cells as well as removal of waste products (Lee and Mooney, 2001). An example of a porous gellan hydrogel network is presented in Fig. 2.1.

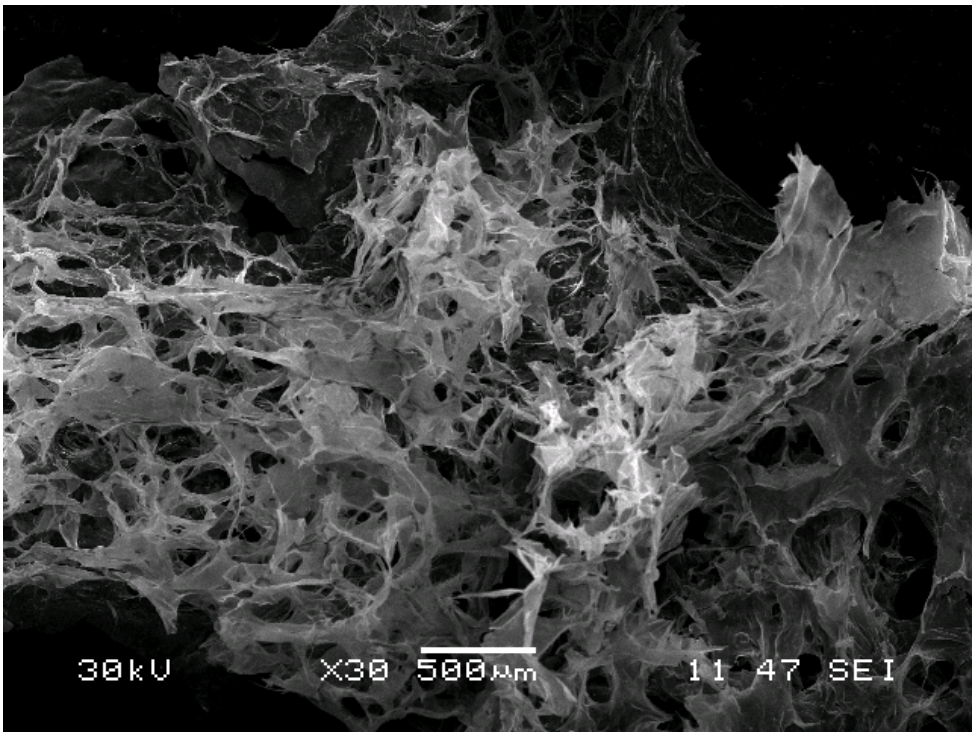

Figure 2.1– A freeze-dried, porous gellan gum hydrogel network observed with scanning electron microscopy/SEM

Cell culture media can be placed onto a hydrogel surface and components diffuse through the porous network supplementing encapsulated cells. Waste products can also diffuse out through hydrogel matrices and be easily removed via aspiration. As a result, cells encapsulated in hydrogel scaffolds can be cultivated in the similar conditions as monolayer cultures where supplemented media is changed every 2-3 days.

2.1.3 Structural and mechanical properties

Hydrogel scaffolds also have the capacity to replicate certain ECM properties. While the exact composition of ECM varies between tissues, certain primary components are present unanimously such as collagenous proteins and proteoglycans. Cells in native ECM are surrounded by hydrated proteoglycan gels that act as barriers against compressive forces. When encapsulated in biopolymer hydrogels, cells are presented with a similar environment comprised of a hydrated polymer gel network. The hydrated network can withstand compressive forces from cells without undergoing significant deformation. Additionally, external mechanical loads placed on a hydrogel network can trigger mechanotransduction in encapsulated cells leading to expression of tissue-specific genes (Drury and Mooney, 2003).

Furthermore, cells encapsulated in biopolymer hydrogels have been widely reported to synthesise and deposit collagen into the surrounding matrix (Bhat and Kumar, 2012, Bian et al., 2011). This results in a 3D environment containing both hydrated polymer gels and a collagenous network, further reflecting native tissue culture conditions.

As well as providing support during culture of new tissue, certain biopolymer hydrogels such as alginate also undergo degradation which can potentially facilitate replacement by newly synthesised ECM *in vivo* Furthermore, the mechanical and physical properties can also be easily tuned to suit the tissue to be cultured (Drury and Mooney, 2003).

2.1.4 Tunability

Porosity, stiffness and elasticity of hydrogels are all directly related to the polymer used for fabrication. Modifying hydrogel formulations is an efficient method for tailoring gel properties for tissue specific applications. Mechanical strength can be effectively tuned by changes in either polymer concentration or changes in concentration of any required cross-linkers. Hydrogel networks are formed by cross-linking of polymer molecules. Increasing concentration of either polymer or cross-linker (where required) results in a larger quantity of such interactions, thus enhancing gel

strength. Some polymers require ionic interactions to facilitate cross-linking and, in such cases, an increase in ionic concentrations further promotes cross-linking of molecules resulting in a gel with greater mechanical strength. Similarly, changes in polymer or cross-linker concentrations can be used to tune hydrogel porosity by directly modifying density. An increase in either concentration results in a hydrogel of greater density (Chavda and Patel, 2011). Density and porosity are inversely related such that in increase in density leads to a reduction in porosity (Hall and Hamilton, 2015). Therefore, both mechanical strength and porosity of biopolymer hydrogels can be easily tuned with modifications in polymer/cross-linker concentration. This, therefore, aids the design of biopolymer scaffolds with tissue-specific structural and mechanical properties.

Changes in polymer/cross-linker concentrations, however, can affect cell behaviour, even in hydrogels formed by physical cross-linking. For example, Çelik et al., (2016) demonstrated that increasing $CaCl_2$ concentrations in alginate hydrogels had a negative effect on cell behaviour (Çelik et al., 2016). Alginate hydrogels with high ionic content exhibited a greater density of cross-linking leading to nutrient depletion, a significant reduction in intracellular space and inadequate oxygenation. While this presents potential issues, it has also been shown that hydrogel properties can be easily tuned without modifying polymer/cross-linker concentration (Taylor et al., 2012, Moxon and Smith, 2016).

Many biopolymer substances have been investigated for the fabrication of tissue-culture scaffolds with natural polysaccharides, proteins and synthetic polymers explored extensively. This work will focus primarily on two natural polysaccharides, namely gellan gum and agarose, with a third polysaccharide and two proteins (alginate, collagen and gelatin respectively) briefly explored for tissue culture applications.

2.2 Polysaccharide Hydrogels

2.2.1 Gellan gum

Gellan gum (herein referred to as gellan) is a microbial extracellular polysaccharide extracted from multiple genus and species of the bacteria, the most common being *Pseudomonas elodea* and *Sphingomonas elodea*. The chemical structure of gellan is comprised of a repeating tetrasaccharide unit containing a molar ratio of 2 D-glucose:1 D-glucuronic acid:1 L-rhamnose (Fig. 2.3). Gellan polymer units carry a net negative charge due to the presence of carboxylate groups on glucuronic acid residues (Stevens et al., 2016). Two types of gellan are commercially available, high acyl gellan and low acyl gellan with names relating to the degree of acetylation (Fig 2.2).

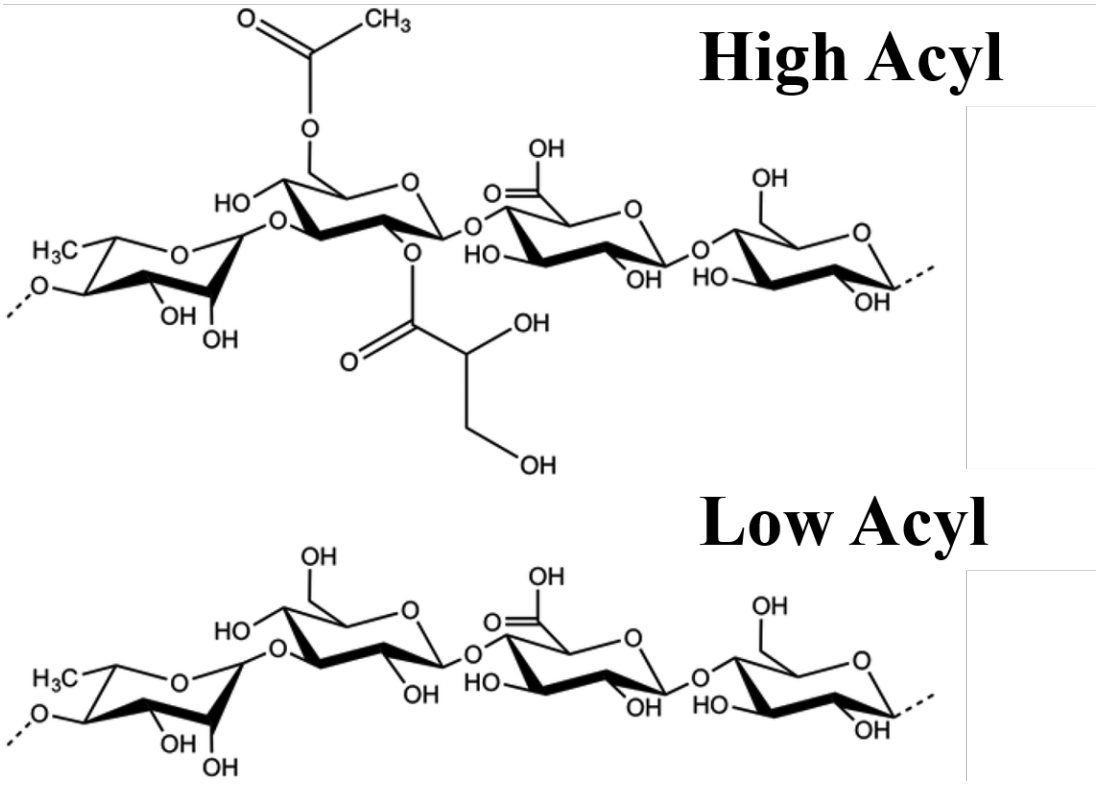

Figure 2.2 - The chemical structure of the tetrasaccharide repeat of low acyl and high acyl gellan (reproduced from Stevens et al. 2016 with permissions from Elsevier)

Both forms of gellan form polymer hydrogel networks but mechanical properties vary significantly. Hydrogels of LA gellan are generally strong, stiff and brittle while HA gellan networks are soft,

elastic and ‘putty-like’ (Morris et al., 2012) due to fundamental differences in gelation mechanics of each polymer.

Gelation of gellan is mediated by temperature and cationic linking of polymer helices. When dispersed in deionised water at temperatures greater than 80°C, molecules of gellan adopt a disordered conformation. Upon cooling, gellan undergoes a rapid phase transition from random coiled structures to more ordered double helices. In the absence of cations, solutions of gellan remain in this phase. Introduction of cations results in aggregation and cross-linking of gellan helices with multivalent ions creating stronger, more stable gels than monovalent cations. Additionally, it has been previously demonstrated that the ions present in cell culture media are sufficient to trigger gelation, thus allowing for formation of a hydrogel saturated with cell supplements (Smith et al., 2007). It is thought that monovalent ions ions such as Na^{+} suppress the repulsive charge exhibited by carboxyl groups located on glucuronic acid residues, thus facilitating aggregation. Divalent ions such as Ca^{2+} act as junctions between polymer helices forming stronger cross-linking by directly bridging carboxylate groups (Fig. 2.3).

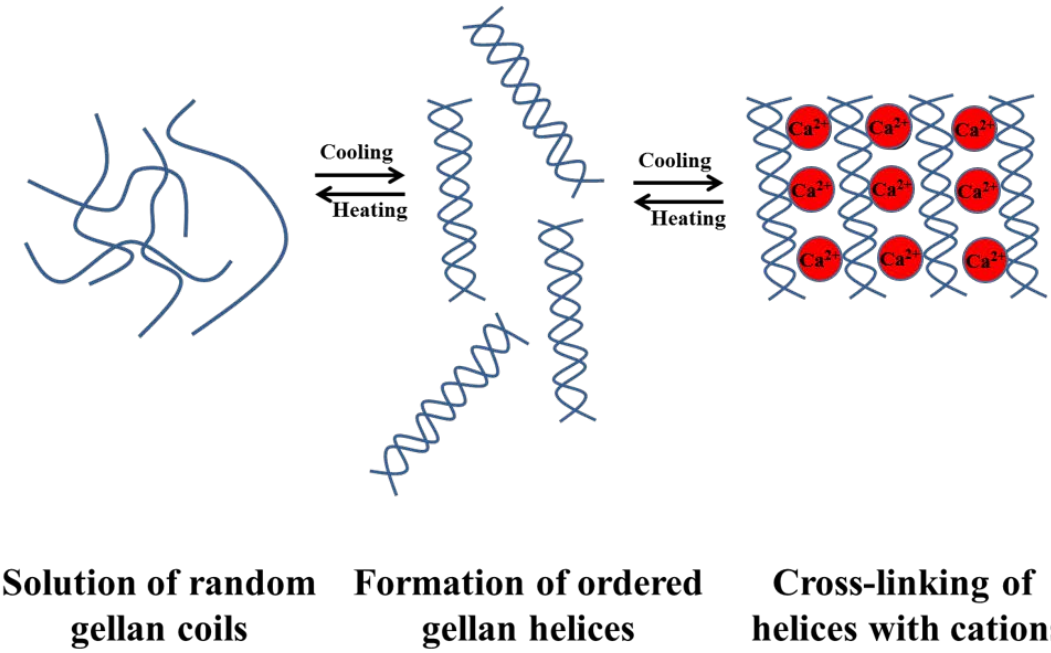

Figure 2.3 - A cartoon representation of phase transitions of gellan molecules from random coils to an ordered, cross-linked network during hydrogel formation

However, the presence of acyl groups in HA gellan is thought to inhibit ion-mediated gelation by blocking aggregation of helices resulting in formation of softer, more elastic gels. Conversely, a lack of acyl groups in LA gellan facilitates helix aggregation allowing for formation of a stiff hydrogel. As a result, low acyl gellan is predominantly used for tissue engineering as scaffolds need to provide significant support for developing tissues. Categorising a matrix as soft or stiff is a highly subjective process, however and is subjected to interpretation with each application of a material. In the context of this work hydrogels exhibiting a modulus on the kPa scale and above are considered 'stiff'.

2.2.2 Agarose

Agarose is the primary gelling agent in agar and is used widely in microbiology. It is extracted from red algae/seaweed with the main sources being *Gelidium* and *Gracilaria* genera. It is commonly used in biology for procedures such as gel electrophoresis of PCR products with recent promise shown as a tissue engineering scaffold.

Chemically, agarose is a hydrophilic, linear polysaccharide with no significant net charge. Polymer molecules are comprised of a repeating disaccharide unit of β-D-galactose and α-L-3,6-anhydrogalactose as shown in Fig. 2.4 (Ghorbal et al., 2013).

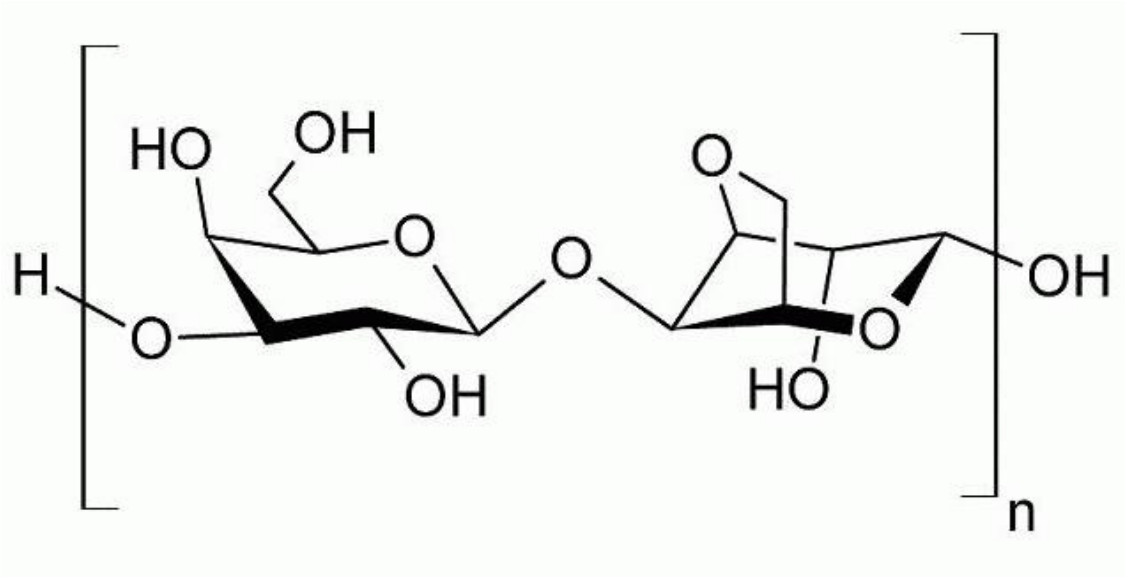

Figure 2.4 - Chemical structure of the repeat unit of agarose shows the 1,3 linked β-D-galactose residue and the 1,4 linked 3,6-anhydro-α-L-galactose residue (reproduced from Thermo Fisher Scientific)

When dispersed in deionised water (pH 7.8) at temperatures above ~80 °C agarose molecules are in a disordered state. Gelation of agarose is triggered by cooling leading to self-assembly of ordered polymer helices facilitated by conformational changes in molecular structure. Helices aggregate and cross-link independent of ionic content.

Agarose has a similar capacity to form hydrogels as gellan in terms of required concentration with a capability to undergo sol-gel transitions into ordered polymer networks at concentrations of <1% w/w. Mechanical properties of agarose hydrogels can be easily tuned with variations in polymer concentration with a capacity to form strong, durable and highly porous scaffolds. Agarose hydrogels are prone to syneresis (loss of water through gel contraction) but this has not been reported to have a significant impact on tissue culture applications.

2.2.3 Alginate

Alginate is a polysaccharide found in seaweed and often extracted from a class of brown algae called *Phaeophyceae*. It is a linear polysaccharide comprised of two different uronic acid residues β-D-mannuronate and α-L-guluronate that occur randomly throughout the polymer chain as blocks of guluronate, blocks of mannuronate and heteropolymeric blocks of both monomers (Park et al., 2009). (Fig. 2.5).

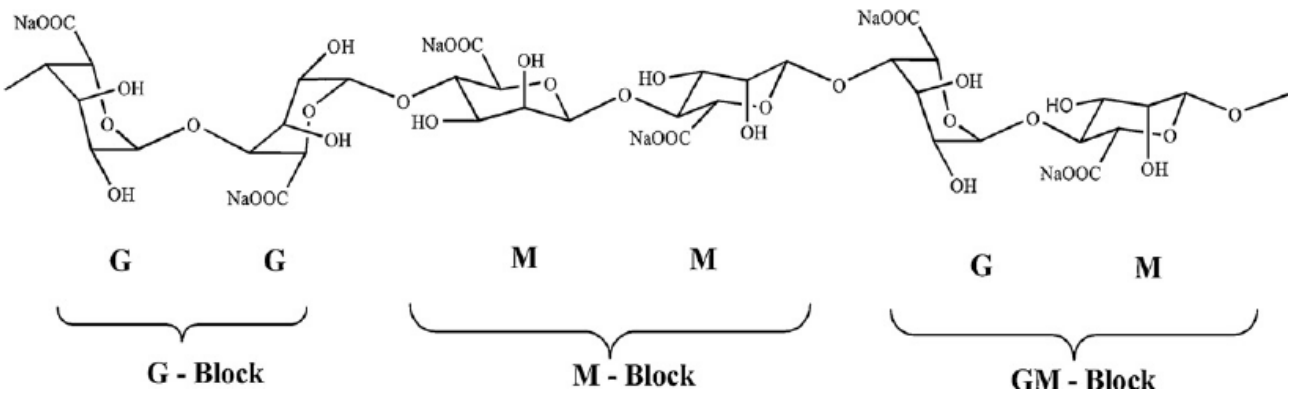

Figure 2.5 - Chemical structures of G and M block confirmations in alginate (reproduced from Park et al., 2009 with permissions from Elsevier)

Alginate has an affinity for divalent cations and can physically cross-link in the presence of divalent cations such as Ca^{2+} to form a gel. Cross-linking of alginates is mediated by interactions between the cations and carboxylic acid groups in the G-blocks. As such, ratios of G and M blocks in alginate have a direct impact on subsequent hydrogel strength with 'high-G' alginate producing stronger gels than 'low-G' alginate (Park et al., 2009). Depending on the source, M/G ratios of alginates can vary with a range of 10%-75% G alginates commercially available. Additionally, it has been shown that the so called 'blockiness' of alginate polymer chains can influence gel mechanical properties (Funami et al., 2009). NMR spectroscopy of alginate has been previously used to determine the frequency of monad (G or M), diad (GG, MM, GM, MG) and triad (MMM, GGG, MMG, MGG, GGM, GMM) blocks in alginate polymer chains (Grasdalen et al., 1981). By determining such frequencies, the average G block length can be determined. This has been shown to directly influence mechanical properties with longer G block alginates producing stronger, stiffer gels than shorter G block alginates.

Alginate is often explored for tissue engineering applications due to desirable gelation properties. Cell suspensions can be mixed with alginate solutions and gelled into cell-loaded hydrogel constructs in a controlled manner, as unlike gellan culture media does not trigger gelation. This is because the concentration of calcium ions in cell culture media is not sufficient to initiate gelation. Introduction of additional divalent cations is required and this results in aggregation and cross-linking of G-blocks and a transition from a disordered sol to ordered gel phase. Relatively low concentrations of alginate (typically between 2% and 5% w/w) are required for fabrication of tissue culture scaffolds, albeit slightly higher than is required for gellan and agarose.

2.3 Protein Hydrogels

2.3.1 Collagen

Collagen is the most abundant protein in mammals and acts as the main structural component in connective tissues. To date 29 different types of collagen have been identified, each with a unique amino acid sequence (Chattopadhyay and Raines, 2014). However each type shares a generic 3D structure of 3 polypeptide chains wrapped in a left-handed helix (Fig. 2.6). Hydrogen bonds between chains stabilise helices with each chain containing approximately 1000 amino acids. Chains contain a common amino acid sequence of Gly-X-Y where X and Y can be any amino acid. High glycine content of collagen polypeptide chains allow for tight packing into structure of high tensile strength.

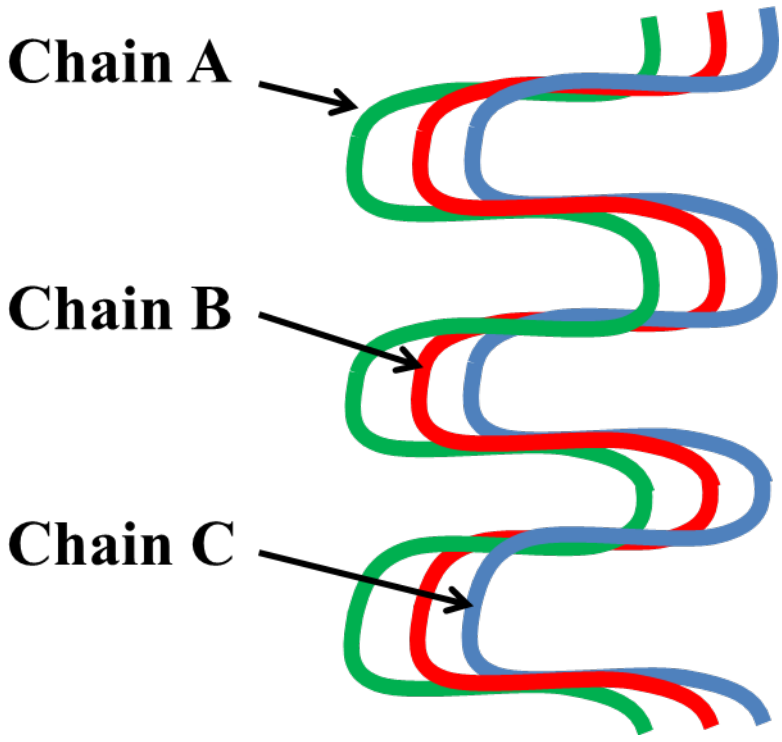

Figure 2.6 - A simplified representation of a left-handed collagen triple helix

Type I collagen, often sourced from rat tails, is the predominant choice for biomedical applications and is classed as a fibrous collagen due to an ability to undergo fibrillogenesis (formation of collagen fibrils). During this process collagen molecules adjacently pack together into a tight structure. Segments at the end of collagen molecules form cross-linking bonds between 2 C-terminus residues

of one collagen molecule and 2 N-terminus residues of another. This results in a fibrous network of high tensile strength.

Gelation of purified collagen biomaterials is complex and often involves control of pH and temperature. As with many protein gels gelation is triggered by an increase in temperature. Thus, physiological temperature can often be utilised to trigger gelation. As a result, collagen has numerous biomedical applications and has been extensively explored as a material for bone and cartilage tissue engineering (Murphy et al., 2010, Rodrigues et al., 2003, Dai et al., 2010).

2.3.2 Gelatin

Gelatin is a protein manufactured primarily from type I collagen in bone. It is highly soluble in water and available in two types, type A (treated with acid) and type B (treated with alkali). Variance in production of types of gelatin results in a different isoelectric point (pH at which the molecule carries no net charge). The isoelectric points of types A and B are ~8.0 and ~4.9 respectively resulting in different charges exhibited at physiological pH (Ghosh, 1927, Hitchcock, 1924). As a result, each type of gelatin will exhibit a different charge at physiological pH. This can subsequently impact on cell culture applications with charge density of tissue culture scaffolds shown to directly influence cell attachment to the matrix (Schneider et al., 2004).

The structure of gelatin is comprised of partially reformed collagen helices as a result of denaturation of native collagen in the production process. Gelation is triggered by cooling gelatin solutions triggering a transition from random coils to more ordered structures with confirmations reflecting that of native collagen. Gelatin molecules penetrate each other, however, thus preventing a full reversion back into collagen (Guo et al., 2003). A representation of fundamental differences in helix confirmations of gelatin and collagen is illustrated in Fig. 2.7.

In summary, both gelatin and collagen are comprised of the same primary structure, i.e. ‘Chain A’ in collagen has the same amino acid sequence as ‘Chain A’ in gelatin. However, because gelatin is

denatured from collagen, the tertiary structure of gelatin is much less ordered and is not comprised of the organised, left handed helix observed in collagen.

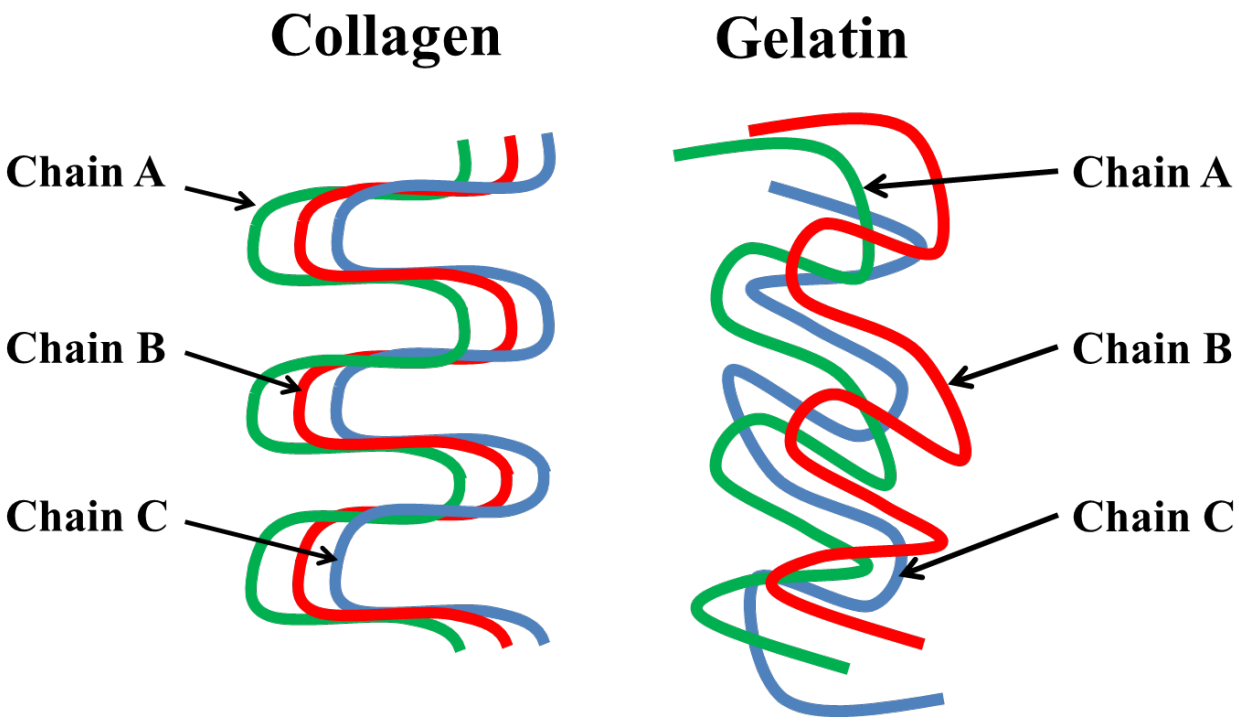

Figure 2.7 - A simplified representation of conformational differences between collagen and gelatin helices

Temperatures used in the extraction process of gelatin influence molecular weight, resulting in a 'bloom value'. A higher bloom indicates a higher molecular weight and, thus, stronger gels can be formed.

2.4 – Recent Innovations in Tissue Engineering Applications of Biopolymers

Each material introduced in section 2.3 exhibits unique properties that can be manipulated for tissue engineering applications. This has led to a variety of innovative studies that represent significant progress in the use of biopolymer hydrogels for tissue regeneration.

Arguably, one of the most exciting recent advancements in tissue engineering is the incorporation of biopolymers into rapid prototyping mechanisms such as 3D printing and additive layer manufacturing (ALM). Such methods have been widely used in other industries with 3D printing becoming a major manufacturing technique (Lipson and Kurman, 2013). Rapid prototyping of tissue culture scaffolds

could provide a promising way of creating complex, customisable 3D structures for treatment of patient specific tissue defects. Consequently, various studies have been conducted demonstrating the potential applications of rapid prototyping in tissue culture scaffold fabrication.

One such example by Zopf et al. (2015) used the gelation properties of collagen hydrogels in the rapid prototyping of patient specific implants for subcutaneous cartilage regeneration (Zopf et al., 2015). As mentioned previously (section 2.3.1), collagen hydrogels undergo a sol-gel transition when temperature is increased. This means cell-loaded collagen hydrogels can be fabricated by seeding a cell/collagen suspension at room temperature and placing in a cell culture incubator at 37 °C to trigger gelation. In this study, patient-specific scaffolds were designed by computer aided design (CAD). Based on CAD models, 3D porous structures were fabricated from fibrillogenesis (PCL). Scaffolds were then seeded with chondrocytes suspended in a collagen solution and transfer into a cell culture incubator triggered collagen gelation via an increase in temperature. Consequently, a complex and implantable 3D structure was created containing a chondrocyte-loaded collagen hydrogel supported by a PCL porous network. Scaffolds exhibited sufficient mechanical properties to allow for subcutaneous implantation and retained structure post-implantation (Fig. 2.8). Histological analysis of chondrocytes seeded in PCL-collagen scaffolds revealed evidence of chondrogenic responses comparable to those observed in native mouse tissue. Therefore, it was concluded that this represents a very promising new approach to manufacturing of patient-specific implants for repair of complex, subcutaneous cartilage tissue.

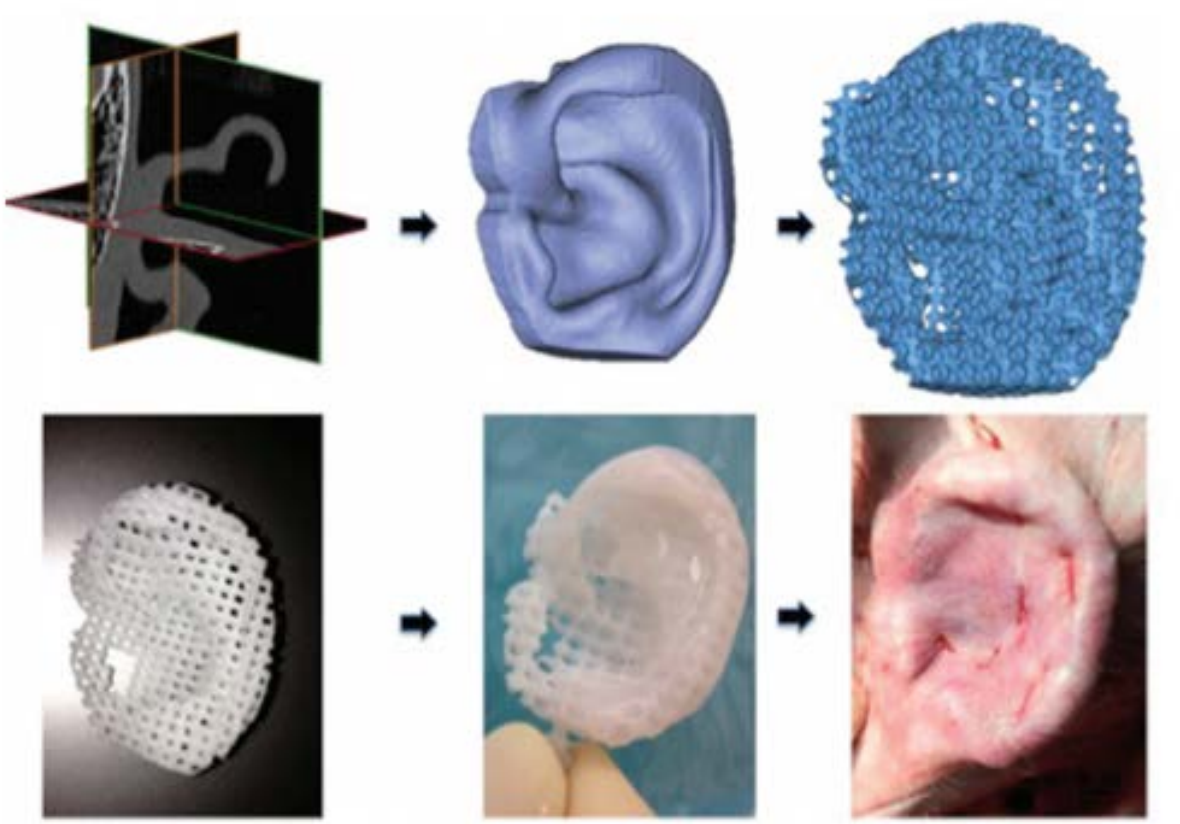

Figure 2.8 - CAD and subsequent manufacture of a cell-seeded collagen hydrogel supported by a porous PCL network and implantation into an *in vivo* culture model (reproduced from Zopf et al. 2015 with permissions from SAGE Publishing)

Gelation properties of gelatin have also been manipulated for rapid prototyping of tissue culture scaffolds. One example is a study by Billiet et al. (2014) with the cooling-triggered gelation of gelatin utilised to allow 3D printing of a porous, gelatin scaffold (Billiet et al., 2014). By printing at temperatures below what was required for gelation (in this case printing at 24.5-30°C), it was possible to layer fibres of gelatin on top of each other, thus fabricating a highly porous scaffold. It was also demonstrated that gelatin seeded with human hepatocytes could be printed to form a cell-loaded scaffold with encapsulated cells showing high viability (Fig. 2.9).

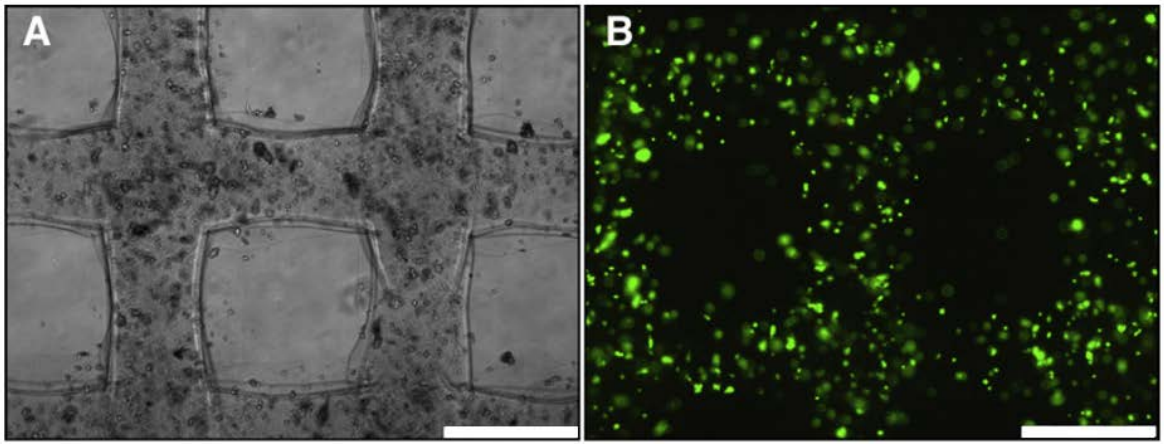

Figure 2.9 – High viability (indicated by green fluorescence) of human hepatocytes encapsulated in a 3D printed, porous gelatin scaffold. A) shows bright field microscopy images of the ordered 'waffle-like' scaffold architecture while B) shows live human hepatocytes attached to the scaffold network (reproduced from Billiet et al. with permissions from Elsevier – scale bar represents 500 µm)

Additionally, evidence of native phenotype retention was demonstrated in the form of a high proliferative capacity, a characteristic hepatocyte marker. Scaffolds demonstrated tunable mechanical properties and retained structure throughout a 14-day culture period. This, therefore, represents another promising way in which tissue culture scaffolds can be fabricated from biopolymers. Theoretically, gelatin could be seeded with a range of cell types and printed to form a customisable, porous scaffold. While this study focussed on liver tissue, it is feasible that cell types such as osteoblasts or chondrocytes could be incorporated to create bone and cartilage scaffolds.

Another promising avenue for exploration of biopolymers in tissue culture is materials that can undergo gelation *in situ*. This can facilitate the injection of a cell-laden biopolymer solution into tissue defects where hydrogel formation is triggered by physiological conditions such as temperature, pH or ionic interactions (Zhu et al., 2015). Gellan, for example, can be gelled by either ionic interactions or changes in pH and gelation is temperature dependent. As such it has been investigated for potential applications that utilise *in situ* gelation of cell-loaded tissue culture scaffolds. One study by Oliveira et al. (2010) highlighted the potential applications of *in situ* gelation of gellan in cartilage repair models (Oliveira et al., 2010). It was demonstrated that gellan gum solutions seeded with rabbit chondrocytes and stem cells could be injected as a solution into simulated rabbit cartilage defects. *In*

situ gelation was successfully triggered by temperature and ionic interactions. This resulted in formation of autologous cell-loaded gellan implants that fully filled simulated defects. Cells encapsulated in implanted hydrogels were shown to exhibit native chondrogenic phenotype with high expression levels of chondrogenic markers. Additionally, encapsulated cells displayed evidence of cartilage ECM synthesis with collagen and GAG deposition. This resulted in increased tissue repair with the greatest degree of healing observed in gels seeded with chondrogenically differentiated stem cells (ASC + GF – Fig. 2.10). This highlights the promise of gellan gum as a material for repair of cartilage defects, with *in situ* gelation properties allowing for injection and formation *in vivo* of cell-loaded scaffolds.

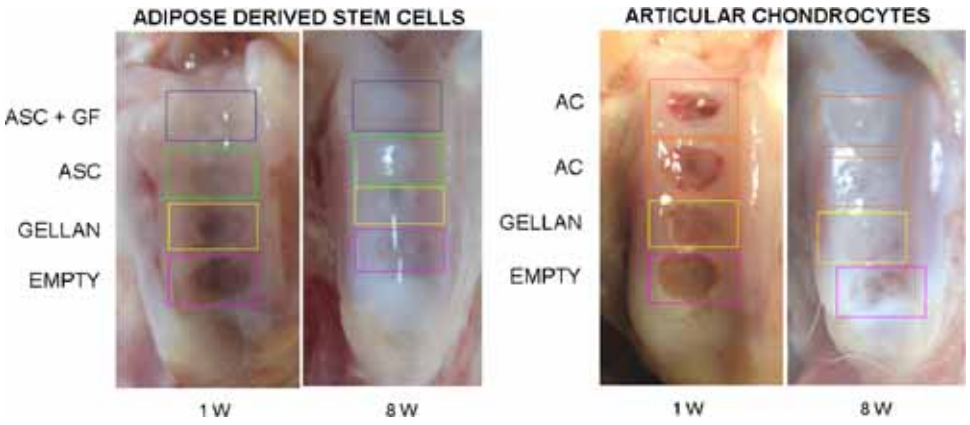

Figure 2.10 – Repair of rabbit cartilage defects using cell-loaded gellan gum hydrogels (reproduced from Oliveira et al. 2012 with permissions from John Wiley & Sons)

To further facilitate native phenotype expression, another area of exploration is in modification of biopolymers that are not naturally cell adhesive such as gellan, alginate and agarose. Various studies have been conducted in chemically modifying such polymers to contain a cell-attachment motif, thus allowing cells to adhere to a hydrogel matrix. This is important for cell types where a key factor in native phenotype expression is proliferation as cells will not proliferate without the ability to adhere to a surface and progress through the cell replication cycle (Guadagno et al., 1993).

One example of such a method is modification of agarose with cell-adhesive peptides derived from laminin (Yamada et al., 2012). Cell adhesive agarose gels with tunable matrix stiffness were

fabricated and seeded with multiple cell types of high proliferative capacity such as fibroblasts, neuronal cells and endothelial cells. All cell types displayed evidence of attachment and proliferation in modified agarose matrices, with the level of attachment observed to be directly proportional to matrix stiffness. More interestingly, seeding of modified agarose with neuronal and endothelial cells resulted in exhibition of native cellular phenotypes (Fig. 2.11). Neuronal cells attached to stiff agarose matrices displayed evidence of neurite development. This is a key step in neurogenesis and highlights the presence of developing neurons. Additionally, endothelial cells attached to stiff agarose matrices showed evidence of capillary formation.

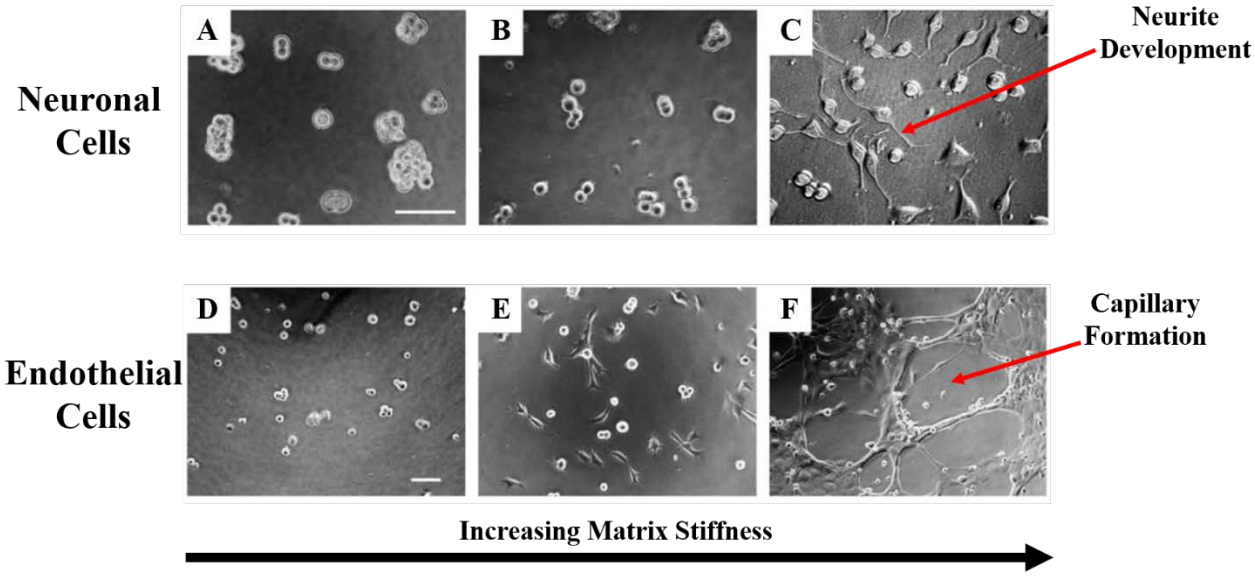

Figure 2.11 – Induction of native phenotype expression in neuronal cells (A-C) and endothelial cells (D-F) when seeded on modified cell-adhesive agarose matrices of varying matrix stiffness (adapted from Yamada et al. 2012 with permissions from Elsevier – scale bar = 100 µm)

Therefore, by tailoring agarose hydrogels to contain a cell binding motif, it was possible to induce native cell behaviour that could not be obtained from un-modified agarose.

Similar work has also been conducted with alginate, this time incorporating the RGD (arginine, glycine, aspartic acid) binding motif of fibronectin to create cell adhesive alginate gels for cardiac tissue regeneration (Shachar et al., 2011). In this study, rat cardiomyocytes were seeded into RGD-modified and unmodified alginate gels and subsequently cultured. It was shown that RGD-alginate promoted adhesion of cardiomyocytes to the hydrogel matrix and prevented apoptosis. In comparison,

cells were unable to attach to hydrogels composed of native alginate. More significantly, evidence of regeneration of ordered, myocardial tissue was observed in cells encapsulated within RGD-alginate, something not observed with cells in native alginate. Furthermore, cardiomyocytes in RGD-alginate synthesised an ordered network of myofibrils that was surrounded by non-myocytes. This was highly reflective of native myocardial tissue and such results were not observed in native alginate (Fig. 2.12). Therefore, this represents an intriguing development alginate scaffolds for myocardial tissue regeneration.

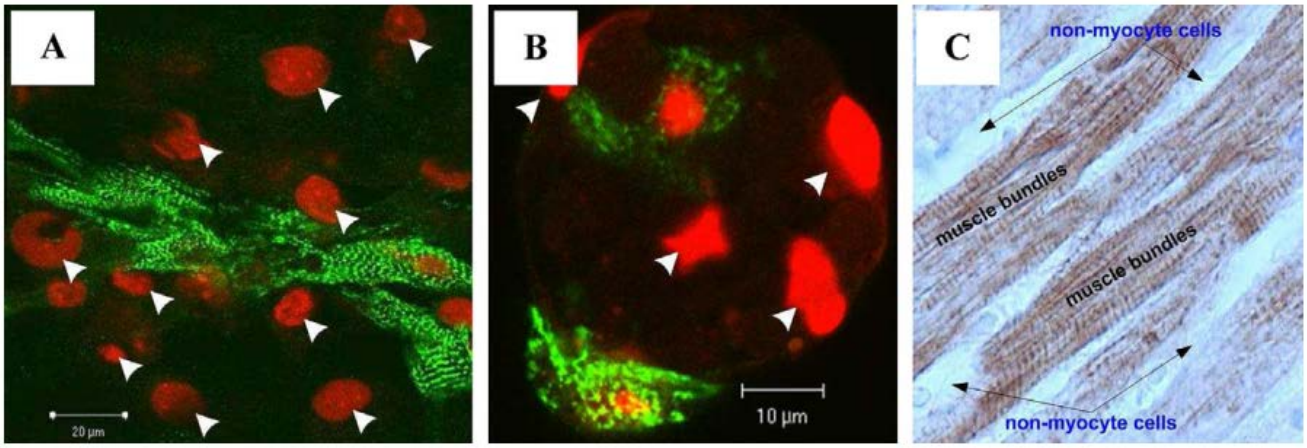

Figure 2.12 – Organisation of cardiomyocytes and myofibrils in A) RGD-alginate, B) native alginate and C) native tissue (reproduced from Shachar et al. 2011 with permissions from Elsevier – arrows in A and B represent non-myocytes (red), green represents cardiomyocytes in myofibril network

While all the studies highlighted so far in this section represent a promising step forward in tissue engineering applications of biopolymers, one common limitation is shared. Each study involved the use of biopolymers to fabricate scaffolds for regeneration of a single tissue type. A lot of progress has been made in engineering of single tissue types using biopolymers but significantly fewer advances have been made in biopolymer models for layered/interfaced tissue repair e.g. the osteochondral interface. Some studies have reported developments in biopolymer scaffolds for repair of layered tissue. For example, Pereira et al. (2014) presented a layered hydrogel structure of un-mineralised gellan and gellan mineralised with hydroxyapatite as shown in Fig. 2.13 (Pereira et al., 2014). Differences in density between both materials were used to facilitate deposition of gellan on top of gellan-hydroxyapatite inside a mould. Gelation was then triggered with the addition of cations

to create a single structure. However, the construct did not contain any cells and the size/shape of each layer could not be easily controlled.

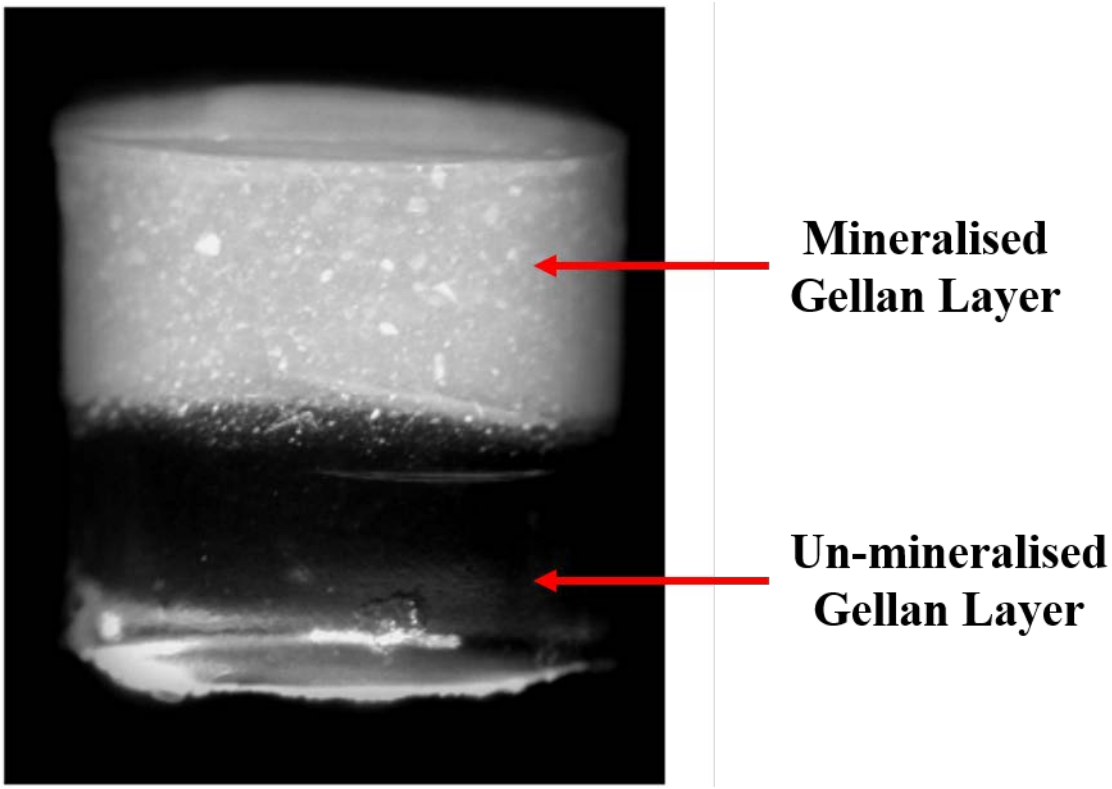

Figure 2.13 – A layered gellan/gellan-hydroxyapatite scaffold for osteochondral tissue engineering (reproduced from Perreira et al. 2014 with permissions from Trans Tech Publications Ltd.)

Studies outlined in this section highlight the many ways in which properties of biopolymers can be manipulated to suit tissue culture applications. This work aims to build on such progress to develop methods for culture of complex tissues from biomedical biopolymers.

Chapter 3 – Rheological Characterisation of Biopolymer Materials

3.1 Introduction to Rheology

The importance of the mechanical properties of tissue engineering scaffolds is well documented from a physical handling perspective and the influence on cellular function. An important part of the work in this thesis therefore, involves physical characterisation of scaffold candidate materials performed using rheological techniques. This chapter outlines fundamental principles behind the rheological methods used to study each material.

The literal translation of rheology is 'flow science' and is derived from the two Greek words 'rheo' and 'logos'. Rheology can be simply defined as the study of the flow although, in reality, it is more complex. It is based on multiple principles and is valuable in the field of tissue engineering as it allows for determination of mechanical properties exhibited by potential scaffold materials (Rao et al., 1986).

A fundamental concept to rheology is studying the way in which a material behaves under the application of stress. Materials can be classified as either 'solid-like' or 'liquid-like'. For each classification there is an extreme that represents a 'perfect' material, namely a Newtonian fluid or a Hookean solid. Each model is based on the principle that the application of stress to a material results in strain (Han, 2007). By studying how a material responds to stress and strain it is possible to evaluate whether it can be classed as an elastic, 'solid-like' material or a viscous, 'liquid-like' material. An elastic material will respond to applied stress by undergoing fractural deformation while a viscous material will respond by flowing. Therefore, stress and strain are integral to rheological characterisation of materials and it is important to understand how they influence mechanical properties of a material.

3.2 Stress and Strain

By determining stress and strain, rheological properties of a material can be evaluated by extrapolating into a series of equations.

Stress is force (F) applied per unit area (A) and can be determined using Equation 3.1.

$$\text{Stress (Pa)} = F/A \qquad \textbf{Equation 3.1}$$

There are three ways stress can be applied. These are tension/compression, shear and bulk stress. Compression and tension are defined as the application of perpendicular force either towards the centre of mass (compression), thus shortening an object, or away from the centre of mass (tension), thus lengthening an object. Shear stress is longitudinal force and bulk stress is isotropic forces applied from all areas. Strain can be calculated using Equation 3.2 where l is sample length prior to application of stress and Δl is the change in length.

$$\text{Strain (unitless)} = \Delta l/l \qquad \textbf{Equation 3.2}$$

Relationships between stress and strain can be used to determine mechanical properties of a material. Since the direction in which force is applied varies among each type of stress, the way in which mechanical properties are calculated also varies dependent upon the type of stress applied. By studying relationships between stress and strain, a value can be determined that represents the overall strength of a material. This is referred to as a modulus with each form of stress allowing for analysis of different moduli.

3.2.1 Young's modulus

Young's modulus (E) is determined by the application of perpendicular stress to materials either via tension or compression. It can be used to analyse the relative strength of solid materials with a defined size and shape and self-supporting capabilities. It is based on Hooke's law which states stress is proportional to strain and independent of strain rate. A perpendicular force is applied to materials

resulting in compression and storage of energy. When the applied stress is released stored energy results in recovery (Wortman and Evans, 1965). A perfect example is a spring that undergoes deformation as a result of compression but exhibits full recovery when applied stress is released. Young's modulus is calculated by dividing perpendicular stress by strain using Equation 3.3.

$$E\ (Pa) = \tau/\varepsilon \qquad \textbf{Equation 3.3}$$

3.2.2 Shear modulus

Shear modulus (G) utilises shear stresses to determine mechanical properties. Materials characterised by shear modulus are often soft and not fully self-supporting and, thus, G is more useful in soft materials such as biopolymer gels than Young's modulus. In determination of G, materials are subjected to longitudinal forces (shear stress) resulting in deformation through a specific angle (θ). The resulting shear strain exhibited by a material as a result of shear stress is calculated using Equation 3.4 where θ represents angle of deformation and Δl and l represent the tangential displacement and sample thickness respectively.

$$\gamma = \Delta l/l = \tan(\theta) = \theta \qquad \textbf{Equation 3.4}$$

From calculation of shear strain, G can be determined using Equation 3.5 where σ represents shear force and γ represents shear strain.

$$G\ (Pa) = \sigma/\gamma \qquad \textbf{Equation 3.5}$$

3.2.3 Bulk relaxation modulus

Bulk modulus (K) is rarely used in characterisation of soft materials such as biopolymer gels but it is based on the principle that all matter can undergo compression. It is defined as the modulus of volume expansion. When isotropic stresses are placed on solid materials, a relative change in volume is observed. The ratio of the two is defined as the bulk compression modulus and can be calculated using Equation 3.6, where bulk stress is represented by σ_v and volumetric strain is represented by ε_v.

$$K\ (Pa) = \sigma_v/\varepsilon_v \qquad \textbf{Equation 3.6}$$

Differences between the three types of stress used to determine moduli of materials are summarised in Fig. 3.1.

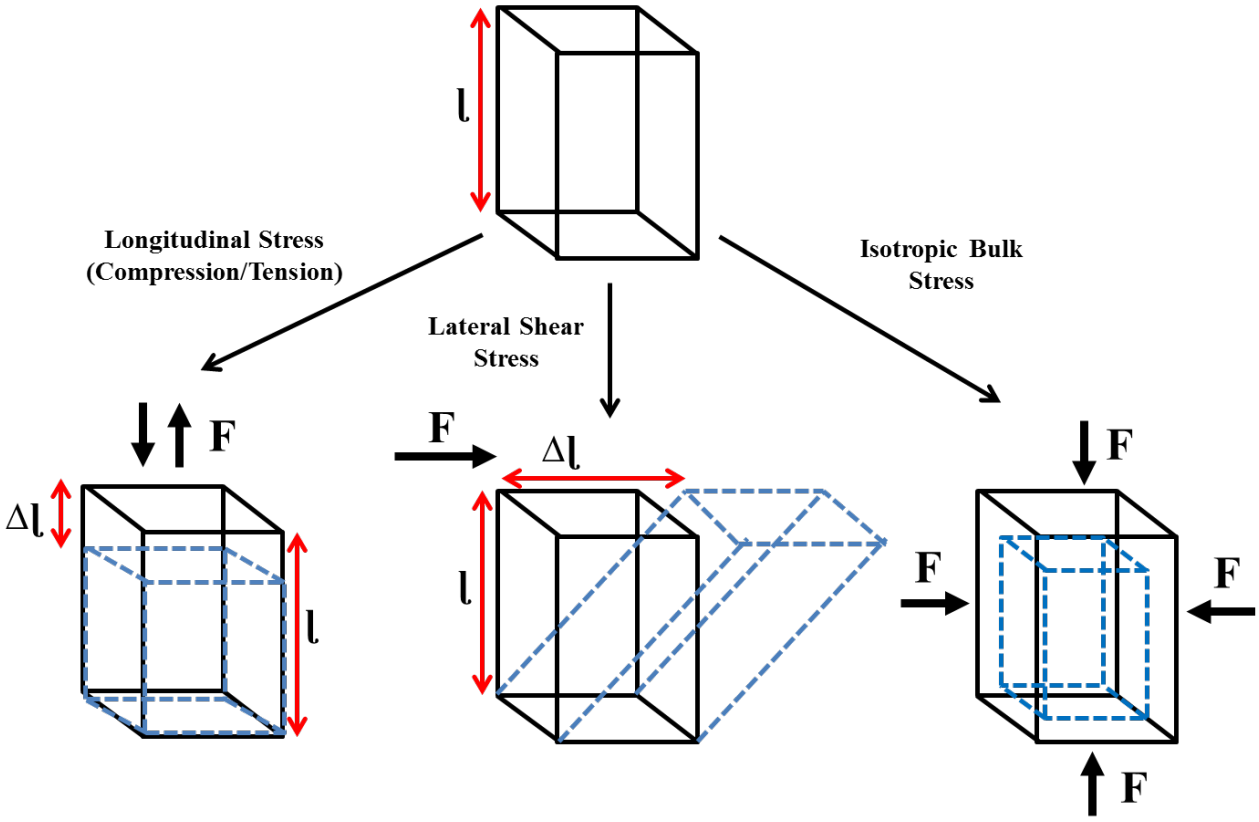

Figure 3.1 – A schematic demonstrating differences between types of force applied in longitudinal, lateral and isotopic stress testing of solid materials (Mahdi, 2016)

3.3 Rheological Analysis of Biopolymers

In order to successfully interpret rheological analysis of materials such as biopolymers, it is necessary to understand fundamental principles that measurements are based on. The concept of materials exhibiting ‘liquid-like’ or ‘solid-like’ behaviour is based on characteristics such as viscosity and elasticity. These are key principles and form the basis of many rheological measurement techniques, including those used throughout this thesis.

3.3.1 Viscosity

Viscosity can be defined as resistance to flow. It is a direct result of interactions between neighbouring molecules resulting in entanglement (Lewis, 1996). Calculation of viscosity is based on Isaac Newton's principle stating the flow of a liquid is directly proportional to the applied stress. Therefore viscosity can be determined by using Equation 3.7 where η represents viscosity, σ represents shear stress and $\dot{\gamma}$ represents rate of shear.

$$\eta \text{ (Pas)} = \sigma / \dot{\gamma} \qquad \textbf{Equation 3.7}$$

Consequently, a Newtonian fluid exhibits a viscosity that is fully independent of shear rate. Under certain conditions, some materials have the capacity to display Newtonian behaviour (such as water and oils). However, a truly Newtonian fluid is a theoretical principle and, in reality, materials exhibit Non-Newtonian behaviour when sufficient stress is applied.

3.3.2 Newtonian vs. Non-Newtonian systems

Non-Newtonian fluids exhibit shear rate-dependant viscosity i.e. as shear rate changes so does viscosity. There are multiple classes of Non-Newtonian systems which can be characterised by flow curves. Each model exhibits a specific required stress to trigger breakdown of molecular entanglements and subsequent flow of a fluid. This is defined as yield stress and biopolymer materials generally show Non-Newtonian behaviour when the yield stress is exceeded. (Poslinski et al., 1988). Non-Newtonian systems are therefore classified by relationships between shear rate and shear stress and the yield stress (Fig. 3.2).

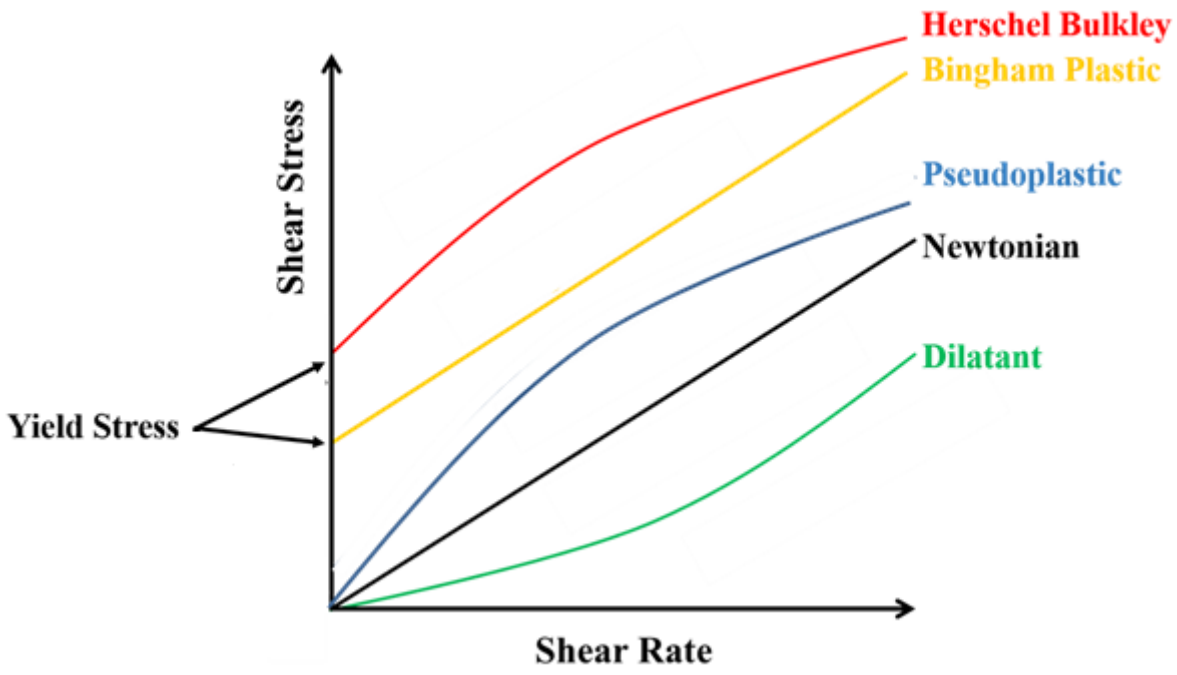

Figure 3.2 – Flow curves outlining differences between flow behaviour of Newtonian and Non-Newtonian systems (Adapted from Miri 2011)

Each classification of Newtonian and non-Newtonian system has a separate law for prediction of viscosity. However, each is adapted from the power law as it allows for analysis of shear thinning, Newtonian and shear thickening behaviour (Equation 3.8).

$$\sigma\ (\text{Pa}) = k\,\dot{\gamma}^{n} \qquad \textbf{Equation 3.8}$$

In Equation 3.8, the consistency index and flow index are represented by k and n respectively. In a Newtonian system n = 1 while n > 1 represents a shear thickening (dilatant) material and n < 1 represents a shear thinning material.

If Newtonian flow is observed once a yield stress has been exceeded, a material is characterised as exhibiting behaviour of a Bingham plastic. Stress can be calculated using Equation 3.9 which involves modification of the power law to include yield stress (σ_o).

$$\sigma\ (\text{Pa}) = \sigma_o + \eta\dot{\gamma} \qquad \textbf{Equation 3.9}$$

If viscosity of a fluid decreases as applied shear rate increases the material is described as showing shear thinning properties and is characterised as being pseudoplastic. When materials have a yield stress and then exhibit pseudoplastic flow this is described as Herschel Bulkley flow behaviour as shown in Equation 3.10.

$$\sigma\,(\mathrm{Pa}) = \sigma_o + k\,\dot{\gamma}^n \qquad \textbf{Equation 3.10}$$

If viscosity of a material increases with an increasing shear rate it is known as a dilatant material. Biopolymer solutions however, generally exhibit pseudoplastic behaviour with the extent of shear thinning dependent upon multiple factors such as molecular weight, confirmation and net charge. Furthermore, viscosity of polysaccharide solutions can be varied without changes in shear rate by modifying polymer concentration or environmental factors such as pH and temperature (Koliandris et al., 2008).

Reduction in viscosity by shear thinning is a result of the rate at which polymer chains become dis-entangled and re-entangled. When polymer solutions are subjected to shear rates greater than the yield stress, the rate of dis-entanglement exceeds the rate of re-entanglement. This causes a transition from a constant entanglement density to a density that decreases with increasing shear rate resulting in a reduction in viscosity (Graessley and Shinbach, 1974).

3.3.3 Characterising flow behaviour

Rheological analysis can be used in order to evaluate if a fluid exhibits shear thinning or shear thickening behaviour when a yield stress is exceeded. One such example is a shear ramp which exposes a material to increasing shear rates at a constant temperature. As applied shear rate rises, the viscous response of a material is measured and is often termed as dynamic viscosity. If viscosity decreases with increasing shear rate, a sample is classed as shear thinning. Conversely, an increase in viscosity with shear rate indicates a material is shear thickening (Fig. 3.3).

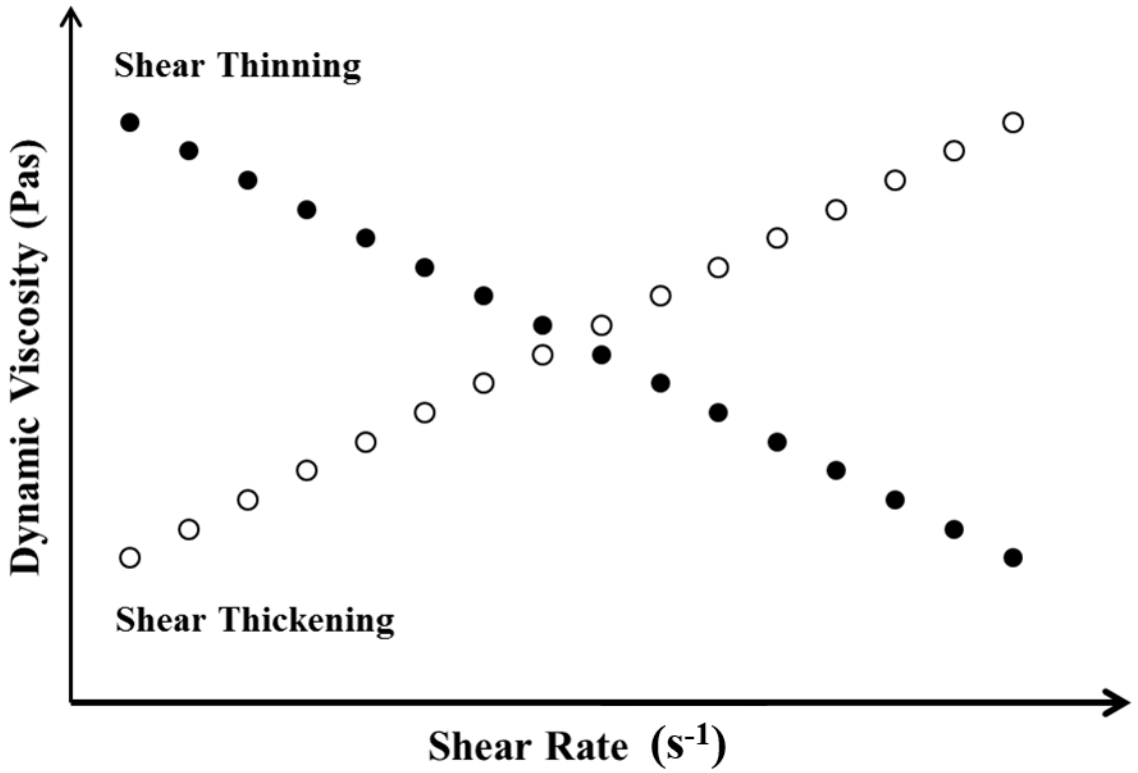

Figure 3.3 – Typical changes in dynamic viscosity of shear thinning and shear thickening materials in response to increasing shear rate

3.3.4 Intrinsic Viscosity

Another key factor in determining rheological properties of a material is the intrinsic viscosity. Intrinsic viscosity can be simply defined as the degree to which a material (polymer molecule for example) contributes to the viscosity of a solution in which it is dispersed. It has a close relationship with molecular weight such that it is often used to determine molecular weight of biopolymers. Molecular weight and thus, intrinsic viscosity are fundamental to a material's mechanical properties. This is because size of a polymer molecule has a direct effect on frequency of molecular entanglements and, thus viscosity. Additionally, molecular weight can also impact on the degree of crosslinking between polymer molecules, influencing the resulting modulus.

Intrinsic viscosity, however, is not determined in the same way as dynamic viscosity. While previously outlined techniques involved loading samples in between two plates on a rheometer, analysis of intrinsic viscosity is performed with a viscometer. In this work, intrinsic viscosity was determined using an Ostwald Viscometer (Fig. 3.4).

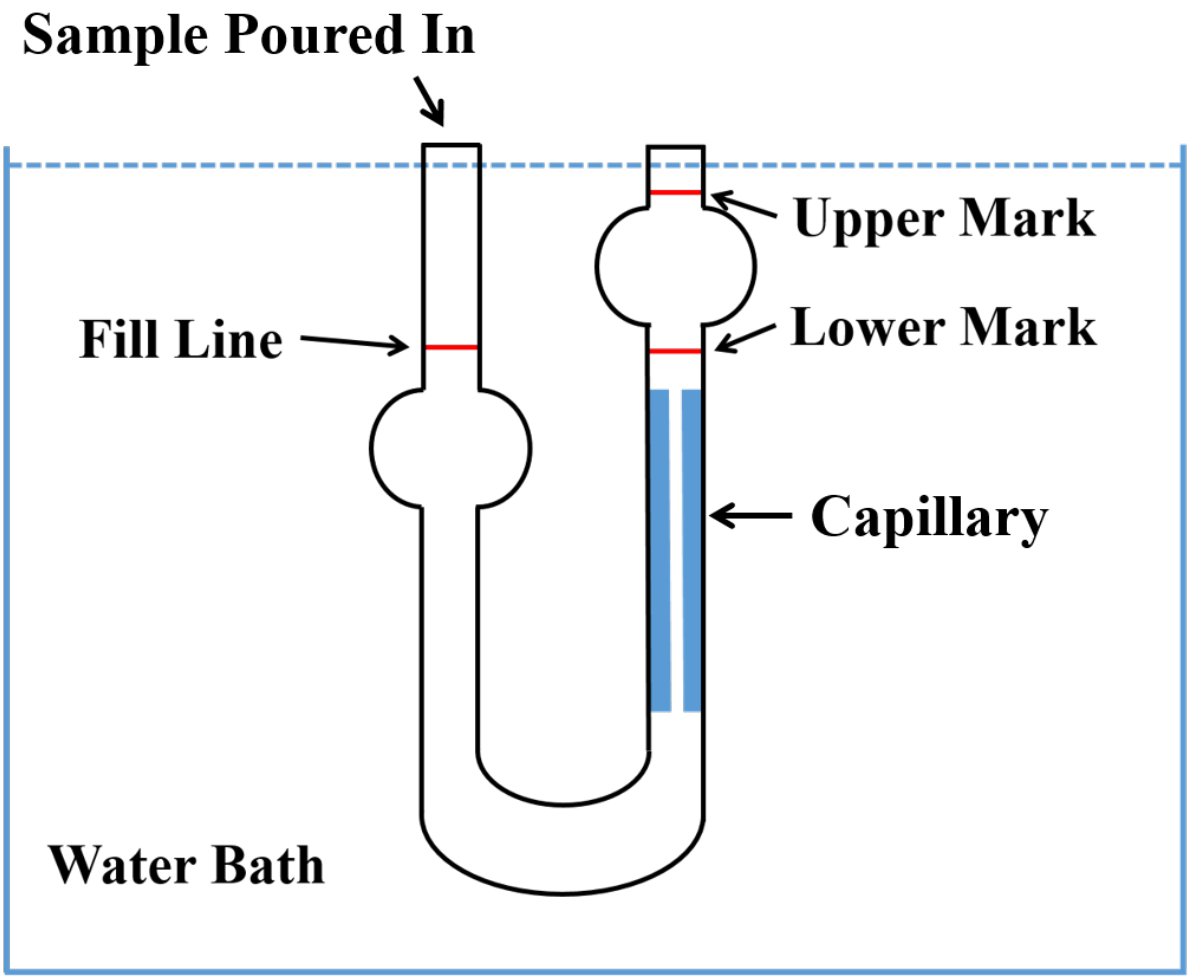

Figure 3.4 – Cartoon representation of and Otswald Viscometer immersed in a water bath

Viscometers are often immersed in a water bath at set temperature as intrinsic viscosity is highly temperature dependent. A series of polymer samples are diluted to increasingly lower concentrations (all low enough to prevent intermolecular interactions) and then viscosity measurements are extrapolated to a polymer concentration of zero. Each concentration is tested separately by pouring into a viscometer until there is sufficient volume to meet the 'fill line'. Suction is then applied at the opposite end of the viscometer using a pipette bulb which pulls the sample (e.g. a biopolymer solution) through a capillary and to the 'upper mark'. Suction pressure is then released from the pipette bulb causing the sample to flow to the 'lower mark'. The time taken to flow from the upper to lower mark is recorded and used to determine relative viscosity which is the first step of calculating intrinsic viscosity.

The relative, η_{rel} and specific viscosities, η_{sp} are calculated as described in Equations 3.11 and 3.12 respectively:

$$\eta_{rel} = \left(\frac{t}{t_0}\right)\left(\frac{\rho}{\rho_0}\right) \qquad \textbf{Equation 3.11}$$

$$\eta_{sp} = \eta_{rel} - 1 \qquad \textbf{Equation 3.12}$$

where t is the average (n=3) flow time of a sample solution at each concentration, t_o is the flow time of the solvent (usually water or salt solutions when measuring intrinsic viscosity of biopolymers), ρ is the sample density at each concentration and ρ_o is the density of the solvent. Due to the low concentrations used in determining intrinsic viscosity, $\rho/\rho_o = 1$.

Measurements are then extrapolated to infinite dilution using both Equations 3.13 (Huggins, 1942) and 3.14 (Kraemer, 1938):

$$\frac{\eta_{sp}}{c} = [\eta](1 + K_H[\eta]c) \qquad \textbf{Equation 3.13}$$

$$\frac{\ln(\eta_{rel})}{c} = [\eta](1 - K_K[\eta]c) \qquad \textbf{Equation 3.14}$$

where the intrinsic viscosity $[\eta]$ is taken as the mean of the intercepts from Equations 3.13 and 3.14 and K_H and K_K are the Huggins (1942) and Kraemer (1938) constants respectively. An example of a Huggins Kraemer plot used to determine intrinsic viscosity is represented in Fig. 3.5. The intercept between both trends is taken as the intrinsic viscosity.

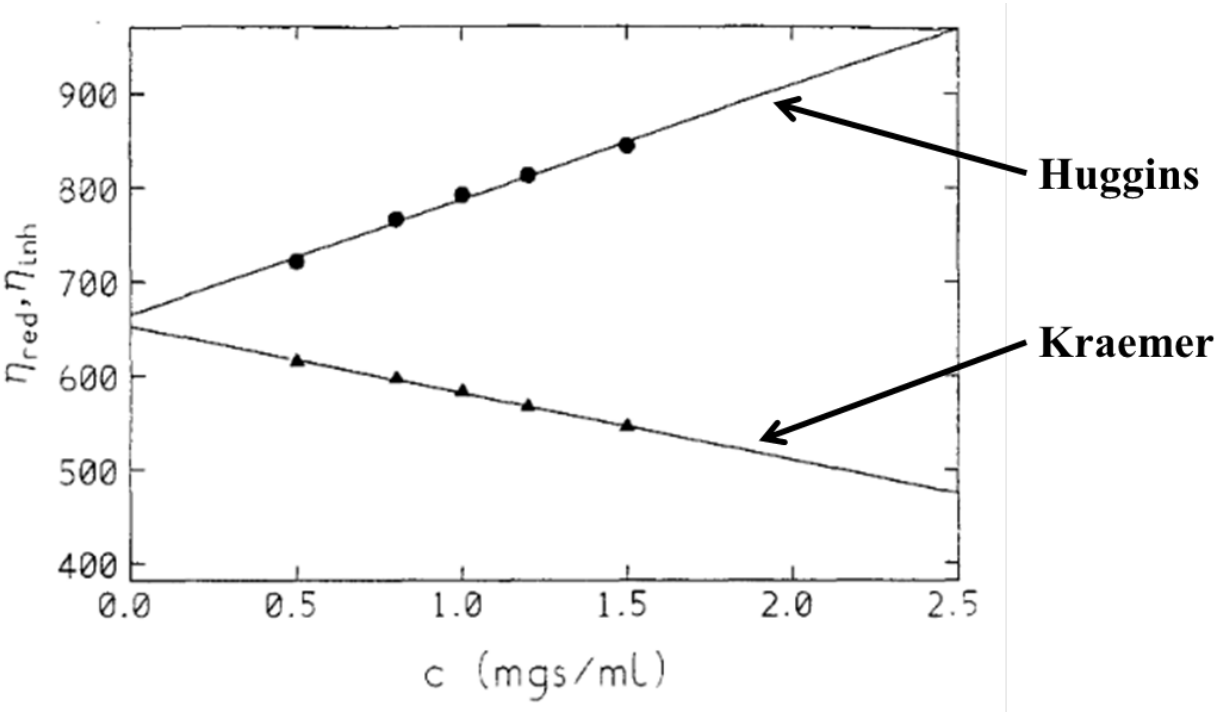

Figure 3.5 - An example of a Huggins/Kraemer plot used for determination of intrinsic viscosity (Reproduced from Harding, 1997 with permissions from Elsevier)

3.3.5 Viscoelasticity

Another important rheological property of biopolymer materials often investigated is viscoelasticity. A viscoelastic material is neither entirely Hookean nor Newtonian but instead exhibits intermediate properties. Consequently, viscoelastic materials display both 'solid-like' and 'liquid-like behaviour. Due to this, mechanical properties of viscoelastic materials are best evaluated via techniques that allow for simultaneous analysis of both elastic and viscous responses to applied stress (Picout and Ross-Murphy, 2003). A popular method for studying viscoelastic responses in materials is the use of oscillating shear stress rheology.

Rheological characterisation of viscoelastic materials using oscillation involves application of sinusoidal stress (or strain) to a sample immobilised between two plates. Commonly, the bottom plate remains stationary while the top plate applies an oscillatory stress. For the majority of techniques, the top, stress loading geometry is either a flat, parallel plate or a truncated cone and the geometry used can directly impact results obtained. This is due to differences in the ways stress is transmitted with parallel and coned plates. When using a coned plate, stress is applied uniformly across the geometry

diameter. Consequently, stress is homogenously applied to a sample fixed between the top and bottom plate. However, with a parallel plate, applied stress is a function of the shear rate that is applied which can show variance dependent upon geometry diameter. Therefore, shear stresses at the outer radius of a parallel plate can vary to those applied at the inner radius (Ewoldt et al., 2015). It is, therefore, often advisable to conduct rheological analysis using a geometry that allows for application of uniform stress as subsequent evaluation of mechanical properties is heavily based upon how a material responds to applied stress.

Stress is transmitted through a material as a result of applied sinusoidal strain. The manner in which transmission occurs can be subsequently used to determine material properties. Stress is dissipated by friction in viscous materials and transmitted in elastic materials. This results in different relationships between oscillation phases of stress and strain between viscous and elastic materials. Stress and strain are defined as being in phase for an elastic material and out of phase for a viscous material. Equation 3.15 can be used to determine sinusoidal shear stress with σ_o representing shear stress amplitude and δ, the phase lag. Angular frequency (rad/s) is represented by ω and t is the time corresponding to plate position.

$$\sigma = \sigma_o \sin(\omega t + \delta) \qquad \textbf{Equation 3.15}$$

A purely elastic material displays no phase lag and, thus, $\delta = 0$. Purely viscous materials exhibit a δ value of 90° due to viscous losses resulting in out of phase stress and strain (Miri, 2011). For a viscoelastic material, phase lag falls between 0 and 90° (Fig. 3.6).

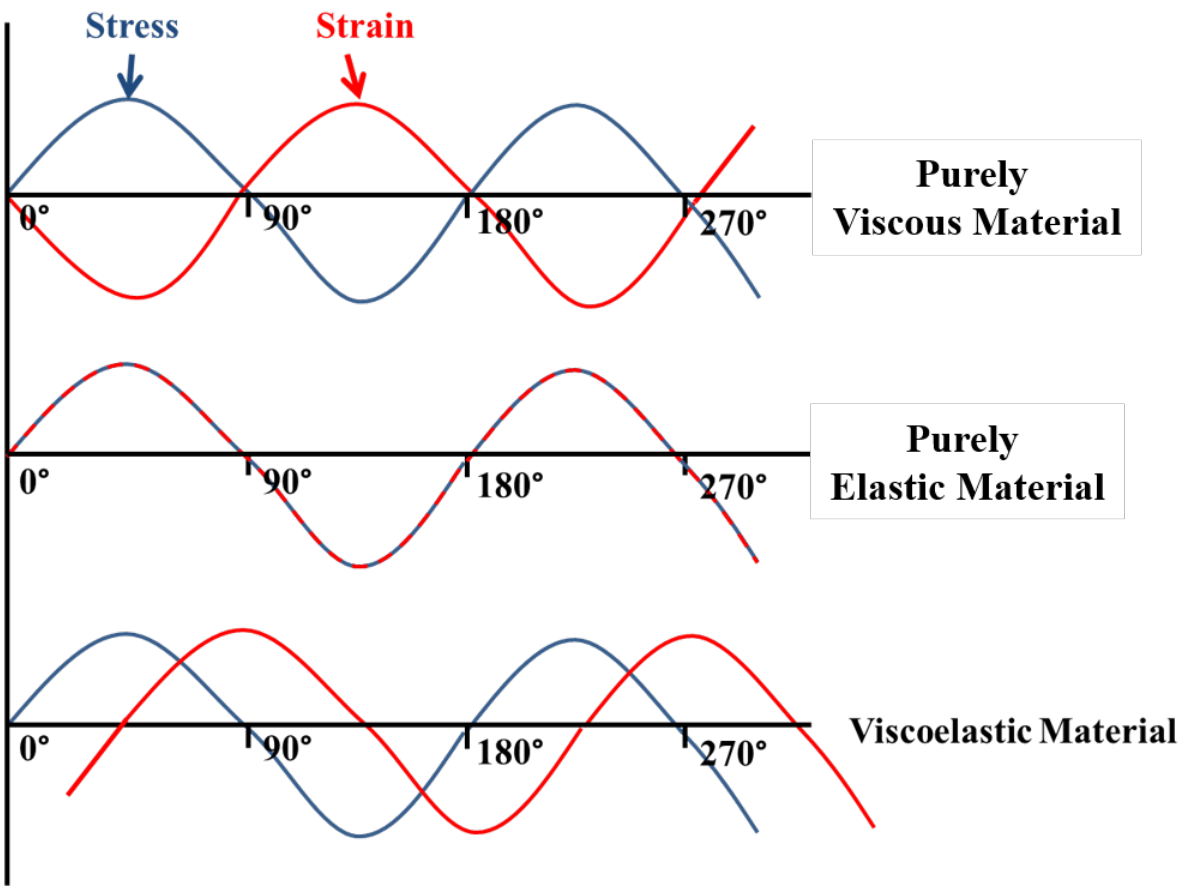

Figure 3.6 – Differences in phase lag between stress and strain when transmitted in purely elastic, purely viscous and viscoelastic materials

Biopolymer gels are good examples of viscoelastic materials and certain rheological measurements can be used to accurately define their properties. By studying in-phase and out-of-phase behaviour several key parameters can be derived that demonstrate mechanical properties. The elastic component of a viscoelastic material is represented by the elastic/storage modulus (G′). This is representative of the amount of energy stored in a material and how much is recovered per stress/strain cycle. Conversely, the viscous component is represented by the viscous/loss modulus (G″) and represents the amount of energy dissipated per cycle. Additionally, the overall stress response is represented by the complex modulus (G*) which is reflective of the ratios of stress and strain amplitudes regardless of storage or loss responses.

Furthermore, G′ represents the ratio of in-phase stress divided by strain. In a Hookean model G′ is completely independent of oscillatory frequency or shear stress. However, viscoelastic materials such

as biopolymers show dynamic changes in G′ as a response to changes in frequency or stress. G′ can be subsequently calculated using Equation 3.16.

$$G' \text{ (Pa)} = (\sigma°/\gamma°) \cos\delta \qquad \textbf{Equation 3.16}$$

Conversely, G″ is defined as the ratio of out-of-phase stress divided by strain and can be calculated using Equation 3.17.

$$G'' \text{ (Pa)} = (\sigma°/\gamma°) \sin\delta \qquad \textbf{Equation 3.17}$$

Complex modulus can be determined by incorporating G′ and G″ into Equation 3.18.

$$G^* \text{ (Pa)} = \sqrt{(G')^2 + (G'')^2} \qquad \textbf{Equation 3.18}$$

Additionally, the complex modulus can be used to determine another key parameter in viscoelastic materials, namely the complex dynamic viscosity (η*). This is representative of the ratio between G* and the frequency of oscillation (ω) and can be calculated using Equation 3.19.

$$\eta^* \text{ (Pas)} = G^*/\omega \qquad \textbf{Equation 3.19}$$

More simply, G′ is a representation of how ‘solid-like’ a viscoelastic material is and G″, how ‘liquid-like’. For example, a solid gel exhibits a G′ that is higher than G″ as the material is more solid like. If G′ is much greater than G″, a material is considered to be stronger than if the difference between them is smaller. Conversely, if G″ is higher the material is more liquid like. Based on relationships between G′, G″ and η* in response to changes in oscillatory frequency, mechanical spectra of viscoelastic materials can be determined and placed into 1 of 4 classifications as outlined in Fig. 3.7.

1. Dilute polymer solution – This classification is characterised by a dominance of G″ over G′. Both moduli rise with increasing frequency while complex viscosity is independent of frequency. This is because, at such low concentrations, polymer molecules do not interact and become entangled, thus viscosity remains constant.

2. Concentrated polymer solution – At low frequencies, a concentrated polymer solution is also characterised by a dominance of G″ over G′. However, as frequency increases, concentrated polymer solutions exhibit elasticity and G′ becomes greater than G″. This is because, at low frequencies, there is sufficient time between each oscillation to allow detachment of entangled polymer molecules. As frequency increases, reduced time between each oscillation makes molecules become harder to detach, thus triggering a rise in elasticity. Dynamic viscosity of a concentrated polymer solution also transitions from being frequency independent to inversely proportional to frequency.

3. Ordered polymer solutions – Ordered polymer solutions exhibit different relationships between G′ and G″ to concentrated solutions due to variances in how polymer molecules interact. In concentrated solutions, polymer molecules become entangled whereas ordered solutions are a network of rigid, ordered structures associated at junction zones. An ordered polymer solution is characterised by a G′ that is higher than G″ with both values being frequency independent. Viscosity decreases with increasing frequency and a weak gel can be poured, however an elastic response can be observed in response to small deformations. Ordered polymer solutions have commonly been termed 'weak gels' due to a dominance of G′ over G″. However, this term has come under recent debate due to behaviour exhibited by ordered polymer solutions in response to high stress. Conventional, 'true' gels respond to high stress by fracturing. Conversely, weak gels respond by flowing, thus exhibiting behaviour that is more typical of solutions rather than gels (Clark and Ross-Murphy, 2009).

4. True gel – Similar to a weak gel, a true gel exhibits a G′ that is higher than G″, however differences between the two values is much greater. Viscosity also reduces with increased frequency but true gels are solid and cannot be poured.

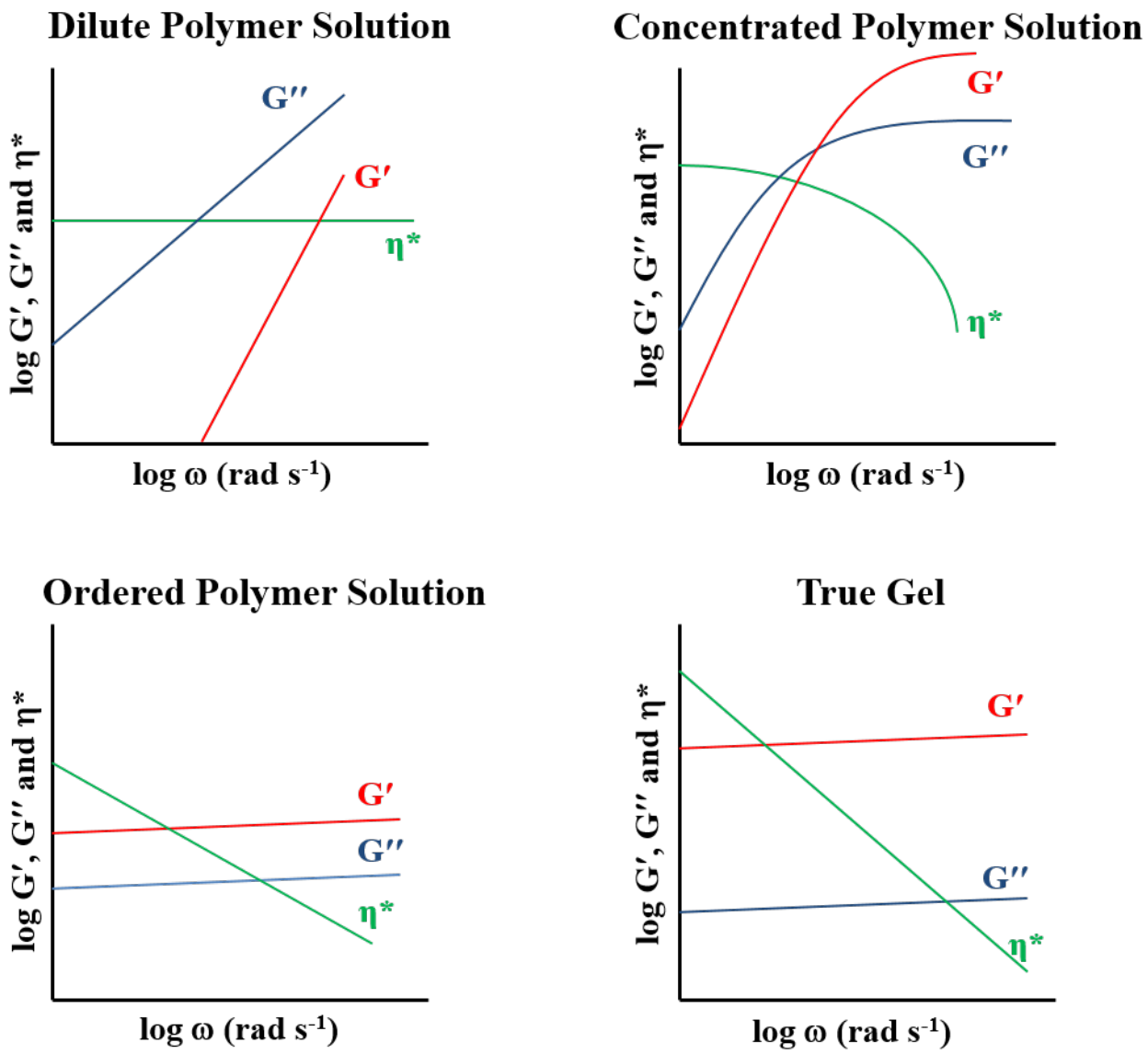

Figure 3.7 – Differences in mechanical spectra exhibited by dilute polymer solutions, concentrated polymer solutions, ordered polymer solutions and true gels

3.3.6 The linear viscoelastic region

When determining mechanical properties of viscoelastic materials, it is also important to consider the linear viscoelastic region (LVR). The LVR is a stress range within which a material exhibits a proportional strain response (Coleman and Noll, 1961). Therefore, within the LVR, a viscoelastic material exhibits behaviour reflective of a Hookean model. Since storage and loss moduli are determined based on stress/strain relationships, G′ and G″ are unaffected by stresses within the LVR. However, when a viscoelastic material is subjected to stresses that exceed the upper LVR limits, large deformation is triggered and G′ often declines as a material undergoes fracture (Winter and Chambon,

1986). This is a direct result of large deformation triggering loss of Hookean behaviour. Strain becomes inversely proportional to stress (Fig. 3.8) and the sample often fails.

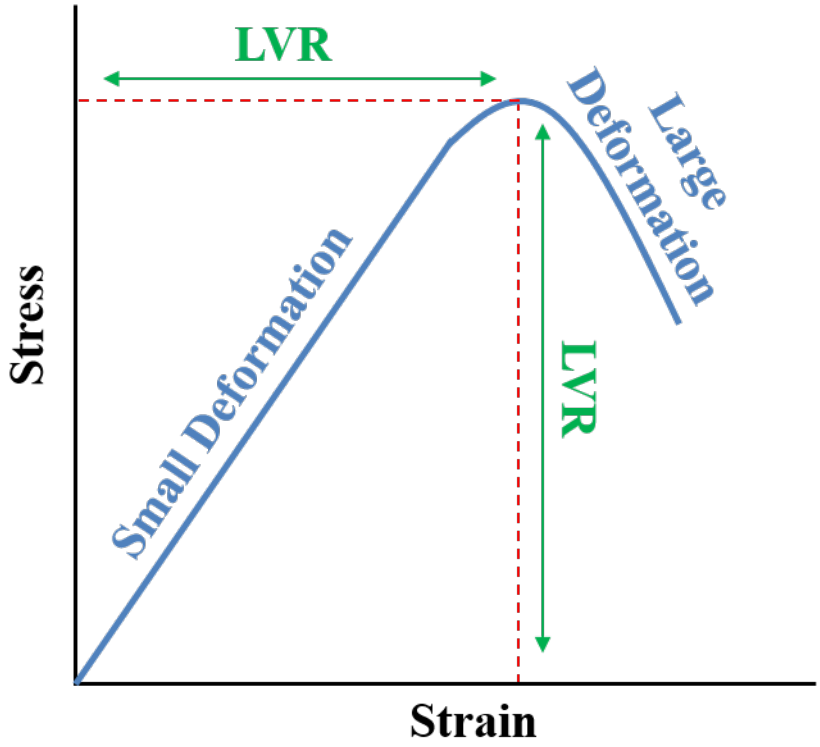

Figure 3.8 – Commonly observed relationships between stress in strain both within and outside the linear viscoelastic region of viscoelastic materials

It is often necessary to characterise the LVR of a viscoelastic material in order to allow for accurate determination of rheological properties. For example, in order to study the effect of oscillatory frequency to obtain mechanical spectra of a material, it is necessary to conduct measurements in a stress/strain range where a material exhibits elastic behaviour. If such a measurement is conducted outside the LVR, elasticity can be lost due to large deformation and fracture. Conducting such experiments within the LVR therefore allows for characterisation of relationships between viscoelasticity and molecular structure.

3.3.7 LVR determination

In order to determine the LVR, it is necessary to subject a material to range of shear stresses. Stress sweeps (or strain sweeps) are often therefore used. During a stress sweep a sample is kept at a constant

temperature but subjected to increasing oscillatory stresses. Strain responses to applied stress are measured and can be used to determine both G′ and G″. Stress is gradually increased until a material exhibits a decline in modulus as a result of stress-triggered deformation (Fig. 3.9). This indicates an onset of non-linear elasticity and reveals the stress at which a material will begin to break down.

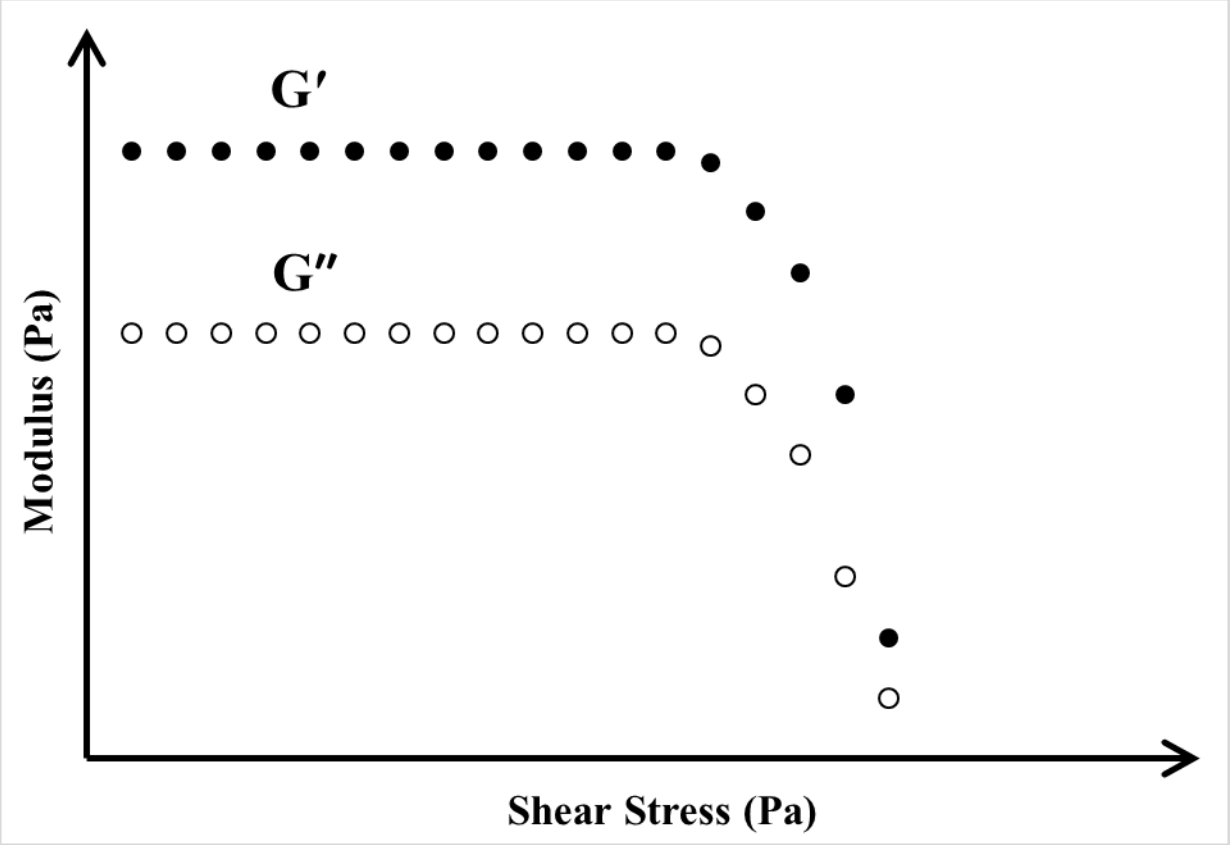

Figure 3.9 – Trends in elastic and viscous moduli associated with a linear to non-linear transition in response to increasing shear stress

The stress and strain ranges within which G′ and G″ remain constant represent the LVR. Once the LVR is determined subsequent rheological analyses can be carried out with an applied stress (or strain) that falls within this range. One such example is a frequency sweep which can be used to obtain mechanical spectra similar to those observed in Fig. 3.7.

3.3.8 Frequency Sweeps

During a frequency sweep, samples are subjected to changes in oscillatory frequency at a constant temperature and a constant stress or strain. G′ and G″ can be monitored in response to changes in

oscillatory frequency in order to determine mechanical spectra of the material as illustrated in Fig. 3.7.

3.3.9 Temperature sweeps

Analysis of moduli within the LVR can also be used to determine gelation properties of a material. Through modification of parameters such as temperature or *in situ* introduction of crosslinkers, gelation can be initiated in a sample loaded onto a rheometer. To monitor gelation, shear stress (or strain) and oscillatory frequency are kept constant with G′ and G″ monitored temperature. Prior to gelation, polymer solutions exhibit a higher value of G″ and lower value of G′. Progression through a sol-gel transition triggers a dramatic increase elastic modulus such that it becomes significantly higher than the viscous modulus. This is indicative of gelation into a solid, 'true gel' network that does not flow and is not pourable. Sol-gel transitions in biopolymers outlined in this thesis are triggered by a decrease in temperature (with the exception of collagen) and gelation profiles resemble that outlined in Fig. 3.10.

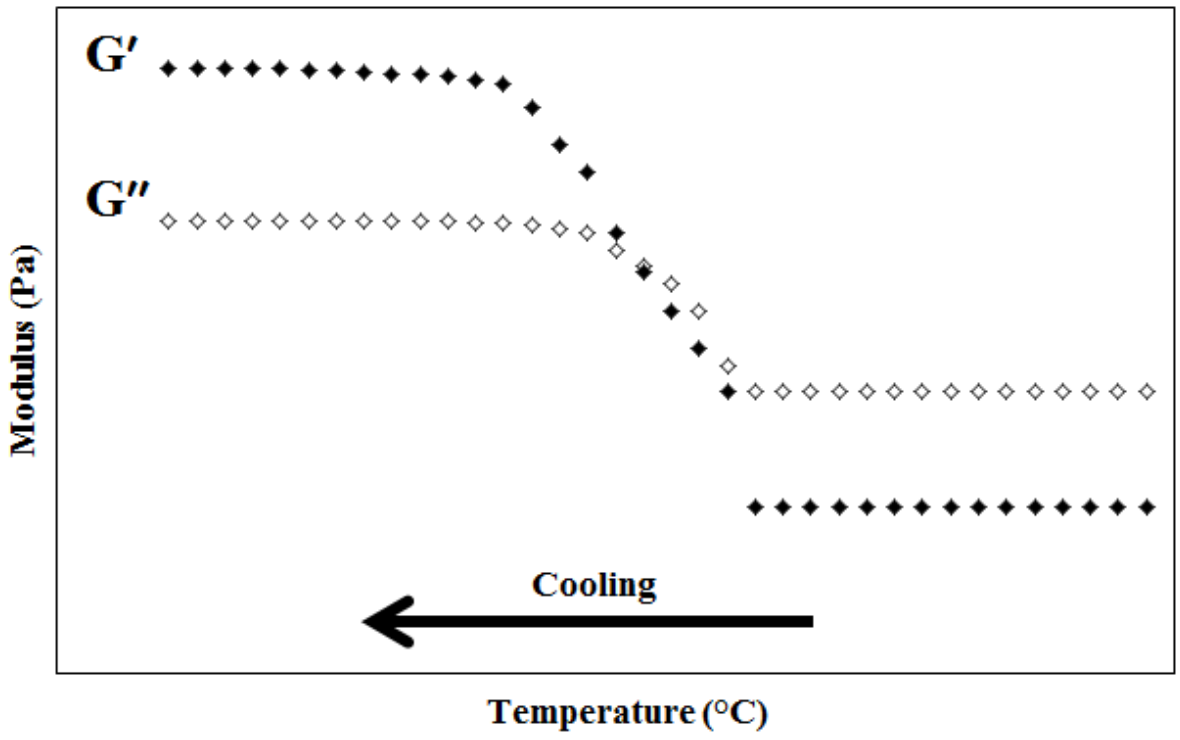

Figure 3.10 – A diagrammatical representation of changes in elastic and viscous moduli during a characteristic, temperature-dependant biopolymer sol-gel transition

Analysis of modulus during cooling can be used to evaluate the gelation temperature of a material. This is important in tissue culture applications as the required conditions for gelation of a biopolymer scaffold should not compromise cell viability i.e. gelation temperature should, ideally, be ~37°C.

Throughout this thesis, the significance of rheology in developing 3D culture models is outlined. Therefore, shear sweeps, stress sweeps, frequency sweeps and temperature sweeps are used extensively. Rheology is an effective way of determining properties such as matrix stiffness and elasticity. These are important factors to consider when studying viscoelastic materials such as biopolymer hydrogels. Such properties have a profound impact on cells encapsulated in 3D culture systems and, consequently, characterising rheological behaviour of biopolymer hydrogels is fundamental to the work in this thesis.

Chapter 4 – Tuning the Rheology of Gellan Gum Hydrogels for Cell Culture Applications

Results presented in this chapter are published in the International Journal of Biological Macromolecules

Moxon, S. R. & Smith, A.M. (2016) Controlling the Rheology of Gellan Gum Hydrogels in Cell Culture Conditions International Journal of Biological Macromolecules 84, pp. 79-86

4.1 Introduction

In previous chapters the importance of hydrogel mechanical properties to tissue engineering applications has been outlined. The modulus and elasticity of a gel, for example, are key to the successful engineering of a tissue with recent studies highlighting the integral role such properties have in determining *in vitro* cell behaviour (Wells, 2008). Certain tissue types develop much more efficiently in stronger, stiffer gels i.e. gels with a much higher elastic modulus (G′) while other tissue types are more suited to weaker, softer gels with a lower G′ value. This has previously been demonstrated in mesenchymal stem cell differentiation where matrix elasticity was shown to directly influence stem cell lineage specification (Engler et al., 2006). The exact mechanism behind how hydrogel/ECM mechanical properties influence cell behaviour is not fully understood but a complex system of cellular mechano-transduction provides a favoured hypothesis (Harley et al., 2008, Leipzig and Shoichet, 2009). It is theorised that cells apply tension and compression forces on a hydrogel matrix or native ECM. Through a pathway of mechano-transduction, cells are thought to be able to 'sense' the required force to deform a matrix, thus determining matrix stiffness and elasticity. Isoforms of myosin II, an ATP-dependent protein involved in contraction of muscle, trigger tension in actin resulting in transmission of intracellular forces to the surrounding matrix via focal adhesions (Fig. 4.1).

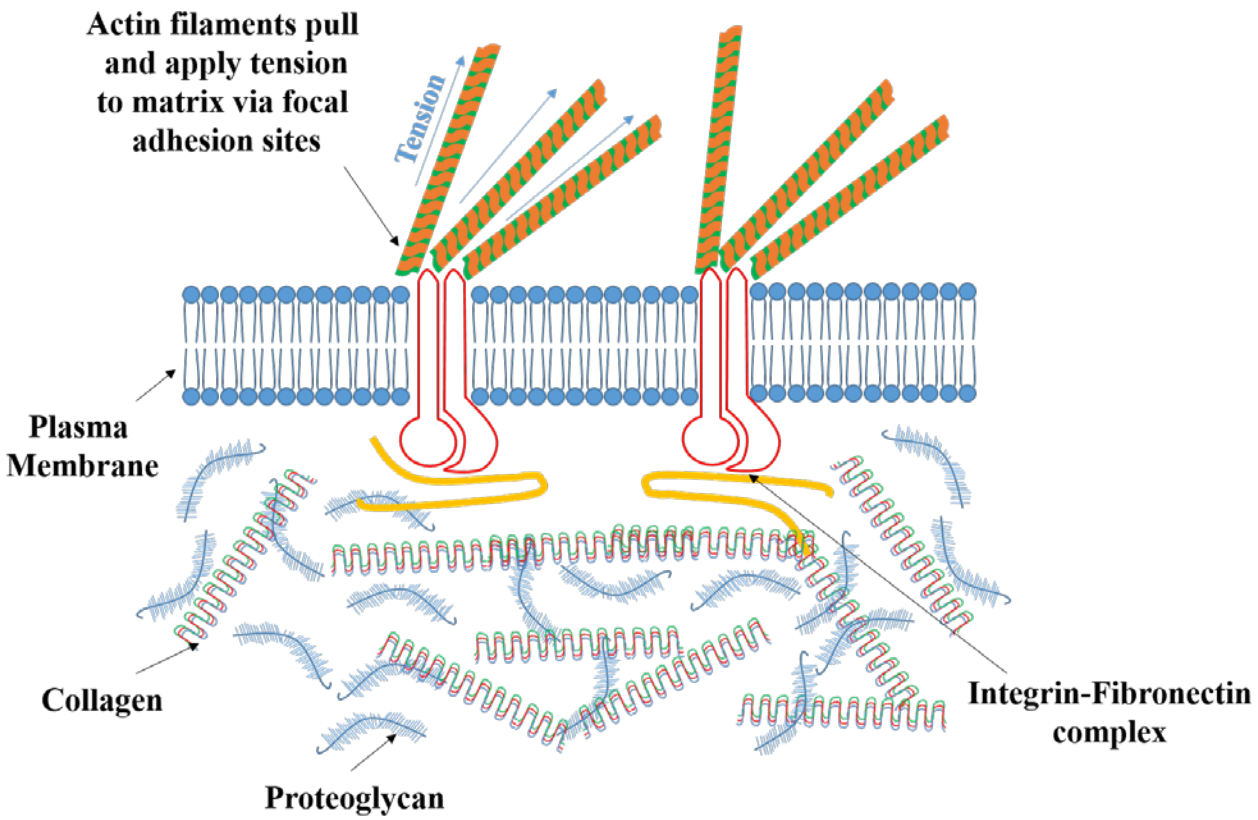

Figure 4.1 – Schematic demonstrating cell attachment to ECM via integrin-fibronectin binding complexes and application of tension to the matrix by actin filaments

While the exact mechanism is yet to be confirmed, many studies have been published highlighting the importance of scaffold mechanical properties in engineering of specific tissues. For example, it has been shown that engineering of bone tissue requires a strong and relatively stiff gel (Dessì et al., 2013). Conversely, the engineering of tissues such as cardiac or corneal tissue requires a matrix to exhibit a much more soft and elastic environment (Rafat et al., 2012, Annabi et al., 2013). In order to optimise a hydrogel for culturing a specific tissue these factors should therefore be considered. Thus, by tailoring the mechanical properties of a hydrogel to suit that of the tissue to be cultured, an *in vitro* mechanical behaviour could potentially be exhibited that is more reflective of the *in vivo* environment. Generally, the main ways to achieve variations in mechanical properties of hydrogels are either through varying the concentration of crosslinking agents or varying the polymer concentration. This can also impact on other factors however such as porosity and permeability as well as the osmotic

environment. A method of tuning mechanical properties without varying such factors could, therefore, be beneficial to the field.

Previous studies on gellan gum have demonstrated tunability of rheological behaviour by the application of pulsed sonication to gellan solutions (Taylor et al., 2012, D'Arrigo et al., 2012). Energy transmitted by pulsed sonication is sufficient to break gellan molecules into fragments of lower molecular weight. This results in a reduction in multiple rheological properties such as viscosity of gellan solutions and stiffness of gellan hydrogels. However, the full extent to which rheology of gellan can be tuned by sonication has not been investigated. Furthermore, the potential effects of using sonication to modify gellan hydrogel matrix applications are yet to be explored in the context of tailoring mechanical environments to influence cell behaviour. This chapter highlights the effects of tuning gellan rheology using sonication on native phenotype expression by mouse pre-osteoblast cells.

Mouse calvaria-derived/MC3T3-E1 cells are widely used in bone culture models. As osteoblast pre-cursors, MC3T3's have the ability to express multiple markers associated with osteogenic differentiation (Shiga et al., 2003, Choi et al., 1996, Franceschi and Iyer, 1992). One such marker is the expression of alkaline phosphatase/ALP which plays a key role in the deposition of calcium mineral deposits during osteogenesis. ALP promotes mineralisation by decreasing extracellular concentrations of pyrophosphate and increasing the concentration of inorganic phosphate (Golub and Boesze-Battaglia, 2007). A colorimetric assay based on hydrolysis of p-nitrophenyl phosphate to p-nitrophenol by ALP can be used to determine its activity (Dean, 2002). Since matrix stiffness is integral to the success of tissue culture, varying mechanical properties could have an effect on expression of differentiation markers.

In this study sonication was investigated as a mechanism to tune mechanical properties of gellan gum hydrogels cross-linked with cell culture media without altering concentrations used in the gelation

process. The effect of tuning matrix stiffness via sonication on ALP activity and viability of encapsulated MC3T3 cells was investigated.

4.2 Materials and Methods

4.2.1 Materials

Cell culture plastics were purchased from Sigma-Aldrich (Dorset, UK). Differentiation supplements and TrypLE™ dissociation enzyme were purchased from Thermo Fisher Scientific (Runcorn, UK). Low acyl gellan gum, herein referred to as 'gellan', was purchased from Kalys (Bernin, France). The StemTAG™ colorimetric alkaline phosphatase assay kit used for determining ALP activity was purchased from Cambridge Bioscience (Cambridge, UK). All other reagents and cell culture media and supplements were purchased from Sigma-Aldrich (Dorset, UK) unless otherwise stated and used without further purification.

4.2.2 Preparation of gellan gum solutions

Gellan solutions were prepared in 200 ml batches of 1% weight for weight. A desired final mass was prepared using deionised water i.e. for a 200 ml 1% solution, 200 g of deionised water and 2 g of low acyl gellan gum powder were used. Deionised water was heated to 85 °C using a magnetic hotplate stirrer. Gellan powder was then dispersed slowly in the water to prevent clumping and stirred at 900 rpm until fully dissolved. After complete hydration of gellan into solution, batches were re-weighed and any water lost through evaporation was replaced using a plastic Pasteur pipette. The gellan solutions were then transferred to airtight bottles and allowed to cool, preventing further evaporation.

4.2.3 Sonication of gellan solutions

Prepared solutions of gellan (1% w/w) were split into 20 ml aliquots in universal tubes. Pulsed sonication was applied using a Sonics Vibra Cell ultrasonic probe (Sonics®, Market Harborough, UK). A constant frequency of 20 kHz was applied to all samples but at different amplitudes varying from 10%-100%. Samples were sonicated using a fully immersed probe for 5 minutes with a 1 second

on/off pulse resulting in a total test time of 10 minutes. The amplitude of ultrasonic waves was varied among samples with a starting parameter of 10% amplitude and increasing up to 100%. Once a sample had been sonicated at a specific amplitude, the sample was not further sonicated at other amplitudes.

4.2.4 Rheology

The aim of this study was to investigate if pulsed sonication could be used to tune mechanical properties of gellan hydrogels and subsequently influence cell behaviour. However, before focussing on cell culture applications, the extent to which mechanical properties of gellan can be modified by sonication was investigated.

Rheological analyses were conducted to gain a more fundamental understanding regarding the effects of pulsed sonication at varying amplitudes on strength, elasticity and stiffness of gellan gels. Additionally, effects on dynamic viscosity and intrinsic viscosity were analysed. Stress sweeps, frequency sweeps, and gelation studies were conducted in order to investigate if gel modulus and elasticity could be directly controlled by sonication amplitude. Shear sweeps were used to demonstrate tunability of gellan solution viscosity. Moreover, the effect of sonication on intrinsic viscosity of gellan was used to determine if sonication could be used to tune molecular weight and, thus, provide a potential explanation for changes in rheological properties. Further rheological analysis then focused on studying how sonication affects mechanical properties of gellan hydrogels in conditions more specific to cell culture protocols.

Two different rheometers were used to analysis any changes in mechanical properties of gellan as a result of pulsed sonication. Tests were conducted on either a Bohlin Gemini rheometer or a Kinexus Pro rheometer. Both instruments were purchased from Malvern Instruments (Malvern, UK). All samples were tested in triplicate for each procedure with the average values for each data point plotted.

4.2.5 Stress sweeps

Samples were gelled prior to loading on a Bohlin Gemini rheometer by mixing 1% gellan (un-sonicated and gellan sonicated at 100% amplitude) with DMEM in a 1:1 ratio at 60°C using a hot plate stirrer. This resulted in a final gellan concentration of 0.5% w/w. Solutions were then allowed to cool to room temperature in 6-well plates with 3 ml gellan pipetted in each well. Hydrogels were subsequently formed via physical cross-linking mediated by cations present in DMEM (Table 4.1). In order to prevent batch to batch variance on ionic content of any DMEM used to create hydrogels, all gels were formed using media from the same single bottle of DMEM.

Table 4.1 – Ionic composition of Dulbecco's Modified Eagle's Medium

Salt	Concentration (mM)
NaH_2PO_4	1.0
NaCl	116.0
KCl	5.4
$MgSO_4$	0.75
$CaCl_2$	1.8

Elastic modulus (G′) and viscous modulus (G″) were measured in response to an increasing shear stress using a 20 mm serrated plate. Shear stress was increased from 1-1000 Pa with a constant frequency of 10 rad/s.

4.2.6 Dynamic measurements of modulus during cooling

Prior to loading on the rheometer, 1% gellan solutions sonicated at varying amplitudes were transferred into bottles (used to prevent water loss through evaporation) and heated to 95 °C in a water bath. This ensured gellan solutions maintain a disordered polymeric state and did not gel prior to sample loading. Gellan solutions were then mixed with DMEM in a 1:1 ratio resulting in final concentrations of 0.5% gellan gum and placed immediately back into a water bath at 95 °C until they were used for rheological analysis. Samples were loaded onto a Kinexus Pro rheometer with the top and bottom geometry maintained at 90 °C using an in-built software feature. Dynamic measurements

of G′ and G″ were performed at a frequency of 10 rad/s and a constant strain of 0.5%. Samples were cooled at a rate 2 °C per minute decreasing from 90 °C to 10 °C (total test time of 40 minutes). All measurements were performed within the linear viscoelastic region with a 55 mm cone and plate geometry. Prior to sample loading, the bottom plate and geometry of the rheometer were both heated to 90 °C to ensure samples did not cool prior to tests. Un-sonicated gellan was used as a control.

4.2.7 Frequency sweeps

Frequency sweeps were conducted to analyse the effect of changes in stress frequency on the modulus of gellan gum gels and if sonication changed such mechanical properties. Hydrogels of 0.5% gellan sonicated at 0%, 50% and 100% amplitude were formed as in 4.2.5 and moduli of resulting gels were analysed with increasing frequency from 1-100 rad/s using a Bohlin Gemini rheometer and a 25 mm serrated plate geometry.

4.2.8 Viscosity measurements

Shear sweeps were conducted on 0.5% w/w gellan exposed to varying amplitudes of sonication to analyse any changes in viscosity or flow behaviour. Samples were exposed to increasing shear rates from 1 rate of 1000 s^{-1} using a 45 mm coned geometry at a constant temperature of 20°C

4.2.9 Intrinsic viscosity and molecular weight

Intrinsic viscosity of all samples was determined using a U Tube Viscometer (Rheotek, Burnham-on-Crouch, UK) using calculations outlined in Chapter 3. The viscometer was immersed up to the fill level indicator in a water bath at 25°C. Samples were prepared at a variety of dilutions ranging from 0.02% to 0.06% gellan gum. Each sample dilution was made by mixing 1% gellan with water containing 10 mM NaCl. This was done in order to counteract the electroviscous effect that is reported to occur with gellan gum dispersed in water (D'Arrigo et al., 2012). Additionally, 10mM NaCl was used as the reference point. Time (in seconds) taken by each sample to flow between two reference points on the viscometer was measured. All samples were tested in triplicate.

The relative, η_{rel} and specific viscosities, η_{sp} were calculated as described in equations 4.1 and 4.2, respectively:

$$\eta_{rel} = \left(\frac{t}{t_0}\right)\left(\frac{\rho}{\rho_0}\right) \qquad \textbf{Equation 4.1}$$

$$\eta_{sp} = \eta_{rel} - 1 \qquad \textbf{Equation 4.2}$$

where t is the average (of 3 replicates) flow time of the gellan solution at each concentration, t_o is the flow time for the 10 mM NaCl solution, ρ is the density of the gellan solution at each concentration and ρ_o is the density of the 10 mM NaCl solution. Due to the low concentrations used, $\rho/\rho_o = 1$ (Harding, 1997).

Measurements were extrapolated to infinite dilution using both equations 4.3 (Huggins, 1942) and 4.4 (Kraemer, 1938):

$$\frac{\eta_{sp}}{c} = [\eta](1 + K_H[\eta]c) \qquad \textbf{Equation 4.3}$$

$$\frac{\ln(\eta_{rel})}{c} = [\eta](1 - K_K[\eta]c) \qquad \textbf{Equation 4.4}$$

where the intrinsic viscosity $[\eta]$ is taken as the is the mean of the intercepts from equations (3) and (4) and K_H and K_K are the Huggins and Kraemer constants respectively (Huggins, 1942, Kraemer, 1938).

The resulting intrinsic viscosities were then used to calculate molecular weight using the Mark-Houwink equation (Equation 4.5) where M represents molecular weight and the Mark-Houwink constants are represented by K and α. For gellan, K and α have been reported to be 0.00746 and 0.91 respectively (Bajaj et al., 2007).

$$\eta = KM^{\alpha} \qquad \textbf{Equation 4.5}$$

4.2.10 Rheology in cell culture conditions

The main focus of this study was the effect of sonication on cell culture applications of gellan gum. Rheological analysis of mechanical properties under cell culture conditions was, therefore, conducted.

4.2.11 Effect of sonication on gelation time of gellan in cell culture conditions

The effect of sonication on gelation time of gellan was measured using a customised controlled ion delivery stage mounted on the bottom plate of a Bohlin Gemini rheometer (Mahdi et al., 2016). Gellan samples were loaded onto dialysis tubing (MWCO 14,000 Da) that sat on filter paper inside a petri dish. The filter paper was soaked with 5 ml DMEM to trigger gelation before a 55 mm parallel plate geometry was lowered onto the sample (Fig. 4.2).

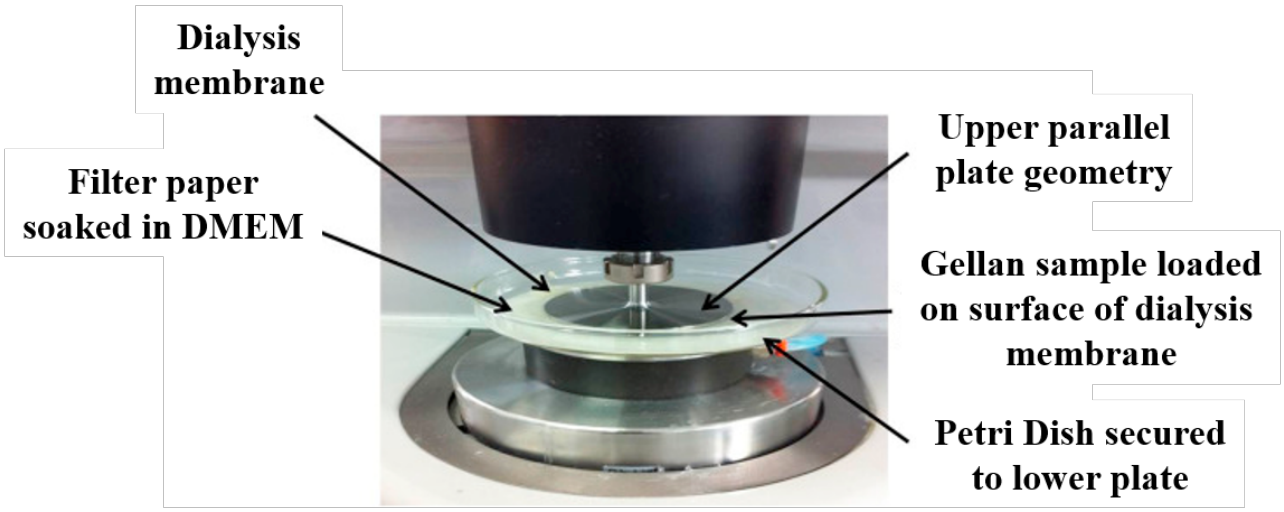

Figure 4.2– Controlled ion delivery system mounted on a Bohlin Gemini rheometer used to study gelation time of gellan hydrogels (adapted from Mahdi et al. 2016 with permissions from Elsevier)

Elastic and viscous moduli vs. time were observed to monitor any changes in gelation mechanics. Temperature was maintained at 37 °C using a Peltier temperature controlled parallel plate system and a strain amplitude of 0.5% was used at a constant frequency of 10 rad/s.

4.2.12 Frequency sweeps in cell culture conditions

To analyse the effect of sonication on rheological properties of cell culture hydrogels, samples were sonicated as in 4.2.3 and prepared in cell culture conditions. Un-sonicated, 50% sonicated and 100% sonicated gellan (1% w/w, autoclaved prior to use) was mixed with DMEM in a 1:1 ratio (3 ml with 3 mL) at 37 °C in wells of a 6 well plate and left for 30 minutes triggering gelation into 0.5% gellan gum hydrogels. Frequency sweeps were conducted with a 25 mm serrated parallel plate geometry using a Bohlin Gemini rheometer. Oscillatory frequency was increased from 1-100 rad/s and G′ and G″ were measured at a constant temperature of 37 °C at 0.5% strain with a geometry gap set at 1 mm.

4.2.13 Cell culture

After changes in rheology as a result of sonication had been investigated, the effect of tuning gellan gum properties with pulsed sonication on cell phenotype was evaluated using mouse MC3T3 pre-osteoblasts. Cells were cultured and passaged following standard culture procedures including aseptic technique, seeding and passaging as detailed below.

4.2.14 Cell culture – aseptic technique

To prevent contamination of MC3T3 cultures, standard aseptic procedures were followed. All cell culture protocols were carried out in a class II vertical laminar flow cabinet (Atlas Clean Air Ltd. UK). A solution of ~70% v/v ethanol (70% methylated spirits, 30% deionised water) was used to sterilise the cabinet prior to use. Any components requiring sterilisation were autoclaved using a Prestige Medical™ bench top autoclave.

4.2.15 – Seeding and expansion of MC3T3 cultures

Mouse preosteoblasts (MC3T3s) were cultured from stock vials (Sigma Aldrich UK). For cell seeding a single vial containing ~$1x10^6$ cells was removed from liquid nitrogen storage and placed into a water bath at 37 °C (Grant Instruments™ - Fisher Scientific, UK) for rapid defrosting. Once defrosted, contents of the vial were transferred to a centrifuge tube and 9 ml supplemented DMEM (10% FBS, 2.5% L-glutamine, 2.5% HEPES buffer and 1% penicillin/streptomycin) was slowly added before

centrifugation at 1000 RPM for 3 minutes using a Eppendorf Benchtop Centrifuge (ThermoFischer Scientific, UK). Supernatant was discarded and replaced with fresh supplemented DMEM before transfer to a T75 cell culture flask. Cells were cultured at 37 °C and 5% CO_2 in a humidified cell culture incubator (Triple Red, UK). Media was changed every 3 days and cells were passaged at 80% confluence (80% flask surface area coverage by cells).

4.2.16 Passaging of confluent cultures

Cells were detached from cell culture flasks using a trypsinisation protocol with TrypLE™ dissociation reagent. Briefly, media was aspirated from flask cultures and cells were washed with Dulbecco's Phosphate-Buffered Saline/DPBS at a volume equal to the volume of media used for flask culture (5 ml for a T25, 10 ml for a T75 and 20 ml for a T175). DPBS was removed and TrypLE™ was added (1 ml for a T25, 2 ml for a T75 and 4 ml for a T175) before incubation for 2 minutes at 37 °C and 5% CO_2. Cells were then observed with a VWR IT 400 Inverted Microscope (VWR, UK) to ensure all cells had detached. If cells remained attached an extra 2 minute incubation step was added. Once cells were detached enzymatic activity of TrypLE™ was stopped with the addition of supplemented cell culture media at a volume four times greater than the TrypLE™ volume. Cell suspensions were transferred into sterile centrifuge tubes and spun at 1000 RPM for 3 minutes. Supernatant was removed and replaced with the required flask volume of supplemented cell culture media. Cell suspensions were then diluted to 1 in 10 by transferring 10% of the suspension to a new flask and adding the remaining required volume of supplemented media. Flasks were transferred back into an incubator for further culture at 37 °C and 5% CO_2.

4.2.17 Encapsulation of MC3T3 preosteoblasts in sonicated and un-sonicated gellan

MC3T3 cells were cultured through 3 passages and used for encapsulation at passage 4. After detaching the cell monolayer, a cell count was performed using a glass haemocytometer. Based on the calculated cell number, cells were centrifuged at 3000 RPM for 1 minute before being resuspended in fresh supplemented αMEM at a density of $1x10^6$ cells/ml using Equation 4.6.

$$\text{Number of cells/ml} = \frac{\text{Number of cells counted}}{\text{Number of Squares Counted}} \times \text{dilution factor} \qquad \textbf{Equation 4.6}$$

Cell suspension was mixed with 1% sterile gellan (un-sonicated, 50% sonicated or 100% sonicated) at a volume ratio of 10:1 gellan to cells. Cell-loaded gellan (4 ml) was mixed with 4 ml of supplemented DMEM and left for 30 minutes to create cell-loaded hydrogels. Supplemented DMEM (3 ml) was placed on the surface of the gels and replaced every 3 days. Cell-loaded hydrogels were cultured in petri dishes for 7 days at 37°C, 5% CO_2 (Fig. 4.11).

4.2.18 Live/dead staining

To assess the proportions of live and dead cells within gellan constructs a live/dead staining protocol using calcein AM and propidium idiode was used. Media was aspirated and gels were washed with 3 ml DPBS. Excess DPBS was removed and replaced with 3 ml fresh supplemented DMEM. Live/dead staining was carried out with the addition of 5 µl calcein AM and 25 µl propidium iodide. Samples were incubated at 37 °C for 30 minutes in the absence of visible light before visualisation at 520 nm using an Olympus Fluorescence Microscope (Olympus Microscopes, UK).

4.2.19 Cell viability

Viable cell counts were obtained via MTT assays on cell-loaded gels. Gels were washed with DPBS and fresh media was added. MTT (0.1 mg/ml in DMSO) was pipetted onto each gel at a volume of 10% of the media volume. Samples were incubated for 4 hours at 37 °C before gels were homogenised and left overnight in DMSO to dissolve MTT crystals. 200 µl of each sample was added to a 96 well plate in triplicate and absorbance at 570 nm was measured using an Inifinte® F50 robotic plate reader (Tecan, UK). Cell counts were extrapolated using a standard curve of absorbance vs. 3D gellan cultures containing a known cell number (determined by cell counting prior to encapsulation). Each sample in the standard curve was treated in the same way as test samples with MTT incubated for 4 hours before gels were homogenised and left overnight in DMSO.

4.2.20 Alkaline phosphatase activity

Alkaline phosphatase (ALP) activity was determined using an assay based on p-nitrophenyl phosphate hydrolysis. The enzyme catalyses conversion of p-nitrophenyl phosphate to p-nitrophenol and absorbance of p-nitrophenol can be measured at 405 nm. A higher absorbance indicates a higher p-nitrophenol concentration and thus higher ALP activity. A StemTAG™ colorimetric alkaline phosphatase assay kit was used to carry out the reaction.

After 7 days of culture, excess media was removed from the surface of the gels before washing with DPBS. 0.5 ml of cell lysis buffer was added to each gel and samples were incubated for 20 minutes at 4°C. The solution was then removed from each gel and centrifuged separately at 12,000 X g for 10 minutes. Supernatant (cell lysate) was removed from each sample and 50 µl was added to wells of a 96-well plate in triplicate. Excess cell lysate was stored at -20°C. To initiate the reaction, 50 µl of StemTAG™ AP Activity Assay Substrate (p-nitrophenyl phosphate) was added and samples were incubated at 37 °C for 30 minutes before absorbance was read at 405 nm. Results were compared with a standard curve of concentrations ranging from 1-250 nM p-nitrophenol and standardised with MTT results to give a concentration of p-nitrophenol produced per 1000 cells.

4.2.21 Statistical analysis

ANOVA was used to statistically evaluate the experimental data. The Student–Newman–Keuls test was used as a post-hoc test for comparison of means. All statistical analyses were performed using Microsoft Excel and a p-value of <0.05 was considered significant.

4.3 Results

4.3.1 Stress Sweeps of sonicated and un-sonicated gellan hydrogels

Stress sweeps were performed to assess the effects of pulsed sonication at 100% amplitude on both the linear viscoelastic region (LVR) of low acyl gellan gum and the critical stress at which the polymer network deforms and begins to break down. Elastic and viscous moduli of un-sonicated

gellan displayed a greater LVR with increasing stress than sonicated gellan (Fig. 4.3) suggesting sonication reduces the LVR of gellan. Furthermore, sonication of gellan reduced the required stress for both an initial lowering in modulus and major deformation of the polymer network. An average stress of 65 Pa was required to trigger an initial decline in the modulus of un-sonicated gellan. The same decline took place at an average stress of 37 Pa in sonicated gellan. Major network deformation occurred at a stress of 863 Pa in un-sonicated gellan and 282 Pa in sonicated gellan, presenting a significant reduction in critical deformation stress. (Results are summarised in Table 4.2).

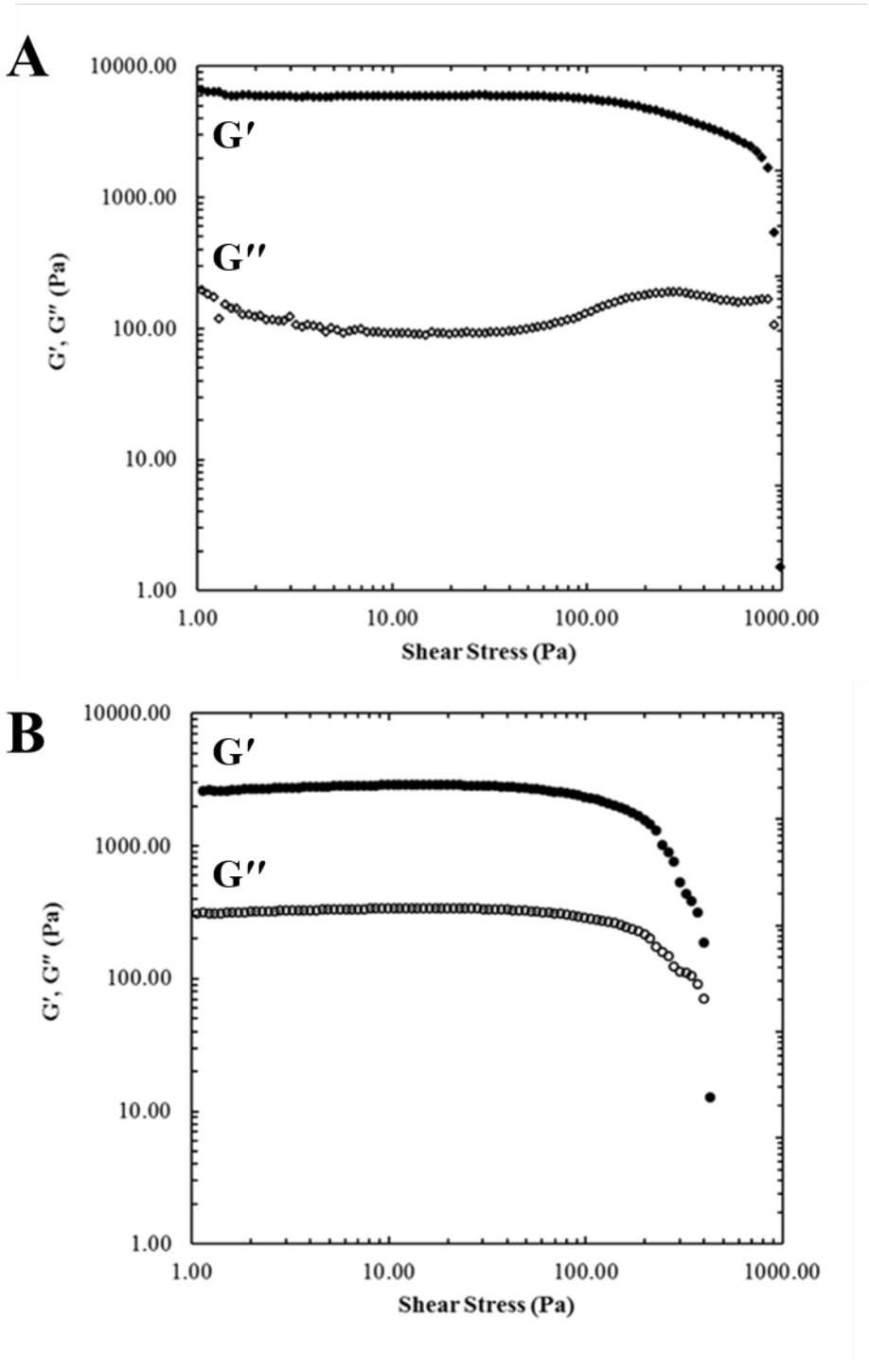

Figure 4.3 - Elastic and viscous modulus of un-sonicated (A) and 100% sonicated (B) 0.5% w/w gellan hydrogels in response to increasing shear stress

Table 4.2 - The effect of sonication amplitude on the modulus of 0.5% gellan gels in response to increasing stress

Sample	Initial G′ (Pa)	Required Stress to Lower Modulus (Pa)	Required stress for major deformation (Pa)
Un-sonicated Gellan	6555	65	863
Sonicated Gellan	2594	37	282

4.3.2 Temperature sweeps of gellan before and after sonication

Temperature sweeps were used to analyse if sonication had any effect on both the strength and gelation temperature of gellan gum hydrogels. Gelation temperature remained unchanged regardless of sonication amplitude with a sol-gel transition initiating at ~46 °C in all samples (Fig. 4.4). Elastic and viscous moduli of gellan gum hydrogels were, however, reduced as a result of sonicating polymer solutions prior to gelation. Furthermore, evidence of modulus tunability as a function of sonication amplitude was observed (Fig. 4.5) with gellan solutions subjected to the highest amplitude of sonication exhibiting the lowest G′ and G″. At a final temperature of 10 °C un-sonicated, 30% sonicated, 70% sonicated and 100% sonicated gellan displayed elastic moduli of 6370 Pa, 2670 Pa, 2495 Pa, and 1944 Pa respectively. This suggests a mechanism whereby gel strength can be tailored with the application of varying amplitudes of pulsed sonication (Results are summarised in Table 4.3).

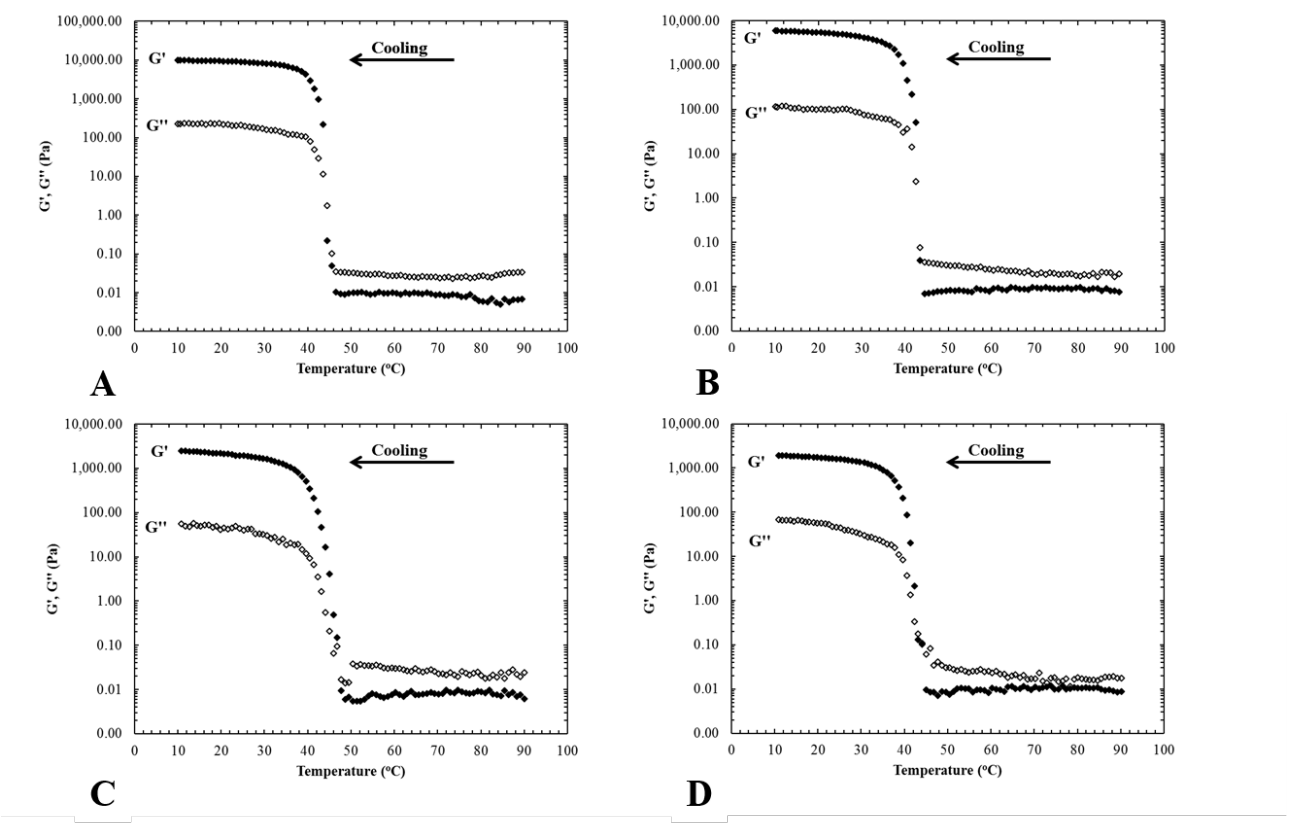

Figure 4.4 – Oscillatory cooling scans displaying both the elastic modulus (G′) and viscous modulus (G″) of 0.5% low acyl gellan hydrogels gelled using DMEM after no sonication (A), 30% amplitude sonication (B), 70% amplitude sonication (C) and 90% amplitude sonication (D)

Table 4.3 – The effect of sonication amplitude on the modulus and gelation temperatures of 0.5% gellan gum gels

Sonication Amplitude (%)	G' at 37 °C (Pa)	G'' at 37 °C (Pa)	G' at 10 °C (Pa)	G'' at 10 °C (Pa)	Gelation Temperature (°C)
0	9880	119	6370	230	46
30	5930	51	2670	113	46
70	930	18	2494	55	46
90	524	15	1944	67	46

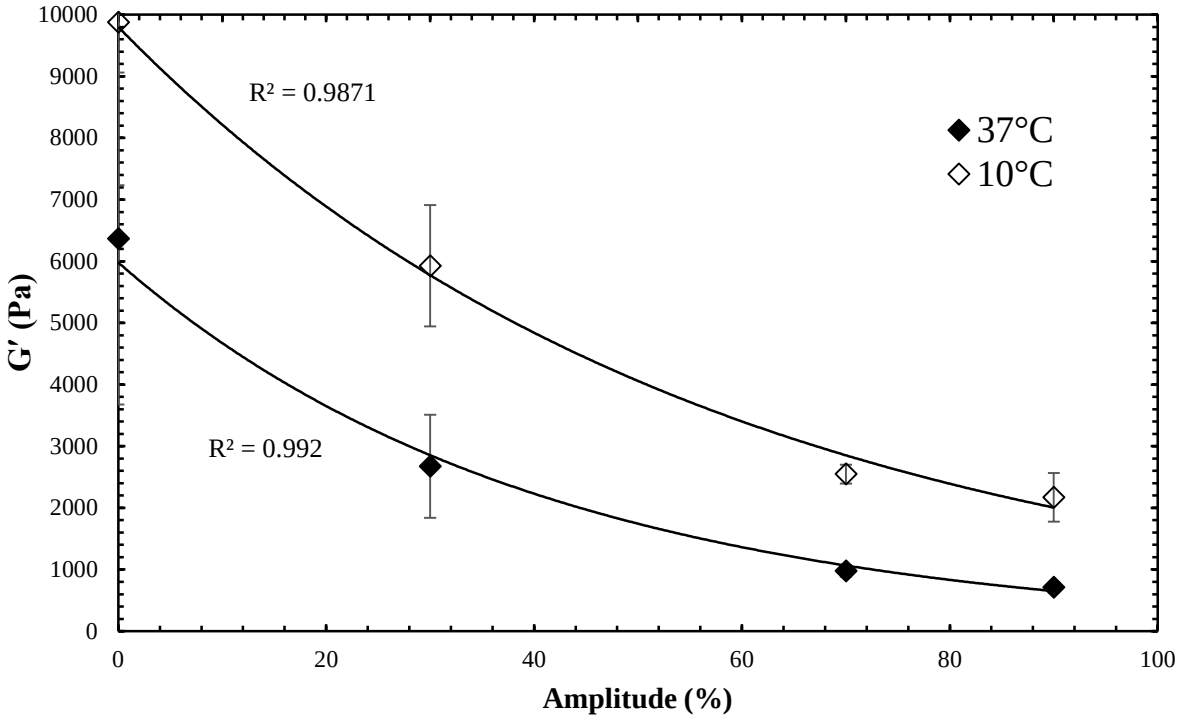

Figure 4.5 – A comparison of the G′ of 0.5% low acyl gellan gum hydrogels at 10 °C and 37 °C with no sonication, sonication at 30% amplitude, sonication at 70% amplitude and sonication at 90% amplitude

4.3.3 Frequency sweeps

Frequency sweeps of sonicated and un-sonicated gellan revealed a similar trend in matrix stiffness as a result of sonication with a reduction in G′ as a result of increasing sonication amplitude (Fig. 4.6). Additionally, samples exhibited an increase in G′ in response to exposure to higher oscillatory frequencies. At a frequency of 1 rad/s un-sonicated, 50% sonicated and 100% sonicated gellan displayed elastic moduli of 1610 Pa, 1421 Pa and 922 Pa respectively. The same samples exhibited moduli of 2621 Pa, 2169 Pa and 1820 Pa at 100 rad/s.

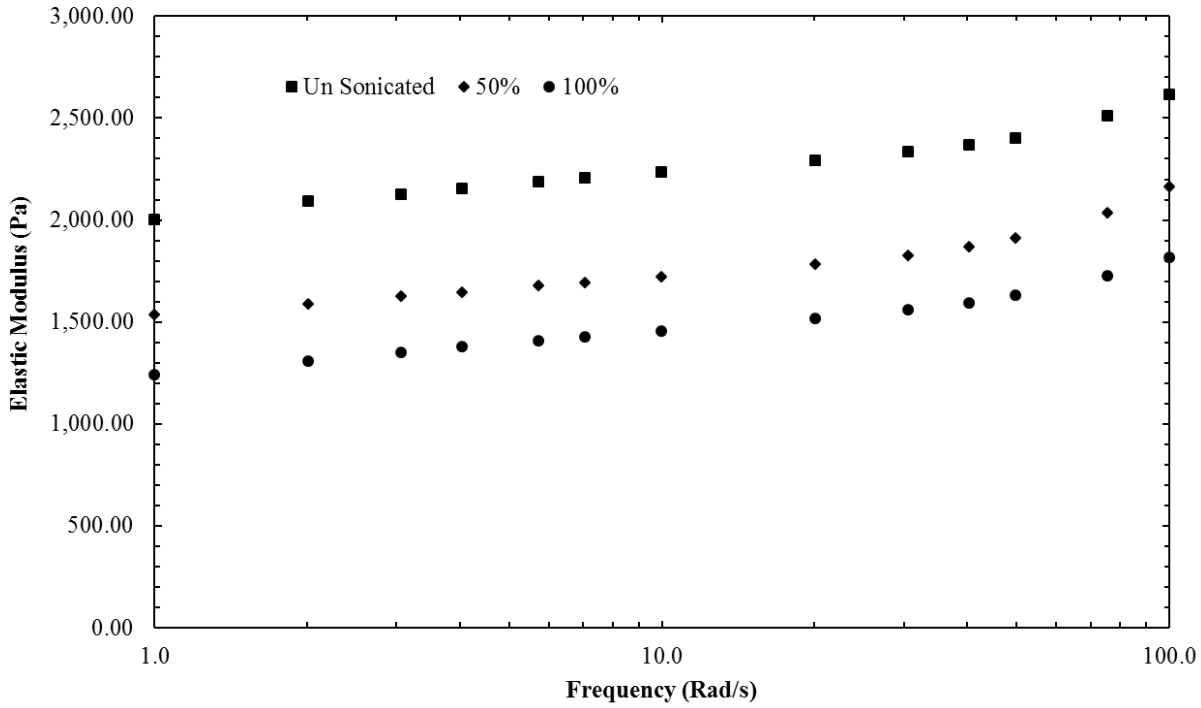

Figure 4.6 – Frequency sweeps of 0.5% low acyl gellan gum mixed with DMEM at 60 °C and gelled at room temperature after no sonication, sonication at 50% amplitude and sonication at 100% amplitude

4.3.4 Shear sweeps of gellan gum

Increasing sonication amplitude resulted in a reduction of instantaneous viscosity with a similar trend observed as in temperature sweeps (Fig. 4.7). A higher amplitude of sonication resulted in a greater reduction in viscosity. This reduction is most pronounce at low shear rates with an almost complete loss of Non-Newtonian behaviour in gellan samples sonicated at 100% amplitude. Therefore, viscosity and flow behaviour of gellan solutions were affected by sonication.

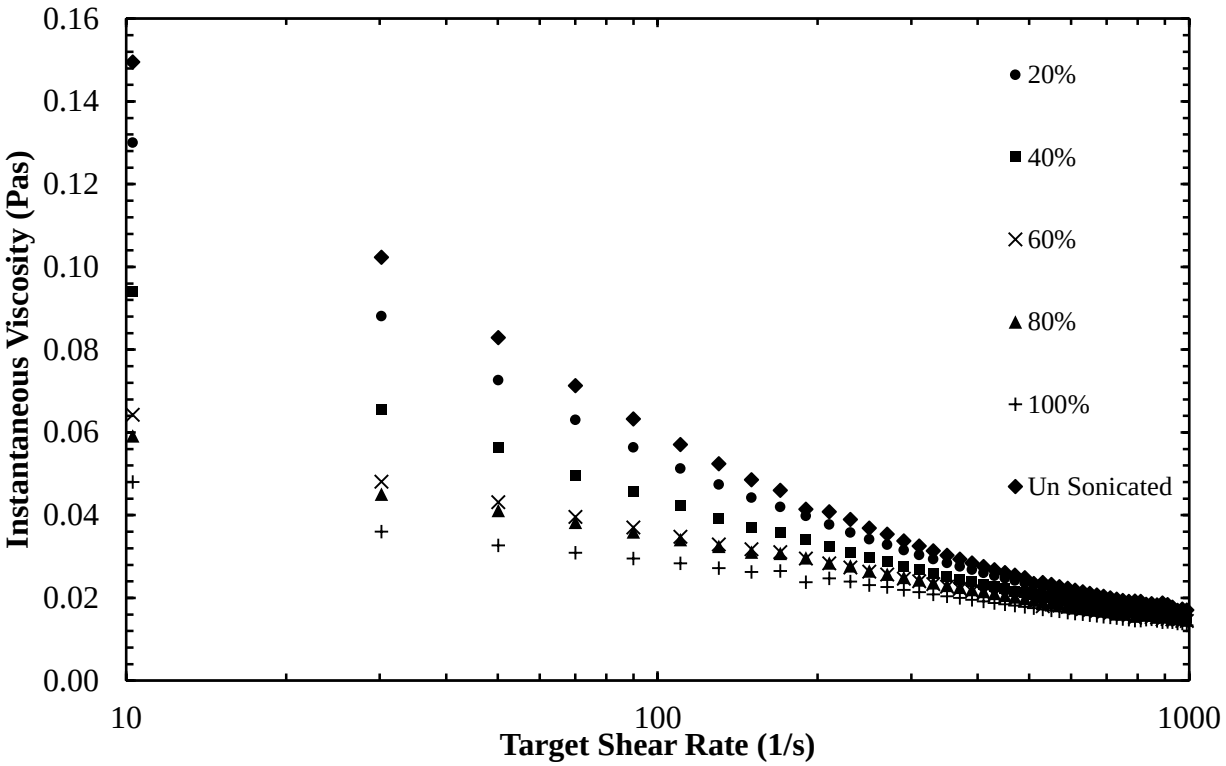

Figure 4.7 – The effect of increasing amplitude (%) of sonication on viscosity of 0.5% low acyl gellan gum in response to increasing shear rate

4.3.5 Determination of intrinsic viscosity and molecular weight

Sonication has been previously reported to lower the molecular weight of gellan gum (Taylor et al., 2012). Intrinsic viscosity and molecular weight are closely associated such that a lower intrinsic viscosity alludes to a reduction in molecular weight (Harding, 1997). Determination of intrinsic viscosity was, therefore, used to analyse if pulsed sonication of gellan gum at different amplitudes could be used to tune the molecular weight. Intrinsic viscosity was found to decrease as a function of increasing sonication amplitude (Fig. 4.8) and a similar trend was observed as in Fig. 4.5. A higher amplitude of sonication resulted in a greater reduction in intrinsic viscosity. This, consequently resulted in a reduction in molecular weight as determined by the Mark-Houwink equation with the same trend observed as with intrinsic viscosity (Table 4.4). Un- sonicated gellan was determined to have an approximate molecular weight of 3612 kDa. Sonication reduced molecular weight with 100% sonicated gellan presenting the lowest value (1269 kDa).

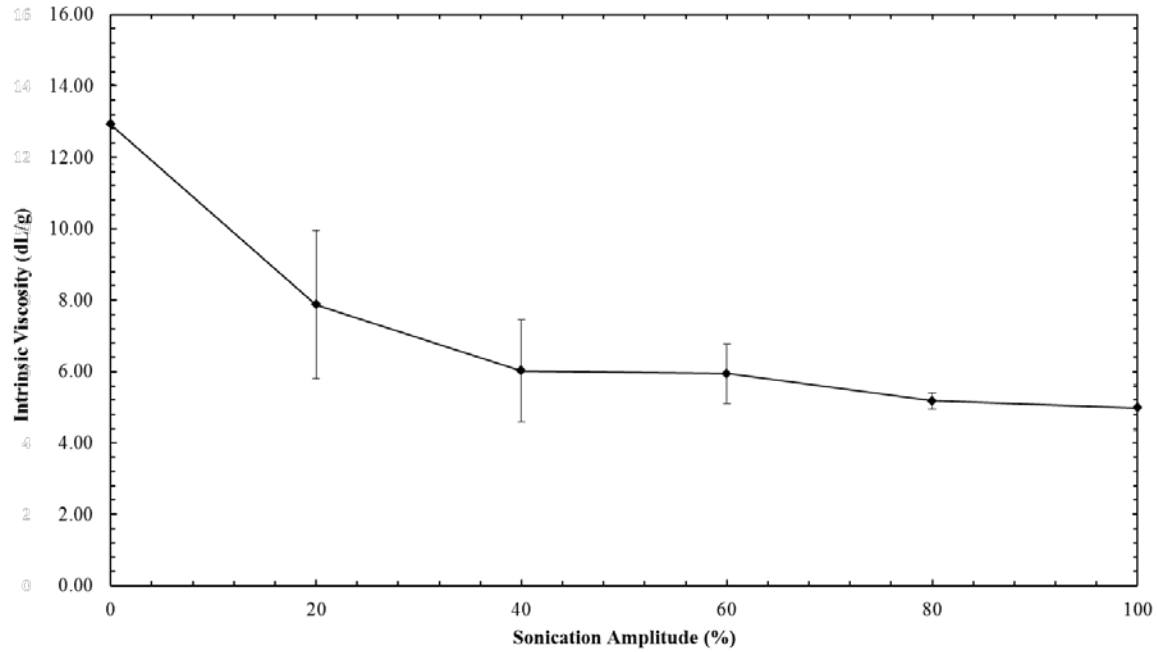

Figure 4.8 – The effect of increasing the amplitude (%) of sonication on the intrinsic viscosity of low acyl gellan gum (error bars represent +/- 1 standard deviation, n = 3)

Table 4.4 - Intrinsic viscosity and resulting calculated molecular weights of gellan subjected to varying amplitudes of sonication

Sonication Amplitude (%)	Intrinsic Viscosity (dL/g)	Calculated Molecular Weight (kDa)
0	12.91	3612.26
20	7.93	2095.23
40	6.01	1559.95
60	5.94	1539.89
80	5.21	1321.41
100	5.02	1269.44

4.3.6 Gelation in cell culture conditions

Gelation profiles were obtained to analyse any changes in gelation mechanics as a result of sonication. Sonication was, again, found to reduce the modulus of resulting hydrogels with un-sonicated gellan exhibiting a final G′ of 443.5 Pa versus 270.1 Pa for gellan sonicated at 100% amplitude. Gelation time when mixed with DMEM was, however, unaffected by sonication of gellan gum solutions (Fig. 4.9). All samples showed a rapid onset of gelation within the first 100 seconds. After the first 100 seconds, increases in G′ plateaued with a final modulus reached at between 330 and 350 seconds post injection of DMEM.

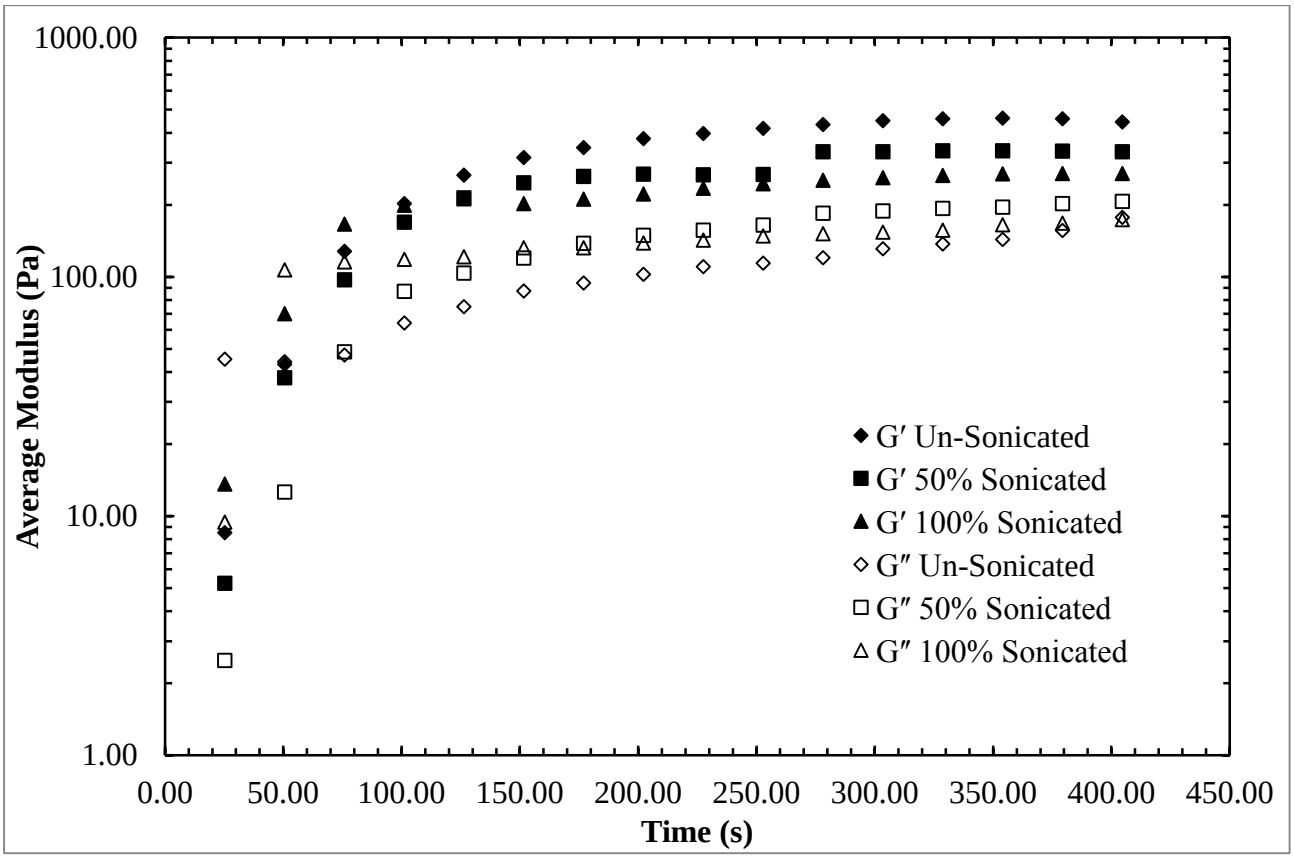

Figure 4.9 – Elastic and viscous moduli (G′ and G″) vs. time for sonicated and un-sonicated gellan when gelation is triggered by ions present in DMEM

4.3.7 Frequency sweeps of hydrogels formed in cell culture conditions

Frequency sweeps were conducted on hydrogel samples formed in cell culture conditions to assess if previous changes in modulus as a result of sonication would be observed. Tunability of mechanical properties as a function of sonication was demonstrated with un-sonicated gellan exhibiting greater elastic and viscous moduli than gellan sonicated at 50% and 100% amplitude (Fig. 4.10). At a frequency of 30 rad/s, for example, hydrogels formed from un-sonicated gellan displayed an average G′ of 1091 Pa. At the same frequency, hydrogels of gellan sonicated at 50% and 100% amplitude had a G′ of 857 Pa and 551 Pa respectively. Matrix stiffness was, therefore, reduced by nearly 50% as a result of sonicating native gellan gum at 100% amplitude prior to gelation into a cell culture scaffold.

All samples exhibited properties of a strong gel with a higher G′ than G″.

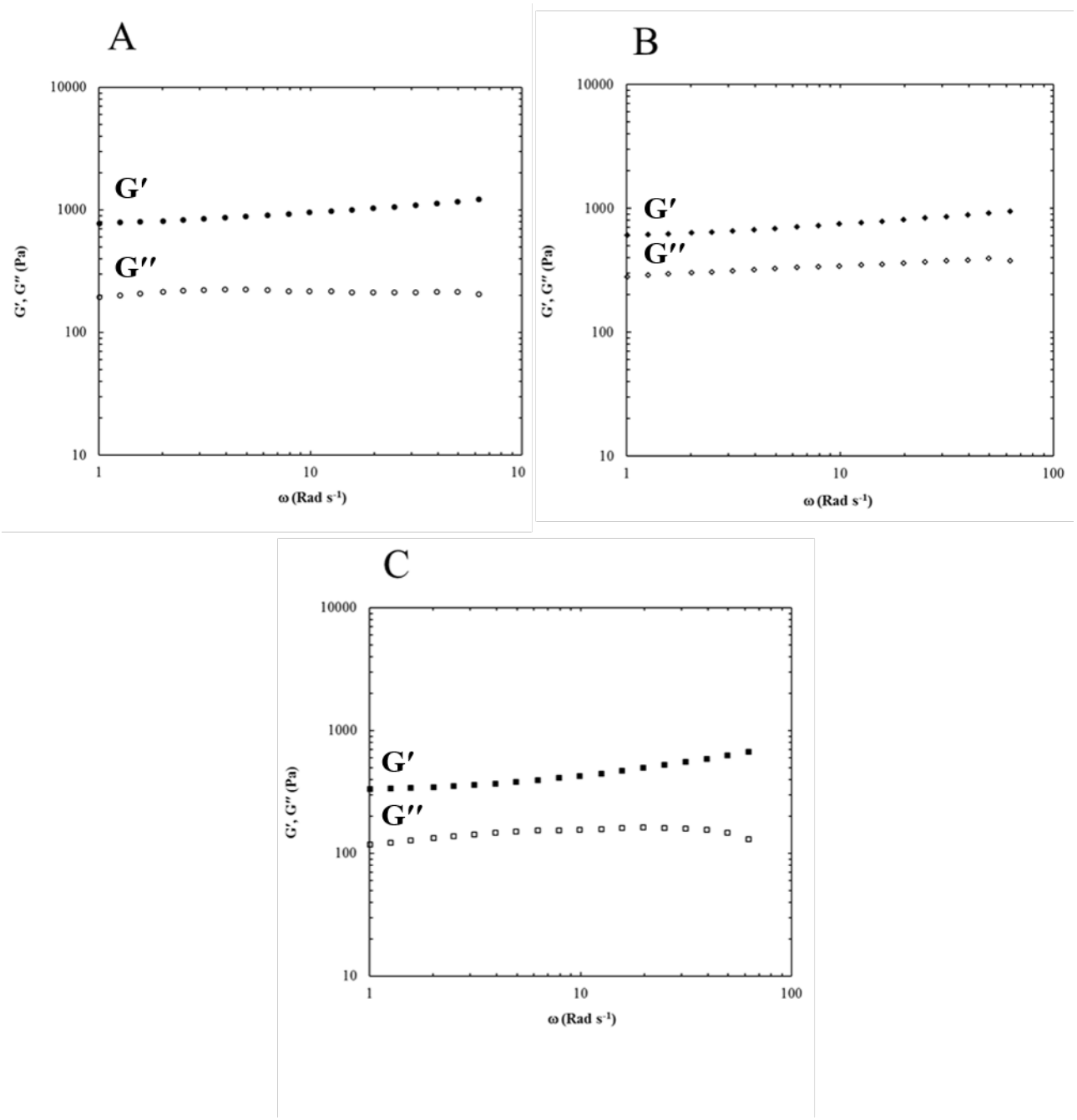

Figure 4.10 – Effect of sonication at (A) 0% amplitude, (B) 50% amplitude and (C) 100% amplitude on G′ and G″ of 0.5% gellan gum cell culture scaffolds in response to increasing oscillatory frequency

4.3.8 Cell-loaded hydrogels

Sonication appeared to have a visual impact on uniformity of hydrogels produced during the encapsulation process (Fig. 4.11). Hydrogels formed from gellan sonicated at 100% amplitude

appeared to be more homogenous whereas gels of un-sonicated gellan were more heterogeneous in appearance.

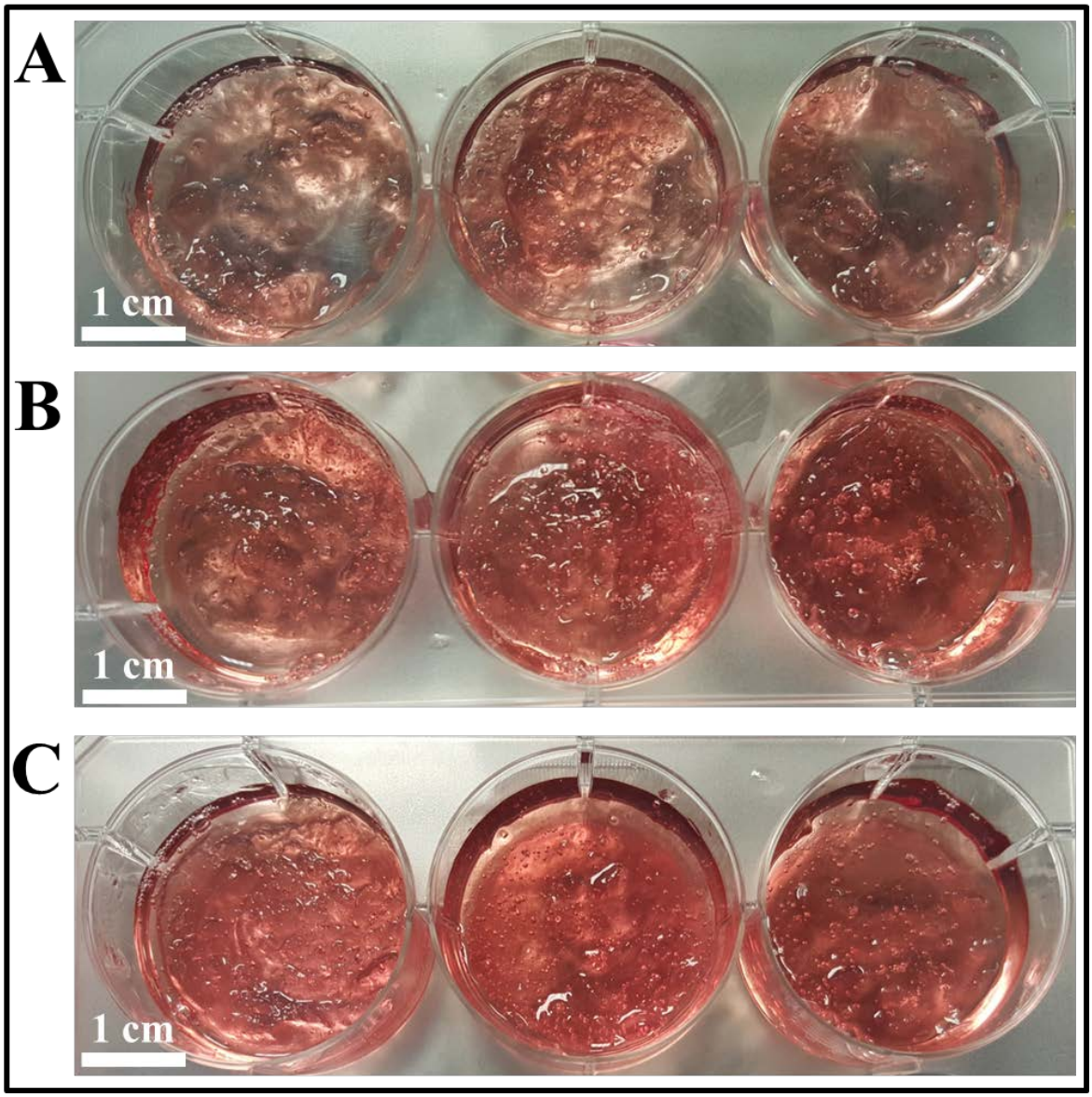

Figure 4.11 – Cell-loaded hydrogels created with A) un-sonicated gellan, B) gellan sonicated at 50% amplitude and C) gellan sonicated at 100% amplitude

4.3.9 Live/dead staining

Live/dead imaging revealed little difference between the three samples (Fig. 4.12). Culture in sonicated and un-sonicated gel yielded high proportions of live cells. No significant numbers of dead cells were present (indicated by the lack of red fluorescence). Cells appear to be dispersed uniformly through hydrogel matrices.

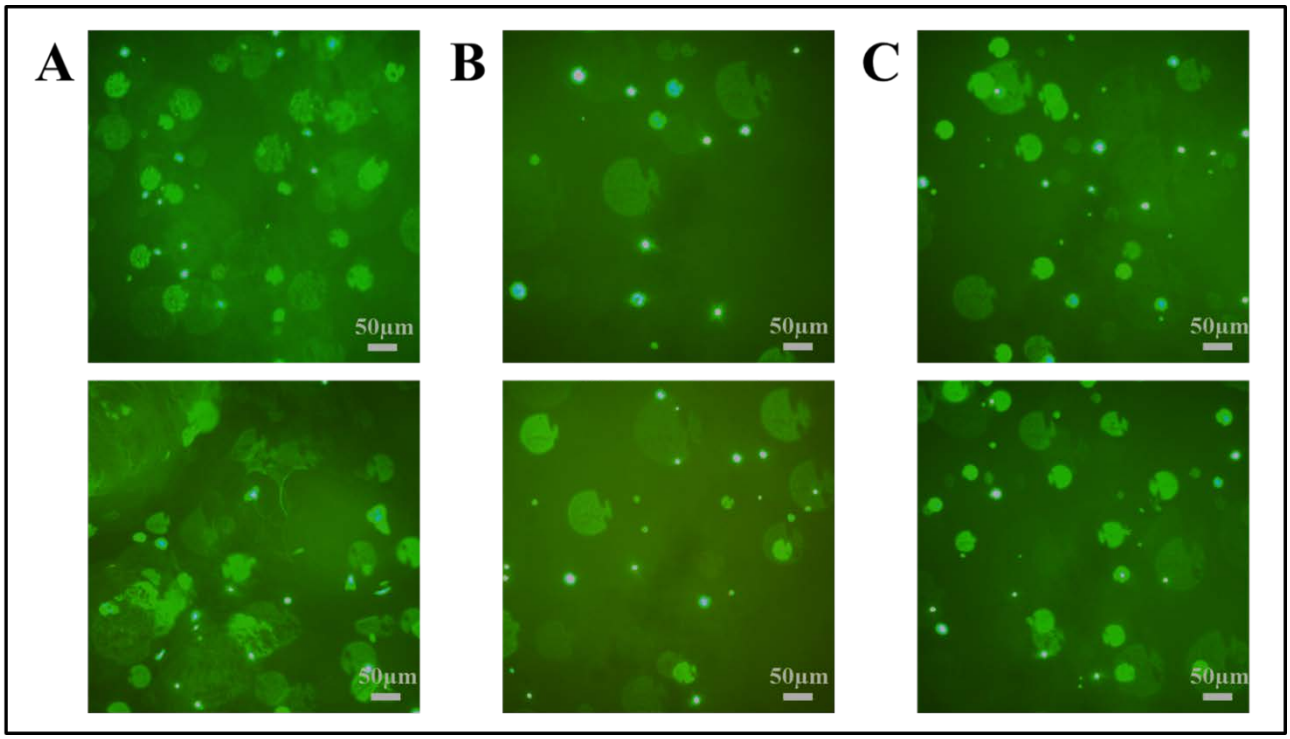

Figure 4.12 – Live/dead staining results for MC3T3's encapsulated in A) un-sonicated gellan, B) gellan sonicated at 50% amplitude and C) gellan sonicated at 100% amplitude – (colour corrected using Microsoft PowerPoint - green spots indicate presence of a live cell)

4.3.10 Cell viability

Cell viability was determined via MTT assays as a means of standardising results of ALP assays. Differences in the number of viable cells 7 days post encapsulation were observed between the three samples (Fig. 4.13). Moreover, variances between number of viable cells in each sample were deemed significant by statistical analysis (p value <0.05). Un-sonicated gellan yielded the lowest number of viable cells with an average of $9.18x10^5$ viable cells. Gellan sonicated at 50% amplitude contained an average of $1.07x10^6$ viable cells with gellan sonicated at 100% amplitude showing the highest average viable cell count ($1.27x10^6$). However, results presented in Fig. 4.12 do not show evidence of significant amounts of cell death in any samples so variances in the average number of viable cells are unlikely to be a result of apoptotic activity.

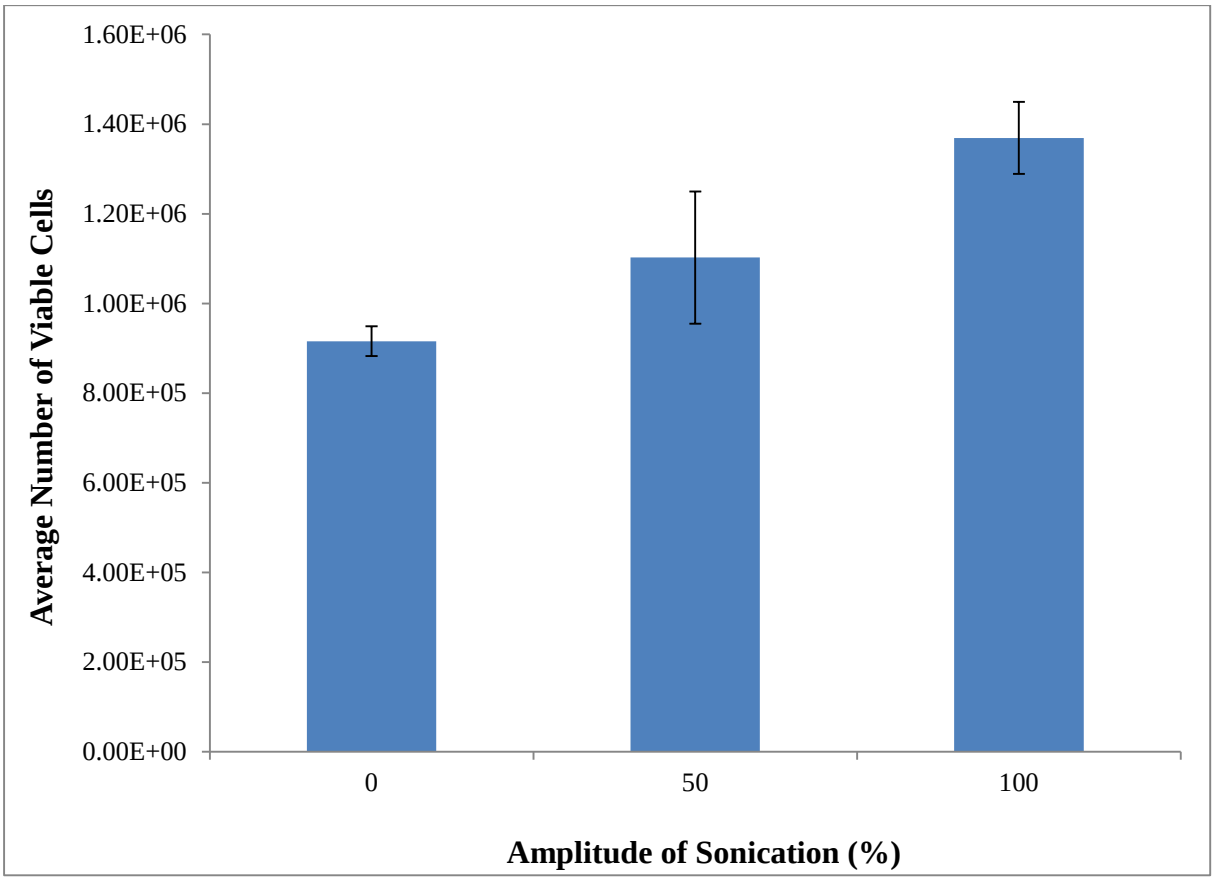

Figure 4.13 – Number of viable cells 7 days post encapsulation determined via MTT assay in un-sonicated gellan, gellan sonicated at 50% amplitude and gellan sonicated at 100% amplitude (error bars represent +/- 1 standard deviation, n = 12)

4.3.11 Effect of gellan sonication on ALP activity in encapsulated MC3T3 cells

ALP activity was found to decrease with increasing sonication amplitude as indicated by a reduction in p-nitrophenol concentration (Fig. 4.14). The concentration of p-nitrophenol produced by each culture was standardised to yield per 1000 cells by incorporating results from the MTT assay using Equation 4.6.

$$[p-nitrophenol]per\ 1000\ cells = \frac{[p-nitrophenol]produced\ by\ all\ cells}{number\ of\ viable\ cells} \text{ x } 1000 \quad \textbf{Equation 4.6}$$

Cells encapsulated in un-sonicated gellan produced the highest p-nitrophenol concentration per 1000 cells (130 pmol). The lowest yield was seen in cells encapsulated in 100% sonicated gellan (50 pmol). When statistical analysis of data was performed results for all samples were found to be significantly different ($p < 0.05$). A summary of statistical results for each sample can be found in Table 4.4.

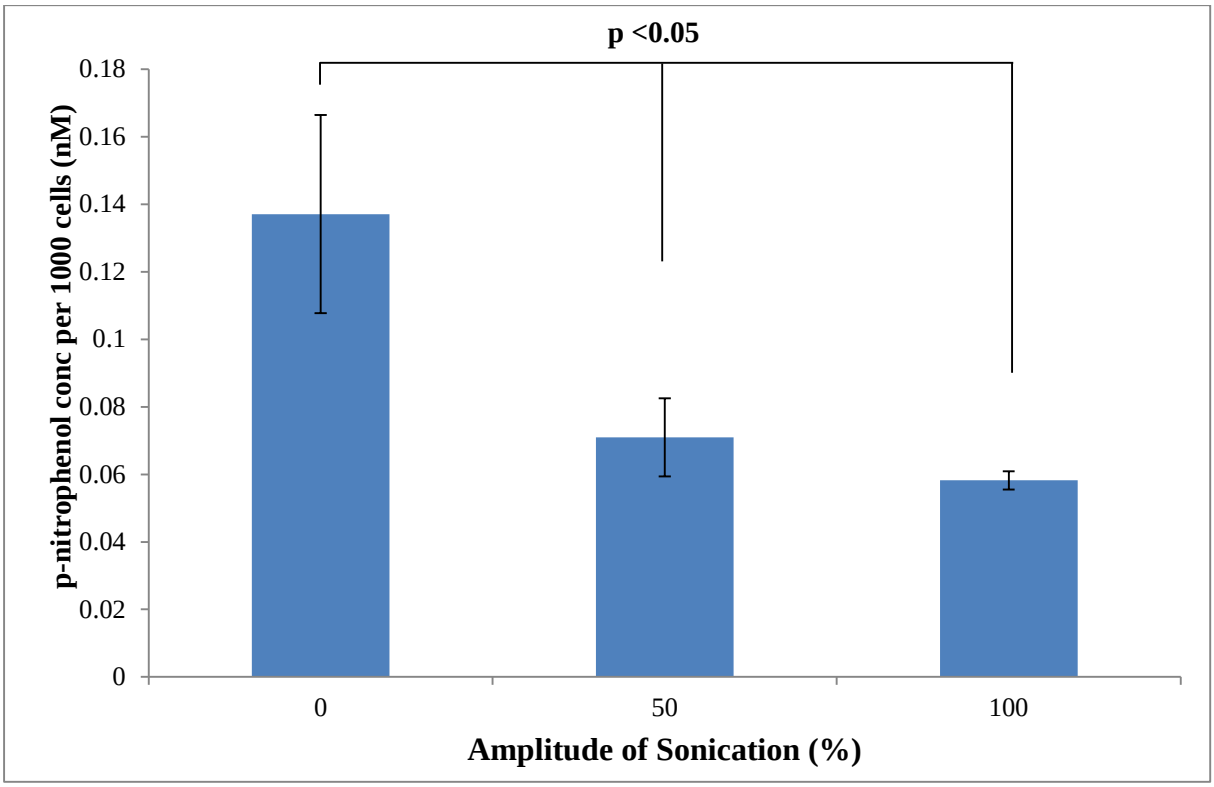

Figure 4.14 – The effect of increasing the amplitude (%) of sonication on the concentration of p-nitrophenol produced per 1000 encapsulated cells provided with p-nitrophenyl phosphate (error bars represent +/- 1 standard deviation, n = 12)

Table 4.5 – A summary of results obtained from statistical analysis of ALP assay data

Results Compared for Statistical Analysis	p-value	Are Results Significantly Different?
[p-nitrophenol] per 1000 cells in 0% sonicated and 50% sonicated gellan	0.0006	Yes
[p-nitrophenol] per 1000 cells in 50% sonicated and 100% sonicated gellan	0.0215	Yes
[p-nitrophenol] per 1000 cells in 0% sonicated and 100% sonicated gellan	0.0001	Yes

4.4 Discussion

The ability to control and tune the mechanical behaviour of biopolymer materials has been of particular interest in tissue engineering over the past decade since it was found that matrix stiffness can directly influence stem cell differentiation (Engler et al., 2006). Here we have shown that various mechanical properties of gellan gum (as a solution and as a hydrogel when cross-linked with DMEM) can be modified by applying varying amplitudes of sonication. The reduction in intrinsic viscosity is perhaps the most significant factor when it comes to explaining the mechanism behind modification of mechanical properties and the ability to tune functional mechanical behaviour. As previously stated, gelation of gellan involves both formation of ordered helices and subsequent aggregation of the helices into a complex 3D structure strengthened by ionotropic crosslinking between polymer molecules. The intrinsic viscosity of a polymer is essentially the capability of that polymer to enhance the viscosity of a solution in which it is dissolved and is therefore, related to molecular weight such that it is often used in molecular weight determination (Harding, 1997). A decrease in molecular weight therefore usually results in a decrease in intrinsic viscosity and vice versa.

Increasing the amplification of sonication resulted in a reduced intrinsic viscosity and therefore, it can be inferred that there was a reduction in molecular weight (Fig. 4.8). This supports work conducted previously by D'Arrigo et al., (2012) who showed that sonication of gellan gum reduces the molecular weight of gellan without altering its chemical structure (D'Arrigo et al., 2012). Furthermore, Taylor et al., (2012) showed that there was in increase in gellan oligomers following sonication at only 30% amplitude which resulted in a reduction in apparent viscosity, as a result of reduced intermolecular entanglement (Taylor et al., 2012). In the present study it was shown that by varying sonication amplitude from 0% to 100% a reduction in viscosity can be tuned to the level required for the application (Fig 4.7), from small reductions in viscosity at low amplitudes to dramatic reductions and an almost complete loss of non-Newtonian behaviour at 100% sonication amplitude and importantly this can be achieved without altering polymer concentration.

Modulation of sonication amplitude can also control the stiffness of resulting hydrogels cross-linked in DMEM. When gellan solutions cool they undergo a two-part gelation mechanism that is normal for gellan (Morris et al., 2012) but a sample of subjected to higher amplitudes of sonication produced a weaker gel (Fig. 4.3-4.6). Since intrinsic viscosity results infer a decrease in molecular weight, reduction in gel modulus is likely attributable to a decrease in polymer chain length resulting in fewer crosslinks between each molecule. The exponential reduction in elastic modulus from 10000 Pa in the un-sonicated gellan to ~3000 Pa (at 10°C) when sonicated at 90% amplitude (Fig. 4.4 - 4.5) highlights how gel stiffness (when cross-linked with DMEM) can be controlled and predicted. The modulus therefore, can be controlled to suit an application by simply applying varied amplitudes of sonication.

As well as tuning both the modulus and viscosity of the polymer, sonication also affects the elasticity of hydrogels. This is demonstrated in Fig. 4.3 where hydrogels formed from sonicated gellan displayed a smaller LVR and a reduced critical stress than hydrogels formed from gellan that was not subjected to sonication. This change adds a new dimension to the sonication protocol whereby elasticity of a hydrogel can also be tuned along with modulus and viscosity to further mimic matrix properties for the tissue to be cultured. Again, reductions in intrinsic viscosity present the most likely explanations for this. Since sonicated gellan has a lower intrinsic viscosity and therefore a lower hydrodynamic volume, the distance of molecular interactions would be expected to be reduced. Therefore, cross-linked hydrogels formed from sonicated gellan pack together in a tighter structure, due to the smaller molecular size and reduced length of interactions. This results in a gel that is significantly less elastic compared with un-sonicated gellan where interaction length is greater.

In cell culture conditions, a similar trend was seen between sonication amplitude and matrix stiffness (Fig. 4.10). Un-sonicated gellan showed the highest modulus while gellan sonicated at maximum amplitude showed the lowest with a ~50% decrease in matrix stiffness. However, gels formed in culture conditions showed a lower modulus than when gelled under conditions outlined in section 4.2.5. Results in Fig 4.10 are far more reflective of the mechanical behaviour of each sample under cell culture conditions as gelation was triggered at 37°C. Conversely, results presented in Fig 4.4-4.5 were obtained by mixing gellan with DMEM at 90 °C and slowly cooling to form a stable hydrogel. This difference in approach is likely the cause of changes in mechanical behaviour. The onset of gelation shown illustrated in Fig. 4.4 takes place at 46 °C so when DMEM is mixed at 37 °C (as occurs when preparing for cell culture) gelation is triggered instantly as the gellan comes into contact with the ions in DMEM. Moreover, when gelled in cell culture conditions samples are gently stirred to promote mixing and as a result imparts a small shear force during the sol-gel transition. This results in a suspension of gel particles, otherwise known as a fluid gel or sheared gel rather than a continuous bulk gel (Mahdi et al., 2014, Sworn et al., 1995). A consequence of this is that the collective strength of the structure is reduced. Interestingly, sonication also seemed to affect physical appearance of cell loaded gellan structures (Fig. 4.11). Gels formed from sonicated gel appeared to be more uniform. However, study of gelation profiles showed no change in gelation time for samples subjected to sonication (Fig. 4.9). This rules out the likelihood of this being attributed to a longer ordering time for gel networks of sonicated gellan. It is, therefore, likely due to reduced viscosity of gellan solutions as a result of sonication promoting more homogeneous mixing with DMEM.

Changes to rheological properties did not appear to impact on viability in cell loaded hydrogels. Similarly sonication does not lead to any potentially harmful contamination of polymer sample with cytotoxic metal particles that may have been released from the sonic probe. It is worth noting that the duration of sonication for each sample was relatively short reducing the chances of such contamination. Both are indicated by results in Fig. 4.12 where all samples yielded a very high

proportion of cells emitting green fluorescence as a result of a calcein AM/propidium iodide assay. This is indicative of live cells as a green fluorescence is emitted when live cells cleave calcein AM to calcein with the use of intracellular esterases (Bratosin et al., 2005). A presence of dead cells would be indicated by red fluorescent signals as a result of propidium iodide penetrating compromised membranes and binding to nucleic acids in dead/dying cells (Banerjee et al., 2014).

A decrease in p-nitrophenol concentration with increasing sonication amplitude (Fig. 4.14) is indicative of reduced p-nitrophenyl phosphate hydrolysis and thus a decrease in alkaline phosphatase activity. As a key marker for osteogenic differentiation, ALP activity levels can indicate the extent of osteogenesis within a tissue engineering construct (Choi et al., 1996). The most common method to promote osteogenic differentiation is to supplement the cell culture media with specific differentiation promoting reagents. In this study, however, no differentiation supplements were added. Any differentiation therefore, would more likely be a result of mechanical stimuli from the surrounding gel matrix.

Rheological measurements showed that sonicating gellan resulted in structures with lower moduli. Reducing the modulus of the structures appeared to cause a reduction in ALP activity in encapsulated MC3T3's. Interestingly, the extent of reduction for both seems to be of similar proportion, with ALP activity and matrix stiffness decreasing by ~50% in gellan sonicated at 100% amplitude. This could be indicative of a mechanism whereby sonication reduced matrix stiffness and had a negative impact on osteogenic differentiation. A higher amplitude of sonication resulted in a further decrease in ALP activity for encapsulated cells. This seems to correspond with previous work showing how matrix stiffness can impact differentiation (Engler et al., 2006). Osteogenesis requires a more stiff and rigid culture environment so a decrease in gel modulus can have a negative impact on osteogenic potential. While data appears to show a negative trend, the reduction in ALP activity as a result of gellan sonication acts as a proof of concept for the level control that can be exhibited over mechanical properties of a gellan scaffold using sonication. ALP assay results show that reductions in scaffold

matrix stiffness were significant enough to have an impact on cell culture conditions. This provides potential for the use of sonication in tuning gel properties to optimise a structure for culture of specific tissues. Changes in mechanical properties can be achieved without altering the concentration of polymer or crosslinking ions and thus there is little impact on the osmotic environment within a construct.

4.5 Conclusions

Application of a simple sonication method was shown to reduce the viscosity and elasticity of gellan gum hydrogels cross-linked with DMEM. ALP activity of encapsulated MC3T3 cells showed variance as a result of changes in scaffold properties via sonication and cell viability was good in all constructs. This was achieved without changing the concentrations of the polymer or the crosslinking ions and was a likely direct result of the sonication method breaking gellan polymer chains into fragments of lower molecular weight as demonstrated previously (Taylor et al., 2012). Results obtained further support the potential of gellan gum for tissue engineering applications as the ability to tune mechanical properties is integral to the success of such procedures. However, while this study outlined a method for varying mechanical properties in a single tissue engineering scaffold, native tissue is more complex containing distinct regional areas and interfaces that have different and often anisotropic mechanical behaviour. Therefore, a system that facilitates fabrication of scaffolds exhibiting multiple mechanical properties is of great interest. In Chapters 5 and 6 a method is proposed to achieve this via integration of multiple materials and cell types into a single structure to greater mimic native tissues *in vitro*. Chapter 5 will outline method development, proof-of-concept testing and initial evaluation of potential cell culture applications. In Chapter 6, subsequent use of the method to fabricate layered, multicellular constructs for osteochondral tissue regeneration will be presented.

Chapter 5 – Development of an Additive Layer Manufacturing Technique for 3D Rapid Prototyping of Hydrogel Substrates

Aspects of this chapter are published in *Advanced Materials*.

Moxon, S. R. Cooke, M. E. Cox, S. C. Snow, M. Jeys, L. Jones, S. W. Smith, A. M. Grover, L. M. (2017) Suspended Manufacture of Biological Structures, Advanced Materials, 1605594.

5.1 Introduction

Rapid prototyping of 3D tissue engineering substrates has emerged as a promising method for synthesising structurally precise culture scaffolds. It overcomes issues associated with generating complex 3D polymer structures such as flow of material prior to gelation resulting in loss of structure and an inability to modify scaffolds post-gelation (Peltola et al., 2008). The technique has been implemented into areas where creation of complex, shaped tissue culture substrates is required such as fabrication of patient-specific, tissue engineering scaffolds. Implantation is still a widely used technique for treatment of various medical defects and greater demand has been placed on the adaptation and implementation of tissue engineering methods into implant fabrication with investigation still on-going (Ye and Peramo, 2014, Schek et al., 2005, Woodfield et al., 2009). The focus is on fabricating a structure that enhances tissue repair and does not negatively impact patient health. By using autologous patient cells and creating a construct comprised of naturally occurring raw materials, scaffolds can potentially be engineered to meet all such criteria (Lu et al., 2011).

A critical factor in generating tissue engineered scaffolds for such an application is the ability to control the shape and size of structures. The majority of implants are patient-specific and, as a result, the ability to easily create such specific structures is critical to the success of treatment (Chuan et al., 2013, Sapkal et al., 2016). Current approaches for designing scaffolds of specific morphologies often

incorporate the use of moulds or stamps. However, use of such systems is reliant on the generation of a new mould for every implant that is engineered (Yeh et al., 2006, Gillette et al., 2008, Khademhosseini and Langer, 2007).

Secondly, such procedures rarely facilitate fabrication of complex, layered structures thus inhibiting the ability to replicate multi-material and multi-cellular *in vivo* environments such as articular cartilage and the osteochondral interface. Little control can be exhibited over precise distribution of cells and scaffold materials and resulting scaffolds are often comprised of a single substance and cell type (Wu et al., 2005, Stevens et al., 2005). This is not reflective of structural ordering in native tissue and, as such, alternative approaches are required to address current limitations (Yeong et al., 2004). Consequently, there is a lot of focus on developing new methods that could allow for creation of tissue engineering scaffolds that better mimic *in vivo* tissue development environments.

Additive layer manufacturing (ALM) has emerged as a promising new rapid prototyping technique for replication of complex tissues. It involves fabrication of structures comprised of multiple materials by adding layer upon layer (de Carvalho and Djabourov, 1997). ALM provides the potential to exhibit greater control over distribution of both cells and supporting matrix and is now widely used in many sectors. However, current applications often utilise hard materials, with ALM using soft materials still providing a much greater challenge due to their rheological behaviour (Pfeifer et al., 2012). Layering soft materials such as biopolymer hydrogels in a gelled state does not allow for integration of multiple materials into a single, tiered structure. Additionally, layering in sol form does not allow for control over integration and flow due to biopolymer solutions often exhibiting viscosities similar to that of water (Capron et al., 2001). Therefore, a degree of manipulation is required in order to facilitate greater control over rheological behaviour of biopolymers to allow for incorporation into ALM technologies. This is something that has proved challenging with ALM techniques still heavily focussed on use of hard rather than soft materials.

Progress has been made with soft materials, nonetheless, with one notable study revealing fabrication of ‘nose-like’ structures of alginate using a ‘drop by drop’ manufacturing technique (Boland et al., 2007). Despite recent advancements, however, structures created from ALM with soft materials often lack complexity (Costantini et al., 2016). Consequently, replication of complex structures such as the 4-tier structure of cartilage or the 2-tier structure of the osteochondral interface remains a challenge. Various research groups have utilised different techniques to try and overcome problems in creating complex structures, with examples involving suspension in high viscosity fluids or use of hard materials for support (Melchels et al., 2016, Kang et al., 2016, Sachlos et al., 2006). Removal of supporting materials, however, is difficult and leads to poor clinical translation with structures often deforming during recovery. This study presents a method for overcoming such issues by utilising a suspension of particulate gels, often referred to as a fluid gel, for the supporting media.

A fluid gel is formed by allowing a polymer solution to pass through a sol/gel transition under an applied shear rate. As a result of the applied shear, gelation does not result in formation of a single polymer network. Instead, the gel that is formed is a suspension of much smaller gel micro particles. A fluid gel displays viscoelastic properties and the particles themselves are comprised of a typical cross-linked network but on a micro scale (Norton et al., 1999). Gel particles formed in this manor are described as being ‘hairy’ and can interact with one another to form weak bonds resulting in a paste-like material which can be reverted back to a pourable liquid with the application of a small shear force (Fig. 5.1). However, if left for a short period of time particles will reform bonds with neighbouring particles and return the gel to a paste-like state. This gives fluid gels so called ‘self-healing’ properties.

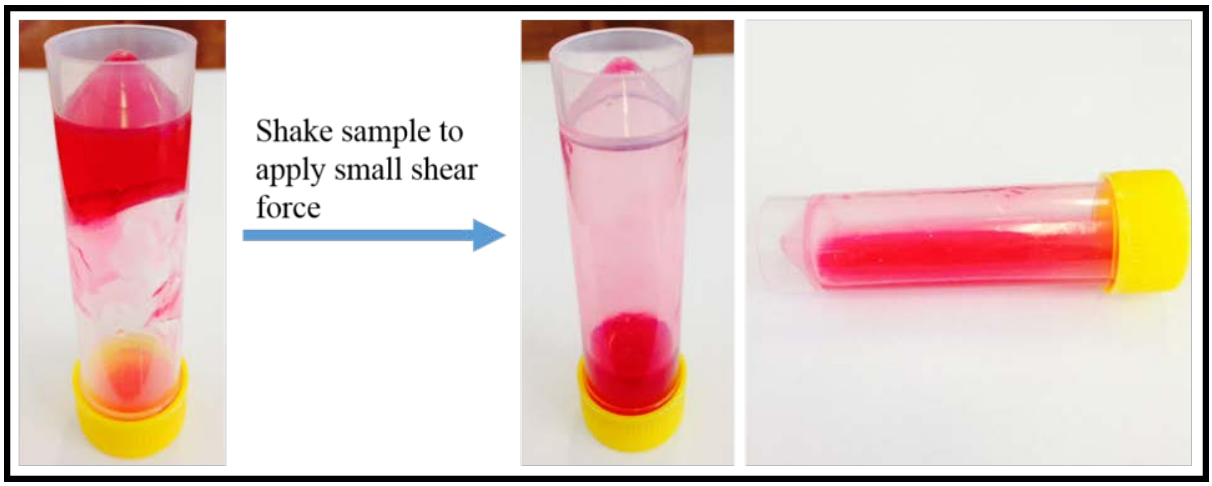

Figure 5.1 - Transition of a fluid gel from a self-supporting paste-like material to a pourable viscoelastic liquid after application of a small shear force

A molecular model for the formation of fluid gel particles was presented by Norton et al., (1999). When a polymer transitions from a sol to gel state, molecules often exhibit a shift from a disordered to more ordered form. In the case of gellan, for example, polymer molecules undergo a conformational change from random coils to ordered helices (Morris et al., 2012). This transition leads to an increase in polymer solution viscosity as molecular domains aggregate together. Applied shear forces separate nucleation sites of neighbouring polymer molecules thus limiting molecular ordering to formation of gel micro-particles (Norton et al., 1999). This is in contrast to the mechanism of quiescent cooling where a lack of shear force facilitates aggregation of polymer molecules into a single, ordered network (Fig. 5.2).

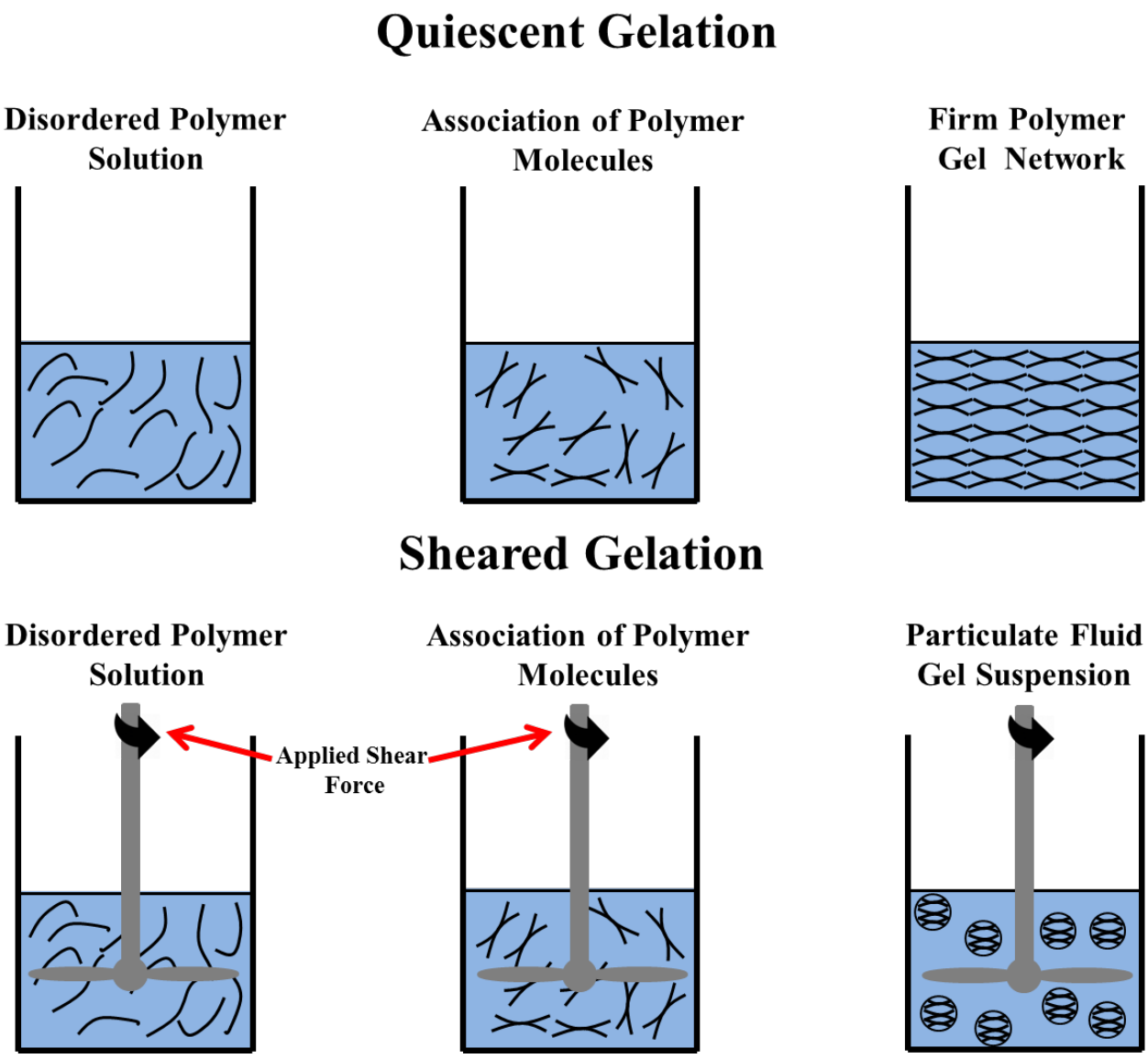

Figure 5.2 – Schematic diagram showing differences between polymer gels subjected to quiescent and sheared gelation (Mahdi, 2016)

There are multiple hypotheses that describe what triggers aggregation and growth of fluid gel particles. One theory attributes particle growth to recruitment of un-gelled polymer molecules from solution (de Carvalho and Djabourov, 1997) while another suggests shear flow promotes polymer aggregation (Norton et al., 1999). Growth and morphology of fluid gel particles is often dependent upon multiple factors such as shear rate, polymer concentration and cooling rate (in thermally gelling systems). This has led to studies into tuning fluid gel properties for biomedical applications (Mahdi et al., 2014, Mahdi et al., 2015, Mahdi et al., 2016).

Fluid gels could potentially solve issues with rapid prototyping of soft materials by acting as highly supportive and easily removable ALM supporting media. Solid-like properties of a fluid gel may facilitate the suspended deposition and controlled gelation of polymer solution. Additionally, the pourable, fluid-like properties of a particulate gel suspension could allow easy extraction of a gelled construct. This may provide a platform for creation of highly customisable, shaped constructs without the requirement for pre-fabrication of support systems such as stamps or moulds. Furthermore, fluid gel suspension could also present a simple method for incorporation of multiple materials and cell types within a single, layered hydrogel construct (Fig. 5.3).

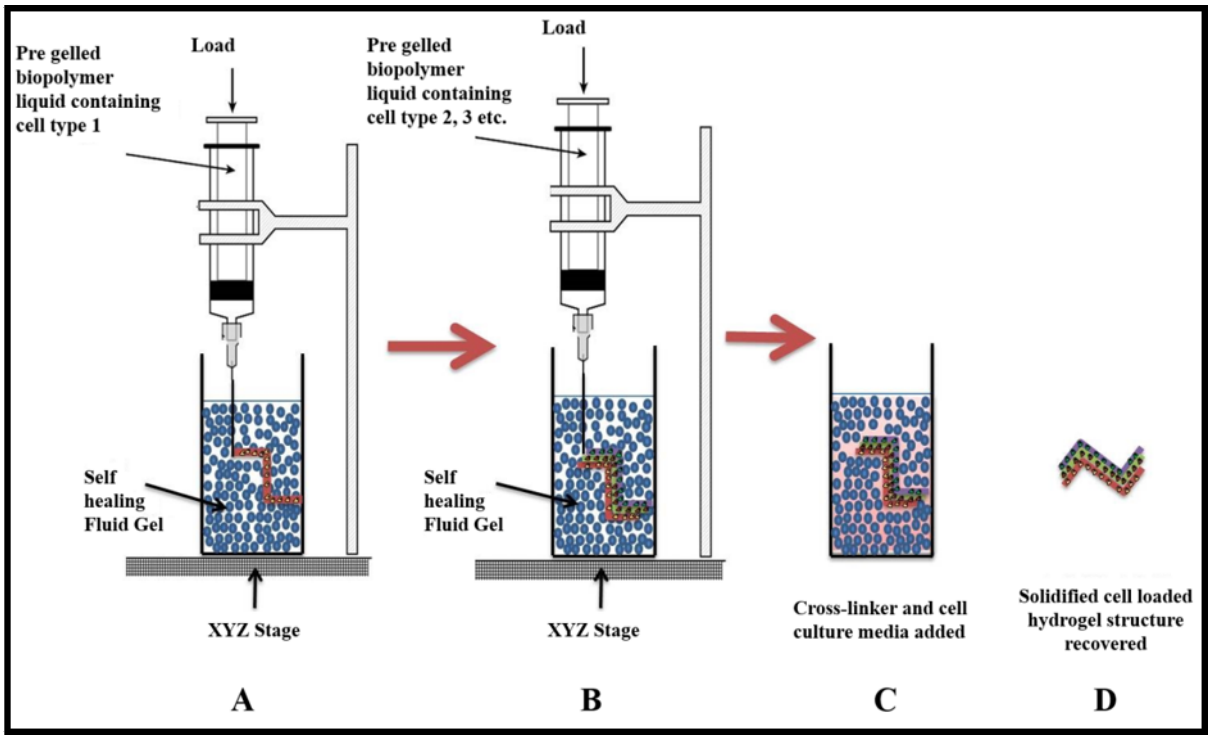

Figure 5.3 - Schematic showing a proposed fluid gel ALM technique. A) Cell loaded biopolymer injected into fluid gel. The polymer remains in liquid form but does not flow due to support from self -healing fluid gel. B) Multiple layers added containing different cell types or molecules such as growth factors (all biopolymers still in liquid form). C) Cross-linker added to completed structure to trigger gelation and immobilise the cells. D) Solidified gel structure/implant can be recovered from the fluid gel when required

A similar mechanism has been previously reported in a study by Hinton et al., (2015) where gelatin microparticles were used as a support bath for 3D printing of soft structures using biopolymers such as alginate (Hinton et al., 2015). The study demonstrated an ability to fabricate complex structures from soft materials. This allowed for formation of hydrogels exhibiting a similar morphology to

biological tissues such as femurs and coronary arteries. However, constructs had to be printed at no higher than 22 °C to prevent the gelatin bed from melting and losing supportive properties. In addition, following fabrication the particle beds had to be heated to 37 °C to allow for extraction of structures. Additionally, structures fabricated using this method were only comprised of a single material and cell type. Structures could not be cultured *in situ* and no clinical implications of the method were investigated.

This chapter aims present a similar approach by suspending biopolymer structures in a fluid gel particle bed. However, by using biopolymers that form hydrogels that exhibit thermal stability at 37°C, it may be possible to allow for printing of structures at physiological temperature. This could facilitate suspended manufacture of multi-material, cell-loaded structures from soft materials suitable for implantation into tissue defects. In this chapter method development for use of fluid gels in ALM of soft material structures is presented. Mechanical boundaries of such a system are explored, with the success of the suspension evaluated in respect of fluid gel viscosity, shear modulus and particle size. . Tunability of construct resolution is also demonstrated as a function of multiple deposition parameters. Proof-of-concept of the fabrication of complex structures is provided with creation of layered, osteochondral-like structures and a complex polymer helix comprised of a gellan/hydroxyapatite blend. Finally, an initial evaluation of cell culture applications with 3T3 fibroblasts is presented.

5.2 Materials and Methods

5.2.1 Materials

Gellan was purchased from Kalys (Benin, France). Agarose, gelatin (type A) and alginate (analytical grade, M:G ratio of 0.39:0.61) were purchased from Sigma Aldrich (Dorset, UK). Type I collagen was purchased from Cell Systems (Troisdorf, Germany). Cell culture plastics, syringes and hypodermic needles were purchased from Sigma-Aldrich (Dorset, UK). All other reagents and cell

culture media and supplements were purchased from Sigma-Aldrich (Dorset, UK) and used without further purification.

5.2.2 Fluid gel formation

Fluid gels were formed using either agarose or gellan solutions of varying concentrations (0.1% - 1% w/w). Hot solutions were allowed to cool to 10 °C under a constant shear rate generated by a magnetic stirrer rotating at 700 rpm. In the case of gellan, sodium chloride was added to the polymer solution prior to cooling (as a source of crosslinking ions) to give a final concentration of 100 mM NaCl..

To create sterile fluid gels for cell culture applications, polymer solutions were autoclaved prior to cooling and subsequently stored in sterile Schott® bottles to maintain sterility.

5.2.3 Fluid gel concentration tests

In order to evaluate the minimum required properties for a fluid gel to act as an ALM supporting media in this system, an experiment was designed whereby 1% solutions of gellan were suspended in gellan fluid gels of decreasing concentration. The fluid gel at which extruded solutions were not fully supported was deemed to contain the minimum required gellan concentration. Rheological analysis was subsequently used to quantitatively outline the required strength and viscosity of a fluid gel to support deposition of polymer solutions.

Gellan fluid gels were prepared as in 5.2.2 using a constant NaCl concentration of 100 mM and varying polymer concentrations. The highest concentration of gellan was 1% w/w and concentration was gradually decreased until fluid gel samples showed loss of self-healing properties and lack of sufficient support for suspending 1% gellan solutions. Supporting baths were created by pipetting 60 ml of each fluid gel concentration into separate 60 mm petri dishes. Depositions of 1% gellan were then created using a 10 ml syringe and a 21 gauge needle (337 µm inner diameter). The needle was immersed beneath the surface of a fluid gel and solutions were extruded at 125 µl/s while the needle was moved laterally to create shaped structures. A 50 mM $CaCl_2$ solution (10 ml) was then added to

the surface of fluid gels loaded with suspended structures to trigger gelation into shaped hydrogel constructs. Constructs were left for 40 minutes before being extracted post-gelation using a spatula and excess fluid gel was washed away with deionised water.

5.2.4 Rheology

Once the minimum gellan concentration for a fluid gel was determined, various rheological tests were conducted in order to quantitatively define the rheological boundaries that could apply to the system. Fluid gels prepared from varying concentrations of gellan and agarose were analysed to determine the required elastic modulus, viscosity and particle size distribution to support suspension of 1% gellan solutions.

5.2.5 Frequency Sweeps

Fluid gels were prepared at 5 different gellan concentrations (shown in Table 5.1). The modulus of each fluid gel was measured in response to increasing oscillatory frequency using a 55 mm cone geometry and a Bohlin Gemini rheometer. Oscillatory frequency was increased from 0.1-100 rad/s with a constant temperature and strain of 20 °C and 0.5% respectively. Agarose fluid gels (0.25%, 0.5%, 0.75% and 1% w/w) were testing using the same parameters and geometry to ensure the same stresses and strains were applied to the samples.

Table 5.1 – Fluid gel samples prepared for rheological analysis

Fluid Gel Sample	Gellan Concentration (% w/w)	NaCl Concentration (mM)
1	1.00	100
2	0.75	100
3	0.50	100
4	0.25	100
5	0.10	100

5.2.6 Shear Ramps

Shear ramps were performed using a Gemini rheometer with a 55 mm coned geometry on all 5 concentrations of gellan fluid gel and all 4 concentrations of agarose fluid gel detailed in 5.2.3. Shear rate was increased from 0-100 s^{-1} over a 10 minute period and temperature was kept constant at 20°C.

5.2.7 Particle size analysis

Another fluid gel property that could affect capacity to support deposited structures is particle size as it can directly influence mechanical properties (Mahdi et al., 2014). Therefore, upper and lower limits regarding fluid gel particle size distribution were evaluated. Additionally, the same evaluations were carried out on 0.5% agarose fluid gels to determine if particle size distribution also fell within the required boundaries.

Fluid gel samples were loaded onto glass slides and allowed to dry under a coverslip for 10 minutes. Samples were then visualised on Keyence VHX 2000 digital microscope (Keyence, UK). Particle sizes were analysed with VHX 2000 communication software. Particle size distribution was calculated using images of fluid gel particles within an area of 135 µm by 120 µm. Images were divided into 12 grids of 11.25 µm by 10 µm. Within each grid, the number of particles was recorded and separated into categories based on size. A total of 96 grids were analysed for each fluid gel sample. Particle size distribution was then determined by comparing the number of particles within each size range and calculating cumulative frequency of each particle size. This method was, however, only used to quantify micro particles. Nano particles (particles of <0.5 µm in size) could not be accurately counted and were therefore not included in the final distribution.

5.2.8 Tuning construct resolution

To further explore the limits of construct resolution, the effect of multiple deposition parameters were investigated. A 0.5% w/w agarose fluid gel was formed and gellan solutions of varying viscosity (controlled by concentration) were deposited in separate aliquots of fluid gel (contained in petri dishes of 60 mm diameter and 15 mm depth). Gellan was extruded through a hypodermic needle with an

inner diameter of 337 µm. Once suspended, gelation was triggered via injection of 200 mM $CaCl_2$ directly around suspended solutions using a 5 ml syringe and 18 gauge needle (838 µm inner diameter). Samples were left for 30 minutes before being extracted with a spatula. Excess fluid gel was washed away with deionised water and the resolution of each construct was measured using electronic callipers.

To further tune construct resolution, gellan samples with the highest viscosity were then extruded into agarose fluid gel through hypodermic needles with varying inner diameters. Gelation, extraction and measurement of construct width and height were conducted as described previously.

Following results from tuning resolution with viscosity and needle aperture, a final experiment was used to investigate if varying the speed of polymer deposition could further increase construct resolution. High viscosity gellan was extruded through a 260 µm diameter hypodermic needle with variations in the speed at which solutions were laterally deposited.

In all 3 experiments extrusion rate was kept constant at 125 µl/s.

5.2.9 Creating complex hydrogel structures using suspended manufacture

Once required properties and customisability of the system had been demonstrated, creation of more complex structures was explored using multiple materials to create a variety of different structures.

5.2.10 Fabricating layered structures of specific dimensions

To demonstrate the degree of control that can be placed on construct fabrication, structures of specific height and width were created, each containing two different materials. Materials were selected with a focus on fabricating a structure that could act as an osteochondral model. Structures were designed to contain both an osteogenic and a separate, integrated chondrogenic layer. Multiple combinations of biopolymers and ceramics were investigated as shown in Table 5.2 with a circular layer (3 mm thick, 10 mm diameter) of gellan deposited initially and a variety of different materials used for a second, top layer of 7 mm thickness and 10 mm diameter. These dimensions were chosen to

demonstrate the level of control that can be exhibited over size and shape of depositions and to mimic size ratios between the bone and cartilage layers of osteochondral tissue (Campbell et al., 2012). Type I collagen was chosen as one potential osteogenic layer due to its high abundance in bone (Viguet-Carrin et al., 2006). Nanocrystalline hydroxyapatite (nano-HA) was incorporated into non-collagenous osteogenic layers for the same reason. Gellan was chosen for a possible chondrogenic layer due to structural similarities with GAGs found in cartilage ECM (Oliveira et al., 2010, Fan et al., 2010, Silva-Correia et al., 2011, Khang et al., 2015).

Table 5.2 – Materials used for creation of osteochondral mimetic constructs

Construct	Material Used for 3 mm Chondrogenic Layer	Material Used for 7 mm Osteogenic Layer
1	1.5% Gellan	30% Gelatin with 5% nano-HA
2	1.5% Gellan	1.5% Low Acyl Gellan with 5% nano-HA
3	1.5% Gellan	3% Alginate with /5% nano-HA
4	1.5% Gellan	0.5% Type I Collagen

Constructs were created by an initial deposition of a circular gellan layer of 10 mm diameter and 3 mm height using a 5 ml syringe and 23 gauge needle (337 µm inner diameter). A second material was then deposited on top to create a second circular layer of 10 mm diameter and 7 mm height. All constructs were extruded by hand into a 0.5% agarose fluid gel supporting bath. Gelation was triggered with the injection of 200 mM $CaCl_2$ around constructs with extraction performed 45 minutes later. The only construct where this procedure differed was for ‘Construct 4’ (gellan bottom layer and collagen top layer – Table 5.2) where $CaCl_2$ was not injected until 30 minutes post-suspension due to the long gelation time of type I collagen. This ensured both polymers passed through the sol-gel transition at a similar time, creating a single structure. After extraction, constructs were washed with deionised water and imaged with a Nikon D3300 Digital SLR camera (Jessops, Leeds, UK).

5.2.11 Fabrication of mineralised polymer helical structures

To demonstrate the complexity of structure that can be created using the suspended manufacture technique, an intricate, 3D helical structure was fabricated composed of gellan mixed with nano HA. Prior to fabrication, nano HA was synthesised using a precipitation method (Mobasherpour et al., 2007). Solutions of 0.24 M $Ca(NO_3)_3.4H_2O$ and 0.29 M $(NH_4)_2HPO_4$ were prepared separately in deionised water. Temperature of $Ca(NO_3)_3.4H_2O$ was maintained at 25 °C and the pH was modified to 11 using ammonia solution. To trigger the precipitation reaction $(NH_4)_2HPO_4$ was slowly added drop wise to $Ca(NO_3)_3.4H_2O$ under constant stirring at 700 RPM with a magnetic stirrer. At a time point of 1 hour post-initiation the resulting suspension was aliquotted and centrifuged at 4,400 RPM for 10 minutes in 50 ml centrifuge tubes. The supernatant was washed and re-suspended in 40 ml deionised water and centrifuged a second time using the same parameters. This was repeated a third time but the pellet was not resuspended after the supernatant was removed. The resulting end product was a paste-like sol phase of nano HA which was later incorporated in gellan solutions for fabrication of mineralised polymer helices.

Helices were formed by suspension in 5 ml of 0.5% agarose fluid gel inside plastic 7 ml bijoux tubes. Gellan was used as the polymer with nano HA incorporated to enable high resolution image reconstruction using X-ray computed tomography (CT-imaging). . Solutions of 1.5% w/w gellan mixed with 10% nano HA at 60 °C (formulated by precipitation method) were extruded into fluid gel samples through a hypodermic needle with a 337 µm inner diameter using a 5 ml syringe. The suspensions were then left at room temperature for 40 minutes to enable gelation to occur. Prior to extraction, samples were observed using micro CT (Bruker Skyscan 1172 – Bruker, Belgium) and reconstructed in 3D using CTVox software (Bruker, UK). Helices were then extracted and excess fluid gel was washed away with deionised water.

5.2.12 Initial evaluation of cell culture applications

Cell culture procedures were conducted using mouse-derived 3T3 fibroblasts. Fibroblasts were seeded, expanded and passaged following the same procedures outlined in Chapter 4, Section 4.2.

Cell culture applications of ALM using fluid gels were initially evaluated by fabricating shaped structures comprised of a single layer with an aim to create more complex, layered structures pending proof-of-concept.

3t3 fibroblasts were trypsinised at passage 12. Cells were then counted using a haemocytometer, centrifuged at 1000 RPM for 3 minutes and re-suspended to a density of $3x10^6$ cells/ml. Once re-suspended, cells were mixed with gellan to create a gellan:cell suspension with a volume ratio of 10:1. Cell-loaded gellan was injected into 3 separate 0.5% agarose fluid gels contained within petri dishes. Three different structures were created. The first was a series of straight lines across the diameter of the petri dish, the second the Greek symbol Σ and the final was a complex spiral to demonstrate flexibility of the system. Constructs were visualised using a VWR IT 400 Inverted Microscope (VWR, UK) to determine if suspension had been successful. After 14 days of culture a live/dead assay was performed as in previous sections to ensure the suspension of cell-loaded structures did not result in significant cell death.

5.3 Results

5.3.1 Fluid gel concentration tests

For concentration tests two different types of structures were suspended in fluid gels. The first was a long, linear construct and the second was a denser, cylindrical structure. Both were found to be suspendable in all concentrations of the fluid gel (Fig. 5.4). However, at the lowest concentration, evidence of loss in fluid gel self-healing properties can be seen around the suspended structure. When injected, some of the polymer solution dispersed among the fluid gel rather than being suspended in it. Both structure types were recovered from each fluid gel sample but recovery from the 0.1% gel

was difficult as the structure was fragmented at regular intervals. Conversely, fluid gels of 1% gellan provided a great deal of support to suspended gellan solutions but extraction was hindered by a greater difficulty in separating gelled constructs from particulate gel. Therefore, 0.1% and 1% gellan fluid gels can be considered as the lower and upper limits for suspended manufacture when producing constructs from 1.5% gellan solutions.

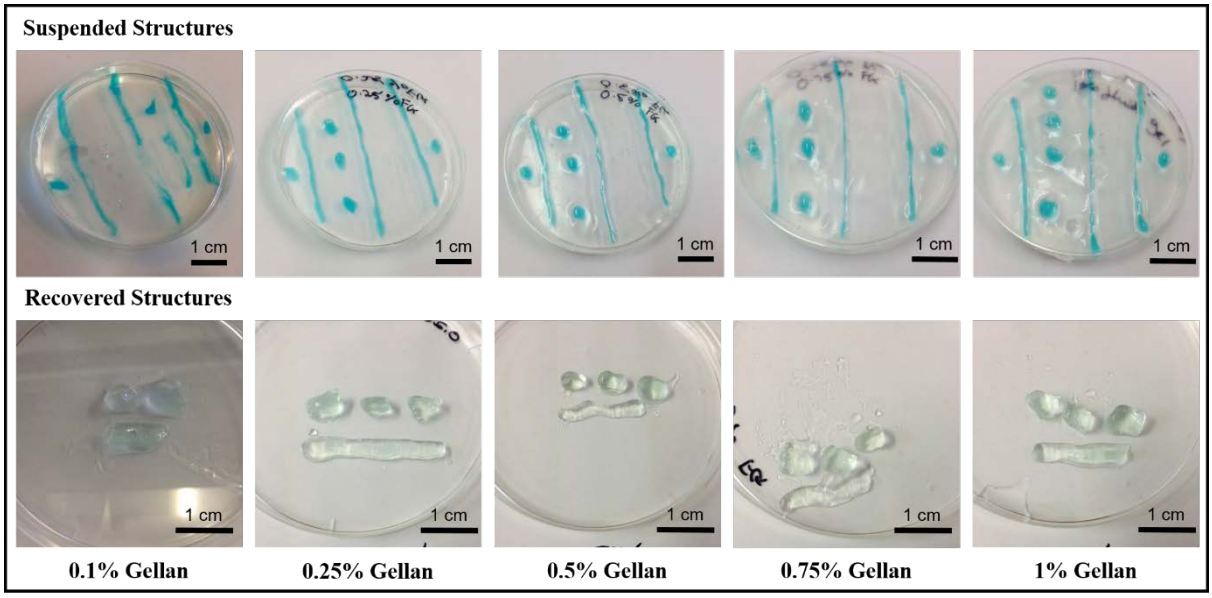

Figure 5.4 - Suspended deposition, gelation and recovery of 1% gellan in fluid gels with a varying gellan concentration and a constant NaCl concentration of 100 mM

5.3.2 Rheology of gellan fluid gels

Elastic moduli of fluid gel formulations were found to decrease as a function of reductions in gellan concentration with 1% gellan exhibiting the highest G′ (359.12 Pa at 1 rad/s) and 0.1% gellan exhibiting the lowest (3.92 Pa at 1 rad/s - Fig. 5.5). Each sample exhibited a slightly frequency-dependant elastic modulus. Therefore, when considering required fluid gel properties, data should ideally be extrapolated from a single frequency. Gellan fluid gels investigated exhibited an elastic modulus of between 3.92 Pa and 359.12 Pa at a frequency of 1 rad/s. Each fluid gel concentration demonstrated a capacity to support suspension of 1% gellan, although some loss of rapid self-healing properties was observed in 0.1% gellan fluid gels (Fig. 5.4). Therefore, it is probable that a gellan

fluid gel exhibiting a G′ of <3.92 Pa at 1 rad/s would not have sufficient self-healing capacity to allow for suspension of 1% gellan solutions.

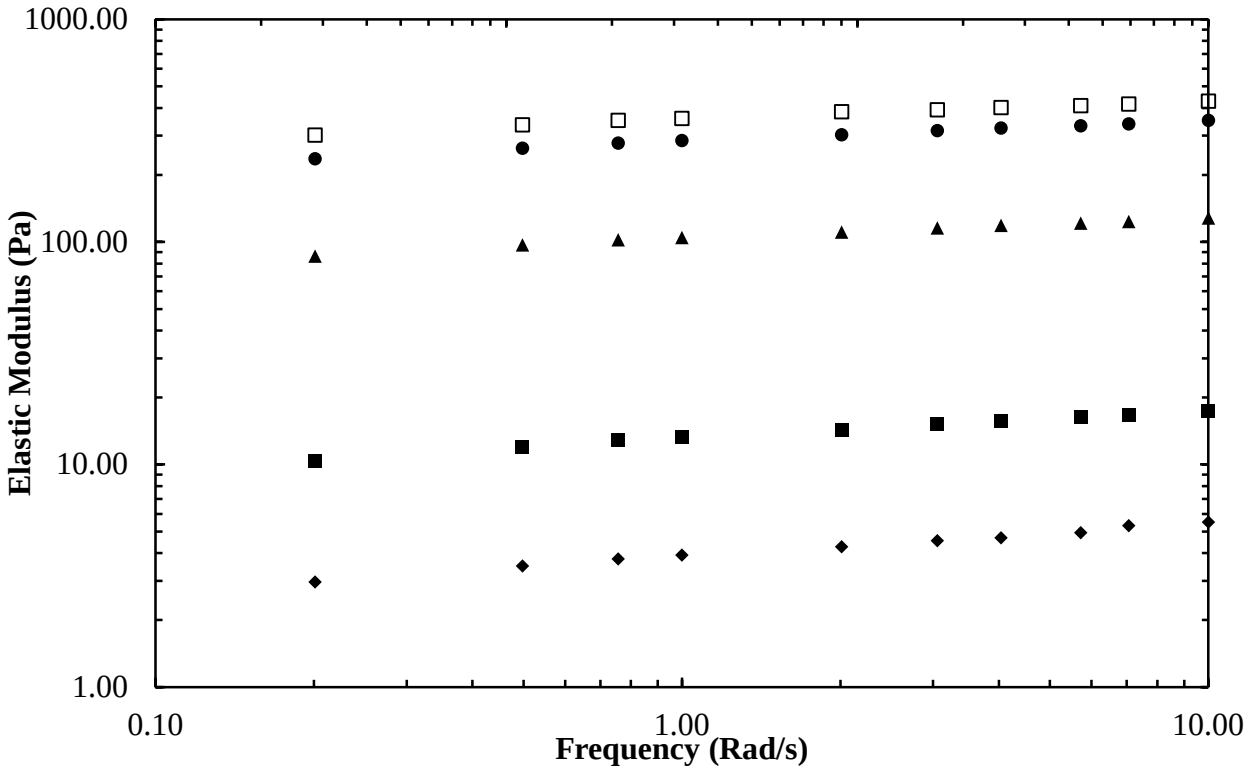

Figure 5.5 - Elastic modulus (G') in response to an increasing frequency of fluid gels made with 1% gellan (clear squares), 0.75% gellan (black circles), 0.5% gellan (black triangles), 0.25% gellan (black squares) and 0.1% gellan (black diamonds and a constant concentration of NaCl of 100 mM

Dynamic viscosity of fluid gels also decreased with a reduction in gellan concentration. All samples showed shear thinning behaviour but varying viscosities. A 1% gellan fluid gel was found to have an initial viscosity of 14.73 Pas, decreasing to 0.52 Pas at higher shear rates. At the lowest concentration of gellan the initial viscosity was 0.71 Pas decreasing to 0.03 Pas at the highest shear rate (Fig. 5.6).

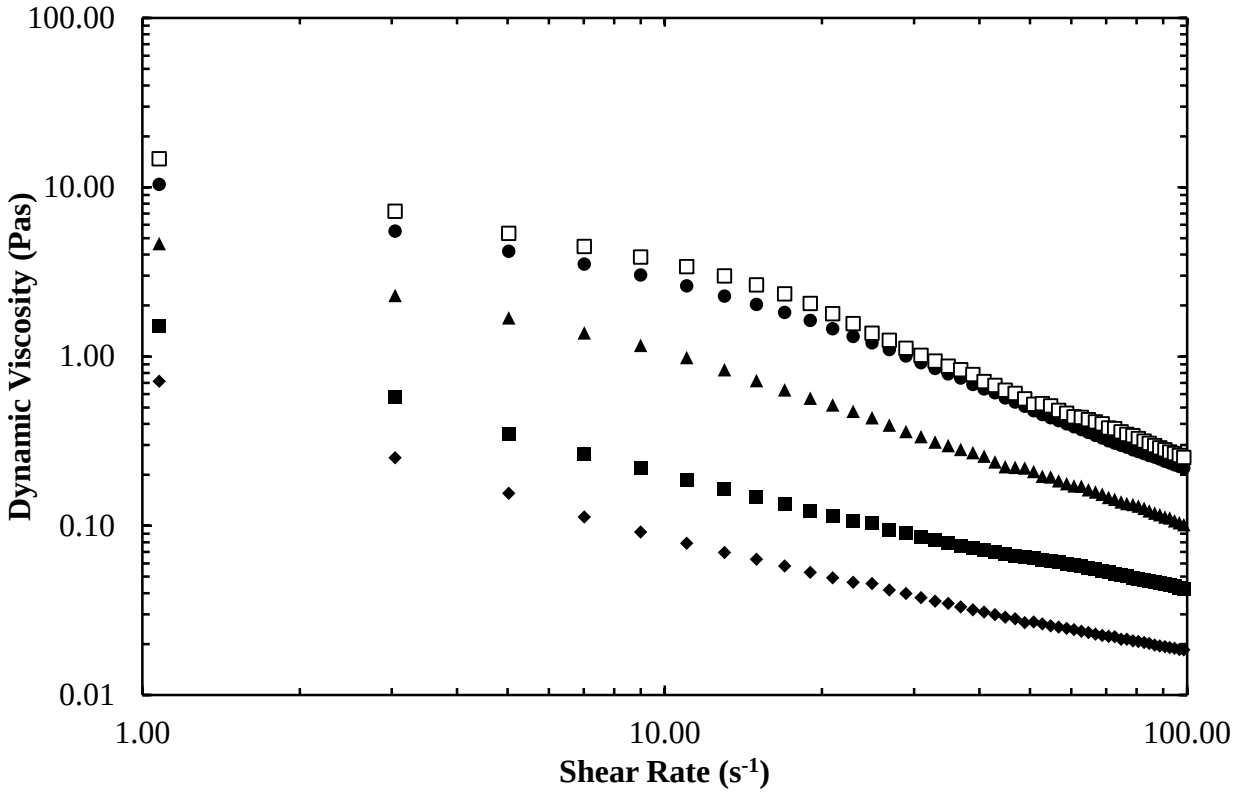

Figure 5.6 - Dynamic viscosity in response to an increasing shear rate of fluid gels made with 1% gellan (clear squares), 0.75% gellan (black circles), 0.5% gellan (black triangles), 0.25% gellan (black squares) and 0.1% gellan (black diamonds and a constant concentration of NaCl of 100 mM

Again, shear ramp data can be used to determine the required viscosity of gellan fluid gels in order to support suspension, gelation and extraction of 1% gellan solutions. It can be concluded that fluid gels should exhibit a dynamic viscosity of at least between 0.71 Pas and 14.73 Pas at a shear rate of 1 s^{-1}. Fluid gels with a viscosity of <0.71 Pas at 1 s^{-1} may not provide sufficient support to 1% gellan solutions.

5.3.3 Rheology of agarose fluid gels

A similar trend in elastic moduli was exhibited by agarose fluid gels with G′ decreasing as agarose concentration was reduced. Fluid gels of 1% agarose exhibited an average G′ of 197.04 Pa at 1 rad/s with 0.25% agarose fluid gels exhibiting an average modulus of 4.43 Pa at the same frequency. At a frequency of 1 rad/s, fluid gels of 0.5% and 0.75% agarose displayed a G′ of 32.11 Pa and 44.92 Pa respectively (Fig. 5.7).

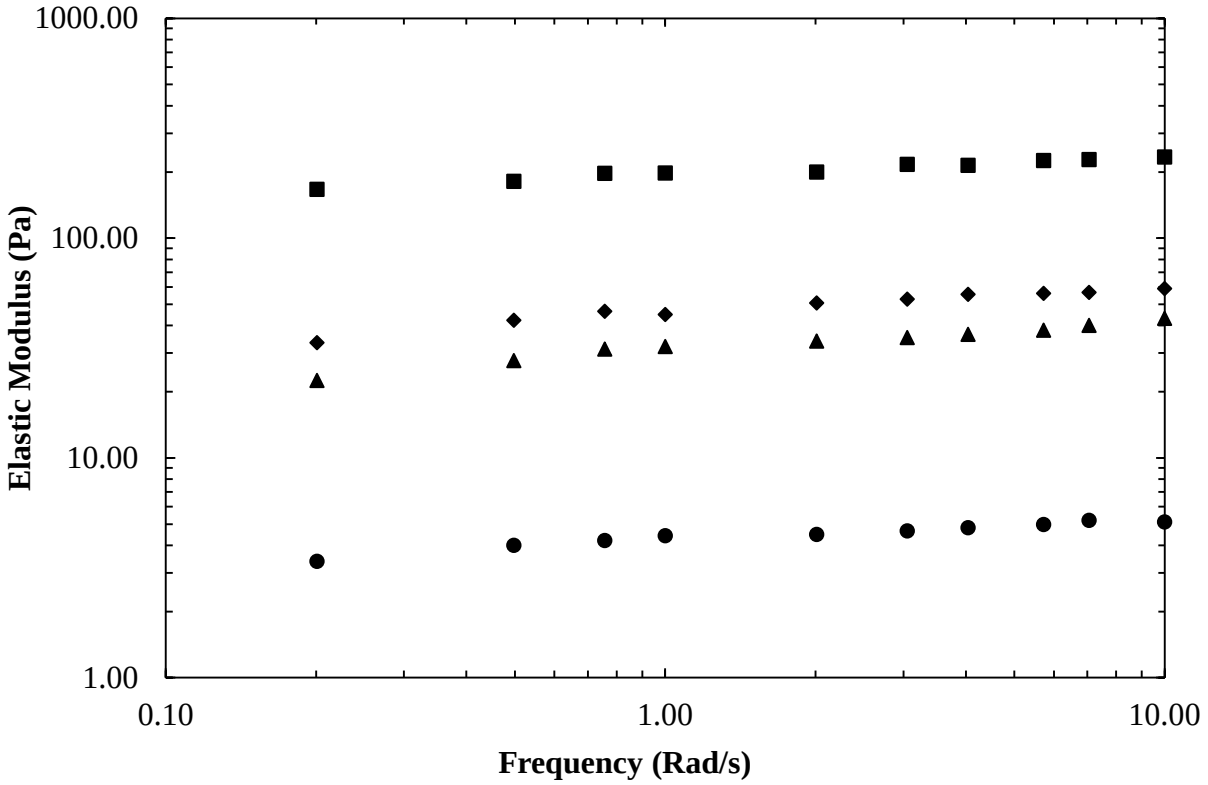

Figure 5.7 - Elastic modulus (G') in response to an increasing frequency of fluid gels made with 1% agarose (black squares), 0.75% agarose (black diamonds), 0.5% agarose (black triangles) and 0.25% agarose (black circles)

Similarly, dynamic viscosity decreased with a reduction in agarose concentration. However, all samples did not fall within the recommended viscosity range for suspension of 1% gellan (0.71 Pas and 14.73 Pas at 1 s^{-1} (Fig. 5.6). Fluid gels of 0.25% agarose exhibited a viscosity of 0.43 Pas at a shear rate of 1 s^{-1}, consequently falling below the minimum requirement of 0.71 Pas at the same shear rate. Fluid gels of 0.5%, 0.75% and 1% agarose exhibited viscosities of 1.42 Pas, 1.88 Pas and 4.19 Pas at 1 s^{-1}.

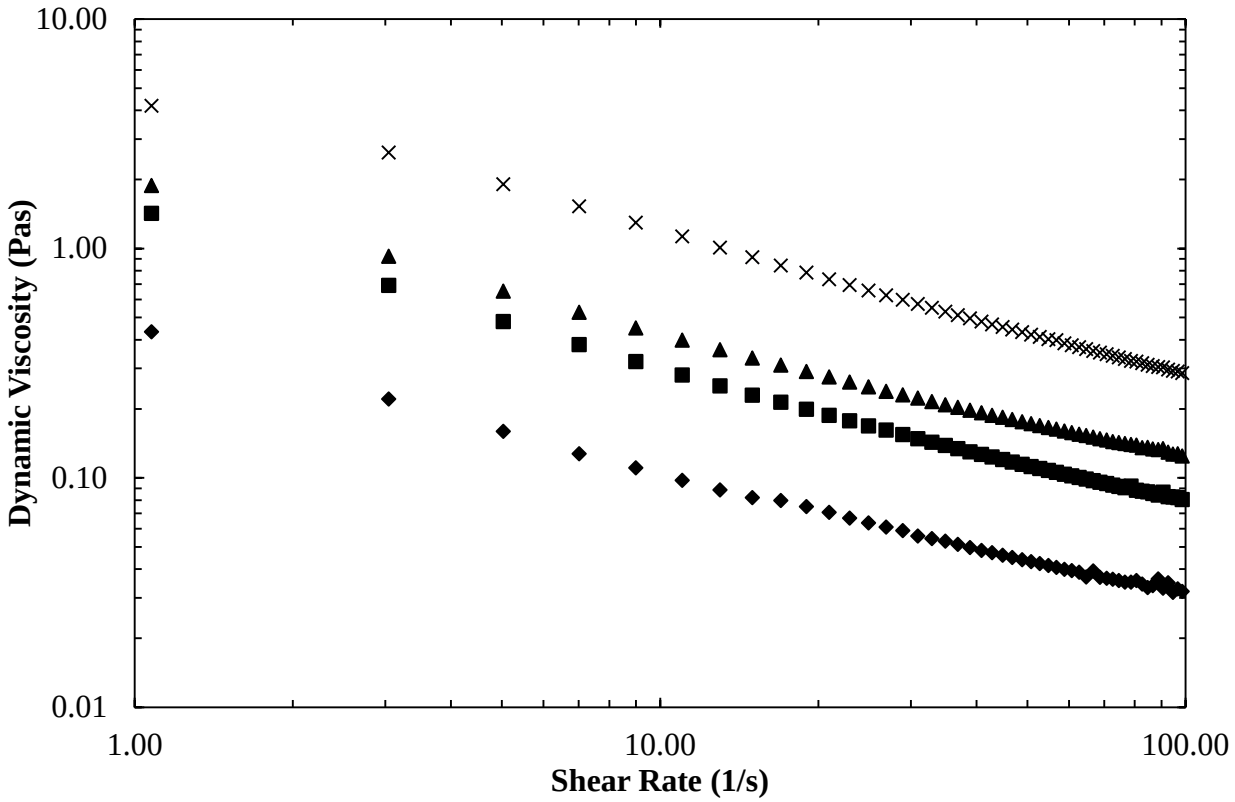

Figure 5.8 - Elastic modulus (G') in response to an increasing frequency of fluid gels made with 1% agarose (black squares), 0.75% agarose (black diamonds), 0.5% agarose (black triangles) and 0.25% agarose (black circles)

After analysing rheological properties of gellan and agarose fluid gels, the next aim was to find an optimal fluid gel composition for creating complex, gellan structures. By selecting a single fluid gel sample, it would be possible to evaluate the impact of factors other than fluid gel mechanical properties on the capacity to create suspended gellan structures. It was concluded that an agarose fluid gel would be better suited due a lack of affinity for cations (Letherby and Young, 1981). Consequently, cations introduced into the system would only interact and cross-link gellan suspensions, thus allowing for greater control over construct gelation. A fluid gel of 0.5% agarose was chosen for further investigation because shear ramps demonstrated viscosity should be sufficient to allow for suspension of gellan structures. Additionally, elastic modulus was far higher than that exhibited by 0.1% gellan fluid gels. Particle size analysis was subsequently used to determine if particle size distribution of 0.5% agarose fluid gels fell between that of 0.1% and 1% agarose fluid gels, thus further suggesting a capacity to suspend gellan structures.

5.3.4 Particle size analysis

Analysis fluid gel particles revealed differences in particle size distribution between 0.1% gellan, 1% gellan and 0.5% agarose fluid gels. This can be observed visually in Fig. 5.9 where 0.1% gellan fluid gels appear to be comprised of a large quantity of smaller particles. In contrast, 1% gellan fluid gels appear to be comprised of a smaller number of much larger particles while fluid gels of 0.5% agarose seem to represent a median. This is supported by particle distribution data outlined in Fig. 5.10-5.12. For example, 63.5% of all particles in a 0.1% gellan fluid gel were in a size range of 0.5-1.5 µm (Fig. 5.10). With 1% gellan fluid gels, the same size range only represented 30.5% of all particles in the sample (Fig. 5.11) while 44.7% of 0.5% agarose fluid particles measured 0.5-1.5 µm in size (Fig. 5.12). Additionally, the maximum observed particle sizes for 0.1% gellan, 1% gellan and 0.5% agarose were 7.5 µm, 13.5 µm and 10.5 µm respectively. Consequently, regarding particle size distribution, 0.5% agarose fluid gels appear to fall in the middle of 0.1% and 1% gellan fluid gels. When combined with rheological properties falling within the required limits for suspension of 1% gellan, this suggested a fluid gel of 0.5% agarose was a suitable sample for further investigation.

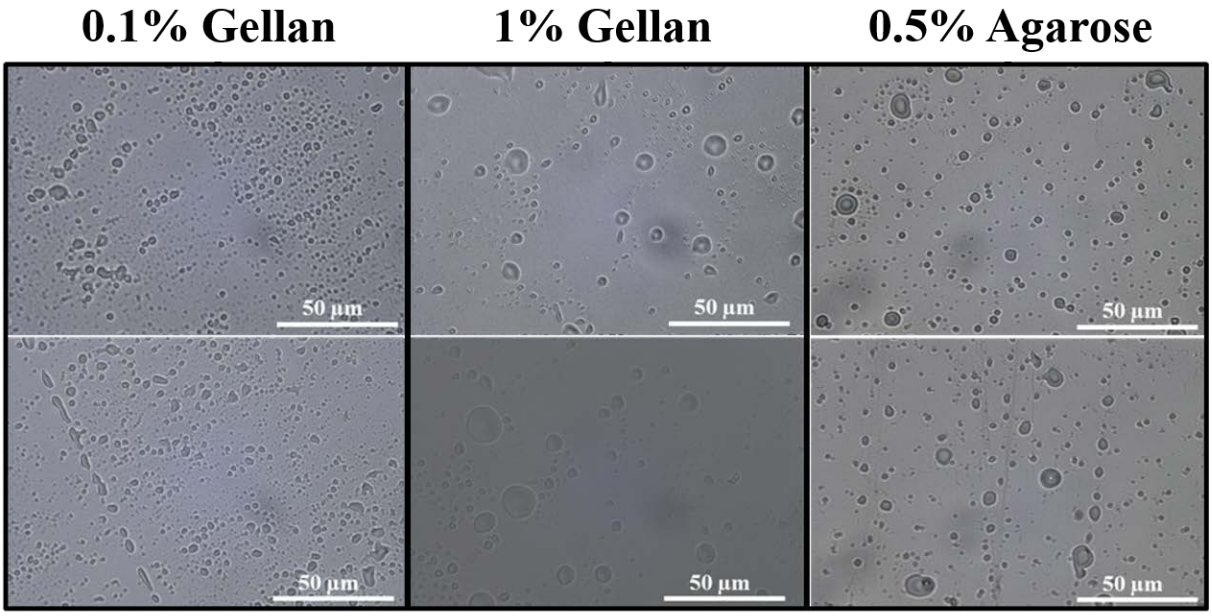

Figure 5.9 – Microscope images of 0.1% gellan, 1% gellan and 0.5% agarose fluid gel particles

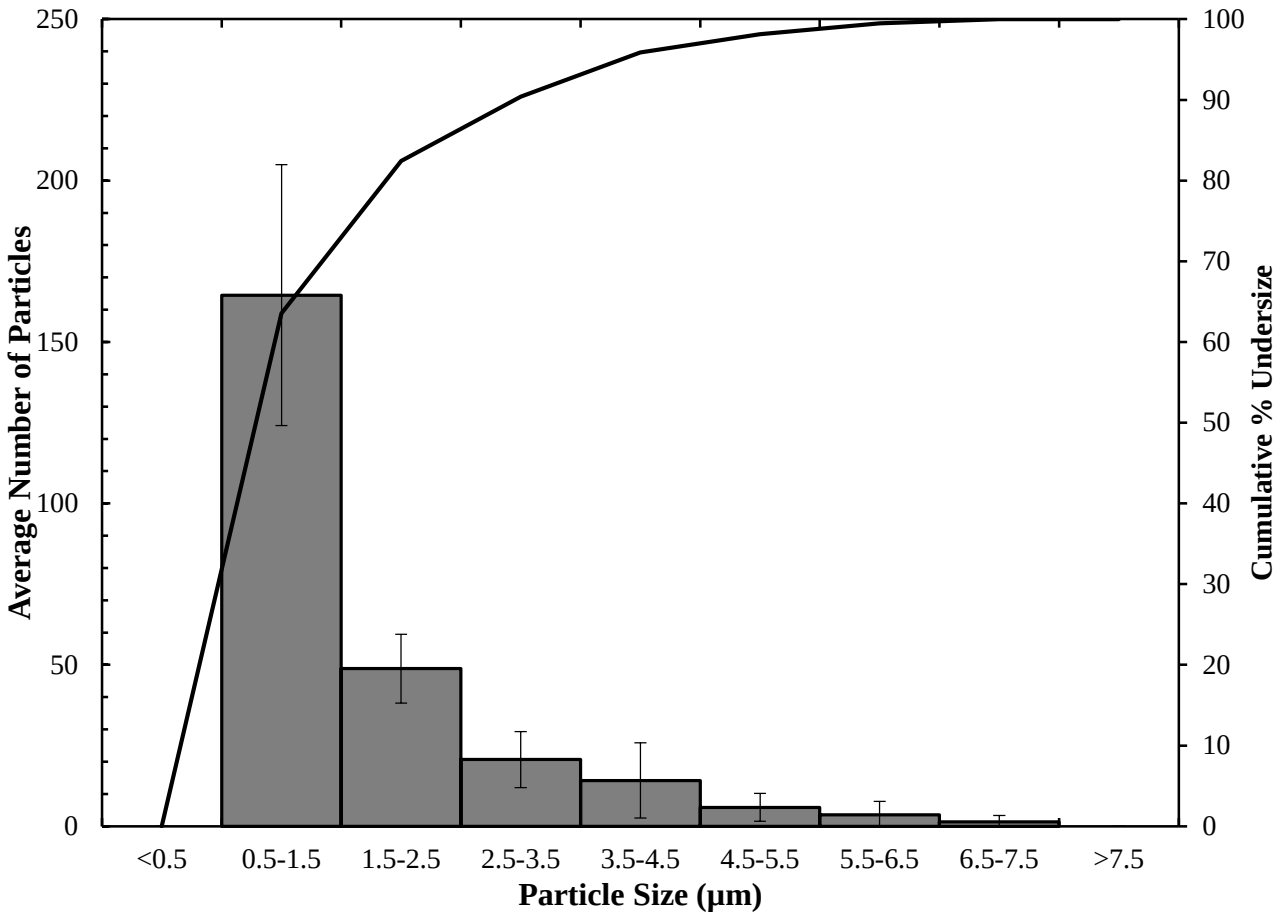

Figure 5.10 – Particle size distribution of 0.1% gellan fluid gels represented by average number of particles in a specific size range and % of particles under a specific size (error bars represent +/- 1 standard deviation, n = 8)

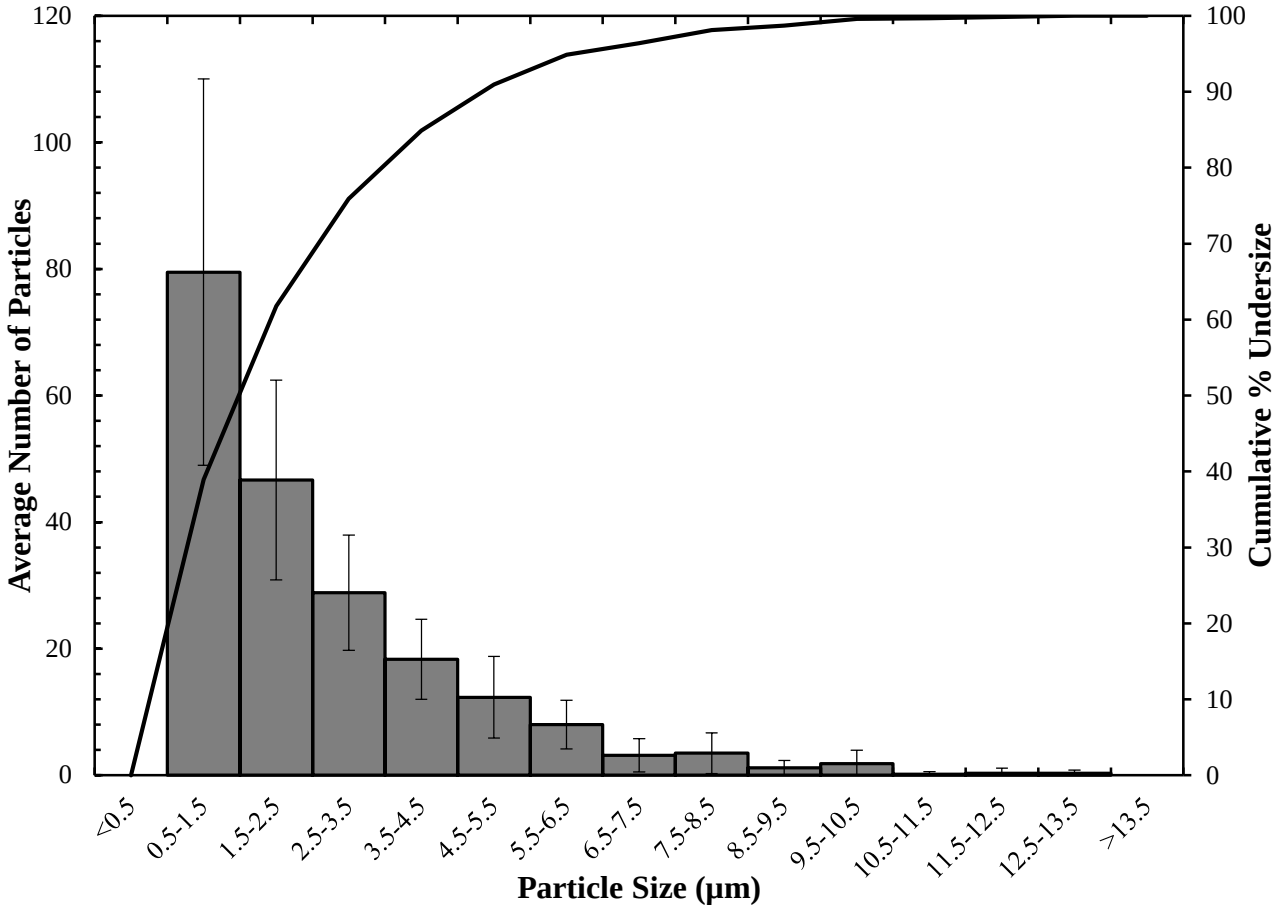

Figure 5.11 – Particle size distribution of 1% gellan fluid gels represented by average number of particles in a specific size range and % of particles under a specific size (error bars represent +/- 1 standard deviation, n = 8)

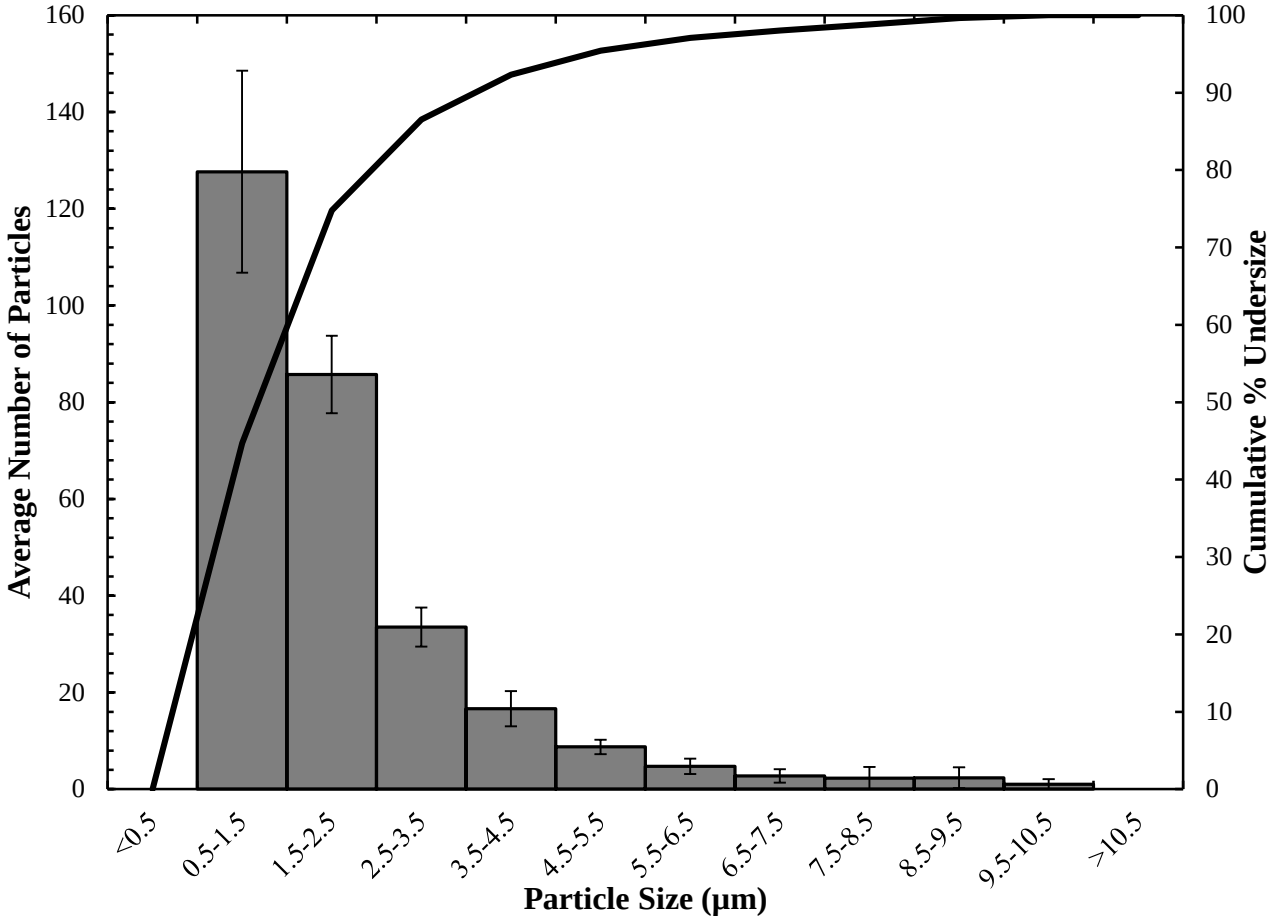

Figure 5.12 – Particle size distribution of 0.5% agarose fluid gels represented by average number of particles in a specific size range and % of particles under a specific size (error bars represent +/- 1 standard deviation, n = 8)

5.3.5 Tuning construct resolution

With mechanical boundaries for suspending solutions of 1% gellan determined, the next stage of development was to determine how the resolution could be tuned to allow control over size and shape of fabricated constructs. Viscosity of extruded solution, inner diameter of hypodermic needles used and the rate at which polymer solutions were laterally deposited were all found to influence construct resolution (Fig. 5.13-5.15). Construct resolution increased as a function of viscosity (Fig. 5.13) with structures fabricated of high viscosity (0.81 Pas at 1 s^{-1}) gellan showing a greater than two-fold reduction in average height (10.31 mm vs. 4.78 mm). This correlated with an increase in construct height from 1.40 mm at low viscosity (0.06 Pas at 1 s^{-1}) to 3 mm at high viscosity (0.81 Pas at 1 s^{-1}). The resulting trend infers viscosity of deposited gellan solutions can be modified to facilitate greater control over polymer deposition facilitating fabrication of more intricate structures.

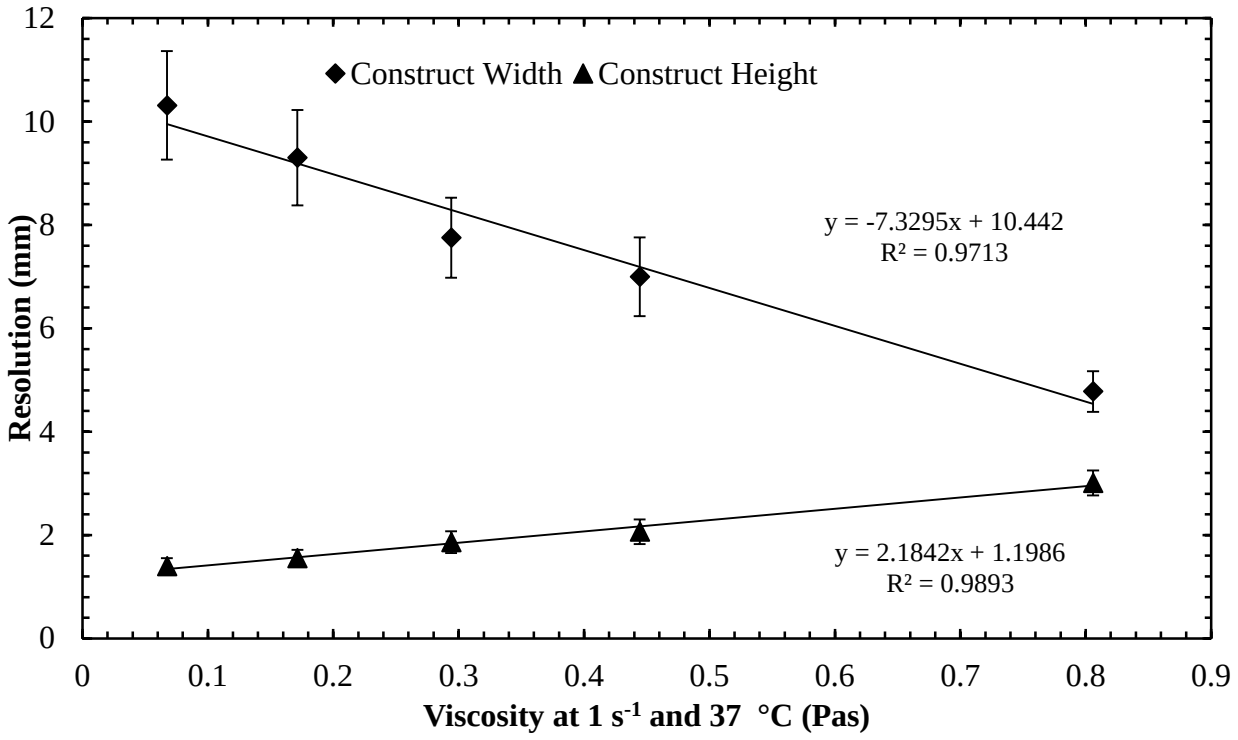

Figure 5.13 – The effect of solution viscosity at 1 s^{-1} on width and height of resulting extruded constructs deposited at a rate of 125 µl/s (error bars represent +/- 1 standard deviation, n = 6)

Further tuning of construct resolution was achieved by varying needle aperture for deposition (Fig. 5.14). By extruding high viscosity gellan (0.81 Pas at 1 s^{-1}) through a hypodermic needle with a 0.26 mm inner diameter, constructs were fabricated with an average height and width of 2.32 mm and 3.51 mm respectively. Increasing the needle inner diameter resulted in constructs with greater height and width and, thus, a lower resolution.

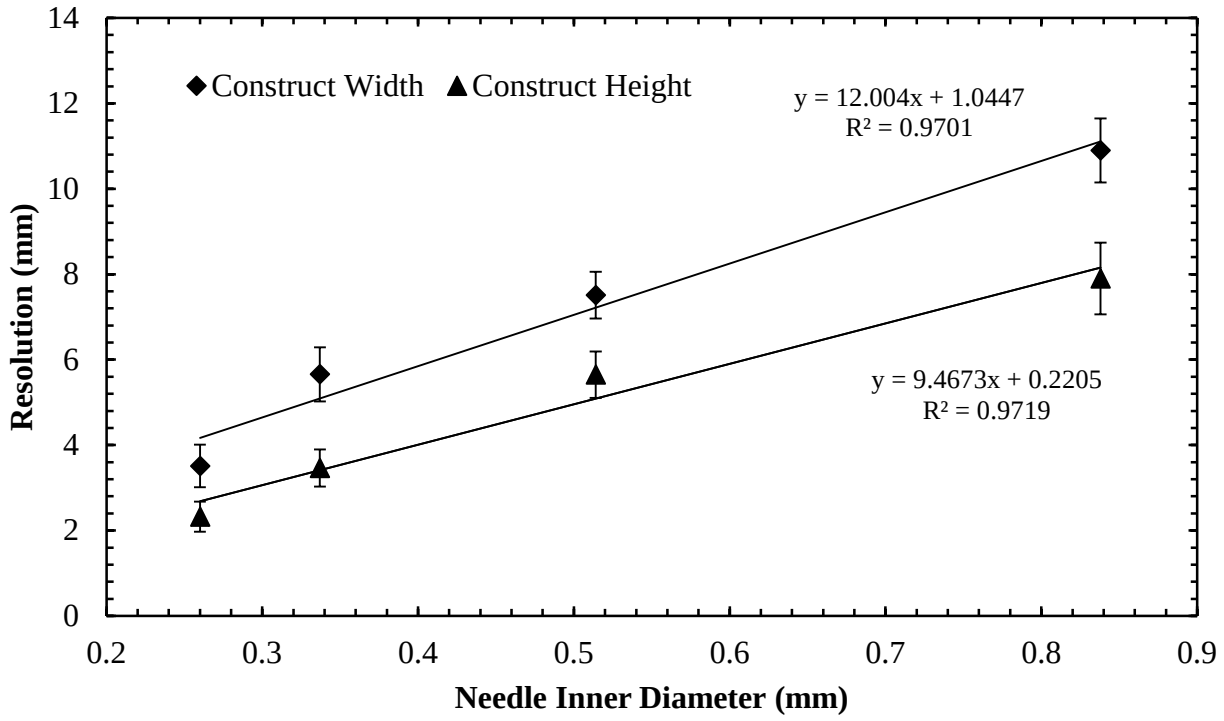

Figure 5.14 – The effect needle inner diameter on width and height of resulting extruded constructs deposited at a rate of 125 µl/s (error bars represent +/- 1 standard deviation, n = 6)

Average height and width of constructs decreased with an increase in lateral deposition speed (Fig. 5.15). Combining high viscosity of gellan, a 260 µm inner diameter needle and a lateral deposition speed of 2.5 cm/s resulted in the highest construct resolution of all three experiments. Average width and height were tuned to 1.30 mm and 2.60 mm respectively.

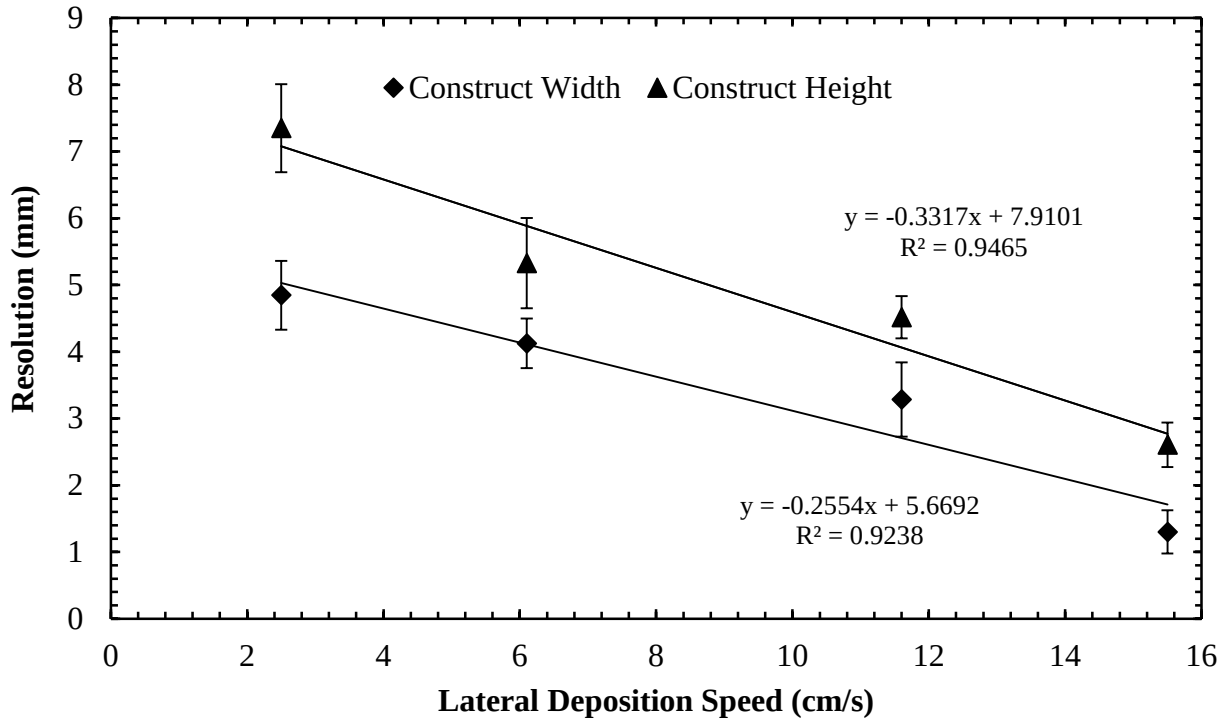

Figure 5.15 – The effect of lateral deposition speed on width and height of resulting extruded constructs deposited at a rate of 125 µl/s (error bars represent +/- 1 standard deviation, n = 6)

5.3.6 Formation of multi-layered structures

Initial evaluation revealed a capacity to fabricate layered hydrogel structures comprised of two different soft materials via suspended deposition in 0.5% agarose fluid gels (Fig. 5.16). Sufficient control can be exhibited to facilitate deposition of separate layers and integration into a similar structure. Additionally, the capacity to integrate multiple materials is not impaired by differences in density between materials. This is best demonstrated in structure C in Fig. 5.16 where 30% gelatin with 5% nano HA was deposited on top of 1.5% gellan. The top layer remained suspended and did not sink into the bottom layer, resulting in formation of a single construct of two integrated materials. Integration in each structure was sufficient to prevent separation of the two layers upon extraction. However, structure A (collagen and gellan) exhibited some weak points around regions in the interface suggesting the two materials did not fully integrate prior to and during gelation possibly due to differences in gelation time between the two materials.

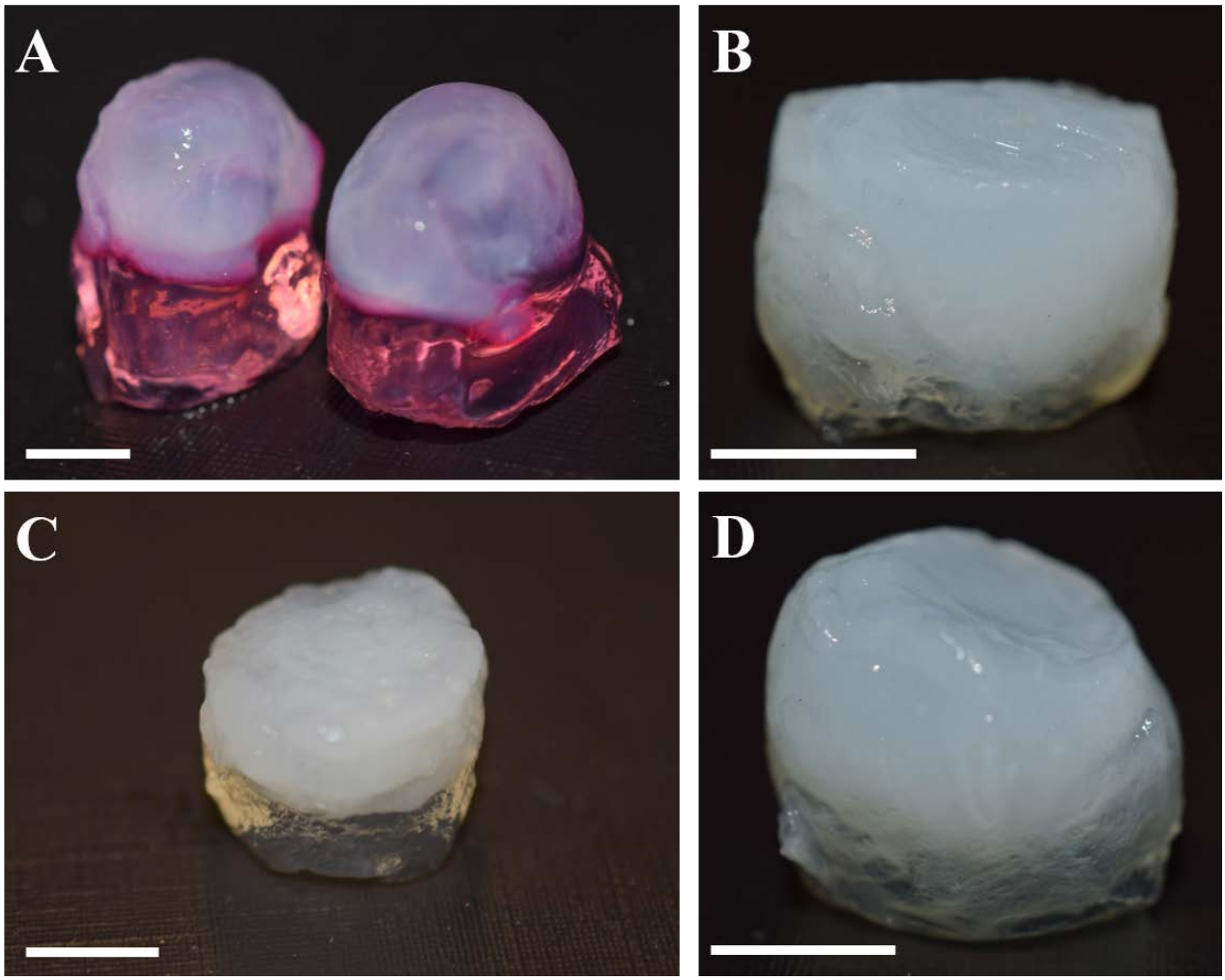

Figure 5.16 – Fabrication and extraction of structures containing a layer of 1.5% gellan and a second layer of A) 0.5% type I collagen, (construct appears pink due to being dyed with culture media for easier deposition) B) 3% alginate with 5% nano HA, C) 30% gelatin with 5% nano HA and D) 1.5% gellan with nano HA (scale bars represent 5 mm)

5.3.7 Fabrication of mineralised gellan helices

Investigation into fabrication of more intricate structures resulted in successful generation of a mineralised gellan helix (Fig. 5.17). A helical structure was successfully deposited in agarose fluid gel and subsequently recovered without compromising structural integrity. Due to the presence of nano HA, CT images were successfully generated indicating complexity of the suspended structure. This further demonstrates the control that can be exhibited over fabrication of complex, high resolution hydrogel constructs.

Figure 5.17 – Fabrication of a mineralised gellan helix (A), micro CT image demonstrating complexity of suspended helical structure (B) and extraction of mineralised gellan helix (C) (scale bars represent 5 mm)

5.3.8 Cell culture proof-of-concept

Multiple cell-loaded, shaped gellan hydrogels were successfully fabricated, cultured and extracted (Fig. 5.18). Live/dead staining revealed high cell viability in each structure as indicated by green fluorescence emitted by encapsulated fibroblasts. This provides a proof-of-concept for further investigation into use of suspended deposition in fluid gel supporting media for fabrication of tissue engineering scaffolds from soft materials.

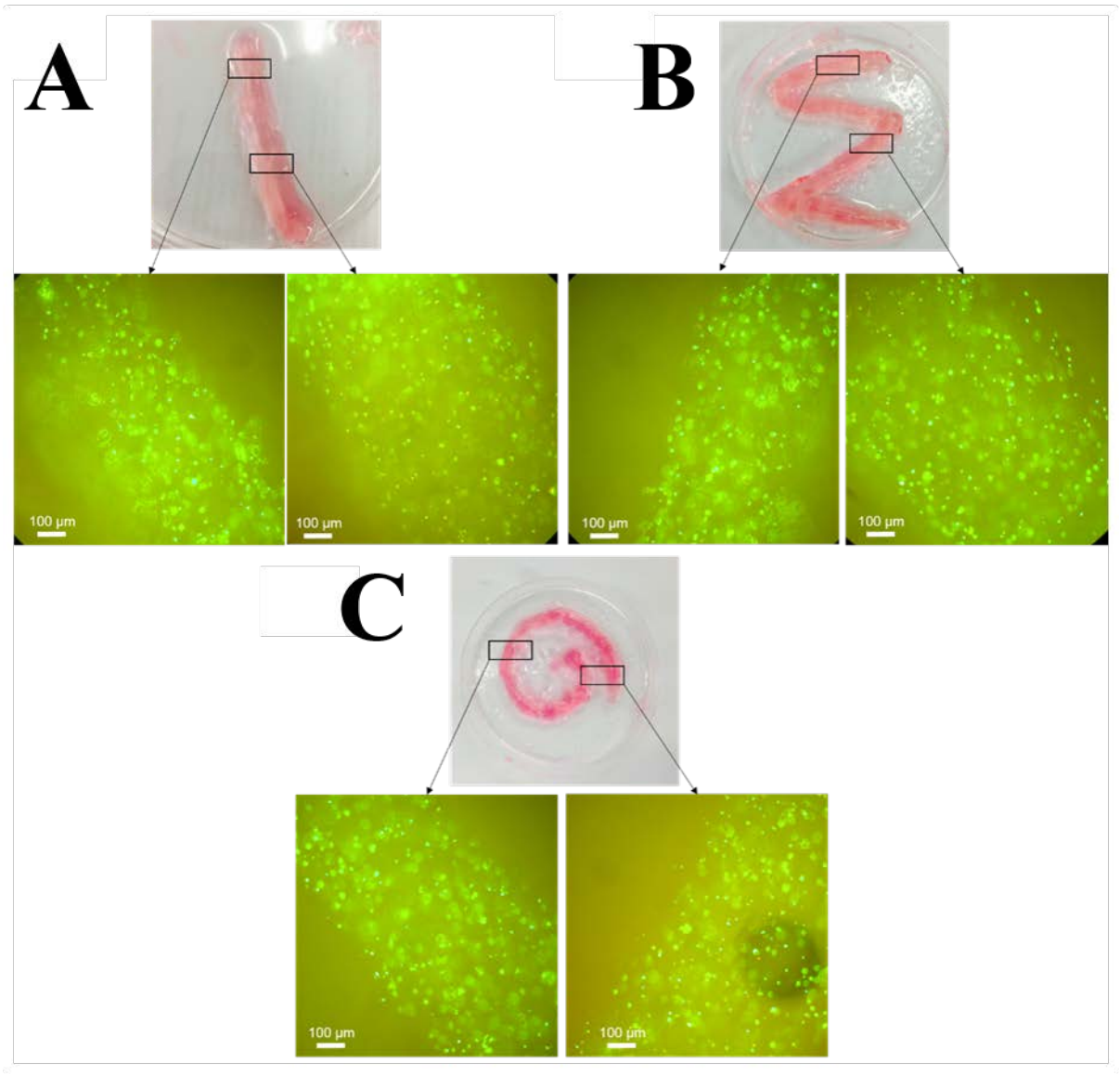

Figure 5.18 - Recovery and live/dead staining of 3T3 fibroblast-loaded gellan hydrogels suspended in A) linear 3D structures B) the shape of the Greek symbol 'Sigma'/Σ and C) the shape of a spiral

5.4 Discussion

The nature of particle-particle interactions in a fluid gel system presents perhaps the most likely explanation for their fluid-supporting properties. Fluid gels can be distinguished from the high viscosity solutions that are often utilised as ALM supporting media because, while they exhibit flow properties, fluid gels are rheologically classified as gels rather than solutions. This is because fluid gels exhibit a higher G′ than G″ with high viscosity fluids displaying the opposite (Sworn et al., 1995). Fluid gel viscosity is mediated by particle-particle interactions rather than molecular entanglement

meaning particles will form bonds with each other but not with suspended polymer solutions. Interactions between particles, therefore allow for suspension and support of a secondary phase even if polymer concentration and subsequent density vary greatly. This is demonstrated in Fig. 5.16 where a gelatin solution with a 65% water content was suspended in a fluid gel of 99.5% water. The gelatin solution did not sink through the fluid gel allowing it to be deposited in a controlled manner such that it could be suspended on top of 1.5% gellan solution.

Minimum required elastic modulus, dynamic viscosity and particle size distributions for a fluid gel to act as supporting media for 1% gellan solutions was determined via characterisation of a formulation containing 0.1% gellan and 0.5% NaCl (Fig. 5.4, 5.5 and 5.9-5.12). Since loss of rapid self-healing capabilities in the supporting media was seen with this formulation it can be suggested that any fluid gel exhibiting weaker gel properties, a lower viscosity and reduced particle size would likely rupture further and not support deposited fluids. This can be explained by the relationship between particle size, stiffness, aggregation and resulting fluid gel viscosity. It has previously been shown that fluid gel particles form bridges with neighbouring particles in order to create a paste-like phase as described previously (Norton et al., 1999). An increase in particle stiffness and size as a result of higher polymer concentration promotes more frequent interactions between particles. This allows particles to pack together more tightly such that a greater shear force is required to break the bonds between them and fluid gel viscosity subsequently increases (Farrés et al., 2014). Such a trend was observed in rheological characterisation of each fluid gel with elastic modulus, viscosity and particle size found to reduce with polymer concentration (Fig. 5.5-5.9). Inability to rapidly self-heal and subsequent loss of structure in gellan solutions suspended in a 0.1% gellan fluid gel (Fig. 5.4) suggests there is a threshold in fluid gel strength below which it can no longer act as a supporting media. Below the threshold, it is likely that there is insufficient aggregation of fluid gel particles (demonstrated by low viscosity) as a result of reduced particle size and strength. When polymer solutions are therefore deposited, the shear force applied by deposition is greater than the required

shear force to separate fluid gel particles and the network ruptures, resulting in flow of suspensions. Conversely, at higher polymer concentrations, a much larger shear force is required to separate fluid gel particles. While this better facilitates support of deposited polymer solutions, upper limits apply as when require shear force to separate particles is too high, extraction of softer structures can be impaired by difficulties in removing excess fluid gel (Fig. 5.4). However, there is potentially a large spectrum of required fluid gel properties such that they could be tailored to suit fabricating constructs of varied mechanical properties. For example, a stronger, more viscous fluid gel with greater particle sizes could be used to fabricate structures from strong and stiff polymer formulations while less viscous fluid gels with smaller particles could be used to create much softer structures.

A fluid gel of 0.5% agarose was chosen for further investigation due to particle size distribution falling in the middle of the required size for this application (Fig. 5.9-5.12). Additionally, the elastic modulus was significantly higher than that of a 0.1% gellan fluid gel (32.11 Pa vs. 3.92 Pas at 1 Hz). Moreover, viscosity was higher than in a 0.1% gellan fluid gel (1.42 Pas vs. 1.08 Pas at 1 s^{-1}) but significantly lower than observed in 1% gellan fluid gels (14.73 Pas at 1 s^{-1}). As a result, it was concluded that low viscosity a 0.5% agarose fluid gel should facilitate easy extraction of gelled constructs. Additionally, by exhibiting a higher modulus and particle size than that of 0.1% gellan fluid gels, it was suggested that 0.5% agarose could exhibit sufficient self-healing properties for use as a supporting media in this application. This is evidenced by successful fabrication of layered structures, a mineralised gellan helix and cell loaded, gellan constructs (Fig. 5.16-5.18).

Resolution of suspended structures is, however, viscosity dependant (Fig. 5.13). In order to fabricate a high resolution suspended structure such as the mineral helix presented in Fig. 5.17, sufficient viscosity is required to prevent viscous flow of extruded solutions. This is highlighted by a reduction in construct resolution when low viscosity gellan solutions were suspended. It is possible that at low viscosities, deposited fluids have a capacity to flow between fluid gel particles, thus reducing the control over the precision with which structures can be fabricated. Moreover, construct resolution can

be further tuned by variations in needle aperture during extrusion and lateral deposition speed (Fig. 5.14-5.15). It is likely that a reduction in needle inner diameter reduces droplet size when polymer solutions are extruded (Tripp et al., 2016), thus facilitating deposition of smaller structures. Depositing using an increased lateral speed reduces the number of droplets extruded across the length of a construct, further increasing resolution. When combined, all three factors can be used to tune resolution of fabricated structures providing a platform for customising the shape and size of resulting hydrogel scaffolds with relative ease.

Fabrication of mineralised gellan helices highlights the control that can be exhibited to facilitate creation of complex structures (Fig. 5.17). Helices of polymer solution were successfully suspended, something that is not possible without use of supporting media. Moreover, structural integrity was not compromised during extraction. This is of significance as gellan gum hydrogels are highly brittle (Sworn et al., 1995). When extracted the helix retained its shape, demonstrating successful support provided by the particulate gel network. Moreover, a lack of structural failure indicates the level of ease with which gelled structures can be separated from fluid gel supporting media.

Successful generation of a single construct comprised of multiple, separately added layers of different materials provides a proof-of-concept for fabrication of layered, multicellular tissue engineering scaffolds as outlined in Fig. 5.3. While integration of the two materials used in each structure shown in Fig. 5.16 was successful, constructs of collagen and gellan showed weak integration in comparison to the other fabricated structures. This could be attributable to significant differences in gelation time between gellan and collagen. Gelation of gellan is rapid while collagen has a much longer onset of gelation. As a result, it is likely that the layer of gellan gelled before the collagen, thus impairing integration of the two materials. In contrast, interfaces between alginate/HA, gelatin/HA and gellan/HA and gellan were much stronger as each material has a similar, rapid onset facilitating simultaneous gelation of two materials into a single structure. Each structure displayed in Fig. 5.16 could potentially be used as an osteochondral model due to successful formation of a 2-layered

structure with an interface. Constructs fabricated from gelatin/HA-gellan could be used for cell delivery in an osteochondral defect, for example. This is due to gelatin often exhibiting a melting temperature below the physiological value of 37 °C (Eldridge and Ferry, 1954). Therefore, cell loaded scaffolds could be fabricated and implanted into *in vivo* defects whereby gelatin would melt and release cells from the scaffold. Similarly, breakdown of alginate *in vivo* as a result of ion exchange could also facilitate such an application (Thomas, 2000). Scaffolds fabricated from gellan/HA-gellan and collagen-gellan would be more suited as implants for long term 3D culture as neither material undergoes rapid breakdown in physiological conditions. Moreover, collagen is natively cell adhesive and incorporation of 5% HA or greater in gellan has also been shown to facilitate cell adhesion (Jamshidi et al., 2015). Such structures could be implanted into osteochondral defects and cultured without undergoing rapid breakdown, thus supporting longer periods of cultivation.

Another significant result is the high cell viability in constructs fabricated by suspended manufacture (Fig 5.18). When cell-loaded constructs are generated using this method, a polymer/cell suspension is extruded through a hypodermic needle. A shear force is applied to the polymer when pressure is applied to the syringe plunger. This results in flow as a result of shear thinning and allows for extrusion of materials through a needle. However, the same shear force is also applied to cells suspended in the polymer solution. A similar mechanism is often employed in other bioprinting mechanisms and it has been shown that shear forces applied in printing can compromise cell viability if they are too great (Farrés et al., 2014). However, viability in fabricated constructs was high suggesting shear forces required to extrude materials in this system are not above the threshold at which cell viability can be compromised.

5.5 Conclusions

Fluid gels have been presented as possible platforms for rapid prototyping of 3D tissue culture substrates by acting as a supporting media for ALM. Rheological boundaries were characterised and tunability of the system was successfully demonstrated. The system allows for generation of complex, intricate structures such as a 3D helix and facilitates incorporation of multiple materials into a single construct. Cell-loaded structures were also successfully fabricated with a high viability exhibited by encapsulated 3T3 fibroblasts. Fabricated cell-loaded structures were, however, fairly simple and comprised of a single material. As a result, Chapter 6 highlights the significance of such a system from a more clinical perspective with a focus on addressing healthcare issues associated with damage to layered osteochondral tissue. A study was subsequently designed to evaluate use of ALM with fluid gel supporting media to fabricate layered, cell-loaded culture scaffolds for repair of damaged/degraded osteochondral tissue.

Chapter 6 – Fabrication of a Layered Tissue Culture Scaffold for Repair of Human Osteochondral Defects

Aspects of this chapter are published in *Advanced Materials*.

Moxon, S. R. Cooke, M. E. Cox, S. C. Snow, M. Jeys, L. Jones, S. W. Smith, A. M. Grover, L. M. (2017) Suspended Manufacture of Biological Structures, Advanced Materials, 1605594.

All experiments involving use of human tissue samples and cells were conducted in accordance to ethical guidelines (Ethics Reference Number – 12/EE/0136).

6.1 Introduction

Osteochondral tissue is key to joint function and contains an interface between subchondral bone and hyaline cartilage. Damage to osteochondral tissue can lead to significant discomfort and impaired function of joints. The most notable example of osteochondral degeneration is osteoarthritis (OA), an age-related degenerative disease caused by damage and breakdown of hyaline cartilage and underlying, subchondral bone (Buckwalter and Mankin, 1997). Current estimates stipulate ~40% of people aged over 65 suffer from OA, thus presenting it as a significant health problem affecting quality of life with occurrences likely to increase with improved global life expectancy (Dunlop et al., 2001). Consequently, research into methods for treatment of damaged osteochondral tissue is widespread with numerous techniques approved for clinical use such as reparative surgery, autografts, allografts and implantation of autologous chondrocytes for tissue regeneration (Brittberg et al., 2001, Rönn et al., 2011). However, current treatments are hugely limited by aspects such as lack of donor availability and poor formation of fibrocartilage. Furthermore, current methods often inflict additional damage to osteochondral tissue before triggering repair (Schaefer et al., 2000). As such, a great deal of emphasis is placed on the requirement for new methods of repairing damaged

osteochondral tissue with a focus on integration of tissue engineering scaffolds as osteochondral analogues for regeneration of healthy tissue. Understanding the complex structure of osteochondral tissue is critical to the process of developing new therapeutic approaches, especially regarding design of 3D tissue culture scaffolds (Martin et al., 2007).

Structurally, osteochondral tissue can be broken down into three layers, namely hyaline cartilage, subchondral bone and calcified cartilage with the latter serving as the interface. Integration of each layer is critical in facilitating the normal function of osteochondral tissue (Li et al., 2015). Collagen fibres penetrate across each layer providing joints with resistance to shear stress with the most abundant being types I, II and X (Redler et al., 1975, Levingstone et al., 2014, Nukavarapu and Dorcemus, 2013). Additionally, a gradient in mineralisation is exhibited with transition from un-mineralised cartilage, through calcified cartilage and into the highly mineralised structure of subchondral bone (Seidi et al., 2011). When considering tissue engineering approaches to repairing damaged osteochondral tissue, scaffolds that reflect this tiered structure provide a promising platform for regenerating healthy tissue (Fig. 6.1).

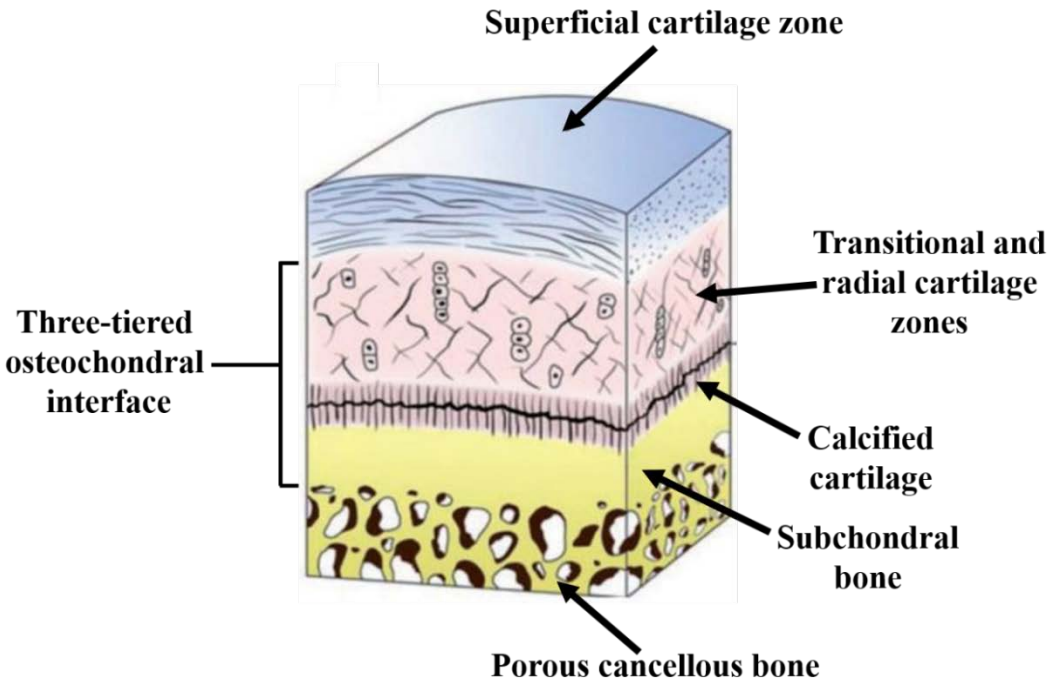

Figure 6.1 – A schematic demonstrating transition from a superficial layer of articular cartilage through an osteochondral interface and into porous, cancellous bone (Adapted from Li et al. 2015 with permissions from Oxford University Press)

Mechanical properties of osteochondral tissue also vary between each layer with hyaline cartilage exhibiting a significantly lower modulus than subchondral bone. A recent study by Campbell et al. in 2012 quantified changes in mechanical behaviour across the three layers of osteochondral tissue by nanoindentation (Campbell et al., 2012). Subchondral bone was shown to exhibit and average indentation modulus of 22.8 GPa with the interface and hyaline cartilage exhibiting moduli of 21.3 GPa and 5.7 GPa respectively. Therefore, a gradient in mechanical strength exhibited by osteochondral tissue coincides with the transition into more mineralised tissue.

Cellular composition also differs in each region of osteochondral tissue with articular cartilage being populated by chondrocytes. Subchondral bone contains populations of the four bone cell types outlined in Chapter 1 (osteoblasts, osteoclasts, osteocytes and bone lining cells), however osteoblasts are the most significant in maintenance and repair due to their role in bone formation (Rawadi et al., 2003). At the interface, chondrocytes are present and known to undergo genotypic changes by up-regulating genes associated with a hypertrophic phenotype. This results in synthesis and deposition

of a Type X collagen matrix and subsequent mineralisation to form the foundation of calcified cartilage (Mahjoub et al., 2012).

Consequently, design of osteochondral scaffolds is very challenging as, in order to more accurately reflect native tissue, substrates composed of multiple materials and cell types are desirable. One promising model is a scaffold containing segregated layers of osteoblasts and chondrocytes, each present in a different mechanical environment (Panseri et al., 2012). For a subchondral bone analogue, it is desirable to present cells with an environment exhibiting high matrix stiffness. Therefore, osteoblasts are often cultured within a mineralised, ordered matrix in order to better stimulate expression of a native phenotype (Kim et al., 2005). Secondly, a material exhibiting much lower matrix stiffness and seeded with chondrocytes is desirable for a cartilage analogue. Most critically, the two materials should be present in distinct layers but also interface in a controlled manner such that they do not separate under shear force. Mechanical behaviour of an osteochondral scaffold should ideally reflect the trend observed in native tissue and, therefore have a gradient in mineralisation across the structure (Mohan et al., 2014, Di Luca et al., 2015). Moreover, for clinical applications, it is desirable for the thickness of each layer to be tunable to reflect variances in relative thickness observed between different joints and individuals (Shepherd and Seedhom, 1999).

Some progress has been made in designing tissue culture scaffolds for osteochondral repair. For example, a study by Khanarian et al., (2012) proposed an agarose-hydroxyapatite (herein referred to as ‘HA’) scaffold seeded with chondrocytes as a potential osteochondral hydrogel-ceramic composite (Khanarian et al., 2012). Chondrocytes seeded in agarose-HA composites showed increased ECM synthesis and activity of enzymes associated with mineralisation such as ALP. However, scaffolds were not layered and, thus did not exhibit any of the required gradients for an optimal osteochondral scaffold. Moreover, a single cell type was seeded rather than multiple cell types. Another study by Cheng et al., (2011) arguably presents a more promising method for creating more analogous osteochondral scaffolds (Cheng et al., 2011). Collagen microspheres seeded with MSC’s were used

to fabricate a layered co-culture of osteoblasts, hypertrophic chondrocytes and chondrocytes, thus mimicking cellular content of osteochondral tissue. Fabrication was complex, however, and layers were comprised of pre-gelled collagen microspheres bringing into question the strength of interface between each layer.

In this chapter, ALM using fluid gel as a supporting media is presented as a method for fabricating a single, multicellular gradient structure for use as an osteochondral plug. Building on proof-of-concept with fabrication of osteochondral-like scaffolds from multiple materials (Chapter 5 - Fig. 5.16), gellan/HA-gellan scaffolds were chosen for further investigation. This was due to ease of gelation into a single, layered structure and an ability to support long-term 3D culture. A study was then designed to apply this to a human cell culture model for regeneration of knee osteochondral defects. The process involved extraction of tissue, defect simulation and isolation of primary osteoblasts and chondrocytes from excess tissue. Defects were then reconstructed with micro-CT and a CAD model was generated and used to guide fabrication of an autologous, cell-loaded osteochondral scaffold for osteochondral defect repair (Fig. 6.2). Rheological properties were evaluated to determine if a mechanical gradient similar to that exhibited by native tissue could be obtained. Autologous, cell-loaded scaffolds were implanted into osteochondral defects and cultured for 30 days before extraction and evaluation of osteogenic and chondrogenic responses by reverse transcription (RT PCR). This study was carried out in collaboration with The University of Birmingham and conducted under strict ethical boundaries for the use of human samples (Ethics Reference Number – 12/EE/0136).

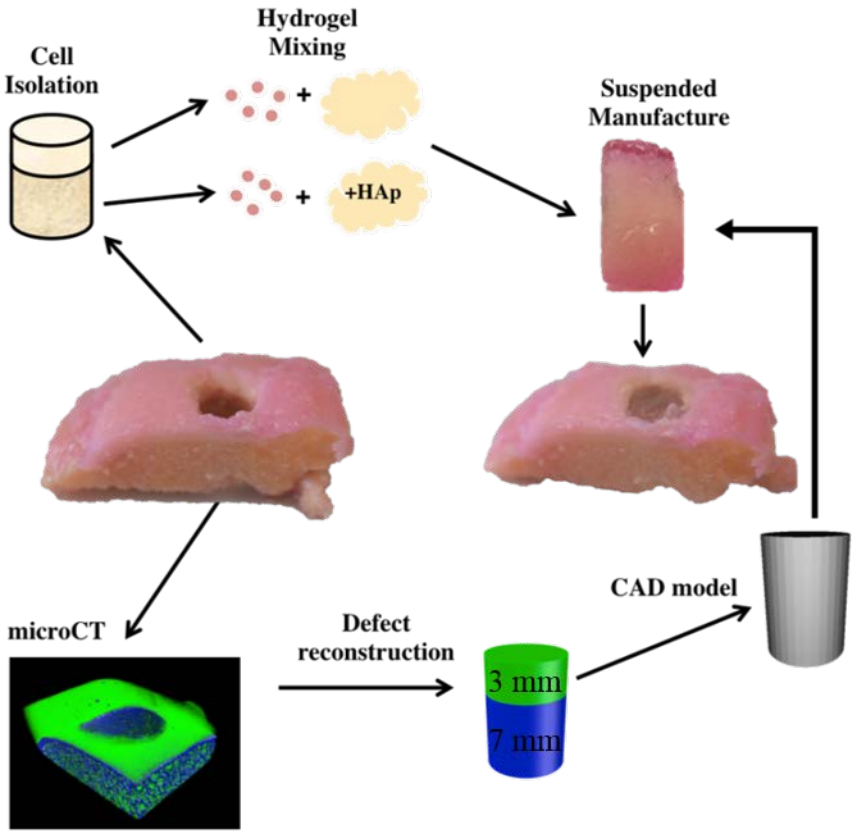

Figure 6.2 – Simulation of a human osteochondral defect and subsequent reconstruction and fabrication of a cell-loaded scaffold for osteochondral repair

6.2 Materials and Methods

6.2.1 Materials

Gellan (low acyl – referred to as 'gellan') was purchased from Kalys (Benin, France). Agarose was purchased from Sigma Aldrich (Dorset, UK). For PCR, primer sequences for each gene were designed using Primer Express 3 software (Applied Biosystems, Warrington, UK) and produced by LifeTechnologies (Cramlington, UK). OneStepPLUS SYBR Green Dye was purchased from PrimerDesign (Eastleigh. UK).

Cell culture plastics, syringes and hypodermic needles were purchased from Sigma-Aldrich (Dorset, UK). All other reagents and cell culture media and supplements were purchased from Sigma-Aldrich (Dorset, UK) and used without further purification.

6.2.2 Extraction and culture of primary human cells

Osteochondral knee tissue was harvested from patients undergoing elective total knee replacement surgery. Sections of cartilage and subchondral bone were surgically removed and cells isolated. Cartilage was removed and minced into 2 mm^3 pieces before enzymatic digestion in 2 mg/ml collagenase at 37 °C for 3 hours to isolate primary chondrocytes. Primary osteoblasts were isolated by culturing 5 mm^3 bone chips in supplemented DMEM (10% FBS, 2.5% L-glutamine, 2.5% HEPES buffer and 1% penicillin/streptomycin) at 37 °C for 14 days. Both cell types were cultured in T75 flasks using supplemented DMEM at 37 °C and 5% CO_2 with media changed every 3 days.

6.2.3 Defect creation and reconstruction

Samples of osteochondral tissue were cultured in supplemented DMEM at 37 °C and 5% CO_2 until required. To simulate an osteochondral defect circular holes were drilled through both the bone and cartilage layers of tissue samples using a sterilised drill. Each tissue block was imaged by microCT and reconstructed in 3D using CTVox software. Guided by dimensions outlined in microCT the defect was reconstructed as a two-layered structure similar to those created in Chapter 5, Fig, 5.16. Gellan (1.5% w/w – sterilised by autoclaving) loaded with $1x10^6$ primary human chondrocytes was deposited in a 0.5% agarose fluid gel in a circular layer of 3 mm thickness and 10 mm diameter. A second layer of 1.5% gellan/5% HA loaded with $1x10^6$ primary human osteoblasts was deposited on top in a circular layer of 7 mm thickness and 10 mm diameter (to match tissue thickness and diameter of defect as determined by micro-CT and CAD reconstruction). Cells used in each construct were extracted from the tissue they were implanted in to ensure scaffolds were autologous.

Once both layers were deposited 200 mM $CaCl_2$ was injected around the suspended structure to trigger gelation. After 45 minutes constructs were extracted with a sterile spatula and excess fluid gel was washed away with sterile deionised water. Acellular scaffolds were also fabricated from the same materials for use in investigation of rheological properties.

6.2.4 Stress sweeps of osteochondral implants

To evaluate changes in mechanical behaviour across constructs, moduli of three acellular scaffolds were analysed via stress sweeps. After gelation and extraction, constructs were sliced laterally into 4 regions using a sterile scalpel (Fig 6.3). Stress sweeps were conducted on each region using a Malvern Kinexus Pro rheometer (Malvern, UK) fitted with a 40 mm serrated parallel plate geometry. Elastic and viscous moduli (G′ and G″) were analysed in response to increasing stress from 1-100 Pa at a constant temperature of 37 °C and a frequency of 10 rad/s. Values were then compared to nanoindentation moduli of the relevant regions in native tissue (sourced from Campbell et al. 2012) to observe any similarities in trends in mechanical behaviour.

6.2.5 Culture of osteochondral implants

Following bioprinting, cells encapsulated in custom-shaped hydrogels were cultured for 30 days in one of four conditions. Test samples were cultured inside simulated defects of human knee tissue with supplemented DMEM. Three control samples were also prepared with implants cultured in DMEM without tissue, cultured in conditioned culture media without tissue or cultured in separate layers of encapsulated chondrocytes or osteoblasts using supplemented DMEM. Constructs were kept at 37 °C in a 20% O_2 humidified incubator and media was changed every 3 days. Conditioned culture media was created by exposing supplemented DMEM to human tissue for 48 hours prior to use.

6.2.6 Reverse transcription PCR (RT-PCR) – RNA Isolation

Cell-loaded osteochondral plugs were extracted from tissue after 30 days culture and sliced into three regions as demonstrated in Fig 6.5. RNA was isolated from gels using TRIzol® reagent. Gel cross-sections were separated and 500 µl TRIzol® reagent was added to each and left for 5 minutes before removal. Samples were transferred in to sterile eppendorf tubes where 100 µl chloroform was added for separation of RNA, protein and DNA. The aqueous RNA-containing phase was removed and RNA was precipitated using 500 µl 100% isopropanol. Samples were then centrifuged for 15 minutes at 12,000 Xg and 4°C. The supernatant was removed and pellet washed in 1 ml 75% ethanol diluted

in RNAse free water, dried in a vacuum desiccator for 15 minutes and re-suspended in RNAse-free water. RNA concentration and A260/280 ratios were quantified by spectrophotometry to determine RNA purity (NanoDrop 2000, ThermoScientific). RNA was stored at -80 °C prior to use.

6.2.7 RT-PCR

Quantification and expression of type I collagen (COL1A1) and type II collagen (COL2A1), key osteogenic and chondrogenic markers, was performed on isolated RNA using precision OneStepPLUS SYBR Green Dye with β-actin used as a housekeeping gene. Primer sequences are shown in Table 1. Gene expression was quantified using the Pfaffl method (Pfaffl, 2001).

Table 6.1 - Primers used for real-time PCR

Gene	**Forward Primer**	**Reverse Primer**
Collagen Type II	ACTGGATTGACCCCAACCAA	TCCATGTTGCAGAAAACCTTCA
Collagen Type I	CTGTTCTGTTCCTTGTGTAACTGTGTT	GCCCCGGTGACACATCAA

6.3 Results

6.3.1 Fabrication of cell-loaded osteochondral implant scaffolds

Layered, multicellular scaffolds were successfully fabricated in cell culture conditions (Fig. 6.3). Both materials were successfully integrated into a single, self-supporting scaffold that could be handled without compromising structural integrity.

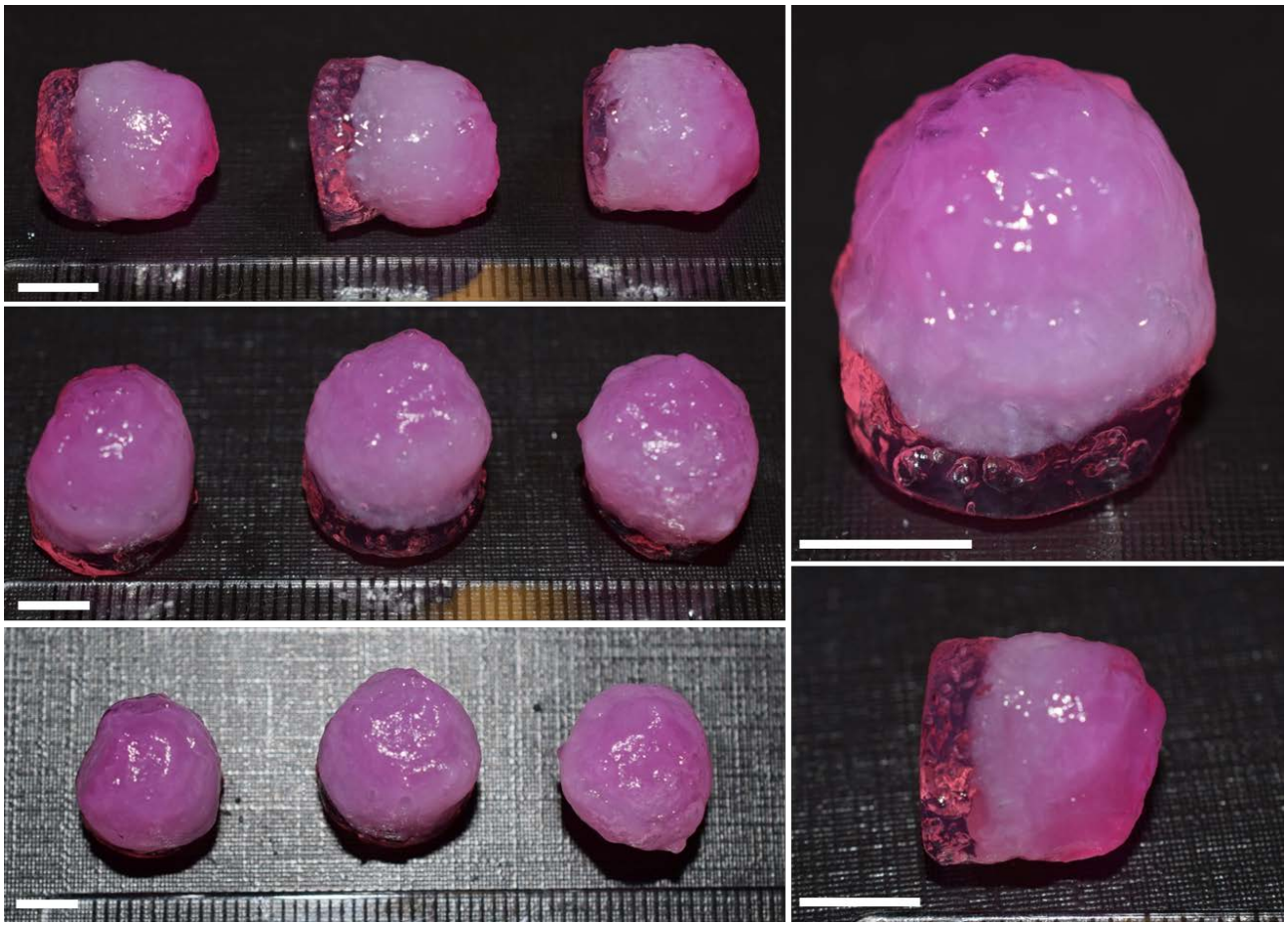

Figure 6.3 – Layered, multicellular scaffolds comprised of chondrocyte-loaded gellan and osteoblast-loaded gellan/HA (scale bar represents 5 mm)

6.3.2 Stress sweeps of osteochondral scaffolds

Stress sweeps of Region A-D revealed a gradient in mechanical properties across osteochondral scaffolds (Fig. 6.4). The trend shows some similarities to trends in mechanical properties observed in the three main regions of osteochondral tissue where Region A represents hyaline cartilage, Region B represents calcified cartilage and regions C and D represent subchondral bone. The highest modulus was observed in Region C of constructs with an average G′ of approximately 42 KPa. Transition through Region B and into Region A resulted in a reduction in modulus with a G′ of 33 KPa and 22 KPa exhibited in Regions B and A respectively. Similarly, in osteochondral tissue, subchondral bone exhibits the highest modulus, hyaline cartilage the lowest and calcified cartilage falls in between. Region D of constructs, however, exhibited the lowest G′ and was the only region not to follow observed trends in mechanical properties across osteochondral tissue.

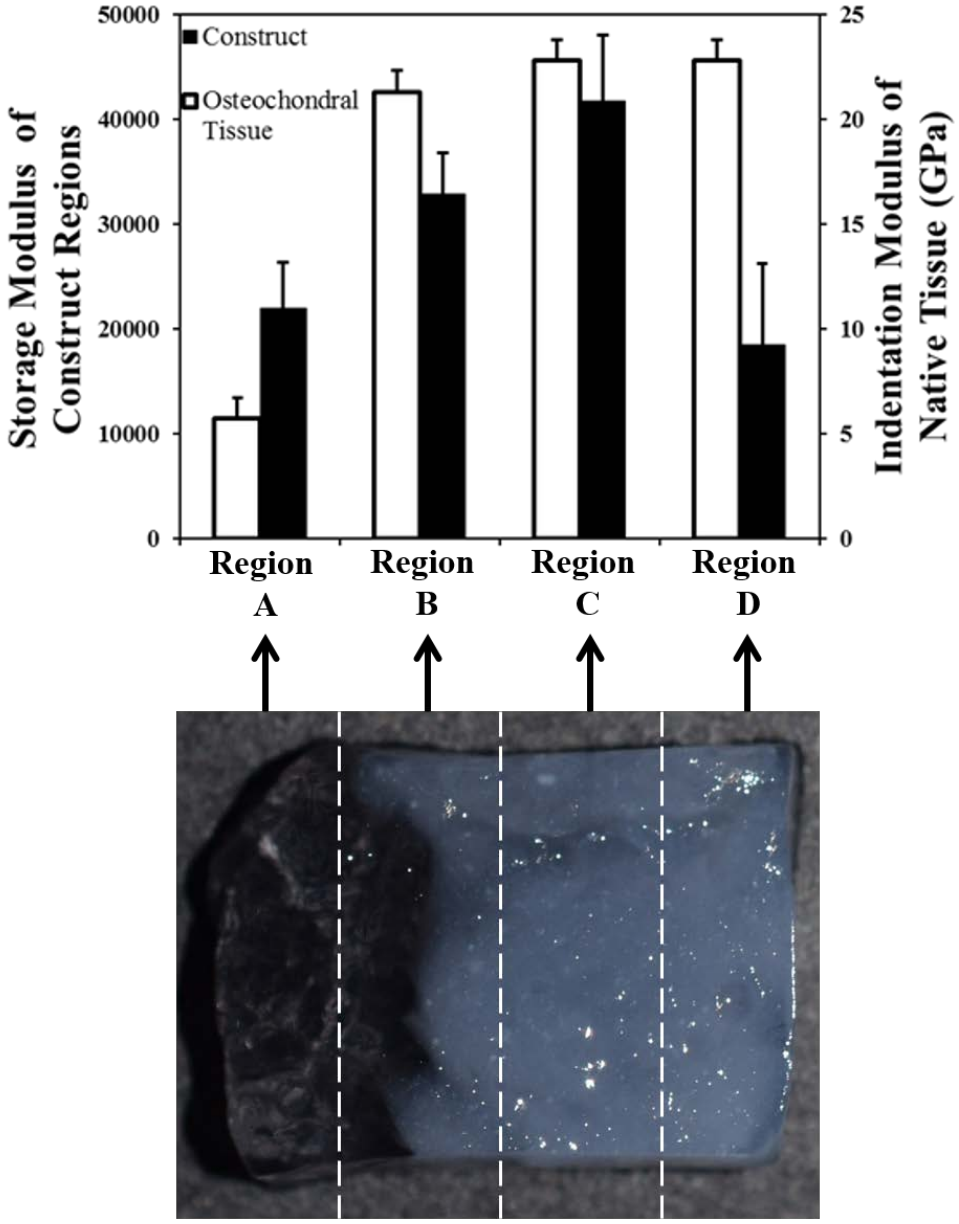

Figure 6.4 – A comparison of storage moduli in 4 regions of osteochondral scaffolds with nanoindentation moduli osteochondral tissue (Nanoindentation moduli extrapolated from Campbell et al. 2012 where Region A represents hyaline cartilage, Region B represents calcified cartilage and regions C and D represent subchondral bone (error bars represent +/- 1 standard deviation, n = 3)

6.3.3 RT-PCR

Constructs were successfully manufactured to fit tightly into simulated osteochondral defects with layer thickness matching that of native tissue (Fig. 6.5). After 30 days *in vitro* culture, layered scaffolds were successfully extracted for analysis of gene expression using RT-PCR. Scaffolds retained their structure throughout the culture process. PCR for types I and II collagen revealed a gradient in ratio of expression after 30 days culture in simulated defects (Fig. 6.5). Expression of

COL2A1, the gene responsible for initiation type II collagen synthesis, was highest in cells located in the cartilage region of scaffolds. Conversely, COL1A1 (responsible for type I collagen) showed the lowest levels of expression in cells within this region. The ratio of type I and II expression changed across the structure with the highest COL1AL expression observed in the bone region. This suggests cells encapsulated in the cartilage region retained a chondrogenic phenotype while cells in the bone region retained an osteogenic phenotype. The change in ratio of COL1A1 and COL2A1 expression across scaffolds suggests potential integration of both materials and cell types.

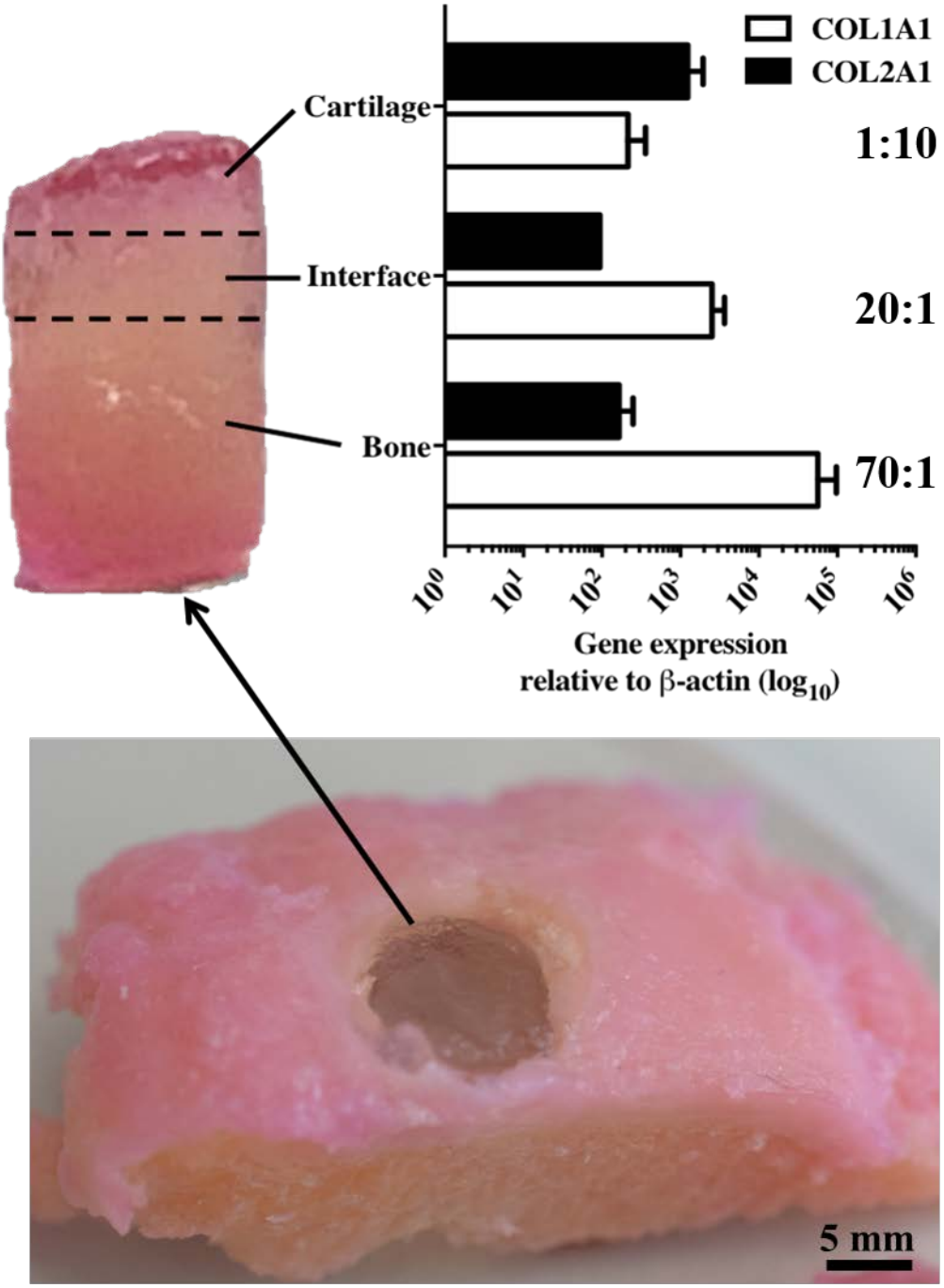

Figure 6.5 – Expression of COL1A1 and COL2A1 30 days post implantation in three regions of a fabricated osteochondral scaffold seeded with human primary osteoblasts and chondrocytes (error bars represent +/- 1 standard deviation, n = 3, PCR data annotated to show ratios of COL1A1 to COL2A1 gene expression)

6.4 Discussion

This study has demonstrated the potential for ALM using fluid gels as a supporting media as a method for manufacturing layered tissue culture scaffolds from soft materials. Scaffolds fabricated in this study were aimed at creating an osteochondral analogue that could be used as an autologous tissue culture implant for defect repair. A construct of two distinct layers, each comprised of a different material, was successfully fabricated in cell culture conditions (Fig. 6.3). Both materials integrated such that a single structure was formed and each layer did not separate during extraction from supporting media. Fabricated scaffolds were successfully manufactured to fit tightly into osteochondral defects with layers that matched the thickness of native tissue (Fig. 6.5). Furthermore, after 30 days of culture in osteochondral defects, scaffolds retained their structure and distinct layers and could be handled without deforming.

Stress sweeps of the osteochondral constructs highlighted the successful integration of two different materials into a single structure with a gradient in G′ observed (Fig. 6.4). Interestingly, the trend in mechanical properties observed in Regions A-C shows some similarity to reported changes in modulus across osteochondral tissue where it was previously demonstrated that subchondral bone exhibited the highest modulus, hyaline cartilage the lowest with calcified cartilage (the interface) falling between the two, albeit closer to the modulus of bone (Campbell et al., 2012). A similar trend was observed in fabricated constructs with Region A (cartilage layer) exhibiting a significantly lower modulus than Region C (bone layer) and Region B (interface) falling between both values. This could be attributed to nanocrystalline HA (nano HA) in the bone layer interacting with gellan chains, thus increasing homogeneity in the gelled network. Such a trend has been reported previously with nano HA shown to significantly increase modulus of gellan hydrogels (Jamshidi et al., 2012). Therefore, an increase in modulus across the structure provides evidence for transition from demineralised gellan into gellan mineralised with nano HA. This could provide further support to the conclusion that a gradient structure had been fabricated. Region D, however, exhibited the lowest modulus despite

being the upper bone region of the construct. This Region should be comprised of gellan/HA and, therefore, would be expected to exhibit a higher modulus than Regions A and B. However, it is possible that this drop in modulus can be attributed to sedimentation and sinking of HA as a result of significant differences in density to gellan (3.16 g/cm^3 vs. 1 g/cm^3). Nano HA was effectively suspended in gellan solution, which does not provide the structural support of fluid gel particles and thus, prior to gelation, the composite may have sunk into the lower regions of the construct bone layer, resulting in a lower modulus in Region D.

Additionally, while trends observed in Regions A-C bare resemblance to that observed in native tissue, it is also worth noting that indentation moduli of native tissue regions were orders of magnitudes greater than storage moduli of respective construct regions. Additionally, methods used to determine both differed greatly. However, parallels between the two trends still highlight the level of control exhibited over mechanical properties within each region of osteochondral constructs.

Expression of COL1A1 and COL2A1 by cells across the structure also revealed evidence in a gradient of cell type. In the cartilage layer of constructs, cells retained a chondrogenic phenotype as demonstrated by high levels of COL2A1 expression (Ghayor et al., 2000). In the bone region, cells retained an osteogenic phenotype with high levels of COL1A1 expression (Dacic et al., 2001). This indicates that while the two sections of the osteochondral scaffold are well integrated (mechanical evidence), the embedded cell population retain their original native phenotype. This is something that has proven challenging with existing technologies for tissue structuring. Moreover, results represent a potential indication of early stages of new bone and cartilage formation. High levels of COL2A1 gene expression by chondrocytes in the cartilage region could be indicative of synthesis and deposition of type II collagen. Type II collagen is a principle component of cartilage ECM and production by chondrocytes is often associated with early cartilage formation (Smits et al., 2001). Additionally, elevated expression of COL1A1 by osteoblasts located in the bone region of constructs eludes to an increase in synthesis of type I collagen. As a principle component of bone, this could

highlight evidence of synthesis and deposition of bone ECM and the early stages of new bone formation (Komori, 2009). At the interface, COL1A1 expression levels fell between those observed in the bone and cartilage layers, suggesting a presence of osteoblasts, albeit in smaller numbers than observed in the bone layer. Interestingly, expression of COL2A1 in this region was the lowest. This could be attributed to presence of a small number of chondrocytes; however an alternative explanation could be chondrocytes in this region undergoing hypertrophy stimulated by the presence of a calcified matrix populated by osteoblasts at the interface. When cartilage and subchondral bone interface in native osteochondral tissue, chondrocytes undergo hypertrophy (Alhadlaq and Mao, 2005). Type X collagen is synthesised by hypertrophic chondrocytes at the expense of type II collagen synthesis. This is because promoters associated with upregulation of COL10A1, the gene associated with type X collagen synthesis, also stimulate suppression of COL2A1. The Runx2 transcription factor is thought to be heavily involved in regulating this change in gene expression by directly triggering onset of a hypertrophic phenotype. (Dong et al., 2006, Von der Mark et al., 1992, Yamasaki et al., 2001). Therefore it is possible that, at the interface, constructs contained both osteoblasts and hypertrophic chondrocytes, thus further replicating the cellular content of osteochondral tissue. However, without analysing expression of COL10A1 in this region, this cannot be fully confirmed.

6.5 Conclusions

This chapter has outlined the potential of using suspended manufacturing with fluid gels as an ALM supporting medium to fabricate layered tissue culture scaffolds. Suspended manufacturing was successfully implemented in the creation of a scaffold that contained 3 distinct regions with different chemical, structural and mechanical properties. Additionally, cellular content of each region also displayed evidence of variation. Bulk properties of the fabricated scaffolds exhibited some analogies to native osteochondral tissue such as trend in mechanical properties, gradients of mineralisation and the presence of separate regions of osteoblasts and chondrocytes. When implanted into human

osteochondral tissue, cells retained a native phenotype with different ratios of COL1A1 and COL2A1 observed in cells located within each region of the construct.

In summary, Chapters 5 and 6 have presented a method for replicating *in vivo* environments for culture of complex, layered tissues by fabrication of scaffolds containing multiple structural and mechanical properties. Chapter 7 will outline an alternative approach to modelling gradient structures in a tissue culture scaffold with hydrogels exhibiting isotropic mechanical properties, but with the ability to deliver different chemical cues throughout the structure. This was explored as a technique for the triggering multi-lineage differentiation of a single mesenchymal stem cell population within distinct regions of a single hydrogel structure.

Chapter 7 – Controlled Multi-Lineage Differentiation of Rat Bone Marrow Stromal Cells within a Single Hydrogel Structure

Aspects of this chapter are currently in preparation for submission to *Biomaterials*.

7.1 Introduction

Mesenchymal stem cells (MSC's) are popular tools for tissue engineering applications due to their capacity to differentiate into multiple different cell types (Pittenger et al., 1999). They can be isolated from multiple tissue sources such as adipose tissue, bone marrow stroma and umbilical cord blood with success rate of isolation varying between each source (Kern et al., 2006). It is possible to culture a number of tissue types such as bone, cartilage, muscle or fat from a single population of MSC's by supplying a variety of specific differentiation cues (Caplan, 2007). Chapters 4-6 have highlighted the impact of varied mechanical cues on cell behaviour and such properties are reported to impact stem cell behaviour (Guilak et al., 2009). For example, one study has demonstrated how different mechanical environments can directly influence stem cell lineage specification (Engler et al., 2006). However, another effective way of directing differentiation into different cell types is by supplying a MSC population with a specific combination of chemical cues. For example, it has been demonstrated that differentiation can be triggered down an osteoblastic lineage by supplementing cell culture media with dexamethasone, ascorbic acid and β-glycerophosphate (Langenbach and Handschel, 2013). Similarly, chondrogenic differentiation can be triggered by supplementing cell culture media using the same chemical cues but with addition of further compounds such as sodium pyruvate and transforming growth factor-beta1/TGF-β1 (Solchaga et al., 2011). Therefore, by tailoring chemical cues, differentiation down multiple different cell lineages can be triggered from a

single stem cell population. Current approaches to using stem cells as tools for tissue engineering often employ similar methods of culture outlined throughout this thesis with 3D scaffolds presenting a preferred platform to 2D monolayer populations (Wang et al., 2005, Mauck et al., 2006, Zhao et al., 2006). Research, however, mainly focuses on culturing a single cell/tissue type from a population of encapsulated MSC's (Shin et al., 2004, Fukuda, 2001, Li et al., 2005). This is due to a difficulty in delivering different media types to stem cell populations in a controlled manner using current 3D culture methods.

When culturing cells within a hydrogel scaffold for example, media is generally applied to the gel surface and allowed to diffuse through the network in order to supply encapsulated cells with nutrients and any differentiation cues the media may contain (Saleh et al., 2012). While this is an effective way of supplementing encapsulated cells, it does not facilitate controlled delivery of media types to specific regions within a hydrogel. Media placed on the surface diffuses isotropically through a hydrogel matrix (Tibbitt and Anseth, 2009). Therefore, using such a technique, it is not possible to deliver multiple chemical cues in the form of different media types to a stem cell population in a controlled manner (Huh et al., 2011). Consequently, this inhibits the capacity to trigger controlled differentiation of MSC's into multiple cell types within select areas of a hydrogel. When designing an osteochondral model for example, osteogenic and chondrogenic differentiation media could be used to create a co-culture of osteoblasts and chondrocytes (Lin et al., 2014). However, if both osteogenic and chondrogenic differentiation media are introduced to a hydrogel surface they will diffuse uniformly through the porous network and create a homogenous mix of media types and thus, both osteoblasts and chondrocytes. Such a co-culture would not be reflective of native osteochondral tissue as a controlled gradient between both cell types is required (Nukavarapu and Dorcemus, 2013). In order to create a 3D osteochondral hydrogel co-culture from a stem cell population, delivery of chemical cues to trigger differentiation should be controlled such that segregated populations of osteoblasts and chondrocytes can cultured. Moreover, an interfacial region between both cell types

should be evident (Gao et al., 2001). This chapter presents a potential method for exhibiting greater control over delivery of specific media types to selective regions of a hydrogel via the use of media channels (Fig. 7.1). By using channelled structures to control diffusion of media it may be possible to develop multiple cell types from a single MSC population and create a controlled interface between the two cell types. This could be of particular interest for modelling *in vivo* environments such as the osteochondral interface.

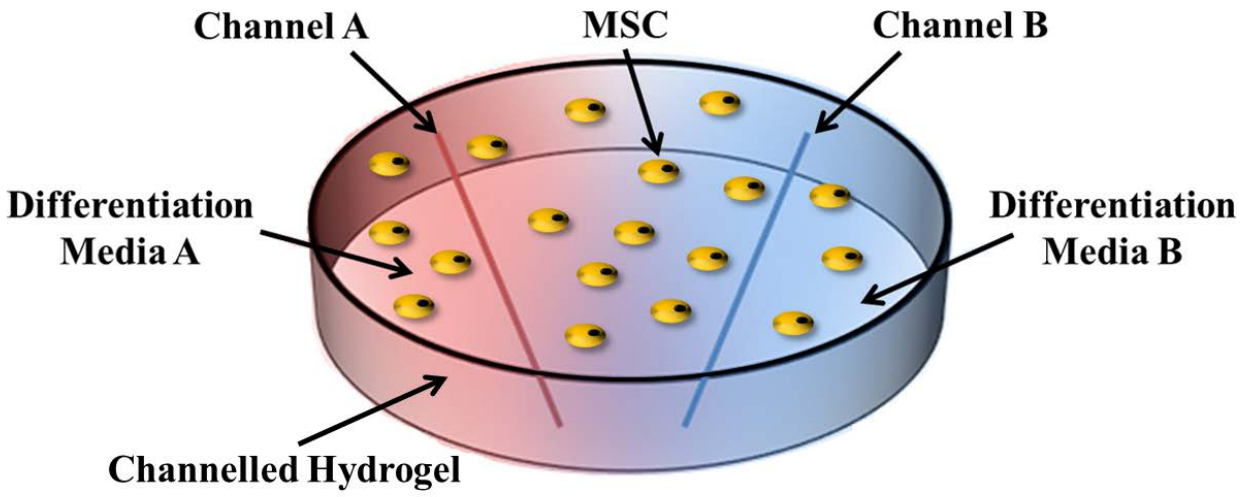

Figure 7.1 – Concept image of how channels could be used to deliver different media types to regions of a cell-loaded hydrogel

This proposed technique involves the use of a mechanism that has shown recent promise in tissue engineering applications known as fluidic system. A microfluidic system allows for control over delivery of small volumes of fluids by injection into channels with dimensions ranging from tens to hundreds of micrometres (Whitesides, 2006). Such systems have shown recent promise as they allow for control over various cell culture parameters such as nutrient supply, pH and metabolite removal (Harink et al., 2014). Various applications of microfluidic systems have been developed and shown to be relevant to tissue culture applications but this chapter focuses on one in particular, namely use of microfluidics to create soluble gradients. Soluble gradients play a key role in cell behaviour during

formation of new ECM and organisation into tissue with cells exhibiting different responses to gradients in chemical cues versus bulk addition (Harink et al., 2013). Consequently, microfluidic systems have been investigated as models for replicating soluble gradients in chemical cues observed in tissue development. For example, it has been demonstrated that a channelled hydrogel system can be used to replicate chemical gradients in neurogenesis, thus directing neural differentiation of adipose-derived stem cells (Choi et al., 2011). This chapter aims to build on such work by developing a channelled microfluidic agarose hydrogel system for creating gradients of osteogenic and chondrogenic differentiation cues with an aim to develop an osteochondral culture. Agarose has been chosen due to a number of desirable properties outlined in Chapter 2 section 2.2.2. Gelation is not ion dependent and consequently not triggered by ionic content in culture media. As a result, agarose solutions can be seeded with cells in culture media and gelation can be managed by temperature alone. This facilitates the easy manipulation of cell-laden agarose, for fabricating channelled hydrogel structures like the example displayed in Fig. 7.1. Furthermore, because agarose is not naturally cell adhesive, encapsulated stem cells will not attach to the hydrogel matrix and proliferate. This is advantageous as osteogenic and chondrogenic differentiation have been shown to occur over a period of up to 4 weeks when chemical cues are added in bulk (Fernandez-Moure et al., 2015). In this system chemical cues will be introduced in much smaller volumes so differentiation could potentially occur over a period greater than 4 weeks. Over such a period, attached stem cells would proliferate and require passaging which is difficult in 3D culture. Moreover, it has been demonstrated that high passage number has a negative impact on stem cell multipotency (Crisostomo et al., 2006, Demerdash et al., 2015, Rastegar et al., 2015). By encapsulating cells in agarose, cell proliferation can be inhibited by a lack of cell adhesion, thereby supporting long term culture. Furthermore, it has been shown that a lack of cell attachment does not inhibit differentiation of MSC's (Jahromi et al., 2011).

In this chapter, the use of channelled agarose hydrogels was investigated, as a mechanism to control the delivery of different chemical cues to different regions of the hydrogel scaffold. It was

hypothesised that by using this method it would be possible to create gradients in chemical cues for differentiation of rat bone marrow stromal cells (rBMSC's) across a single hydrogel structure, with the ultimate aim to produce a 3D osteochondral culture model. Such a model would therefore, contain a controlled co-culture of segregated populations of osteoblasts and chondrocytes with an interface between the two, all cultured from the same rBMSC population within a single structure.

7.2 Materials and Methods

7.2.1 Materials

Plastic cultureware was purchased from Sigma-Aldrich (Dorset, UK). Differentiation supplements and TrypLE™ cell detachment enzyme were purchased from Thermo Fischer Scientific (Runcorn, UK). Agarose powder (microbiology grade, low EEO), cell culture media and all other cell culture reagents were purchased from Sigma-Aldrich (Dorset, UK) and used without further purification. TRIzol® reagent and PCR primers were purchased from Life Technologies (Cramlington, UK) and Precision OneStepPLUS SYBR Green Dye was purchased from PrimerDesign (Eastleigh, UK). Calcein AM and propidium iodide were purchased from Life Technologies (Cramlington, UK). Alkaline phosphatase assay substrate and stop solution were purchased from Cambridge Bioscience (Cambridge, UK). Alizarin red and alcian blue staining dyes were purchased from Sigma-Aldrich (Dorset, UK). Chloroform used for PCR was purchased from Fisher Scientific (Loughborough, UK) and ethanol, 100% isopropanol and RNAse free water were purchased from Sigma-Aldrich (Dorset, UK).

7.2.2 Preparation of agarose hydrogels

Agarose powder was dispersed in deionised water at a temperature of 85 °C, a concentration of 0.5% w/w and in batches of 200 mL. Mixtures were stirred at 900 RPM using a magnetic stirrer until fully dissolved and any water lost through evaporation was replaced. Hydrogels were formed by allowing agarose solutions to quiescently cool to room temperature.

7.2.3 Gelation properties

Rheological analysis was carried out on 0.5% agarose in order to determine both gelation temperature and modulus of resulting hydrogels. Solutions of 0.5% agarose were loaded onto the bottom geometry of a Bohlin Gemini rheometer (Malvern, UK) at 90 °C. Temperature dependence of G′ and G″ were measured during cooling from 90 °C to 10 °C at a rate of 2 °C/min using a 55 mm 2° cone and plate geometry. Oscillation frequency and strain were fixed at 10 rad s^{-1} and 0.5% respectively. All measurements were performed within the linear viscoelastic region.

7.2.4 Diffusion studies

To visualise the effect of time constraints on diffusion through agarose networks 0.5% agarose hydrogels were created with two channels meeting in a T-junction to demonstrate complexity of structures that can be created and to assess if multidirectional diffusion can occur. Hot agarose solutions were poured into modified petri dishes (60 mm diameter) containing retractable glass rods with a 2 mm inner diameter. Once set, rods were removed to create the T-junction channels. Methylene blue (500 µl of 1% w/w) was injected into each channel and allowed to diffuse over a period of 48 hours. Images were taken at various time intervals to map the extent of diffusion.

7.2.5 Channelled hydrogel cell culture proof of concept

Mouse-derived 3t3 fibroblasts were cultured at 37 °C and 5% CO_2 in Dulbecco's Modified Eagle's Media (DMEM) supplemented with 10% FBS, 1% penicillin/streptomycin, 2.5% L-glutamine and 2.5% HEPES buffer. At 70% confluent, cells were detached with TypLE™ dissociation reagent, counted and re-suspended in 0.5% agarose solution (autoclaved for sterility) at a density of $1x10^6$ cells/ml. Cell-laden agarose solution was then poured into a modified 35 mm petri dish containing a single retractable rod and allowed to cool and undergo gelation before the rod was removed. This created a cell-loaded agarose hydrogel with a single central channel. Supplemented DMEM was injected into the media channel using a sterile syringe and cells were then cultured at 37 °C and 5% CO_2. After 24 hours the media channel was flushed with PBS and fresh media was injected and left

for a further 24 hours. This procedure was repeated for a period of 7 days with no media being placed on the gel surface.

7.2.6 Live/dead assay

After 7 days of culture (in which media was only supplied through the media channel), PBS was flushed through the media channel and used to wash the gel surface. Excess PBS was aspirated and replaced with fresh DMEM. Calcein AM and propidium iodide were added at volumes of 7 µl and 25 µl respectively. Samples were incubated at 37 °C for 30 minutes in the absence of visible light before visualisation at 520 nm using an Olympus Fluorescence Microscope (Olympus Microscopes, UK).

7.2.7 Culture and encapsulation of rBMSC's

Primary rBMSC's were isolated from the femurs of a sacrificed Wistar rat via sterile dissection in a class II laminar flow hood. Femurs were cut at both ends and stromal cells were flushed out into separate 50 ml centrifuge tubes via injection of supplemented DMEM through the bone marrow cavity to create two cell suspensions (one from each bone). Cell suspensions were centrifuged for 3 minutes at 1000 RPM and supernatants were removed. Cell pellets were re-suspended in 10 ml fresh DMEM by gentle mixing before transferring to two separate T-75 cell culture flasks for culture at 37 °C and 5% CO_2. At passage 4 cultures were trypsinised, counted and re-suspended in sterile 0.5% agarose solution at a density of $1x10^6$ cells/ml. The suspension was poured into modified 35 mm petri dishes with two parallel, retractable glass rods which were removed post-gelation to create rBMSC-loaded hydrogels with two media channels. Osteogenic media was injected into one channel and chondrogenic media into the other (500 µl of each). Supplemented Alpha Modified Minimum Essential Eagle's Media (αMEM, 2 ml) was pipetted onto the gel surface. After 24 hours of culture media channels were flushed and supplemented αMEM was injected into both channels and cells were cultured for a further 24 hours. This process was repeated for a period of 6 weeks to induce differentiation. Gels were washed every 3 days with fresh media being pipetted onto the surface. As

a control group, an additional four rBMSC-loaded gels were created using the same encapsulation process. However, retractable glass rods were not used so no channels were present. Cells in this group were cultured in supplemented αMEM and not given any differentiation cues. After 7 days a single cell-loaded gel was removed and a live/dead assay was conducted as described in section 7.2.6 to ensure the encapsulation process had not compromised cell viability and cells were being maintained.

7.2.8 Histological Staining of encapsulated rBMSC's

After 6 weeks two cell-loaded gels were washed with PBS and cultures were fixed with 10% buffered formalin for 30 minutes at room temperature. Gels were then sliced in half along the x-axis, thus cutting each channel in half, and the bottom half of one gel was swapped with the top half of another to ensure each sample was exposed to both alizarin red and alcian blue dyes (Fig. 7.2).

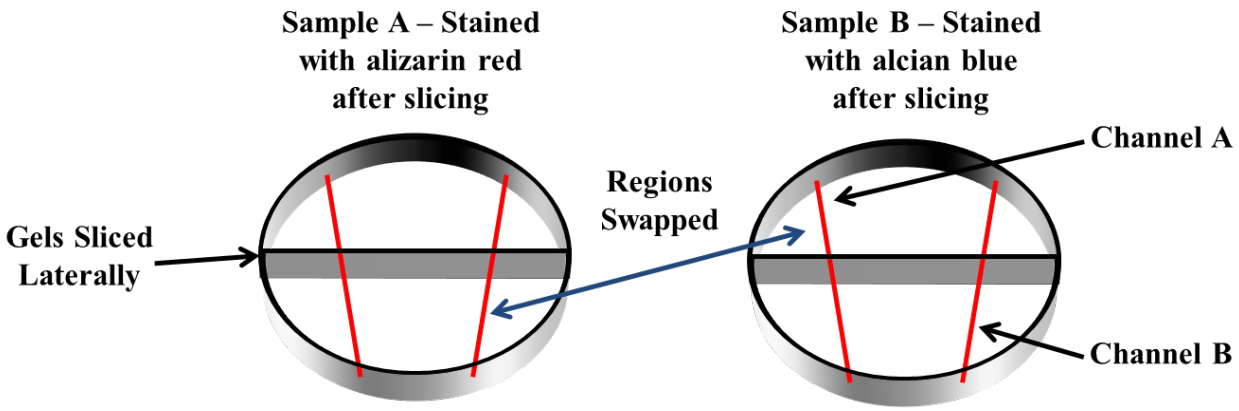

Figure 7.2 – A schematic demonstrating how cell-loaded gels were sliced and arranged. Gel A was stained with alizarin red and gel B was stained with alcian blue

Alizarin red (2 ml) was added to one sample to specifically stain for mineral deposits associated with osteogenesis. Alcian blue (2 ml) was added to the second sample to stain for glycosaminoglycan deposition as a possible indicator for chondrogenesis. Both samples were incubated in the absence of visible light for 30 minutes before the removal of excess dye with thorough washing in deionised water.

7.2.9 Histology of stained cultures

Stained three dimensional cultures were frozen and cross-sectioned using a cryostat (Starlet, Bright Instruments, and UK). Briefly, samples were fixed to a steel plate using cryo-embedding media and flash frozen with cryo spray before being sliced. Cross-sections were placed onto glass slides with a glass coverslip and observed with a Leica compound bright field microscope (Leica Microscopes, UK).

7.2.10 Alkaline Phosphatase Assay

Alkaline phosphatase activity was determined using an assay based on hydrolysis of p-nitrophenyl phosphate substrate to p-nitrophenol which is catalysed by ALP. A higher concentration of p-nitrophenol indicates higher ALP activity. Presence of elevated ALP activity is indicative of osteoblast activity and, thus, is used in this study to highlight potential osteogenic differentiation of rBMSC's.

Cell-loaded hydrogels were sliced parallel to the media channels in order to separate the osteogenic, chondrogenic and interfacial regions. Each region of the gel was homogenised separately and cells were lysed in 500 µl RIPA cell lysis buffer with protease inhibitor for 10 minutes at 4 °C. Cell lysate was then centrifuged in 1 ml eppendorf tubes for 10 minutes at 12,000 x g and 50 µl of supernatant from cells encapsulated in hydrogel regions 1, 2 and 3 (Fig. 7.8) were loaded into a 96-well plate in triplicate. Cell lysate from controls was also loaded in triplicate with cell lysis buffer used as a blank sample. The reaction was triggered with the addition of 50 µl StemTAG™ AP Activity Assay Substrate. Samples were incubated for 30 minutes at 37 °C and 5% CO_2 before the reaction was stopped with 100 µl stop solution. Absorbance was read at 405 nm and activity was calculated from a pre-prepared standard curve of concentrations ranging from 1-250 nM p-nitrophenol. Results were tested for significant differences as in Chapter 4, section 4.2.21.

7.2.11 Reverse transcription PCR (RT-PCR) – RNA Isolation

Cell-loaded gels were sliced into three regions as demonstrated in Fig 7.8 and 7.9. RNA was isolated from gels using TRIzol® reagent. Gel cross-sections were placed into separate wells of a 6-well plate and 500 µl TRIzol® reagent was added to each and left for 5 minutes before removal. Samples were transferred to sterile 1 ml eppendorf tubes and 100 µl chloroform was then added to separate the RNA into a separate, aqueous phase. This was then removed and RNA was subsequently isolated from the aqueous phase via precipitation using 500 µl of pure isopropanol. Samples were then centrifuged for 15 minutes at 12,000 X g and 4°C. The supernatant was removed and pellet washed in 1 ml 75% ethanol diluted in RNAse free water, dried in a vacuum desiccator for 15 minutes and re-suspended in RNAse-free water. RNA concentration and A260/280 ratios were quantified by spectrophotometry (NanoDrop 2000, ThermoScientific). RNA was stored at -80 °C before use for PCR

7.2.12 Real-time quantitative PCR

Precision OneStepPLUS SYBR Green Dye (PrimerDesign) was used with GAPDH housekeeping gene for quantification and expression of collagen type I (COL1A1), a key osteogenic marker and type II (COL2A1), a key chondrogenic marker. The forward and reverse primer sequences were designed with Primer Express 3 software (Applied Biosystems) and produced by LifeTechnologies (UK). Primer sequences are shown in Table 7.1. Variation in gene expression was calculated using the Pfaffl method (Pfaffl, 2001).

Table 7.1 - Primers used for real-time PCR

Gene	Forward Primer	Reverse Primer
COL1A1	CTGTTCTGTTCCTTGTGTAACTGTGTT	GCCCCGGTGACACATCAA
COL2A1	ACTGGATTGACCCCAACCAA	TCCATGTTGCAGAAAACCTTCA

7.3 Results

7.3.1 Rheology

Rheological analysis of 0.5% agarose during cooling revealed the onset of gelation occurred at ~35 °C (Fig. 7.3). As agarose passed through a sol-gel transition, the relationship between the elastic and viscous moduli changed. Prior to gelation the polymer displayed a higher viscous modulus (G″), indicating agarose was present as a disordered polymer solution. Transition into a more ordered hydrogel network triggered a shift in which the elastic modulus (G″) became significantly larger with a G′ of 3231.5 Pa and a G″ of 86.8 Pa at 10 °C indicating formation of a strong gel. It is possible therefore, to mix a suspension of cells with 0.5% agarose at 37 °C as the polymer is still in sol form. Gelation into a cell-loaded gel can then be subsequently triggered by cooling. This does involve temporarily exposing cells to temperatures lower than the optimum of 37°C. However, studies have demonstrated that this does not negatively impact cell viability (Yoon et al., 2003, Furukawa and Ohsuye, 1999)

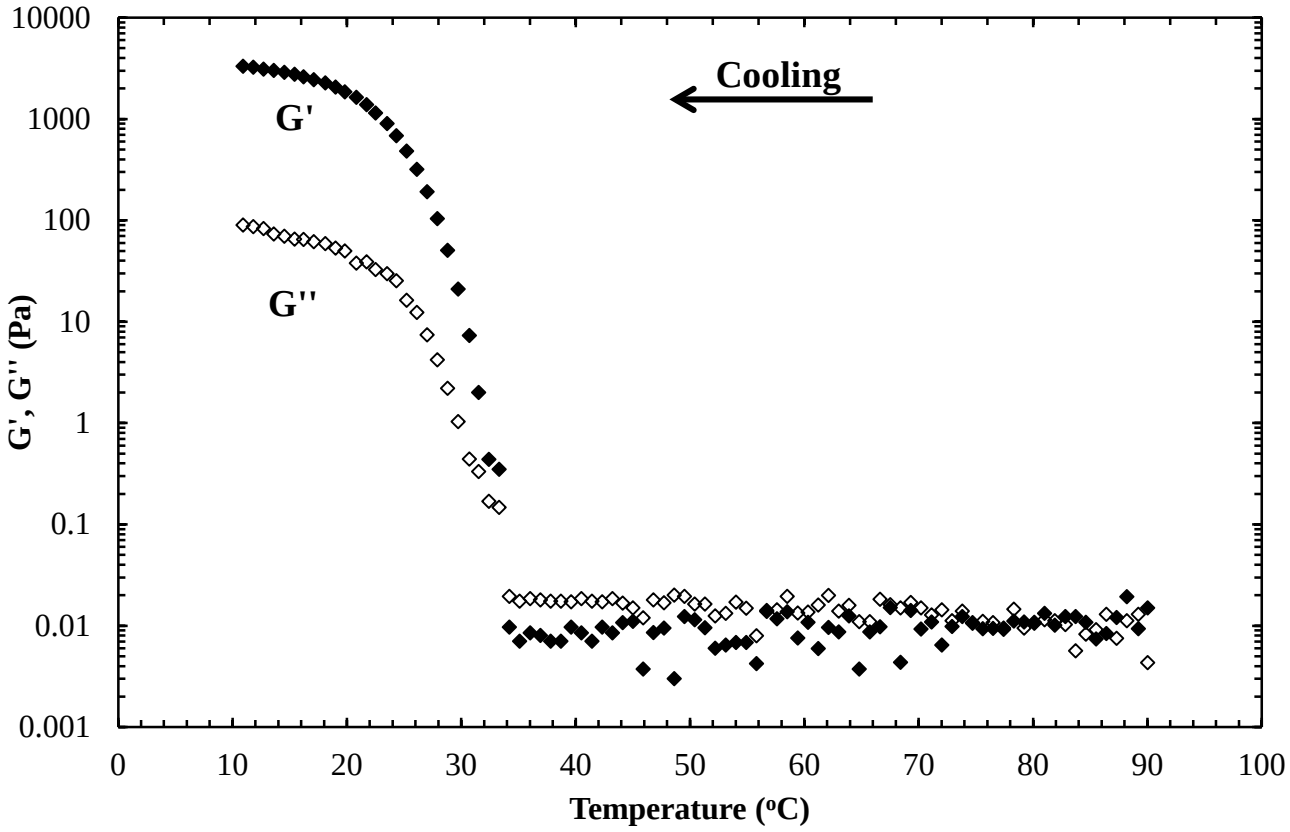

Figure 7.3 – Elastic modulus (G′) and viscous modulus (G′′) of 0.5% agarose (w/w) during cooling

7.3.2 Diffusion studies

Once injected into channels, methylene blue diffused readily through an agarose polymer network (Fig. 7.4). At a time point of 24 hours post-injection, methylene blue had diffused approximately 1.5 cm from each channel in all directions. At 48 hours post-injection, methylene blue had diffused an even greater distance from the channels such that most of the matrix was dyed blue. This model is useful as an indication of how certain components in osteogenic and chondrogenic differentiation media may diffuse through channelled agarose matrices. A critical factor that often affects diffusion of compounds through hydrogel matrices is molecular weight (Drury and Mooney, 2003, Lieleg and Ribbeck, 2011, Smith et al., 2012). Methylene blue has a molecular weight of 319.85 g/mol which is similar to certain osteogenic and chondrogenic media components such as dexamethasone (392.461 g/mol), β-glycerophosphate (216.04 g/mol) and ascorbic acid (176.12 g/mol). Therefore, results presented in Fig. 7.4 could be indicative of how osteogenic and chondrogenic media may diffuse

through agarose hydrogel matrices, providing an idea of required time constraints to restrict diffusion. This suggested that 24 hours may be an appropriate time period for controlling diffusion of such compounds through an agarose network.

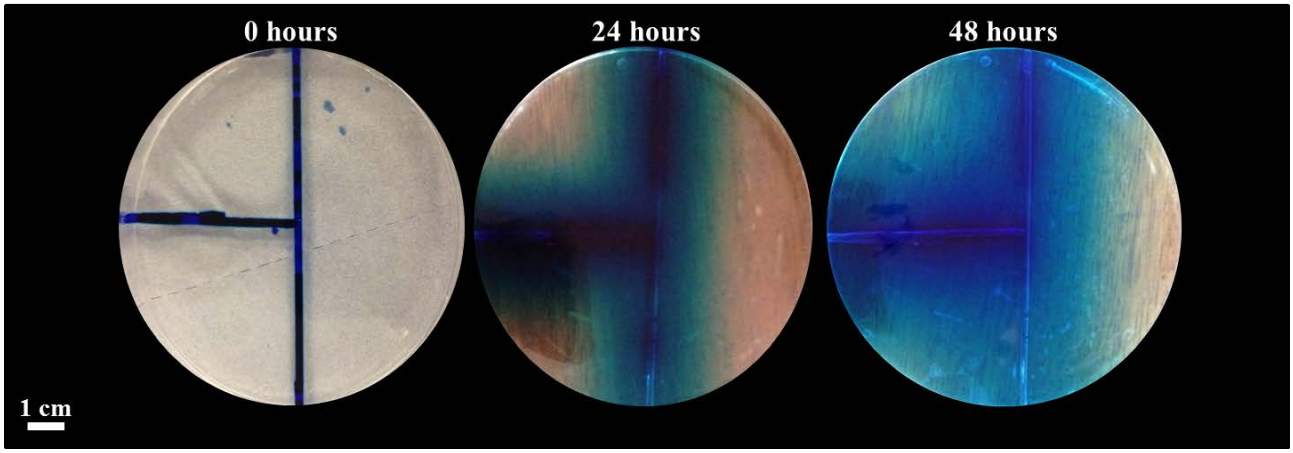

Figure 7.4 – Diffusion of methylene blue through a 0.5% agarose hydrogel over 48 hours after injection into channels

7.3.3 Culture of 3t3 fibroblasts in a channelled structure

After 7 days of culture, live/dead staining revealed an increase in cell death as distance from the central media channel increased (Fig. 7.5). In regions in close proximity to the channel cells were alive as indicated by green fluorescence. In regions greater than 1.5 cm away from the channel, cells had died as shown by red fluorescence. Constraining diffusion of media from the channel to a period of 24 hours restricted delivery to segregated regions of the cell-loaded gel and created controlled regions of live and dead cells. Cell death in regions greater than 1.5 cm from the channel was also supported by the methylene blue diffusion results where, 24 hours post-injection, the dye diffused over a distance of approximately 1.5 cm from each channel (Fig. 7.4).

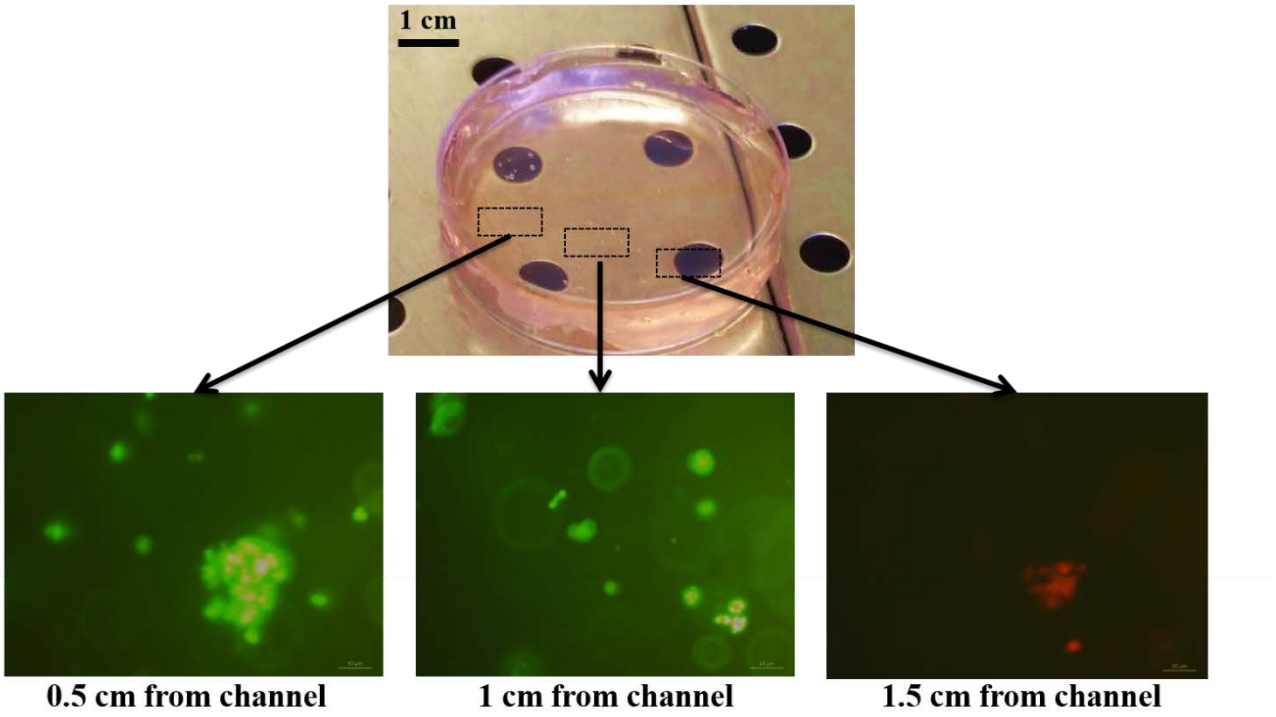

Figure 7.5 – Calcein AM/propidium iodide staining from various regions of a 0.5% agarose hydrogel containing 3t3 fibroblasts cultured for 7 days using a single media channel

7.3.4 Live/dead assay of encapsulated rBMSC's

Live/dead staining of rBMSC's demonstrated that cell viability was not compromised during encapsulation into a channelled gel and cells could be maintained within channelled gels for 7 days (Fig. 7.6). The cells also appeared to be dispersed uniformly through the agarose gel matrix suggesting that the channelled agarose hydrogels were a suitable platform for culturing rBMSC's.

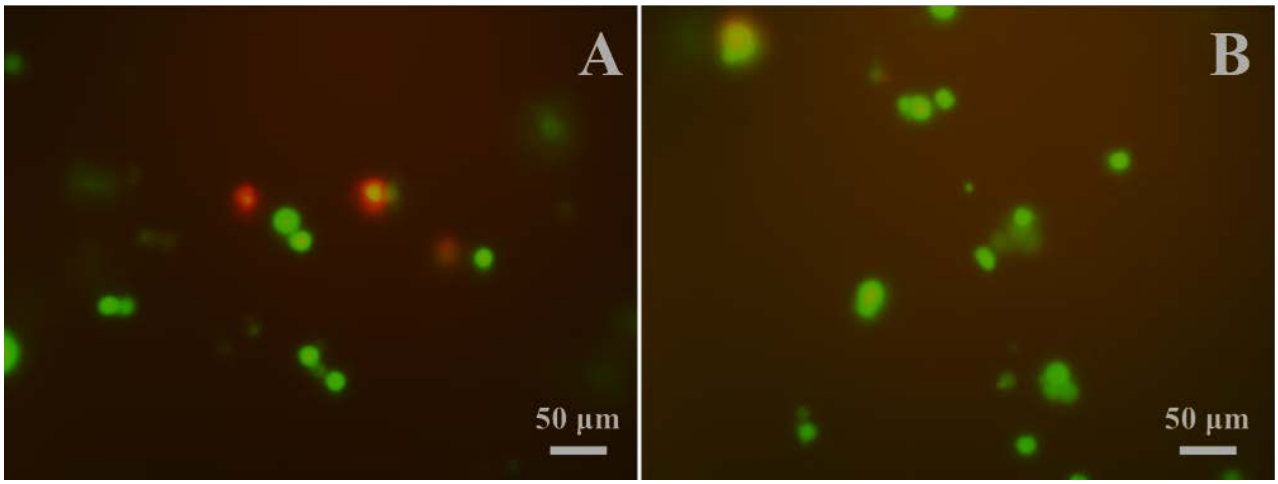

Figure 7.6 – Calcein AM/propidium iodide staining results from osteogenic (A) and chondrogenic (B) regions of a 0.5% agarose hydrogel containing rBMSC's after 7 days of culture

7.3.5 Histological analysis of encapsulated cultures

Alizarin red is used to detect mineralisation associated with early osteogenesis due to an affinity to specifically bind to calcium-based deposits (Gregory et al., 2004). Additionally, alcian blue is used to stain for sulphated and carboxylated glycosaminoglycans; key components of cartilage ECM and indicators of early chondrogenesis (Berg et al., 2009).

Evidence of calcified mineral deposition was observed when specific hydrogel regions were stained with alizarin red (Fig. 7.7). Interestingly little evidence for mineral deposition was seen in outer regions of areas closer to the osteogenic media channel. This is indicated by a very noticeable decrease in specific alizarin red staining of cells and surrounding ECM. When regions closer to the osteogenic channel and further towards the interfacial region were observed there appeared to be a much greater degree of mineralisation. This suggests that cells in the outer regions of the hydrogel showed little osteogenic activity. In regions closer to both the osteogenic channel and interface however, there is an indication of rBMSC differentiation into osteoblasts. Further magnification of samples revealed a matrix that appears to be saturated with highly mineralised nodules towards central regions of the gel. Areas closer to the chondrogenic channel revealed evidence of glycosaminoglycan deposition when stained with alcian blue (Fig. 7.7) with specific blue staining of apparent GAG depositions. GAG's such as chondroitin sulphate and keratin sulphate are key

components of cartilage ECM and markers for early chondrogenesis (Knudson and Knudson, 2001). Therefore, specific staining with alcian blue in regions around the chondrogenic channel is indicative of possible chondrogenesis.

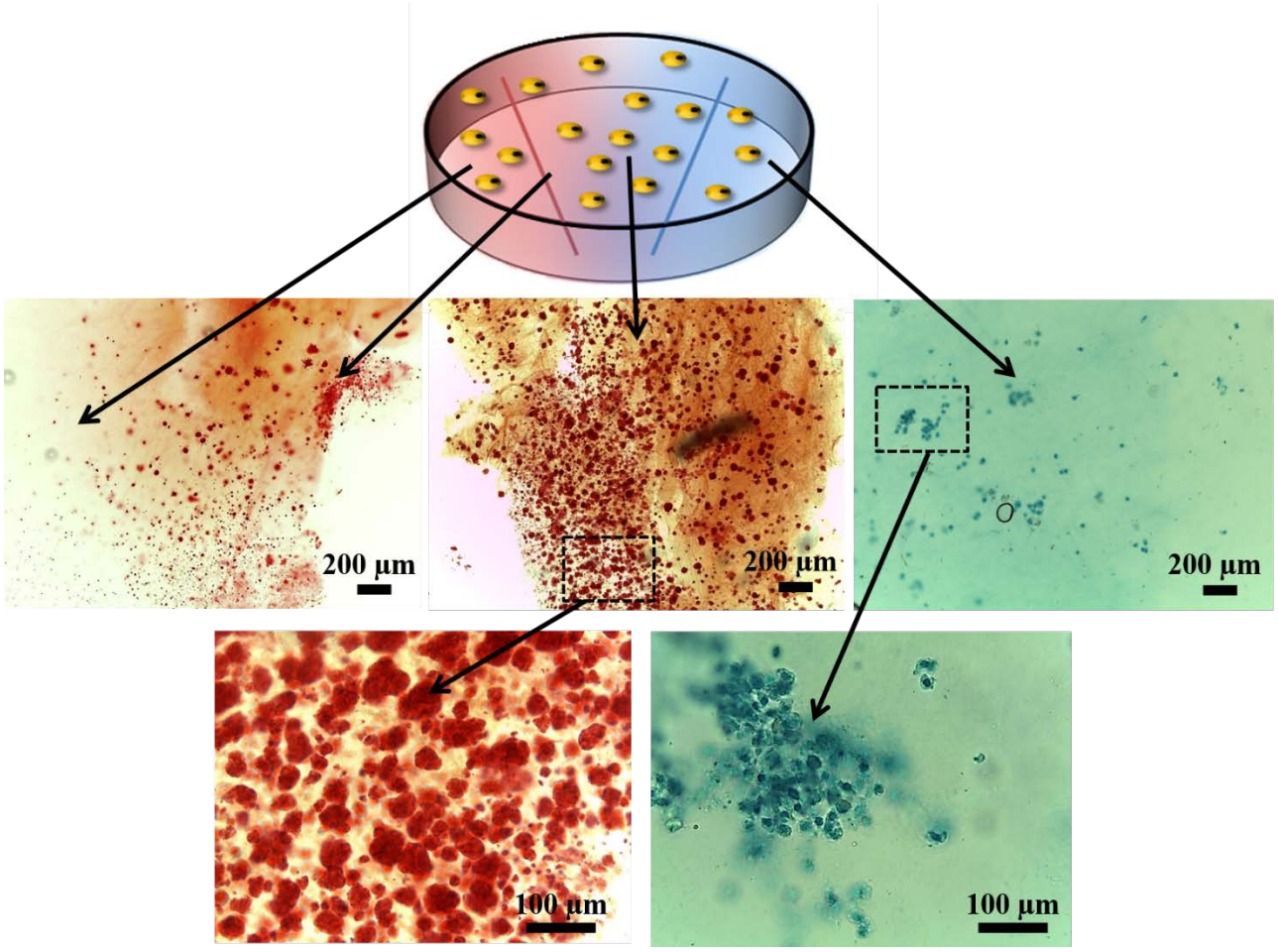

Figure 7.7 – Histology of osteogenic and chondrogenic regions of rBMSC-loaded gel when stained with alizarin red and alcian blue after 6 weeks culture

7.3.6 ALP Assay

Alkaline phosphatase activity of encapsulated rBMSC's was indirectly evaluated by the concentrations of p-nitrophenol measured in the various regions on the hydrogel (Fig 7.8). A higher concentration of p-nitrophenol indicated a greater level of ALP activity. A significant elevation in ALP activity was only seen in region 2 of cross-sectioned hydrogels with a p-nitrophenol yield of 127 nmol (vs. 70 nmol in the control sample). A slight elevation in activity was observed in region 3 with a yield of 88 nmol whereas in region 1 the lowest ALP activity was observed with a p-nitrophenol

concentration of 53 nmol produced. Differences between ALP activity levels were deemed significant as indicated by a p value of <0.05. A surge in ALP activity seen in region 2 appears to coincide with histological results where the greatest degree of mineralisation was observed in similar regions (Fig. 7.7). Similarly the low ALP activity in region 1 provides a potential explanation of low amounts of mineral deposition observed in similar regions stained with alizarin red with ALP being a key protein in mineralisation.

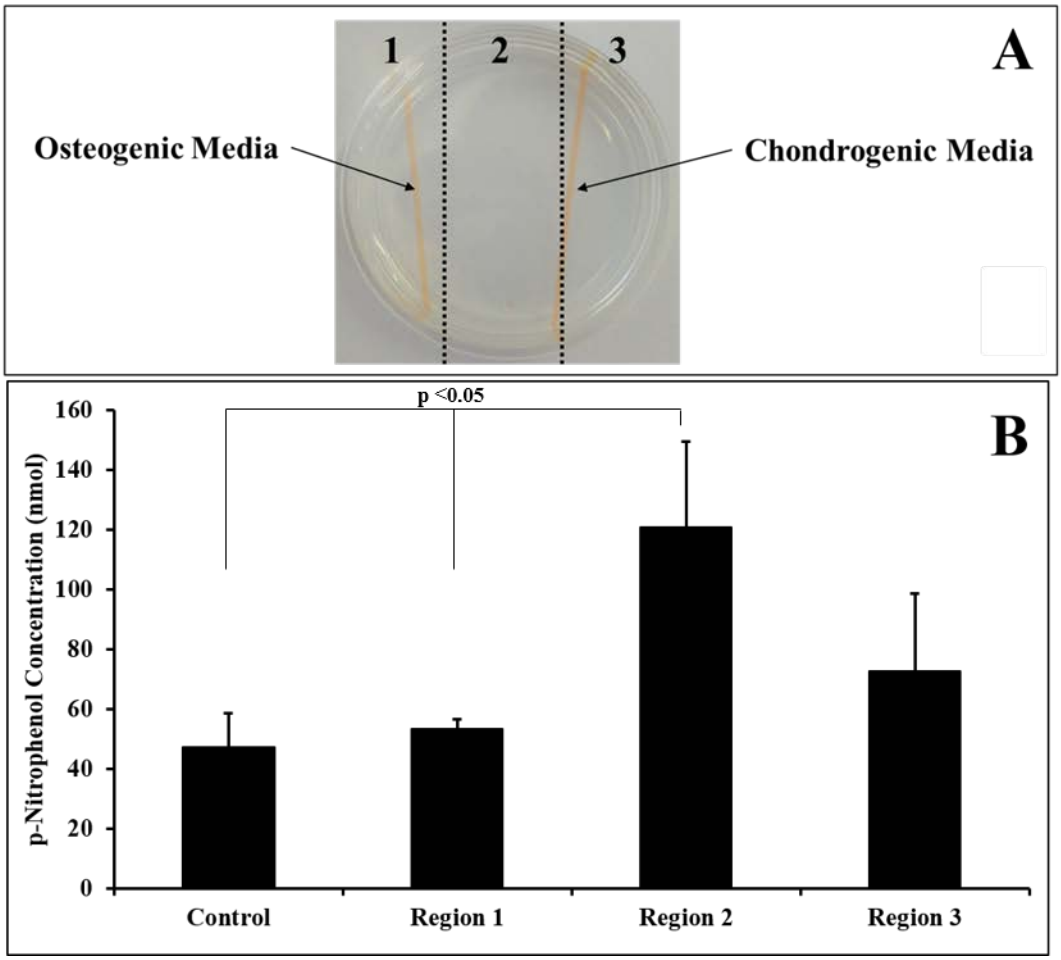

Figure 7.8 – A photographic image demonstrating (A) how cell-loaded gels were sliced for bioassays and PCR combined with (B) results indicating alkaline phosphatase activity as a function of [p-nitrophenol] produced by hydrolysis of p-nitrophenyl phosphate (error bars represent +/- 1 standard deviation, n = 8)

7.3.7 RT-PCR

Gene expression levels of both Col1 and Col2 varied in different regions of hydrogel samples (Fig. 7.9). Elevated Col1 gene expression was observed in region 2 with a value of 3.7 indicting expression was 3.7 times higher than in control samples. In region 1 Col1 expression levels were very similar to

those seen in control values (1.1 times higher than control) with a slighter increase in expression seen in region 3 (1.5). This trend mirrors ALP activity in each region and further alludes to a dominance of cells displaying an osteogenic phenotype in region 2. In region 3 Col2 expression levels were elevated to 2.1 times higher than in control samples further supporting a hypothesis for chondrogenesis in this region. Col2 expression was not significantly elevated in regions 1 and 2 (1.1 and 1.0 respectively) suggesting chondrogenesis did not occur. This, again, coincides with histological results showing evidence for chondrogenesis in region 3 indicated by staining of glycosaminoglycans. A slight elevation in Col1 expression and ALP activity in region 3 also suggests presence of osteoblasts, albeit in lower quantity than region 2.

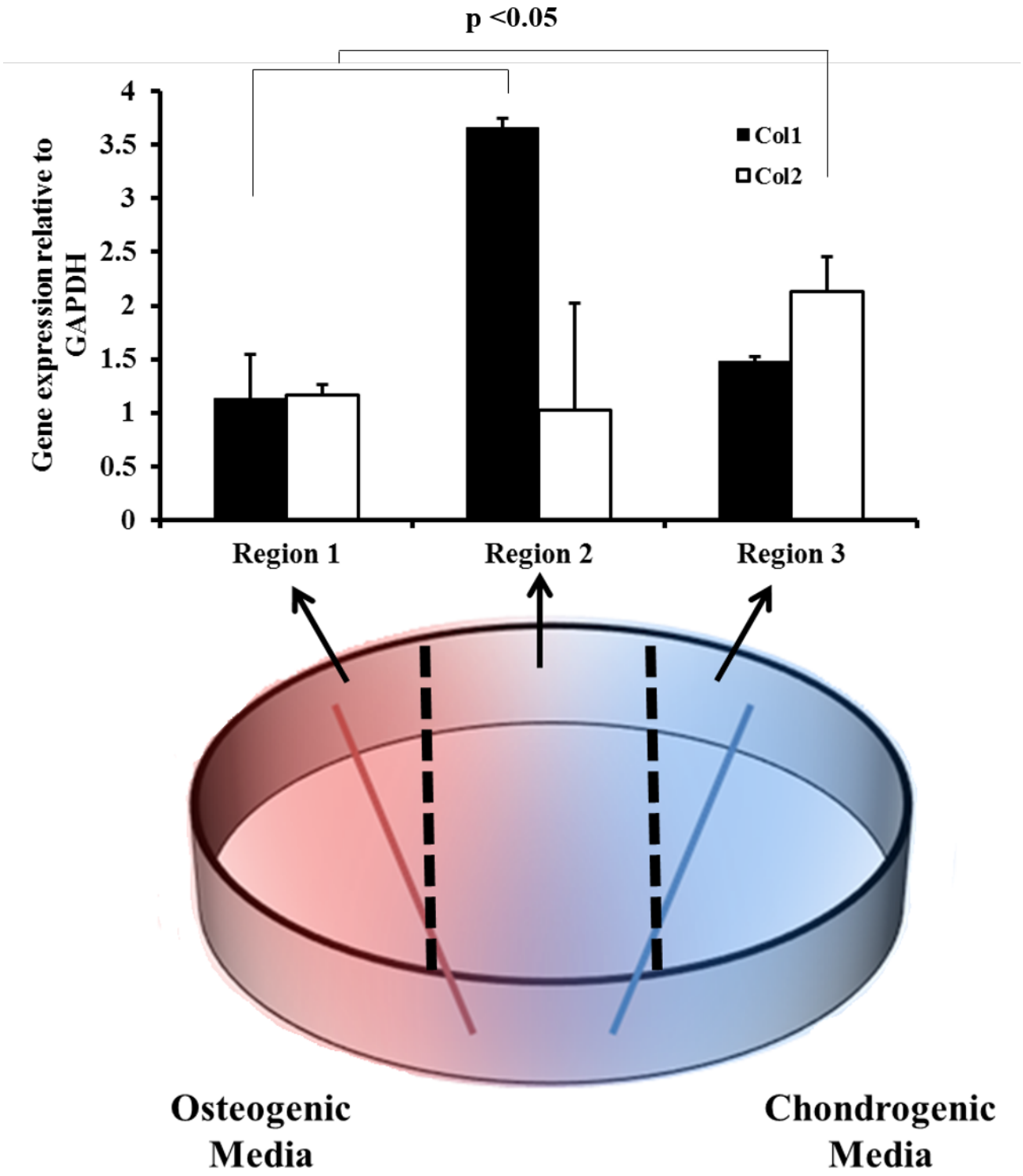

Figure 7.9 – RT-PCR results showing Col1 and Col2 expression relative to GAPDH in three regions of a cell loaded hydrogel (error bars represent +/- 1 standard deviation, n = 6)

7.4. Discussion

Agarose was chosen as the polymer for this study due to rheological properties outlined in Fig. 7.3. At temperatures above 35 °C and a concentration of 0.5% (w/w) agarose is in a liquid, with the polymer in the disordered form. Gelation is occurs at ~35 °C as indicated in a rapid rise in both the elastic modulus (G′) and viscous modulus (G″) at temperatures <35 °C . Consequently, a cell-suspension can me mixed with a 0.5% agarose solution at 37 °C and left to cool, triggering gelation into a cell-loaded structure at 35°C. After gelation the hydrogel exhibited a final elastic modulus of 3232 Pa. G″ was significantly lower than G′ (868 Pa vs. 3319) indicating a strong cell-loaded gel could be formed with 0.5% agarose. Agarose is also commonly reported to show thermal hysteresis. Despite gelation occurring at 35°C, a resulting cell-loaded hydrogel will not melt back into solution when placed in culture conditions of 37 °C as a significantly higher temperature is required, making agarose suitable polymer for this application.

Encapsulation using this protocol does not result in significant cell death as indicated by live/dead assays (Fig. 7.6). This assay was also used to evaluate an initial proof-of-concept for using channels to control media diffusion within a hydrogel (Fig. 7.5). Fibroblasts were encapsulated and only supplied media via injection into a single channel. As distance from the channel increased, the amount of live cells decreased as shown by a change from green, live cells to red, apoptotic cells with significant cell death seen at distances > 1.5 cm from the channel. Increase in cell death as a function of distance suggested that diffusion of supplemented media had been controlled and restricted. This is further supported by methylene blue diffusion results (Fig. 7.4) where a diffusion radius of approximately 1.5 cm was observed 24 hours post-injection of the dye. Theoretically results from both experiments can translate to an rBMSC model whereby cells that are within approximately 1.5 cm of a channel would receive differentiation media via injection in a channel and cells that are greater than 1.5 cm from the channel would not. A period of 24 hours was determined as the optimal time constraint in order to successfully exhibit the desired control over media diffusion.

Applying this to an rBMSC-loaded gel with two channels successfully resulted in the delivery of both osteogenic and chondrogenic media to segregated regions (Fig. 7.7, 7.8 and 7.9). As a result both chondrocytes and osteoblasts were cultured with the potential to develop an interface between the two.

Evidence for osteogenesis within cell-loaded hydrogels can be observed in histology, ALP assay and RT-PCR results (Fig. 7.7, 7.8 and 7.9). Histological staining with alizarin red revealed gradients in mineralisation across hydrogel samples (Fig. 7.7). This can be explained by the observed changes in alkaline phosphatase activity (Fig. 7.8). Alkaline phosphatase is an enzymatic protein found in multiple tissues but elevated levels of expression and activity have been widely reported in early bone formation (Bellows et al., 1991a, van Straalen et al., 1991, Weinreb et al., 1990b). As a result, ALP is now regarded as a key marker for early osteogenesis. The protein actively promotes mineralisation by both hydrolysing extracellular pyrophosphate and increasing intracellular phosphate concentrations. This acts to aid synthesis of hydroxyapatite, the main inorganic component of bone. Elevated ALP activity, therefore, leads to increased mineralisation and this trend is mirrored in results from histology and ALP assays. In regions of samples where little mineralisation was observed (regions 1 and 3), ALP activity was also reduced. In region 2 where ALP activity was highest, the greatest degree of matrix mineralisation was observed (Fig. 7.7 and 7.8).

Further evidence for osteogenesis in region 2 of samples is provided by increased Col1 expression (Fig. 7.9). While hydroxyapatite provides the main inorganic component of bone, the primary organic component is type I collagen. Osteoblasts synthesis type I collagen before mineralising it with calcium-based compounds and type I collagen and ALP are thought to function in synergy. ALP binds to collagen fibrils and, thus, aids in collagen mineralisation. Elevated ALP and Col1 expression paired with alizarin red staining revealing mineralised nodules in region 2 provides strong evidence for presence of mature osteoblasts.

Alcian blue staining results suggested chondrogenesis in region 3 of cell-loaded gels. This was further supported by RT-PCR results for Col2 gene expression (Fig. 7.7 and 7.9 respectively). While GAG deposition is heavily associated with chondrogenesis due to high proportions of proteoglycans in cartilage matrix, other cell types deposit GAGs as part of ECM (Duncan and Berman, 1991, Sugahara and Kitagawa, 2000). A more specific marker for chondrogenesis is a combination of GAG deposition and type II collagen synthesis (Toh et al., 2012). In region 3 of hydrogel samples Col2 expression was elevated and alcian blue revealed an indication of GAG deposition within the same region providing evidence of chondrogenesis.

Interestingly, ALP activity levels are also slightly elevated in region 3 of hydrogel samples. One possible explanation for this is expression of the protein by maturing chondrocytes. While ALP does not play as big a role in chondrogenesis as in osteogenesis, it has been reported to show type II collagen-mediated activity in cartilage (Rastegar et al., 2015). Type II collagen can bind to a receptor expressed on the surface of chondrocytes known as Annexin V. This stimulates an influx of Ca^{2+} ions mediated by Annexin V. Intracellular concentrations of calcium ions become elevated and this triggers an increase in alkaline phosphatase activity. However, a slight up-regulation of Col1 in region 3, albeit not as pronounced as in region 2, was observed (Fig. 7.9) providing a more probable explanation for elevated ALP activity in region 3. Presence of osteoblasts in parts of region 3 but at a lower density than in region 2 would also result in such a trend. When combined with higher Col2 expression, this may allude to a potential interface of osteoblasts and chondrocytes between regions 2 and 3.

In region 1 of the cell-loaded gel ALP activity and expression of both genes were all approximately lower than or equal to the control. This initially suggesting rBMSC's could be undifferentiated in this region despite being close to the osteogenic channel. However, an alternative explanation relates to observations made by Jiang et al.,(2005) where osteoblast and chondrocytes were simultaneously co-cultured. The study involved development of an osteoblast-chondrocyte co-culture with an aim to

develop an osteochondral analogue. It was reported that at the interfacial region, both cell types retained a native phenotype as evidenced by high expression of cell specific markers. Osteoblasts exhibited high levels of type I collagen gene expression while chondrocytes showed high levels of type II collagen. However, there was also evidence to suggest cell-cell interactions at the osteochondral-like interface mediated matrix production with a pronounced effect on mineralisation by osteoblasts. Reduced activity of alkaline phosphatase was reported in osteoblasts neighbouring the osteochondral interface with controls (osteoblasts cultured separately) exhibiting higher ALP activity. This was attributed to cell-cell interactions resulting in secretion of factors that trigger responses in neighbouring cells, mediating mineralisation (Jiang et al., 2005). Since this initial study, various other research groups have reported similar observations of chondrocyte populations directly influencing osteogenesis in osteochondral models. For example, Pan et al.,(2009) highlighted the importance of biochemical signalling between articular cartilage and subchondral bone in regulating ECM synthesis during early osteochondral tissue development (Pan et al., 2009). Moreover, further studies have revealed the MAPKinase signalling pathway in chondrocytes has a direct, inhibitory effect on osteoblast differentiation (Prasadam et al., 2010). Additionally, it has been reported that TGF-β3, a major signalling component of chondrogenesis, can negatively impact mineralisation by osteoblasts neighbouring an osteochondral interface by delaying ALP activity (Guo et al., 2010). Such observations could present an insight into the evidence of reduced mineralisation observed in Region 1 of channelled hydrogels despite the presence of osteogenic differentiation media (Fig. 7.7-7.9). It is plausible that synthesis of key bone ECM components has been inhibited by biochemical signals received from the forming interface between osteoblasts and chondrocytes. The exact mechanism inhibiting matrix formation is not clear but it could be related to the previously reported studies highlighting suppression of osteoblast phenotype expression via biochemical signals produced by chondrocytes in early chondrogenesis.

7.5 Conclusions

Results of histology, ALP activity assays and RT-PCR suggest the successful culture of both osteoblasts and chondrocytes from a single rBMSC population. There is evidence of osteoblast activity in Region 2 of channelled hydrogels as evidence by high ALP activity and type I collagen mRNA synthesis. Increased type II collagen mRNA synthesis and GAG deposition in Region 3 indicates chondrocytic activity. More importantly, there is little evidence of chondrogenesis in Region 2 suggesting both cell types have been successfully segregated. Slight expression of osteogenic markers in Region 3 also suggests that an interface between both cell types may be located between Regions 2 and 3. Furthermore, reduced expression of osteogenic markers in Region 1 could allude to cells at the interface mediating osteogenesis as previously reported, further supporting the conclusion that an osteochondral analogue has been successfully cultured.

Chapter 8 – Summary, Conclusions and Future Recommendations

The purpose of this research was to develop potential new approaches to 3D cell culture using biopolymer hydrogel scaffolds. By manipulating chemical and mechanical properties of biopolymers commonly used in tissue engineering, 3D cell culture models were developed with a capacity to directly influence cell behaviour. A protocol was developed for tuning mechanical properties of gellan gum hydrogels via pulsed sonication. Modification of matrix stiffness in gellan hydrogels directly influenced behaviour of mouse osteoblast precursor cells *in vitro*. This demonstrated the potential implications of modifying a single mechanical property on cell phenotype.

Building on this, a new method was developed for fabricating biopolymer hydrogels exhibiting multiple mechanical properties. Fluid gels were exploited as a support media for ALM of layered cell culture scaffolds. This technique was investigated for fabrication of biphasic scaffolds with potential applications in culture of osteochondral tissue.

Finally, an alternative method for creating anisotropic 3D culture environments was investigated. Gels with a single mechanical property but different chemical properties were created via use of media channels to control diffusion of small molecules through agarose hydrogel matrices. Again, focus was on creating a potential osteochondral model. Key highlights and future prospects for each study are outlined below.

8.1 Tuning the Rheology of Gellan Gum Hydrogels for Cell Culture Applications

Chapter 4 highlighted the potential of using pulsed sonication to exhibit greater control over the rheology of gellan gum hydrogels. Application of sonication resulted in breaking of gellan molecules into smaller fragments of lower molecular weight. This had a direct influence on rheology with a reduction in gellan solution viscosity. Additionally, stiffness and elasticity of gellan hydrogels was

reduced by sonication. Changes in rheological properties could be controlled by varying the amplitude of applied ultrasonic waves with higher amplitudes triggering a greater reduction in viscosity and strength. Furthermore, changes in rheological behaviour triggered variances in behaviour of encapsulated mouse-derived pre-osteoblast cells. Reductions in matrix stiffness had a negative effect on expression and subsequent activity of alkaline phosphatase, an early marker for osteogenesis.

This highlighted the potential of using tunable hydrogels to directly influence cell phenotype expression. However, further work could be conducted to greater understand how tuning hydrogel properties with sonication could influence behaviour of a variety of cell types. Mechanical properties heavily influence cell phenotype expression *in vivo*. To evaluate the extent with which a simple sonication method can be used to stimulate such changes, the effect of sonication on mechanical properties of multiple biopolymer materials could be investigated. Furthermore, multiple cell types could be investigated to evaluate how sonication of hydrogel materials can influence their behaviour. Perhaps the most interesting future recommendation is analysis of how rheological changes presented in Chapter 4 effect stem cell lineage differentiation. It has been shown that matrix elasticity can directly influence stem cell lineage specification (Engler et al., 2006). It could, therefore, be useful to provide insight into if sonication can be used to change rheological properties of biopolymer hydrogels such that stem cell lineage specification can be tuned.

8.2 Fluid Gel as a Supporting Media for ALM of Biological Structures

Chapters 5 and 6 outlined a potential new approach to ALM using soft materials. The aim was to build on work outlined in Chapter 4 by analysing cellular behaviour in scaffolds exhibiting multiple mechanical properties. Use of particulate gel suspensions (fluid gels) as an ALM supporting media was investigated. It was demonstrated that a fluid gel system could be used to support controlled deposition and suspension of biopolymer solutions, albeit provided certain mechanical boundaries were met. Suspended biopolymer solutions were successfully gelled and extracted, allowing for

fabrication of complex structures such as a mineralised gellan helix and biphasic hydrogel scaffolds. Tunability of the system was demonstrated with multiple parameters shown to influence the resolution of suspended structures. Moreover, by using this system it was possible to fabricate a cell loaded, gradient scaffold that exhibited certain properties analogous to native osteochondral tissue. Scaffolds contained a gradient in mineralisation, mechanical properties and evidence of successful co-culture of osteoblasts and chondrocytes with a controlled interface. At the interface between both materials, there was possible indication of chondrocyte hypertrophy with low expression levels of type II collagen. However, further investigation is required to confirm this. Future work could involve studying chondrocyte behaviour at the interface focussing on hypertrophic markers such as type X collagen and ALP expression in chondrocytes (Leboy et al., 1989, Von der Mark et al., 1992).

This technique could potentially hold a great deal of promise in the field of tissue engineering using soft materials. ALM can play an important role in fabrication of patient-specific cell culture scaffolds but current difficulties in printing soft materials place limitations on its integration. Depositing biopolymer solutions into a particulate gel suspension allows for greater control over formation of cell-seeded scaffolds and addresses limitations in layering soft materials into complex structures. Using this technique, it is plausible that many complex *in vivo* environments could be modelled in addition to osteochondral tissue. The 4-tiered structure of articular cartilage, for example, could potentially be modelled by depositing soft materials into fluid gel supporting media. By creating such a structure it may be possible to create scaffolds that can be used to repair damage to this complex tissue. Alternatively, the 5-tiered structure of the cerebral cortex could be modelled, providing a potential *in vitro* 3D culture platform for modelling neurodegenerative diseases such as Alzheimer's. Finally, automation of the system could allow for greater control over construct fabrication, facilitating creation of completely customisable, patient-specific hydrogel scaffolds for tissue repair.

8.3 Controlled Multi-Lineage Differentiation of MSCs within a Single Hydrogel Structure

The final results chapter outlined a study into use of microfluidics in a hydrogel model for triggering controlled multi-lineage differentiation in a single MSC population. Channelled agarose hydrogels were evaluated with a focus on using 2 separate channels for inducing simultaneous osteogenic and chondrogenic differentiation through controlling diffusion of chemical cues. The aim was to create an osteochondral model with segregated populations of osteoblasts and chondrocytes and, additionally, an interface between both cell types. Control over diffusion of small molecules through agarose hydrogels via application of time constraints was successfully demonstrated by an ability to selectively deliver supplemented DMEM to encapsulated fibroblasts. Building on this a stem cell model was evaluated with an attempt to control diffusion of osteogenic and chondrogenic culture media. After 6 weeks of culture histology, bioassays and RT-PCR of encapsulated cells highlighted evidence of potential simultaneous osteogenic and chondrogenic differentiation of a single, encapsulated stem cell population. There was also evidence of an interface between osteoblasts and chondrocytes providing potential support for use of such a system in creating osteochondral models. However, expression of osteogenic markers was the lowest in regions close to the osteogenic channel. While this result was unanticipated, it could be explained by previous observations on the effect of osteochondral culture on osteoblast behaviour (Prasadam et al., 2010, Jiang et al., 2005). Such studies have reported a negative impact on expression of osteogenic markers by osteoblasts but the exact mechanism is, as of yet, unknown. This could, therefore, present an interesting avenue for future investigation. Osteochondral cultures generated by this fluidic system could be used to study how chondrocytes and osteoblasts interact at an interface and the subsequent effect this has on expression of osteogenic markers.

Such a system could also have many other potential future applications in terms of tissue culture systems. While this study focussed on controlled co-culture of 2 cell types with an aim to create an

osteochondral model, other models could be investigated. Hydrogels could be fabricated to contain more than 2 media channels. By doing this, more complex co-cultures could be cultivated such as a neuronal model containing neurons, astrocytes, microglial cells and oligodendrocytes. Again, such a model could be used to study neurodegenerative diseases. Additionally, microfluidic systems within hydrogels could be used to create an artificial vascular system for encapsulated cultures by pumping media through channels at a continuous rate. This could allow for creation of media gradients within hydrogels with a focus on mimicking environments seen in formation of tumours and could allow for more effective screening of potential anti-cancer compounds. By introducing drugs through microfluidic channels and observing diffusion through hydrogel matrices, this could provide a more insightful screening platform than basic 2D monolayer cultures.

Overall this work has further highlighted the potential of biopolymer hydrogel scaffolds as 3D culture models for influencing cell behaviour. Tunability of both mechanical and chemical hydrogel properties can direct phenotype expression in encapsulated cells. Taking this into consideration could allow for fabrication of hydrogel scaffolds that greater mimic *in vivo* tissue culture environments.

References

AHMED, E. M. 2015. Hydrogel: Preparation, characterization, and applications: A review. *Journal of Advanced Research,* 6**,** 105-121.

ALHADLAQ, A. & MAO, J. J. 2005. Tissue-engineered osteochondral constructs in the shape of an articular condyle. *J Bone Joint Surg Am,* 87**,** 936-944.

ANNABI, N., TSANG, K., MITHIEUX, S. M., NIKKHAH, M., AMERI, A., KHADEMHOSSEINI, A. & WEISS, A. S. 2013. Highly elastic micropatterned hydrogel for engineering functional cardiac tissue. *Advanced functional materials,* 23**,** 4950-4959.

BAINO, F., NOVAJRA, G., MIGUEZ-PACHECO, V., BOCCACCINI, A. R. & VITALE-BROVARONE, C. 2016. Bioactive glasses: Special applications outside the skeletal system. *Journal of Non-Crystalline Solids,* 432, Part A**,** 15-30.

BAJAJ, I. B., SURVASE, S. A., SAUDAGAR, P. S. & SINGHAL, R. S. 2007. Gellan gum: fermentative production, downstream processing and applications. *Food Technology and Biotechnology,* 45**,** 341.

BANERJEE, A., MAJUMDER, P., SANYAL, S., SINGH, J., JANA, K., DAS, C. & DASGUPTA, D. 2014. The DNA intercalators ethidium bromide and propidium iodide also bind to core histones. *FEBS open bio,* 4**,** 251-259.

BELLOWS, C., AUBIN, J. & HEERSCHE, J. 1991a. Initiation and progression of mineralization of bone nodules formed in vitro: the role of alkaline phosphatase and organic phosphate. *Bone and mineral,* 14**,** 27-40.

BELLOWS, C. G., AUBIN, J. E. & HEERSCHE, J. N. 1991b. Initiation and progression of mineralization of bone nodules formed in vitro: the role of alkaline phosphatase and organic phosphate. *Bone Miner,* 14**,** 27-40.

BERG, L., KOCH, T., HEERKENS, T., BESONOV, K., THOMSEN, P. & BETTS, D. 2009. Chondrogenic potential of mesenchymal stromal cells derived from equine bone marrow and umbilical cord blood. *Veterinary and Comparative Orthopaedics and Traumatology,* 22**,** 363.

BHAT, S. & KUMAR, A. 2012. Cell proliferation on three-dimensional chitosan–agarose–gelatin cryogel scaffolds for tissue engineering applications. *Journal of Bioscience and Bioengineering,* 114**,** 663-670.

BHOSALE, A. M. & RICHARDSON, J. B. 2008a. Articular cartilage: structure, injuries and review of management. *British Medical Bulletin,* 87**,** 77-95.

BHOSALE, A. M. & RICHARDSON, J. B. 2008b. Articular cartilage: structure, injuries and review of management. *Br Med Bull,* 87**,** 77-95.

BIAN, L., ZHAI, D. Y., TOUS, E., RAI, R., MAUCK, R. L. & BURDICK, J. A. 2011. Enhanced MSC chondrogenesis following delivery of TGF-β3 from alginate microspheres within hyaluronic acid hydrogels in vitro and in vivo. *Biomaterials,* 32**,** 6425-6434.

BILLIET, T., GEVAERT, E., DE SCHRYVER, T., CORNELISSEN, M. & DUBRUEL, P. 2014. The 3D printing of gelatin methacrylamide cell-laden tissue-engineered constructs with high cell viability. *Biomaterials,* 35**,** 49-62.

BOLAND, T., TAO, X., DAMON, B. J., MANLEY, B., KESARI, P., JALOTA, S. & BHADURI, S. 2007. Drop-on-demand printing of cells and materials for designer tissue constructs. *Materials Science and Engineering: C,* 27**,** 372-376.

BONEWALD, L. F. & JOHNSON, M. L. 2008. Osteocytes, mechanosensing and Wnt signaling. *Bone,* 42**,** 606-615.

BRATOSIN, D., MITROFAN, L., PALII, C., ESTAQUIER, J. & MONTREUIL, J. 2005. Novel fluorescence assay using calcein-AM for the determination of human erythrocyte viability and aging. *Cytometry Part A,* 66**,** 78-84.

BRITTBERG, M., TALLHEDEN, T., SJÖGREN-JANSSON, E., LINDAHL, A. & PETERSON, L. 2001. Autologous chondrocytes used for articular cartilage repair: an update. *Clinical orthopaedics and related research,* 391**,** S337-S348.

BUCKWALTER, J. & MANKIN, H. 1997. Articular cartilage: degeneration and osteoarthritis, repair, regeneration, and transplantation. *Instructional course lectures,* 47**,** 487-504.

BUCKWALTER, J. A. & MANKIN, H. J. 1998. Articular cartilage: tissue design and chondrocyte-matrix interactions. *Instr Course Lect,* 47**,** 477-86.

CAMPBELL, S. E., FERGUSON, V. L. & HURLEY, D. C. 2012. Nanomechanical mapping of the osteochondral interface with contact resonance force microscopy and nanoindentation. *Acta Biomaterialia,* 8**,** 4389-4396.

CAPLAN, A. I. 2007. Adult mesenchymal stem cells for tissue engineering versus regenerative medicine. *Journal of Cellular Physiology,* 213**,** 341-347.

CAPRON, I., COSTEUX, S. & DJABOUROV, M. 2001. Water in water emulsions: phase separation and rheology of biopolymer solutions. *Rheologica Acta,* 40**,** 441-456.

CAPULLI, M., PAONE, R. & RUCCI, N. 2014. Osteoblast and osteocyte: games without frontiers. *Archives of biochemistry and biophysics,* 561**,** 3-12.

CARLETTI, E., MOTTA, A. & MIGLIARESI, C. 2011. Scaffolds for tissue engineering and 3D cell culture. *Methods Mol Biol,* 695**,** 17-39.

ÇELIK, E., BAYRAM, C., AKÇAPıNAR, R., TÜRK, M. & DENKBAŞ, E. B. 2016. The effect of calcium chloride concentration on alginate/Fmoc-diphenylalanine hydrogel networks. *Materials Science and Engineering: C,* 66**,** 221-229.

CHATTOPADHYAY, S. & RAINES, R. T. 2014. Review collagen-based biomaterials for wound healing. *Biopolymers,* 101**,** 821-33.

CHAVDA, H. V. & PATEL, C. N. 2011. Effect of crosslinker concentration on characteristics of superporous hydrogel. *International Journal of Pharmaceutical Investigation,* 1**,** 17-21.

CHENG, H.-W., LUK, K. D. K., CHEUNG, K. M. C. & CHAN, B. P. 2011. In vitro generation of an osteochondral interface from mesenchymal stem cell–collagen microspheres. *Biomaterials,* 32**,** 1526-1535.

CHOI, J., KIM, S., JUNG, J., LIM, Y., KANG, K., PARK, S. & KANG, S. 2011. Wnt5a-mediating neurogenesis of human adipose tissue-derived stem cells in a 3D microfluidic cell culture system. *Biomaterials,* 32**,** 7013-7022.

CHOI, J. Y., LEE, B. H., SONG, K. B., PARK, R. W., KIM, I. S., SOHN, K. Y., JO, J. S. & RYOO, H. M. 1996. Expression patterns of bone-related proteins during osteoblastic differentiation in MC3T3-E1 cells. *Journal of cellular biochemistry,* 61**,** 609-618.

CHUAN, Y. L., HOQUE, M. E. & PASHBY, I. 2013. Prediction of Patient-Specific Tissue Engineering Scaffolds for Optimal Design. *International Journal of Modeling and Optimization,* 3**,** 468.

CLARK, A. H. & ROSS-MURPHY, S. B. 2009. *Biopolymer network assembly: measurement and theory,* Elsevier: London, UK.

COLEMAN, B. D. & NOLL, W. 1961. Foundations of linear viscoelasticity. *Reviews of modern physics,* 33**,** 239.

CONCONI, M. T., COPPI, P. D., BELLINI, S., ZARA, G., SABATTI, M., MARZARO, M., FRANCO ZANON, G., GAMBA, P. G., PARNIGOTTO, P. P. & NUSSDORFER, G. G. 2005. Homologous muscle acellular matrix seeded with autologous myoblasts as a tissue-engineering approach to abdominal wall-defect repair. *Biomaterials,* 26**,** 2567-2574.

COSTANTINI, M., IDASZEK, J., SZÖKE, K., JAROSZEWICZ, J., DENTINI, M., BARBETTA, A., BRINCHMANN, J. E. & ŚWIĘSZKOWSKI, W. 2016. 3D bioprinting of BM-MSCs-loaded ECM biomimetic hydrogels for in vitro neocartilage formation. *Biofabrication,* 8**,** 035002.

COVIELLO, T., MATRICARDI, P., MARIANECCI, C. & ALHAIQUE, F. 2007. Polysaccharide hydrogels for modified release formulations. *J Control Release,* 119**,** 5-24.

CRISOSTOMO, P. R., WANG, M., WAIRIUKO, G. M., MORRELL, E. D., TERRELL, A. M., SESHADRI, P., NAM, U. H. & MELDRUM, D. R. 2006. High passage number of stem cells adversely affects stem cell activation and myocardial protection. *Shock,* 26**,** 575-580.

D'ARRIGO, G., DI MEO, C., GAUCCI, E., CHICHIARELLI, S., COVIELLO, T., CAPITANI, D., ALHAIQUE, F. & MATRICARDI, P. 2012. Self-assembled gellan-based nanohydrogels as a tool for prednisolone delivery. *Soft Matter,* 8**,** 11557-11564.

DACIC, S., KALAJZIC, I., VISNJIC, D., LICHTLER, A. & ROWE, D. 2001. Col1a1-Driven Transgenic Markers of Osteoblast Lineage Progression. *Journal of Bone and Mineral Research,* 16**,** 1228-1236.

DAI, W., KAWAZOE, N., LIN, X., DONG, J. & CHEN, G. 2010. The influence of structural design of PLGA/collagen hybrid scaffolds in cartilage tissue engineering. *Biomaterials,* 31**,** 2141-2152.

DE CARVALHO, W. & DJABOUROV, M. 1997. Physical gelation under shear for gelatin gels. *Rheologica Acta,* 36**,** 591-609.

DEAN, R. L. 2002. Kinetic studies with alkaline phosphatase in the presence and absence of inhibitors and divalent cations. *Biochemistry and Molecular Biology Education,* 30**,** 401-407.

DEMERDASH, Z., EL-BAZ, H., MAHER, K., HASSAN, S., SALAH, F., HASSAN, M., ELZALLAT, M., EL-SHAFEI, M. & TAHA, T. 2015. Effect of repeated passaging and cell density on proliferation and differentiation potential of cord blood unrestricted somatic stem cells. *New Horizons in Translational Medicine,* 2**,** 67.

DESSÌ, M., BORZACCHIELLO, A., MOHAMED, T. H., ABDEL-FATTAH, W. I. & AMBROSIO, L. 2013. Novel biomimetic thermosensitive β-tricalcium phosphate/chitosan-based hydrogels for bone tissue engineering. *Journal of Biomedical Materials Research Part A,* 101**,** 2984-2993.

DI LUCA, A., VAN BLITTERSWIJK, C. & MORONI, L. 2015. The osteochondral interface as a gradient tissue: From development to the fabrication of gradient scaffolds for regenerative medicine. *Birth Defects Research Part C: Embryo Today: Reviews,* 105**,** 34-52.

DONG, Y. F., SOUNG, D. Y., SCHWARZ, E. M., O'KEEFE, R. J. & DRISSI, H. 2006. Wnt induction of chondrocyte hypertrophy through the Runx2 transcription factor. *Journal of Cellular Physiology,* 208**,** 77-86.

DRURY, J. L. & MOONEY, D. J. 2003. Hydrogels for tissue engineering: scaffold design variables and applications. *Biomaterials,* 24**,** 4337-4351.

DUNCAN, M. R. & BERMAN, B. 1991. Stimulation of collagen and glycosaminoglycan production in cultured human adult dermal fibroblasts by recombinant human interleukin 6. *Journal of Investigative Dermatology,* 97**,** 686-692.

DUNLOP, D. D., MANHEIM, L. M., SONG, J. & CHANG, R. W. 2001. Arthritis prevalence and activity limitations in older adults. *Arthritis & Rheumatism,* 44**,** 212-221.

EBERLI, D. & ATALA, A. 2006. Tissue engineering using adult stem cells. *Methods Enzymol,* 420**,** 287-302.

ELDRIDGE, J. E. & FERRY, J. D. 1954. Studies of the cross-linking process in gelatin gels. III. Dependence of melting point on concentration and molecular weight. *The Journal of Physical Chemistry,* 58**,** 992-995.

ENGLER, A. J., SEN, S., SWEENEY, H. L. & DISCHER, D. E. 2006. Matrix elasticity directs stem cell lineage specification. *Cell,* 126**,** 677-89.

EWOLDT, R. H., JOHNSTON, M. T. & CARETTA, L. M. 2015. Experimental challenges of shear rheology: How to avoid bad data. *Complex Fluids in Biological Systems.* Springer.

FAN, J., GONG, Y., REN, L., VARSHNEY, R. R., CAI, D. & WANG, D. A. 2010. In vitro engineered cartilage using synovium-derived mesenchymal stem cells with injectable gellan hydrogels. *Acta Biomater,* 6**,** 1178-85.

FARRÉS, I. F., MOAKES, R. & NORTON, I. 2014. Designing biopolymer fluid gels: A microstructural approach. *Food Hydrocolloids,* 42**,** 362-372.

FEDOROVICH, N. E., OUDSHOORN, M. H., VAN GEEMEN, D., HENNINK, W. E., ALBLAS, J. & DHERT, W. J. 2009. The effect of photopolymerization on stem cells embedded in hydrogels. *Biomaterials,* 30**,** 344-353.

FERNANDEZ-MOURE, J. S., CORRADETTI, B., CHAN, P., VAN EPS, J. L., JANECEK, T., RAMESHWAR, P., WEINER, B. K. & TASCIOTTI, E. 2015. Enhanced osteogenic potential of mesenchymal stem cells from cortical bone: a comparative analysis. *Stem cell research & therapy,* 6**,** 1.

FLORENCIO-SILVA, R., SASSO, G. R., SASSO-CERRI, E., SIMOES, M. J. & CERRI, P. S. 2015. Biology of Bone Tissue: Structure, Function, and Factors That Influence Bone Cells. *Biomed Res Int,* 2015**,** 421746.

FOX, A. J. S., BEDI, A. & RODEO, S. A. 2009. The basic science of articular cartilage: structure, composition, and function. *Sports Health: A Multidisciplinary Approach,* 1**,** 461-468.

FRANCESCHI, R. T. & IYER, B. S. 1992. Relationship between collagen synthesis and expression of the osteoblast phenotype in MC3T3-E1 cells. *Journal of Bone and Mineral Research,* 7**,** 235-246.

FUKUDA, K. 2001. Development of regenerative cardiomyocytes from mesenchymal stem cells for cardiovascular tissue engineering. *Artificial organs,* 25**,** 187-193.

FUNAMI, T., FANG, Y., NODA, S., ISHIHARA, S., NAKAUMA, M., DRAGET, K. I., NISHINARI, K. & PHILLIPS, G. O. 2009. Rheological properties of sodium alginate in an aqueous system during gelation in relation to supermolecular structures and Ca 2+ binding. *Food Hydrocolloids,* 23**,** 1746-1755.

FURUKAWA, K. & OHSUYE, K. 1999. Method for animal cell culture. Google Patents.

GAMBLIN, A.-L., BRENNAN, M. A., RENAUD, A., YAGITA, H., LÉZOT, F., HEYMANN, D., TRICHET, V. & LAYROLLE, P. 2014. Bone tissue formation with human mesenchymal stem cells and biphasic calcium phosphate ceramics: The local implication of osteoclasts and macrophages. *Biomaterials,* 35**,** 9660-9667.

GAO, J., DENNIS, J. E., SOLCHAGA, L. A., AWADALLAH, A. S., GOLDBERG, V. M. & CAPLAN, A. I. 2001. Tissue-engineered fabrication of an osteochondral composite graft using rat bone marrow-derived mesenchymal stem cells. *Tissue engineering,* 7**,** 363-371.

GHAYOR, C., HERROUIN, J.-F., CHADJICHRISTOS, C., ALA-KOKKO, L., TAKIGAWA, M., PUJOL, J.-P. & GALÉRA, P. 2000. Regulation of Human COL2A1 Gene Expression in Chondrocytes IDENTIFICATION OF C-Krox-RESPONSIVE ELEMENTS AND MODULATION BY PHENOTYPE ALTERATION. *Journal of Biological Chemistry,* 275**,** 27421-27438.

GHORBAL, A., GRISOTTO, F., CHARLIER, J., PALACIN, S., GOYER, C., DEMAILLE, C. & BRAHIM, A. B. 2013. Nano-Electrochemistry and Nano-Electrografting with an Original Combined AFM-SECM. *Nanomaterials,* 3**,** 303-316.

GHOSH, B. N. 1927. The alleged second isoelectric point of gelatin. *Journal of the Chemical Society***,** 1250-1252.

GILLETTE, B. M., JENSEN, J. A., TANG, B., YANG, G. J., BAZARGAN-LARI, A., ZHONG, M. & SIA, S. K. 2008. In situ collagen assembly for integrating microfabricated three-dimensional cell-seeded matrices. *Nature materials,* 7**,** 636-640.

GOLUB, E. E. & BOESZE-BATTAGLIA, K. 2007. The role of alkaline phosphatase in mineralization. *Current Opinion in Orthopaedics,* 18**,** 444-448.

GRAESSLEY, W. W. & SHINBACH, E. S. 1974. Flow properties of branched polydisperse polymers. *Journal of Polymer Science: Polymer Physics Edition,* 12**,** 2047-2063.

GRASDALEN, H., LARSEN, B. & SMISROD, O. 1981. 13 CN. MR studies of monomeric composition and sequence in alginate. *Carbohydrate Research,* 89**,** 179-191.

GREGORY, C. A., GUNN, W. G., PEISTER, A. & PROCKOP, D. J. 2004. An Alizarin red-based assay of mineralization by adherent cells in culture: comparison with cetylpyridinium chloride extraction. *Analytical biochemistry,* 329**,** 77-84.

GUADAGNO, T. M., OHTSUBO, M., ROBERTS, J. M. & ASSOIAN, R. K. 1993. A link between cyclin A expression and adhesion-dependent cell cycle progression. *SCIENCE-NEW YORK THEN WASHINGTON-*, 262**,** 1572-1572.

GUILAK, F., COHEN, D. M., ESTES, B. T., GIMBLE, J. M., LIEDTKE, W. & CHEN, C. S. 2009. Control of stem cell fate by physical interactions with the extracellular matrix. *Cell stem cell,* 5**,** 17-26.

GUO, L., COLBY, R. H., LUSIGNAN, C. P. & WHITESIDES, T. H. 2003. Kinetics of Triple Helix Formation in Semidilute Gelatin Solutions. *Macromolecules,* 36**,** 9999-10008.

GUO, X., LIAO, J., PARK, H., SARAF, A., RAPHAEL, R. M., TABATA, Y., KASPER, F. K. & MIKOS, A. G. 2010. Effects of TGF-β3 and preculture period of osteogenic cells on the chondrogenic differentiation of rabbit marrow mesenchymal stem cells encapsulated in a bilayered hydrogel composite. *Acta Biomaterialia,* 6**,** 2920-2931.

HALEEM, A. M. & CHU, C. R. 2010. Advances in Tissue Engineering Techniques for Articular Cartilage Repair. *Operative Techniques in Orthopaedics,* 20**,** 76-89.

HALL, C. & HAMILTON, A. 2015. Porosity–density relations in stone and brick materials. *Materials and Structures,* 48**,** 1265-1271.

HAN, C. D. 2007. *Rheology and Processing of Polymeric Materials: Volume 1: Polymer Rheology,* Oxford University Press on Demand.

HARDING, S. E. 1997. The intrinsic viscosity of biological macromolecules. Progress in measurement, interpretation and application to structure in dilute solution. *Progress in Biophysics and Molecular Biology,* 68**,** 207-262.

HARINK, B., LE GAC, S., BARATA, D., VAN BLITTERSWIJK, C. & HABIBOVIC, P. 2014. Microtiter plate-sized standalone chip holder for microenvironmental physiological control in gas-impermeable microfluidic devices. *Lab on a Chip,* 14**,** 1816-1820.

HARINK, B., LE GAC, S., TRUCKENMÜLLER, R., VAN BLITTERSWIJK, C. & HABIBOVIC, P. 2013. Regeneration-on-a-chip? The perspectives on use of microfluidics in regenerative medicine. *Lab on a Chip,* 13**,** 3512-3528.

HARLEY, B. A., KIM, H.-D., ZAMAN, M. H., YANNAS, I. V., LAUFFENBURGER, D. A. & GIBSON, L. J. 2008. Microarchitecture of three-dimensional scaffolds influences cell migration behavior via junction interactions. *Biophysical journal,* 95**,** 4013-4024.

HEINO, T. J., HENTUNEN, T. A. & VÄÄNÄNEN, H. K. 2004. Conditioned medium from osteocytes stimulates the proliferation of bone marrow mesenchymal stem cells and their differentiation into osteoblasts. *Experimental Cell Research,* 294**,** 458-468.

HENCH, L. L., SPLINTER, R. J., ALLEN, W. C. & GREENLEE, T. K. 1971. Bonding mechanisms at the interface of ceramic prosthetic materials. *Journal of Biomedical Materials Research,* 5**,** 117-141.

HEZAVEH, H. & MUHAMAD, I. I. 2013. Modification and swelling kinetic study of kappa-carrageenan-based hydrogel for controlled release study. *Journal of the Taiwan Institute of Chemical Engineers,* 44**,** 182-191.

HINTON, T. J., JALLERAT, Q., PALCHESKO, R. N., PARK, J. H., GRODZICKI, M. S., SHUE, H.-J., RAMADAN, M. H., HUDSON, A. R. & FEINBERG, A. W. 2015. Three-dimensional printing of complex biological structures by freeform reversible embedding of suspended hydrogels. *Science advances,* 1**,** e1500758.

HITCHCOCK, D. I. 1924. THE ISOELECTRIC POINT OF GELATIN AT 40°C. *The Journal of General Physiology,* 6**,** 457-462.

HOYER, B., BERNHARDT, A., LODE, A., HEINEMANN, S., SEWING, J., KLINGER, M., NOTBOHM, H. & GELINSKY, M. 2014. Jellyfish collagen scaffolds for cartilage tissue engineering. *Acta Biomaterialia,* 10**,** 883-892.

HUGGINS, M. L. 1942. The Viscosity of Dilute Solutions of Long-Chain Molecules. IV. Dependence on Concentration. *Journal of the American Chemical Society,* 64**,** 2716-2718.

HUH, D., HAMILTON, G. A. & INGBER, D. E. 2011. From 3D cell culture to organs-on-chips. *Trends in cell biology,* 21**,** 745-754.

HUTMACHER, D. W. 2000. Scaffolds in tissue engineering bone and cartilage. *Biomaterials,* 21**,** 2529-2543.

IGNATIUS, A., BLESSING, H., LIEDERT, A., SCHMIDT, C., NEIDLINGER-WILKE, C., KASPAR, D., FRIEMERT, B. & CLAES, L. 2005. Tissue engineering of bone: effects of mechanical strain on osteoblastic cells in type I collagen matrices. *Biomaterials,* 26**,** 311-318.

JAHROMI, S. H., GROVER, L. M., PAXTON, J. Z. & SMITH, A. M. 2011. Degradation of polysaccharide hydrogels seeded with bone marrow stromal cells. *Journal of the mechanical behavior of biomedical materials,* 4**,** 1157-1166.

JAMSHIDI, P., BIRDI, G., WILLIAMS, R. L., COX, S. C. & GROVER, L. M. 2015. Modification of gellan gum with nanocrystalline hydroxyapatite facilitates cell expansion and spontaneous osteogenesis. *Biotechnology and bioengineering*.

JAMSHIDI, P., MA, P., KHOSROWYAR, K., SMITH, A. M. & GROVER, L. M. 2012. Tailoring gel modulus using dispersed nanocrystalline hydroxyapatite. *Journal of Experimental Nanoscience,* 7**,** 652-661.

JIANG, J., NICOLL, S. B. & LU, H. H. 2005. Co-culture of osteoblasts and chondrocytes modulates cellular differentiation in vitro. *Biochemical and Biophysical Research Communications,* 338**,** 762-770.

JIN, R., MOREIRA TEIXEIRA, L. S., KROUWELS, A., DIJKSTRA, P. J., VAN BLITTERSWIJK, C. A., KARPERIEN, M. & FEIJEN, J. 2010. Synthesis and characterization of hyaluronic acid–poly(ethylene glycol) hydrogels via Michael addition: An injectable biomaterial for cartilage repair. *Acta Biomaterialia,* 6**,** 1968-1977.

KAKUDO, N., SHIMOTSUMA, A., MIYAKE, S., KUSHIDA, S. & KUSUMOTO, K. 2008. Bone tissue engineering using human adipose-derived stem cells and honeycomb collagen scaffold. *J Biomed Mater Res A,* 84**,** 191-7.

KANG, H.-W., LEE, S. J., KO, I. K., KENGLA, C., YOO, J. J. & ATALA, A. 2016. A 3D bioprinting system to produce human-scale tissue constructs with structural integrity. *Nature biotechnology,* 34**,** 312-319.

KARAGEORGIOU, V. & KAPLAN, D. 2005. Porosity of 3D biomaterial scaffolds and osteogenesis. *Biomaterials,* 26**,** 5474-91.

KERN, S., EICHLER, H., STOEVE, J., KLÜTER, H. & BIEBACK, K. 2006. Comparative analysis of mesenchymal stem cells from bone marrow, umbilical cord blood, or adipose tissue. *Stem cells,* 24**,** 1294-1301.

KHADEMHOSSEINI, A. & LANGER, R. 2007. Microengineered hydrogels for tissue engineering. *Biomaterials,* 28**,** 5087-5092.

KHANARIAN, N. T., HANEY, N. M., BURGA, R. A. & LU, H. H. 2012. A functional agarose-hydroxyapatite scaffold for osteochondral interface regeneration. *Biomaterials,* 33**,** 5247-5258.

KHANG, G., LEE, S., KIM, H., SILVA-CORREIA, J., GOMES, M. E., VIEGAS, C., DIAS, I. R., OLIVEIRA, J. M. & REIS, R. 2015. Biological evaluation of intervertebral disc cells in different formulations of gellan gum-based hydrogels. *Journal of tissue engineering and regenerative medicine,* 9**,** 265-275.

KIM, H.-W., KIM, H.-E. & SALIH, V. 2005. Stimulation of osteoblast responses to biomimetic nanocomposites of gelatin–hydroxyapatite for tissue engineering scaffolds. *Biomaterials,* 26**,** 5221-5230.

KIM, S. G., LEE, D. S., LEE, S. & JANG, J. H. 2015. Osteocalcin/fibronectin-functionalized collagen matrices for bone tissue engineering. *Journal of Biomedical Materials Research Part A,* 103**,** 2133-2140.

KNUDSON, C. B. & KNUDSON, W. Cartilage proteoglycans. Seminars in cell & developmental biology, 2001. Elsevier, 69-78.

KOLIANDRIS, A., LEE, A., FERRY, A.-L., HILL, S. & MITCHELL, J. 2008. Relationship between structure of hydrocolloid gels and solutions and flavour release. *Food Hydrocolloids,* 22**,** 623-630.

KOMORI, T. 2009. Regulation of osteoblast differentiation by Runx2. *Osteoimmunology*. Springer.

KRAEMER, E. O. 1938. Molecular weights of celluloses and cellulose derivates. *Industrial & Engineering Chemistry,* 30**,** 1200-1203.

LANGENBACH, F. & HANDSCHEL, J. 2013. Effects of dexamethasone, ascorbic acid and β-glycerophosphate on the osteogenic differentiation of stem cells in vitro. *Stem cell research & therapy,* 4**,** 1.

LEBOY, P. S., VAIAS, L., USCHMANN, B., GOLUB, E., ADAMS, S. & PACIFICI, M. 1989. Ascorbic acid induces alkaline phosphatase, type X collagen, and calcium deposition in cultured chick chondrocytes. *Journal of Biological Chemistry,* 264**,** 17281-17286.

LEE, K. Y. & MOONEY, D. J. 2001. Hydrogels for Tissue Engineering. *Chemical Reviews,* 101**,** 1869-1880.

LEIPZIG, N. D. & SHOICHET, M. S. 2009. The effect of substrate stiffness on adult neural stem cell behavior. *Biomaterials,* 30**,** 6867-6878.

LETHERBY, M. R. & YOUNG, D. A. 1981. The gelation of agarose. *Journal of the Chemical Society, Faraday Transactions 1: Physical Chemistry in Condensed Phases,* 77**,** 1953-1966.

LEVINGSTONE, T. J., MATSIKO, A., DICKSON, G. R., O'BRIEN, F. J. & GLEESON, J. P. 2014. A biomimetic multi-layered collagen-based scaffold for osteochondral repair. *Acta Biomaterialia,* 10**,** 1996-2004.

LEWIS, M. J. 1996. 4 - Viscosity. *Physical Properties of Foods and Food Processing Systems.* Woodhead Publishing.

LI, W.-J., TULI, R., OKAFOR, C., DERFOUL, A., DANIELSON, K. G., HALL, D. J. & TUAN, R. S. 2005. A three-dimensional nanofibrous scaffold for cartilage tissue engineering using human mesenchymal stem cells. *Biomaterials,* 26**,** 599-609.

LI, X., DING, J., WANG, J., ZHUANG, X. & CHEN, X. 2015. Biomimetic biphasic scaffolds for osteochondral defect repair. *Regenerative biomaterials***,** rbv015.

LIELEG, O. & RIBBECK, K. 2011. Biological hydrogels as selective diffusion barriers. *Trends in cell biology,* 21**,** 543-551.

LIESS, C., LÜSSE, S., KARGER, N., HELLER, M. & GLÜER, C.-C. 2002. Detection of changes in cartilage water content using MRI T2-mapping in vivo. *Osteoarthritis and Cartilage,* 10**,** 907-913.

LIN, H., LOZITO, T. P., ALEXANDER, P. G., GOTTARDI, R. & TUAN, R. S. 2014. Stem cell-based microphysiological osteochondral system to model tissue response to interleukin-1β. *Molecular pharmaceutics,* 11**,** 2203-2212.

LIPSON, H. & KURMAN, M. 2013. *Fabricated: The new world of 3D printing,* John Wiley & Sons.

LIU, Z., YIN, X., YE, Q., HE, W., GE, M., ZHOU, X., HU, J. & ZOU, S. 2016. Periodontal regeneration with stem cells-seeded collagen-hydroxyapatite scaffold. *J Biomater Appl,* 31**,** 121-31.

LU, H., HOSHIBA, T., KAWAZOE, N. & CHEN, G. 2011. Autologous extracellular matrix scaffolds for tissue engineering. *Biomaterials,* 32**,** 2489-2499.

MA, P. X. 2008. Biomimetic materials for tissue engineering. *Advanced Drug Delivery Reviews,* 60**,** 184-198.

MAHDI, M., DIRYAK, R., KONTOGIORGOS, V., MORRIS, G. & SMITH, A. M. 2016. In situ rheological measurements of the external gelation of alginate. *Food Hydrocolloids,* 55**,** 77-80.

MAHDI, M. H. 2016. *Development of Gellan Gum Fluid Gels as Modified Release Drug Delivery Systems* Doctor of Philosophy PhD, University of Huddersfield.

MAHDI, M. H., CONWAY, B. R. & SMITH, A. M. 2014. Evaluation of gellan gum fluid gels as modified release oral liquids. *International Journal of Pharmaceutics,* 475**,** 335-343.

MAHDI, M. H., CONWAY, B. R. & SMITH, A. M. 2015. Development of mucoadhesive sprayable gellan gum fluid gels. *International Journal of Pharmaceutics,* 488**,** 12-19.

MAHJOUB, M., BERENBAUM, F. & HOUARD, X. 2012. Why subchondral bone in osteoarthritis? The importance of the cartilage bone interface in osteoarthritis. *Osteoporosis International,* 23**,** 841-846.

MARTIN, I., MIOT, S., BARBERO, A., JAKOB, M. & WENDT, D. 2007. Osteochondral tissue engineering. *Journal of biomechanics,* 40**,** 750-765.

MAUCK, R., YUAN, X. & TUAN, R. 2006. Chondrogenic differentiation and functional maturation of bovine mesenchymal stem cells in long-term agarose culture. *Osteoarthritis and cartilage,* 14**,** 179-189.

MELCHELS, F. P., BLOKZIJL, M. M., LEVATO, R., PEIFFER, Q. C., DE RUIJTER, M., HENNINK, W. E., VERMONDEN, T. & MALDA, J. 2016. Hydrogel-based reinforcement of 3D bioprinted constructs. *Biofabrication,* 8**,** 035004.

MIRI, T. 2011. Viscosity and Oscillatory Rheology. *Practical Food Rheology.* Wiley-Blackwell.

MOBASHERPOUR, I., HESHAJIN, M. S., KAZEMZADEH, A. & ZAKERI, M. 2007. Synthesis of nanocrystalline hydroxyapatite by using precipitation method. *Journal of Alloys and Compounds,* 430**,** 330-333.

MOHAN, N., GUPTA, V., SRIDHARAN, B., SUTHERLAND, A. & DETAMORE, M. S. 2014. The potential of encapsulating "raw materials" in 3D osteochondral gradient scaffolds. *Biotechnology and bioengineering,* 111**,** 829-841.

MORRIS, E. R., NISHINARI, K. & RINAUDO, M. 2012. Gelation of gellan – A review. *Food Hydrocolloids,* 28**,** 373-411.

MOUTOS, F. T. & GUILAK, F. 2008. Composite scaffolds for cartilage tissue engineering. *Biorheology,* 45**,** 501-512.

MOXON, S. R. & SMITH, A. M. 2016. Controlling the rheology of gellan gum hydrogels in cell culture conditions. *International Journal of Biological Macromolecules,* 84**,** 79-86.

MURPHY, C. M., HAUGH, M. G. & O'BRIEN, F. J. 2010. The effect of mean pore size on cell attachment, proliferation and migration in collagen–glycosaminoglycan scaffolds for bone tissue engineering. *Biomaterials,* 31**,** 461-466.

NORTON, I. T., JARVIS, D. A. & FOSTER, T. J. 1999. A molecular model for the formation and properties of fluid gels. *International Journal of Biological Macromolecules,* 26**,** 255-261.

NUKAVARAPU, S. P. & DORCEMUS, D. L. 2013. Osteochondral tissue engineering: current strategies and challenges. *Biotechnology advances,* 31**,** 706-721.

OLIVEIRA, J. T., GARDEL, L. S., RADA, T., MARTINS, L., GOMES, M. E. & REIS, R. L. 2010. Injectable gellan gum hydrogels with autologous cells for the treatment of rabbit articular cartilage defects. *J Orthop Res,* 28**,** 1193-9.

PAN, J., ZHOU, X., LI, W., NOVOTNY, J. E., DOTY, S. B. & WANG, L. 2009. In situ measurement of transport between subchondral bone and articular cartilage. *Journal of Orthopaedic Research,* 27**,** 1347-1352.

PANSERI, S., RUSSO, A., CUNHA, C., BONDI, A., DI MARTINO, A., PATELLA, S. & KON, E. 2012. Osteochondral tissue engineering approaches for articular cartilage and subchondral bone regeneration. *Knee Surgery, Sports Traumatology, Arthroscopy,* 20**,** 1182-1191.

PARK, H., KANG, S.-W., KIM, B.-S., MOONEY, D. J. & LEE, K. Y. 2009. Shear-reversibly Crosslinked Alginate Hydrogels for Tissue Engineering. *Macromolecular Bioscience,* 9**,** 895-901.

PELTOLA, S. M., MELCHELS, F. P., GRIJPMA, D. W. & KELLOMÄKI, M. 2008. A review of rapid prototyping techniques for tissue engineering purposes. *Annals of medicine,* 40**,** 268-280.

PEREIRA, D. R., CANADAS, R. F., SILVA-CORREIA, J., MARQUES, A. P., REIS, R. L. & OLIVEIRA, J. M. Gellan gum-based hydrogel bilayered scaffolds for osteochondral tissue engineering. Key Engineering Materials, 2014. Trans Tech Publ, 255-260.

PFAFFL, M. W. 2001. A new mathematical model for relative quantification in real-time RT–PCR. *Nucleic acids research,* 29**,** e45-e45.

PFEIFER, R., LUNGARELLA, M. & IIDA, F. 2012. The challenges ahead for bio-inspired'soft'robotics. *Communications of the ACM,* 55**,** 76-87.

PICOUT, D. R. & ROSS-MURPHY, S. B. 2003. Rheology of biopolymer solutions and gels. *The Scientific World Journal,* 3**,** 105-121.

PITTENGER, M. F., MACKAY, A. M., BECK, S. C., JAISWAL, R. K., DOUGLAS, R., MOSCA, J. D., MOORMAN, M. A., SIMONETTI, D. W., CRAIG, S. & MARSHAK, D. R. 1999. Multilineage potential of adult human mesenchymal stem cells. *science,* 284**,** 143-147.

POSLINSKI, A., RYAN, M., GUPTA, R., SESHADRI, S. & FRECHETTE, F. 1988. Rheological Behavior of Filled Polymeric Systems I. Yield Stress and Shear-Thinning Effects. *Journal of Rheology (1978-present),* 32**,** 703-735.

PRASADAM, I., FRIIS, T., SHI, W., VAN GENNIP, S., CRAWFORD, R. & XIAO, Y. 2010. Osteoarthritic cartilage chondrocytes alter subchondral bone osteoblast differentiation via MAPK signalling pathway involving ERK1/2. *Bone,* 46**,** 226-235.

RAFAT, M., KOH, L. B., ISLAM, M. M., LIEDBERG, B. O. & GRIFFITH, M. 2012. Highly elastic epoxy cross-linked collagen hydrogels for corneal tissue engineering. *Acta Ophthalmologica,* 90**,** 0-0.

RAO, V. M., DELANEY, R. A. & SKINNER, G. 1986. Rheological properties of solid foods. *Engineering properties of foods***,** 215-226.

RASTEGAR, A. M., PAHLAVANZADEH, F., VAHDANI, R., AZADI, S. & MIRSADEGHI, E. 2015. The effect of cell passage on the viability of mesenchymal stem cells after cryopreservation. *Comparative Clinical Pathology,* 24**,** 403-408.

RAWADI, G., VAYSSIÈRE, B., DUNN, F., BARON, R. & ROMAN-ROMAN, S. 2003. BMP-2 controls alkaline phosphatase expression and osteoblast mineralization by a Wnt autocrine loop. *Journal of Bone and Mineral Research,* 18**,** 1842-1853.

REDDY, N., REDDY, R. & JIANG, Q. 2015. Crosslinking biopolymers for biomedical applications. *Trends in Biotechnology,* 33**,** 362-369.

REDLER, I., MOW, V. C., ZIMNY, M. L. & MANSELL, J. 1975. The ultrastructure and biomechanical significance of the tidemark of articular cartilage. *Clinical orthopaedics and related research,* 112**,** 357-362.

ROACH, P., EGLIN, D., ROHDE, K. & PERRY, C. C. 2007. Modern biomaterials: a review—bulk properties and implications of surface modifications. *Journal of Materials Science: Materials in Medicine,* 18**,** 1263-1277.

RODRIGUES, C., SERRICELLA, P., LINHARES, A., GUERDES, R., BOROJEVIC, R., ROSSI, M., DUARTE, M. & FARINA, M. 2003. Characterization of a bovine collagen–hydroxyapatite composite scaffold for bone tissue engineering. *Biomaterials,* 24**,** 4987-4997.

RÖNN, K., REISCHL, N., GAUTIER, E. & JACOBI, M. 2011. Current surgical treatment of knee osteoarthritis. *Arthritis,* 2011.

RUEL-GARIÉPY, E. & LEROUX, J.-C. 2004. In situ-forming hydrogels—review of temperature-sensitive systems. *European Journal of Pharmaceutics and Biopharmaceutics,* 58**,** 409-426.

SACHLOS, E., GOTORA, D. & CZERNUSZKA, J. T. 2006. Collagen scaffolds reinforced with biomimetic composite nano-sized carbonate-substituted hydroxyapatite crystals and shaped by rapid prototyping to contain internal microchannels. *Tissue Eng,* 12**,** 2479-87.

SAKAI, S., HASHIMOTO, I. & KAWAKAMI, K. 2007. Synthesis of an agarose-gelatin conjugate for use as a tissue engineering scaffold. *J Biosci Bioeng,* 103**,** 22-6.

SALEH, F. A., FRITH, J. E., LEE, J. A. & GENEVER, P. G. 2012. Three-dimensional in vitro culture techniques for mesenchymal stem cells. *Progenitor Cells: Methods and Protocols***,** 31-45.

SALEM, A. K., STEVENS, R., PEARSON, R. G., DAVIES, M. C., TENDLER, S. J., ROBERTS, C. J., WILLIAMS, P. M. & SHAKESHEFF, K. M. 2002. Interactions of 3T3 fibroblasts and endothelial cells with defined pore features. *J Biomed Mater Res,* 61**,** 212-7.

SAPKAL, P. S., KUTHE, A. M., KASHYAP, R. S., NAYAK, A. R., KUTHE, S. A. & KAWLE, A. P. 2016. Rapid prototyping assisted fabrication of patient specific β-tricalciumphosphate scaffolds for bone tissue regeneration. *Journal of Porous Materials,* 23**,** 927-935.

SCHAEFER, D., MARTIN, I., SHASTRI, P., PADERA, R., LANGER, R., FREED, L. & VUNJAK-NOVAKOVIC, G. 2000. In vitro generation of osteochondral composites. *Biomaterials,* 21**,** 2599-2606.

SCHEK, R., TABOAS, J., HOLLISTER, S. & KREBSBACH, P. 2005. Tissue engineering osteochondral implants for temporomandibular joint repair. *Orthodontics & craniofacial research,* 8**,** 313-319.

SCHEPERS, E., DE CLERCQ, M., DUCHEYNE, P. & KEMPENEERS, R. 1991. Bioactive glass particulate material as a filler for bone lesions. *J Oral Rehabil,* 18**,** 439-52.

SCHINDELER, A., MCDONALD, M. M., BOKKO, P. & LITTLE, D. G. 2008. Bone remodeling during fracture repair: The cellular picture. *Seminars in Cell & Developmental Biology,* 19**,** 459-466.

SCHNEIDER, G. B., ENGLISH, A., ABRAHAM, M., ZAHARIAS, R., STANFORD, C. & KELLER, J. 2004. The effect of hydrogel charge density on cell attachment. *Biomaterials,* 25**,** 3023-3028.

SEIDI, A., RAMALINGAM, M., ELLOUMI-HANNACHI, I., OSTROVIDOV, S. & KHADEMHOSSEINI, A. 2011. Gradient biomaterials for soft-to-hard interface tissue engineering. *Acta Biomaterialia,* 7**,** 1441-1451.

SHACHAR, M., TSUR-GANG, O., DVIR, T., LEOR, J. & COHEN, S. 2011. The effect of immobilized RGD peptide in alginate scaffolds on cardiac tissue engineering. *Acta Biomaterialia,* 7**,** 152-162.

SHEKHAWAT, V., LAURENT, M., MUEHLEMAN, C. & WIMMER, M. 2009. Surface topography of viable articular cartilage measured with scanning white light interferometry. *Osteoarthritis and cartilage,* 17**,** 1197-1203.

SHEPHERD, D. & SEEDHOM, B. 1999. Thickness of human articular cartilage in joints of the lower limb. *Annals of the rheumatic diseases,* 58**,** 27-34.

SHIGA, M., KAPILA, Y. L., ZHANG, Q., HAYAMI, T. & KAPILA, S. 2003. Ascorbic Acid Induces Collagenase-1 in Human Periodontal Ligament Cells but Not in MC3T3-E1 Osteoblast-Like Cells: Potential Association Between Collagenase Expression and Changes in Alkaline Phosphatase Phenotype. *Journal of Bone and Mineral Research,* 18**,** 67-77.

SHIN, M., YOSHIMOTO, H. & VACANTI, J. P. 2004. In vivo bone tissue engineering using mesenchymal stem cells on a novel electrospun nanofibrous scaffold. *Tissue engineering,* 10**,** 33-41.

SILVA-CORREIA, J., OLIVEIRA, J. M., CARIDADE, S., OLIVEIRA, J. T., SOUSA, R., MANO, J. & REIS, R. 2011. Gellan gum-based hydrogels for intervertebral disc tissue-engineering applications. *Journal of tissue engineering and regenerative medicine,* 5**,** e97-e107.

SMITH, A. M., HUNT, N. C., SHELTON, R. M., BIRDI, G. & GROVER, L. M. 2012. Alginate Hydrogel Has a Negative Impact on in Vitro Collagen 1 Deposition by Fibroblasts. *Biomacromolecules,* 13**,** 4032-4038.

SMITH, A. M., SHELTON, R. M., PERRIE, Y. & HARRIS, J. J. 2007. An initial evaluation of gellan gum as a material for tissue engineering applications. *J Biomater Appl,* 22**,** 241-54.

SMITS, P., LI, P., MANDEL, J., ZHANG, Z., DENG, J. M., BEHRINGER, R. R., DE CROMBRUGGHE, B. & LEFEBVRE, V. 2001. The transcription factors L-Sox5 and Sox6 are essential for cartilage formation. *Developmental cell,* 1**,** 277-290.

SOLCHAGA, L. A., PENICK, K. J. & WELTER, J. F. 2011. Chondrogenic differentiation of bone marrow-derived mesenchymal stem cells: tips and tricks. *Mesenchymal Stem Cell Assays and Applications***,** 253-278.

STEVENS, L. R., GILMORE, K. J., WALLACE, G. G. & IN HET PANHUIS, M. 2016. Tissue engineering with gellan gum. *Biomaterials Science,* 4**,** 1276-1290.

STEVENS, M. M., MAYER, M., ANDERSON, D. G., WEIBEL, D. B., WHITESIDES, G. M. & LANGER, R. 2005. Direct patterning of mammalian cells onto porous tissue engineering substrates using agarose stamps. *Biomaterials,* 26**,** 7636-7641.

SUGAHARA, K. & KITAGAWA, H. 2000. Recent advances in the study of the biosynthesis and functions of sulfated glycosaminoglycans. *Current opinion in structural biology,* 10**,** 518-527.

SWORN, G., SANDERSON, G. & GIBSON, W. 1995. Gellan gum fluid gels. *Food Hydrocolloids,* 9**,** 265-271.

TAYLOR, D. L., FERRIS, C. J., MANIEGO, A. R., CASTIGNOLLES, P., IN HET PANHUIS, M. & GABORIEAU, M. 2012. Characterization of Gellan Gum by Capillary Electrophoresis. *Australian Journal of Chemistry,* 65**,** 1156-1164.

THOMAS, S. 2000. Alginate dressings in surgery and wound management—Part 1. *Journal of wound care,* 9**,** 56-60.

TIBBITT, M. W. & ANSETH, K. S. 2009. Hydrogels as extracellular matrix mimics for 3D cell culture. *Biotechnology and bioengineering,* 103**,** 655-663.

TOH, W. S., LIM, T. C., KURISAWA, M. & SPECTOR, M. 2012. Modulation of mesenchymal stem cell chondrogenesis in a tunable hyaluronic acid hydrogel microenvironment. *Biomaterials,* 33**,** 3835-3845.

TRIPP, G. K., GOOD, K. L., MOTTA, M. J., KASS, P. H. & MURPHY, C. J. 2016. The effect of needle gauge, needle type, and needle orientation on the volume of a drop. *Veterinary ophthalmology,* 19**,** 38-42.

TSAO, C. T., HSIAO, M. H., ZHANG, M. Y., LEVENGOOD, S. L. & ZHANG, M. 2015. Chitosan-PEG Hydrogel with Sol–Gel Transition Triggerable by Multiple External Stimuli. *Macromolecular Rapid Communications,* 36**,** 332-338.

VAN STRAALEN, J. P., SANDERS, E., PRUMMEL, M. F. & SANDERS, G. T. 1991. Bone-alkaline phosphatase as indicator of bone formation. *Clinica chimica acta,* 201**,** 27-33.

VATS, A., TOLLEY, N., POLAK, J. & GOUGH, J. 2003. Scaffolds and biomaterials for tissue engineering: a review of clinical applications. *Clinical Otolaryngology & Allied Sciences,* 28**,** 165-172.

VIGUET-CARRIN, S., GARNERO, P. & DELMAS, P. 2006. The role of collagen in bone strength. *Osteoporosis International,* 17**,** 319-336.

VON DER MARK, K., KIRSCH, T., NERLICH, A., KUSS, A., WESELOH, G., GLÜCKERT, K. & STÖSS, H. 1992. Type X collagen synthesis in human osteoarthritic cartilage. Indication of chondrocyte hypertrophy. *Arthritis & Rheumatism,* 35**,** 806-811.

VOSKERICIAN, G. 2012. Soft Tissue Structure and Functionality. *Biomimetic, Bioresponsive, and Bioactive Materials.* John Wiley & Sons, Inc.

WANG, H., DWYER-LINDGREN, L., LOFGREN, K. T., RAJARATNAM, J. K., MARCUS, J. R., LEVIN-RECTOR, A., LEVITZ, C. E., LOPEZ, A. D. & MURRAY, C. J. L. 2012. Age-specific and sex-specific mortality in 187 countries, 1970–2010: a systematic analysis for the Global Burden of Disease Study 2010. *The Lancet,* 380**,** 2071-2094.

WANG, Y., BLASIOLI, D. J., KIM, H.-J., KIM, H. S. & KAPLAN, D. L. 2006. Cartilage tissue engineering with silk scaffolds and human articular chondrocytes. *Biomaterials,* 27**,** 4434-4442.

WANG, Y., KIM, U.-J., BLASIOLI, D. J., KIM, H.-J. & KAPLAN, D. L. 2005. In vitro cartilage tissue engineering with 3D porous aqueous-derived silk scaffolds and mesenchymal stem cells. *Biomaterials,* 26**,** 7082-7094.

WEINREB, M., SHINAR, D. & RODAN, G. A. 1990a. Different pattern of alkaline phosphatase, osteopontin, and osteocalcin expression in developing rat bone visualized by in situ hybridization. *J Bone Miner Res,* 5**,** 831-42.

WEINREB, M., SHINAR, D. & RODAN, G. A. 1990b. Different pattern of alkaline phosphatase, osteopontin, and osteocalcin expression in developing rat bone visualized by in situ hybridization. *Journal of Bone and Mineral Research,* 5**,** 831-842.

WELLS, R. G. 2008. The role of matrix stiffness in regulating cell behavior. *Hepatology,* 47**,** 1394-1400.
WHITESIDES, G. M. 2006. The origins and the future of microfluidics. *Nature,* 442**,** 368-373.
WINTER, H. H. & CHAMBON, F. 1986. Analysis of linear viscoelasticity of a crosslinking polymer at the gel point. *Journal of Rheology (1978-present),* 30**,** 367-382.
WOODFIELD, T., GUGGENHEIM, M., VON RECHENBERG, B., RIESLE, J., VAN BLITTERSWIJK, C. & WEDLER, V. 2009. Rapid prototyping of anatomically shaped, tissue-engineered implants for restoring congruent articulating surfaces in small joints. *Cell proliferation,* 42**,** 485-497.
WORTMAN, J. & EVANS, R. 1965. Young's modulus, shear modulus, and Poisson's ratio in silicon and germanium. *Journal of applied physics,* 36**,** 153-156.
WU, L., ZHANG, H., ZHANG, J. & DING, J. 2005. Fabrication of three-dimensional porous scaffolds of complicated shape for tissue engineering. I. Compression molding based on flexible-rigid combined mold. *Tissue engineering,* 11**,** 1105-1114.
XUE, J., FENG, B., ZHENG, R., LU, Y., ZHOU, G., LIU, W., CAO, Y., ZHANG, Y. & ZHANG, W. J. 2013. Engineering ear-shaped cartilage using electrospun fibrous membranes of gelatin/polycaprolactone. *Biomaterials,* 34**,** 2624-31.
YAMADA, Y., HOZUMI, K., ASO, A., HOTTA, A., TOMA, K., KATAGIRI, F., KIKKAWA, Y. & NOMIZU, M. 2012. Laminin active peptide/agarose matrices as multifunctional biomaterials for tissue engineering. *Biomaterials,* 33**,** 4118-4125.
YAMASAKI, A., ITABASHI, M., SAKAI, Y., ITO, H., ISHIWARI, Y., NAGATSUKA, H. & NAGAI, N. 2001. Expression of type I, type II, and type X collagen genes during altered endochondral ossification in the femoral epiphysis of osteosclerotic (oc/oc) mice. *Calcified tissue international,* 68**,** 53-60.
YE, D. & PERAMO, A. 2014. Implementing tissue engineering and regenerative medicine solutions in medical implants. *British Medical Bulletin,* 109**,** 3-18.
YEH, J., LING, Y., KARP, J. M., GANTZ, J., CHANDAWARKAR, A., ENG, G., BLUMLING III, J., LANGER, R. & KHADEMHOSSEINI, A. 2006. Micromolding of shape-controlled, harvestable cell-laden hydrogels. *Biomaterials,* 27**,** 5391-5398.
YEONG, W.-Y., CHUA, C.-K., LEONG, K.-F. & CHANDRASEKARAN, M. 2004. Rapid prototyping in tissue engineering: challenges and potential. *Trends in Biotechnology,* 22**,** 643-652.
YOON, S. K., SONG, J. Y. & LEE, G. M. 2003. Effect of low culture temperature on specific productivity, transcription level, and heterogeneity of erythropoietin in Chinese hamster ovary cells. *Biotechnology and bioengineering,* 82**,** 289-298.
YOSHIKAWA, H. & MYOUI, A. 2005. Bone tissue engineering with porous hydroxyapatite ceramics. *Journal of Artificial Organs,* 8**,** 131-136.
ZHAO, F., GRAYSON, W. L., MA, T., BUNNELL, B. & LU, W. W. 2006. Effects of hydroxyapatite in 3-D chitosan–gelatin polymer network on human mesenchymal stem cell construct development. *Biomaterials,* 27**,** 1859-1867.
ZHU, L., AO, J. & LI, P. 2015. A novel in situ gel base of deacetylase gellan gum for sustained ophthalmic drug delivery of ketotifen: in vitro and in vivo evaluation. *Drug design, development and therapy,* 9**,** 3943.
ZOPF, D. A., MITSAK, A. G., FLANAGAN, C. L., WHEELER, M., GREEN, G. E. & HOLLISTER, S. J. 2015. Computer Aided–Designed, 3-Dimensionally Printed Porous Tissue Bioscaffolds for Craniofacial Soft Tissue Reconstruction. *Otolaryngology--Head and Neck Surgery,* 152**,** 57-62.